FACULTAD DE CIENCIAS BIOLÓGICAS

Departamento de Bioquímica y Biología Molecular-ERI BioTECMED

Doctorado en Biomedicina y Biotecnología

The Fibronectin RGD and synergy sites function in integrin interaction

Tesis Doctoral

María Benito Jardón

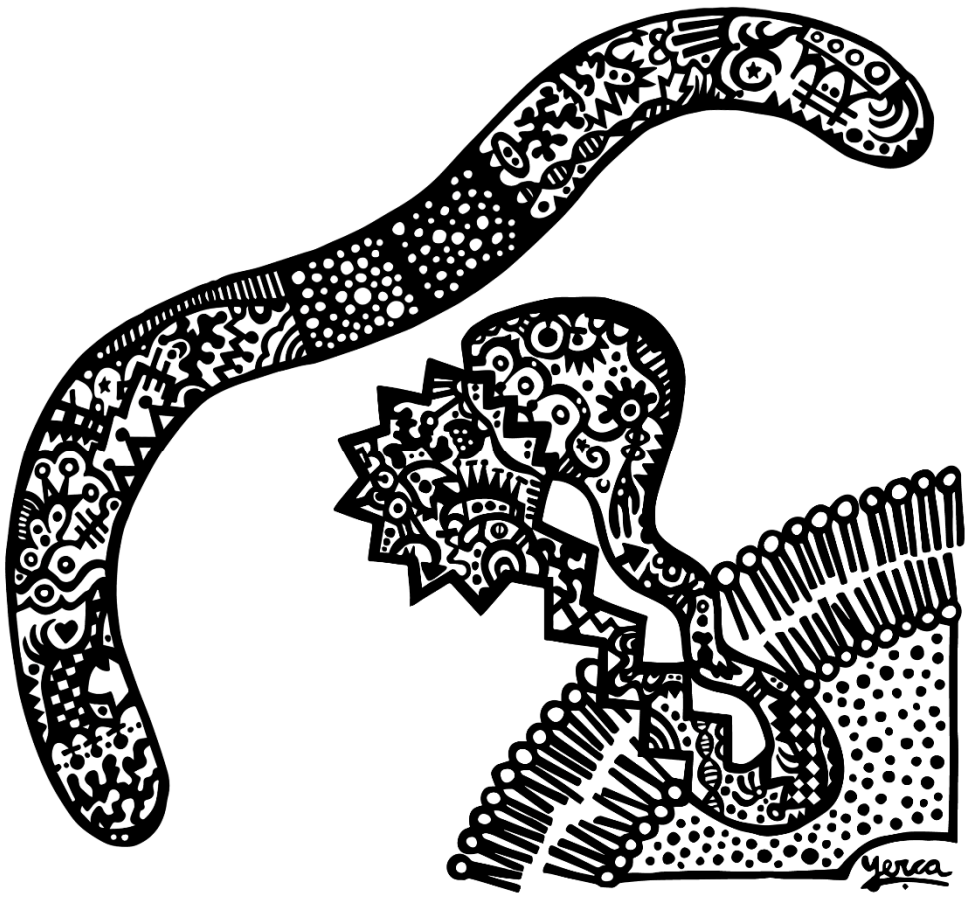

Directora:
Mercedes Costell Rosselló

Valencia, Junio 2018

FACULTAD DE CIENCIAS BIOLÓGICAS

Departamento de Bioquímica y Biología Molecular-ERI BioTECMED

Doctorado en Biomedicina y Biotecnología

The Fibronectin RGD and synergy sites function in integrin interaction

María Benito Jardón

Directora: Mercedes Costell Rosselló

Junio, 2018

To Christoph,

To my parents, Manuel and Almudena

To Lucía

"I am among those who think that science has great beauty. A scientist in his laboratory is not only a technician: he is also a child placed before natural phenomena which impress him like a fairy tale."

Marie Skłodowska-Curie

Acknowledgements

Reaching the end of my PhD thesis there are many people who I would like to thank for their help and support throughout these years.

Mercedes, my PhD supervisor, thank you for giving me the chance of working on these projects and for entrusting me with them since the beginning. I have learnt many things from you, but most importantly: how to be a scientist. Thank you for teaching me to be critical, curious, perseverant and to think independently, and especially for being supportive all the way and giving me the courage to stay on track when things did not turn out as expected.

I also want to thank Markus Moser, my supervisor at the MPI, for all the support and being such a hands-on mentor during my long stay. You have taught me a lot at a technical level. I particularly want to thank you for passing on to me your passion and enthusiasm in research.

My stay at the MPI would not have been possible without the generosity of Prof. Fässler, the head of the Molecular Medicine department. For that, I am deeply grateful.

During these years I had the pleasure of meeting and sharing my working place with people who created a friendly and motivating atmosphere and helped me when necessary, especially my colleagues and good friends Georgina, Franzi, Valeria Soberon, Valeria Samarelli, Marina, Sarah and Irene, who were there for everything: from integrin and mouse discussion, to splitting my cells if needed, to cheering me up with small talk or hanging out and travelling. I also would like to mention my last years´ "lunch crew": Raquel, Silvia, Johannes, Thomas, Peter and Alwin; you have also become more than just colleagues to me and brought animated moments to the daily life in the lab, and not only during lunch time. In addition, I want to thank Raquel for carefully reading the introduction of my thesis. There is also a bunch of colleagues who assisted me with technical issues or with who I had the pleasure of sharing enriching discussions, thank you for being such good lab mates: Julien, Ralph, Madis, Vera, Armin, Michal, Alicjia, Klaus, Ushi, Misha, Sarah, Patricia, Maik, Shiny. Last but not least, I want to thank Irene, Sheila and Olga for accompanying me during the last period (and a pretty hard one) of my PhD: the end!

Finally, I want to thank: Dr. Juan Jose Calvete Chornet, Dra. Roser Sabater Serra, Dra. Sarah Klapproth, Dr. Jerónimo Bravo Sicilia, Dra. Patricia Rico Tortosa and Dr. Frank Suhr, for agreeing to evaluate my thesis.

Index

Index

SUMMARY

Fibronectin (FN) is a large glycoprotein component of the extracellular matrix (ECM). It presents two forms: soluble in plasma or insoluble (fibrillar) within the ECM surrounding the cells in tissues. FN is a dimer with a modular structure containing various binding sites for cellular receptors, growth factors, other ECM proteins and FN itself. The ECM is a highly dynamic network organized in fibrils that acts as a scaffold for cells, supports them and can regulate numerous aspects of cell behaviour such as proliferation, migration or differentiation. FN is one of the most important proteins in the ECM, it directly mediates adhesion, and therefore is essential for several biological processes such as embryonic development or blood clotting. Its involvement in these processes relay in its interaction with the cellular receptors integrins. The major binding site for integrins in FN is the so-called RGD site located in the 10th FN type III repeat ($FNIII_{10}$), which is recognized by α5β1, αIIbβ3 and all the αv-containing integrins. Additionally, the α5β1 and αIIbβ3 integrins can also bind the synergy site (DRVPPSRN) in the 9th FN type III repeat ($FNIII_9$). In this work, we aimed to understand the function of these two different FN binding sites in interaction with integrins and fibrillar ECMs formation. FN is secreted in a globular soluble form within tissues, so to build a matrix it has to be turned into its fibrillar form in a process called fibrillogenesis. FN fibrillogenesis is a cell-mediated process, both *in vivo* and *in vitro.* The cellular receptors integrins are heterodimers which provide a transmembrane link between the ECM and the cytosol. Integrins are linked to F-actin and use intracellular actomyosin contractility to stretch cell-surface FN, thereby generating the characteristic long FN fibrils. When FN fibrillogenesis is disabled either due to insufficient FN production or defective assembly, it can lead to organ or tissue dysfunction. Therefore, it is of great importance to understand the rules governing the process of FN fibrillogenesis. Knowing the process in detail will allow, for example, the design of adequate and functional biomaterials. Integrin interaction with the RGD motif in $FNIII_{10}$ has been considered the backbone of FN fibrillogenesis. Integrin $\alpha5\beta1$ binding to the RGD site promotes the most efficient FN fibrillogenesis. However additional RGD binding integrins, including $\alpha v\beta3$ and $\alpha IIb\beta3$, can substitute for $\alpha5\beta1$ in FN matrix assembly. This work has explored new RGD-independent mechanisms for FN fibrillogenesis. For that purpose, we analysed FN fibrillogenesis by fibroblast which express FN lacking the RGD site ($FN^{\Delta RGD}$). The results from this work showed that despite lacking the RGD site, $FN^{\Delta RGD}$ can be assembled in a disorganized fibrillar matrix. The $FN^{\Delta RGD}$ fibrillogenesis takes place through a different binding site located in the 12-14th FN type III repeat (heparin II) through binding of receptors distinct of integrins, the syndecan family of heparan sulphate. However, $FN^{\Delta RGD}$ fibrillar matrix is disorganized indicating the relevance of the α5β1-FN-RGD adhesion for this process. Although the RGD sequence in the $FNIII_{10}$ domain is the key binding site for integrins, the synergy site (DRVPPSRN sequence in mice) has been demonstrated in adhesion experiments to cooperate in the interaction of the RGD motif with $\alpha5\beta1$ and $\alpha IIb\beta3$ *in vitro.* Despite $FNIII_9$ has no adhesive activity by itself, it causes an about 100-fold increase in cell adhesion to FN via $\alpha5\beta1$. The αv-containing integrins, which bind the RGD site, do not bind to the synergy site. This altogether indicates that the synergy site could contribute to cell adhesion via integrins, modulating cellular functions, integrin usage and signalling. Most of the studies that give evidence of a binding activity of this motif have been done *in vitro* with cultured cells. With the aim of analysing the role of the synergy site *in vivo*, in this project we analysed a mouse strain in which the two arginines in

the sequence DRVPPSRN were substituted with alanines. The synergy site was shown to have a role in Xenopus development and we expected that the mutations would impair $\alpha5\beta1$ and αIIb$\beta3$ functions while leaving αv functions unaltered. The integrin $\alpha5\beta1$ is mostly expressed in mesenchymal cells, and its interaction with FN is essential for development. The αIIbβ3 integrin is only expressed in platelets, which also express $\alpha5\beta1$, and interacts with the plasmatic FN during platelet aggregation. Contrary to our expectations, the mutation does not affect mouse development. However, the mutant synergy mice (*Fn1*$^{syn/syn}$) have prolonged haemorrhages upon vessel injury, indicating that platelet-FN interaction is altered. To further study the function of the synergy site in integrin binding, we developed a series of *in vivo and in vitro* approaches using the mutant mice, different mouse fibroblast lines and purified plasma FN with mutated synergy sequence (FN^{syn}). In this work we show that the synergy site is not essential for cell adhesion or FN fibrillogenesis, but it is important to strengthen the bond to FN under shear forces. The α5β1 adhesion to FN reinforcement allows regulation of integrin-FN downstream signalling, assembly of focal adhesions and reorganization of the cytoskeleton. Integrin-FN reinforcement through the synergy site also modulates cellular adaptation to different rigidities, which is relevant for pathologies such cancer or fibrosis where the abundant ECM hardens the stroma. Moreover, we could demonstrate that the function of the synergy site can be compensated by αv integrins in mesenchymal cells. Fibrinogen, a plasmatic ECM protein which binds αIIbβ3 integrin, can also compensate the lack of function of the synergy site in platelets. Therefore, these two compensatory mechanisms attenuate the lack of synergy site function. When these compensatory mechanisms are lost, the synergy site becomes essential and cells do not form correct adhesions and mice die during development. Taken together, the data presented in this study show that the FN synergy site is important for integrin adhesion reinforcement to FN, but it can be compensated by other mechanisms making it not essential for embryonic development or tissue homeostasis *in vivo*.

I INTRODUCTION

1. The extracellular matrix protein Fibronectin. General aspects

The extracellular matrix (ECM) is a complex collection of molecules secreted by the cells into their extracellular space. The ECM normally consists of a fibrillar array surrounding the cells and gives them mechanical and biochemical support. Each tissue has a different ECM composition. Fibronectin (FN) is a large and ubiquitous ECM glycoprotein. It exists as a soluble protein in blood (plasma FN or pFN) and assembled into a fibrillar network surrounding the cells in tissues (cellular FN or cFN). The pFN is synthetized by hepatocytes in the liver and secreted to the bloodstream and plays a role in thrombosis as it will be discussed in section 4. Several cell types synthetize cFN. Fibroblasts and endothelial cells are the major producers but many other cell types, including some epithelial cells, can synthesize FN at lower levels. FN is encoded by a single gene (*Fn1*) located in the chromosome 2 in humans and in the chromosome 1 in mouse. The protein is secreted as a dimer consisting of two nearly identical subunits of 230-270 kDa each, linked by a disulphide bond at the carboxyl terminal region (Fig 1). FN monomers are not identical as the mRNA contain several splicing sites. Hence, the *Fn1* gene product can be spliced into different isoforms, 20 in humans and 12 in rodents (Singh *et al.*, 2010; Goossens *et al.*, 2009).

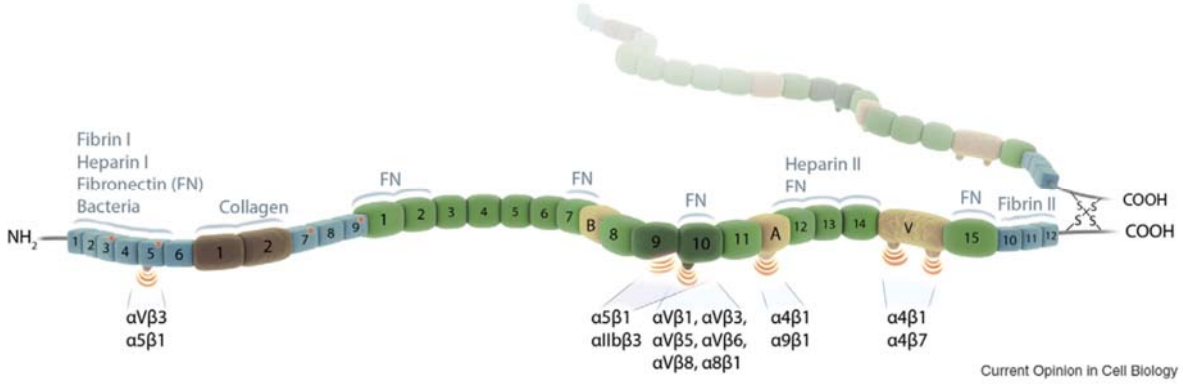

Figure 1. Representation of the FN structure. It is a dimer connected by two disulphide bonds at the C-terminus. Each monomer is a modular protein composed by three different domains: type I (blue), type II (brown) and type III (green). It also contains alternative spliced extradomains A, B and variable region (V), coloured in ochre. The binding sites for integrins and other ECM proteins are indicated along the molecule. From Leiss *et al.* 2009.

FN interacts with several ECM components including heparan sulphate proteoglycans, collagen or fibrin, and even serves as a scaffold for the assembly of collagens (Kadler, *et al.*, 2008; Leiss *et al.*, 2008). Furthermore, FN recruits growth factors and binds to different cellular receptors. All these different interactions are possible by distinct structural and functional motifs contained within the FN molecule (described in section 2). By interacting with cells and others ECM proteins, FN mediates fundamental processes such as organogenesis, haemostasis, angiogenesis and vascular remodelling. It has been demonstrated that mutations in *Fn1* gene lead to glomerulopathy in humans (Castelletti *et al.*, 2008) and deletion of the *Fn1* gene leads to embryonic lethality in zebrafish (Jessen, 2015), frogs (Marsden and DeSimone, 2001) and mice (George *et al.*, 1993). The description of the FN knock-out phenotype in mice ($FN^{-/-}$) was the proof that FN is essential for development in mammals. Mice lacking FN die early in

embryogenesis, at embryonic day 8.5, presenting several abnormalities including shortened anterior-posterior axes, absence of mesenchymal structures such as notochord and somites; and defective heart, blood vessels as well as extraembryonic vasculature (George *et al.*, 1993; Georges-Labouesse *et al.*, 1996; George *et al.*, 1997).

2. Modular structure of fibronectin and binding sites

The extended conformation of FN monomers looks like a slender and flexible elongated fibril in electron microscopy (Fig. 2) (Erikson *et al.* , 1981). They have a complex molecular structure, consisting in sets of modular repeats (modules) which are Ig-like folds. These modules were initially described as protease-resistant units, although later studies showed that FN is composed by a repetition of three types of modules with a defined structure, designed as FNI, FNII and FNIII. These three types of repeats are connected by flexible links and most of them present specific ligand-binding activities (Potts and Campbell, 1996; Mao and Schwarzbauer, 2005; Bingham and Potts, 2010).

Figure 2. Typical EM image of FN fibrils presenting an elongated and flexible morphology. From Erikson *et al.* 1981

2.1. FN type I modules

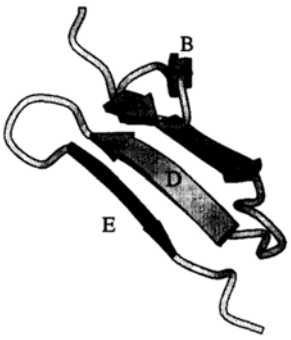

Figure 3. Representative structure of FNI domain. From Potts and Campbell, 1996.

Type I repeats are about 40-45 amino-acid residues in length and contain 4 cysteines forming two disulphide bonds (Potts and Campbell, 1996; Pankov, 2002a). Each of them has β-sheets structures enclosing a hydrophobic core that contains highly conserved aromatic amino acids (Mao and Schwarzbauer, 2006) (Fig. 3). FN contains 12 type I modules located at the N- and C-terminus of the protein. The N-terminal part of FN has a central role in FN multimerization during matrix assembly as different FN dimers interact by the 70 kDa N-terminus containing FNI_{1-5} (Potts and Campbell, 1996). The FNI_5 can interact with $FNIII_1$ (type III FN repeat) for self-association and there is also a cryptic binding site for FN self-association in FNI_1 (Zollinger and Smith, 2017).

The FNI modules also contain binding sites for other ECM proteins and bacteria. Collagen interacts weakly with FNI_6 and FNI_7 and once it is bound, it makes stronger interactions with FNI_{8-9}. It is known that collagen matrix is not deposited in absence of FN and needs direct interaction with FNI modules. For example, deletion of FNI_6 and FNI_9 or blocking of this region prevented collagen fibres assembly (Sottile *et al.*, 2007). Recent studies with FN-FRET probes showed that collagen colocalizes with elongated non-stretched FN fibrils (relaxed fibrils),

suggesting that collagen fibrillogenesis relies on the mechanoregulation of FN matrix (Kubow *et al.*, 2015). The FNI modules also contain fibrin binding sites in the amino-terminal FNI_{1-5} and the carboxyl-terminal FNI_{10-12}. Covalent bonds are formed between FN and fibrin involving residues localized in the FNI_{1-5} region and mediated by thrombin-activated factor XIII during blood coagulation (Corbett *et al.*, 1997), as it will be explained in detail in section 6. FNI_{1-5} also contains a heparin binding site (Heparin I) where heparan sulphate (HS) chains from proteoglycans (GAGs) can bind to. Another heparin-binding module (HepII) located in type III13 is dominant for FN-heparin adhesions (Busby *et al.*, 1995). The FNI can be targeted by bacteria to adhere to tissues and evade host defences. The regions FNI_{1-5} and FNI_{8-9} have been shown to interact with different bacteria (Marjenberg *et al.*, 2011; Maurer *et al.*, 2012), such as *S. aureus* and *S.pyrogenes*, two bacteria of high clinical interest (Henderson *et al.*, 2011).

2.2. FN type II modules

In FN there are two repeats of type II modules and despite being the firsts isolated, they probably are the least studied regions of FN. They contain approximately 60 amino acids and two intramolecular disulphide bonds (Potts and Campbell, 1996; Pankov, 2002). Structure has shown that FNII domains are constituted by two relatively short antiparallel β-sheets, which are almost perpendicular to each other, and two irregular loops separating the β-sheets (Pickford *et al.*, 1997). FNIIs interact weakly with collagen and promote its fibrillogenesis or with gelatine but cannot mediate cell interactions. This region, together with $FNI_{6-9,}$ is important for the interaction with denatured collagenous materials from blood and tissue (Pankov, 2002).

2.3. FN type III modules

The FN type III (FNIII) domains are well characterized. Each FN monomer contains 15-17 FNIII repeats of 90 amino acids, which all together constitute about 90% of the molecule (Pankov, 2002b; Bencharit *et al.*, 2007). Despite the low sequence identity (~30%) among FN type III repeats, their secondary structure is similar and does not contain disulphide bonds (Potts and Campbell, 1996). The individual FNIII repeat is a β-sandwich fold, topologically very similar to that of immunoglobulin constant domains, which encloses a compact hydrophobic core with four β-strand on one side and three on the other (Leahy *et al.*, 1996; Potts and Campbell, 1996; Bencharit *et al.*, 2007). The FNIII repeats contain several motifs for cell receptors binding. These binding sites are often series of key residues situated in the loop regions in between β-strands. The most relevant cell binding sites are EIIIA, $FNIII_5$, $FNIII_{10}$ (RGD), $FNIII_9$ (synergy) IIICS, and $FNIII_{12-14}$ (heparin II), which bind integrins. $FNIII_{12-14}$ bind also syndecans (Fig. 1) and growth factors (Zollinger and Smith, 2017). The $FNIII_{9-10,}$ are the most important cellular binding sites and will be described in section 4.

The EIIIA, EIIIB and the IIICS (or variable region) are present in the FN by alternative splicing. Splicing at EIIIA (located between FN repeats III7 and III8) and EIIIB (located between FN repeats III11 and III12) happens by exon skipping, generating FN molecules which either lack or contain these regions. In contrast, splicing in IIICS can be totally or partially included or excluded since its exon contains various alternative splice acceptors and one donor site, giving

rise to several FN isoforms (Goossens *et al.*, 2009). The number of isoforms that alternative splice in IIICS arises seem to correlate with the evolutionary scale: there are five variants in humans, three in rodents, and two in chickens (White and Muro, 2011). The expression of EIIIA and EIIIB isoforms is higher during embryonic development and decreases after birth and aging. However, it can temporally increase again in adulthood under certain situations such as fibrosis or wound healing (White *et al.* , 2008; Goossens *et al.*, 2009). One of the greatest particularities of the EIIIA and EIIIB domains is that they are only included in cFN and always absent in pFN, although in pathological conditions is possible to find cFN-EIIIA+ in the blood (White and Muro, 2011). Despite the fact that EIIIA and EIIIB are only present in cFN, none of them is required for FN fibrillogenesis (Singh *et al.*, 2010), a process which will be explained in detail section 5. The EIIIA presents the EDGIHEL motif, which is bound by integrins α4β1, α4β7 and α9β1. The IIICS contains two sequences (LDV and REDV) that are recognized by integrins α4β1 and α4β7. Therefore, these regions mediate cell adhesion by these two integrins which are mainly expressed in leukocytes and monocytes (Guan and Hynes, 1990). The α4β1 integrin can also interact with an IDAPS motif located at the $FNIII_{13-14}$ junction (Pankov, 2002a; Leiss *et al.*, 2008). $FNIII_{14}$ also has a secondary α4β1 binding site, the PRARI motif which constitutes a loop within the 14th type III domain structure (Sharma, 1999). The IDAPS and PRARI motives belong to the heparin II (Hep II) region. The Hep II region is a well-defined 30 kDa fragment and its structure present homologies with the $FNIII_{7-10}$ modules. Some studies suggest that it contains two binding sites for heparan sulphate. The major binding site is in $FNIII_{13}$ and there are contributions in $FNIII_{14}$ which may be essential for FN-heparan sulphate interaction (Barkalow and Schwarzbauer, 1991; Sharma, 1999). This interaction is based on ionic contacts between the negatively charged groups of heparan sulphate (sulphate and carboxylate groups) and positively charged residues in FN. The $FNIII_{13}$ consists of 5 arginines and 1 lysine located in 3 different β-strands. This cluster of basic amino acids form a 'cationic cradle' facing the outer part of the β-sheet (Busby *et al.*, 1995). In the $FNIII_{14}$ there is another cluster of positively charged amino acids (3 lysines and 2 arginines). The positively charged amino acids of $FNIII_{13}$ and $FNIII_{14}$ are on the same face of the molecule (Fig. 4) so heparan sulphate could use both binding sites at the same time (Sharma *et al.*, 1999).

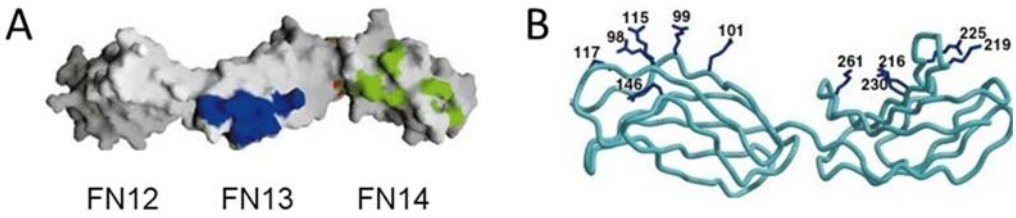

Figure 4. (A) Representation of the $FNIII_{12-14}$. The backbone is coloured in grey, the HBS-1 ($FNIII_{13}$) in blue and the HBS-2 ($FNIII_{14}$) in green. (B) Stereo view of the $FNIII_{13-14}$, the backbone is shown in cyan and the side-chains of the basic residues in dark blue. HBS-1 and 2 locations in the same face of the molecule is appreciated in both images. Modified from Sharma *et al.* 1999.

The $FNIII_{13}$ mediates cell adhesion and focal adhesion assembly by binding to the heparan sulphate lateral chains of the family of syndecan receptors as indicated by many studies using cells and immobilized FN (Stamatoglou and Keller, 1983; Busby *et al.*, 1995; Mahalingam *et al.*, 2007). Syndecans are a family of 4 transmembrane proteoglycans HS and chondroitin sulfate glycosaminoglycans (GAGs) (Fig. 5) (Yoneda and Couchman, 2003). Their extracellular domain is composed by a core protein and several glycosaminoglycans (GAGs) and both mediate interaction with ECM (Choi *et al.*, 2011). The 4 members of the syndecan family (sydecan 1-4) differ in their cytosolic variable region and their ectodomain (Fig 5). Chromatography analysis indicated that interaction between syndecans and $FNIII_{13}$ is specific and requires the N-sulphated disaccharides of the heparan sulphate GAG chains (Mahalingam *et al.*, 2007). Syndecan adhesion to FN triggers signalling events, which promote focal adhesion assembly and cytoskeleton rearragement and can also cooperate with integrin signalling (Bass *et al.*, 2007; Choi *et al.*, 2011). The $FNIII_{12\text{-}14}$ repeats are also a promiscuous binding site for growth factors (GFs), acting as a reservoir for them, which can provide proteolytic degradation and aid the interaction with receptors. The repertoire of GF that can bind FN includes platelet-derived GF (PDFG) or vascular endothelial GF (VEGF), fibroblast GF families and transforming growth factor-β or neurotrophin families (Zollinger and Smith, 2017).

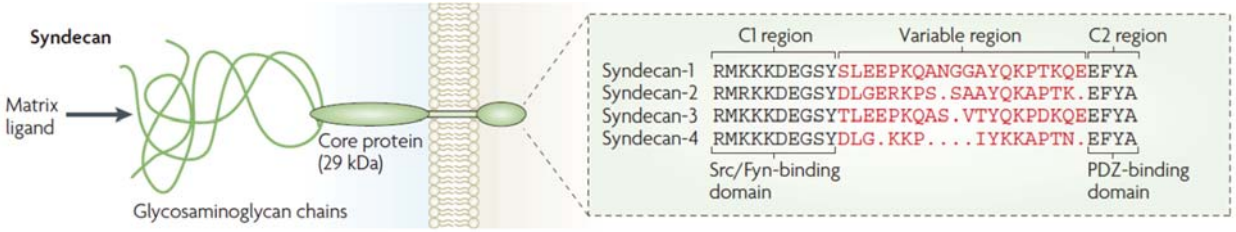

Figure 5. Syndecans are transmembrane proteins with an ectodomain rich in glycosaminoglicans (GAGs). They interact by the ectodomain with the ECM. The four syndecans have different amino acid sequence, although there are two conserved regions in the cytoplasmic domain: the C1 and C2 regions. Modified from Bass *et al.* 2007.

3. Fibronectin receptors: the integrins α5β1 and αvβ3

FN interacts with cell receptors to mediate cell adhesion, migration, growth and differentiation (Pankov, 2002). The major receptors for FN are integrins. Integrins are transmembrane, heterodimeric proteins which act as a link between the ECM and the cytoskeleton. Integrin heterodimers are composed by two non-covalently associated subunits α and β. Mammals express 18 different α and 8 different β subunits that can be combined in 24 different receptors, each with specific properties. The 24 integrins have distinct patterns of expression in cells and tissues and can recognize different ligands (Fig. 6) (Hynes, 2002; Campbell and Humphries, 2011).

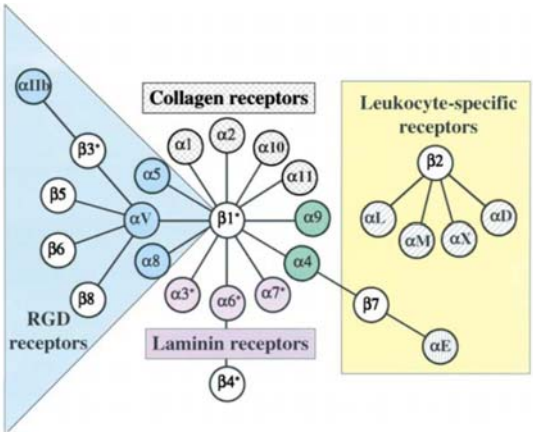

Figure 6. The integrin receptor family. The figure represents the mammalian subunits and their αβ associations: 8β and 18α subunits to form 24 different heterodimers. Each heterodimer can recognize different types of ligands depending on the α and β-subunit which composes them. From Hynes 2000.

Integrins transmit signals bidirectionally across the plasma membrane: from inside to outside ("inside-out") and from outside to inside ("outside-in"). They transduce both chemical and mechanical signals from the ECM triggering intracellular responses which allow cell to adapt to its environment, participating in broad biological processes including development, tissue repair, angiogenesis and haemostasis. Integrins play fundamental roles in such processes by mediating cell adhesion and migration through stablished interactions with the ECM. Despite many integrins share the same ECM ligand, integrins do not have redundant functions. Genetic ablation of distinct α or β integrin subunits in mice causes different phenotypes and severity, reflecting that their roles are non-overlapping (Hynes, 2002; Springer and Wang, 2004; Wickström *et al.*, 2011).

About 11 different integrins are receptors for FN: α5β1, αIIbβ3, α4β1, α4β7, α8β1, α9β1 and all the αv-subunit containing integrins (αvβ1, αvβ3, αvβ5, αvβ6, αvβ8). At least 8 integrins (α5β1, αIIbβ3 and all the αv-subunit integrins) among the FN integrin receptors recognize and bind a RGD motif in $FNIII_{10}$ (Ruoslahti, 1996; Leiss *et al.*, 2008), however, the most studied ones as FN receptors are α5β1 and αvβ3, probably because of being broadly expressed in tissues. It is worth noting that with exception of α5β1 integrin, the rest of integrins binding the FN-RGD site bind other ECM proteins including fibrinogen (αIIbβ3) or vitronectin (αv-class of integrins) (Hynes, 2002). Since FN is the only ligand for **α5β1 integrin**, this integrin is considered the major FN receptor. *In vivo* deletion of the α5β1 integrin (α5-null) causes embryonic lethality around day 10-11, and embryos have severe defects in posterior trunk elongation and mesoderm (Fig. 7) (Yang *et al.*,1993). However, α5-null mutant cells assemble FN, form focal adhesions (FA) and migrate on FN by interactions with αv-containing integrins (Yang and Hynes, 1996). Furthermore, while single deletion of αv integrins causes perinatal lethality (Bader *et al.*, 1998), the double deletion of α5 and αv integrins in mice generates a phenotype similar to the $FN^{-/-}$ (Yang *et al.*, 1999). Taking all into consideration, α5 and αv(β3) integrins are the major receptors for FN and despite some different functions upon FN adhesion, they also have certain overlapping roles (Yang *et al.*, 1999).

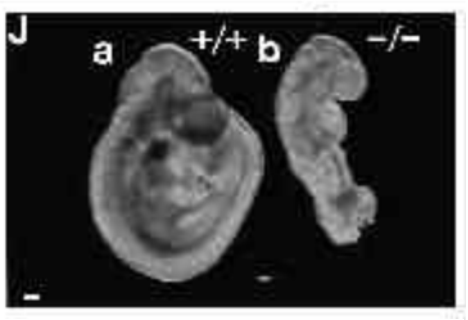

Figure 7. Wild-type (a) and a α5-null (b) embryo from the same litter (E9.5). Note the underdevelopment of the mutant embryo. From Yang *et al.* 1993.

3.1 Integrin structure domains

All integrin dimers have similar shape and size. Each subunit is composed by an ectodomain or extracellular fragment, a transmembrane domain and a cytosolic domain. The ectodomains are the largest part that resemble two "legs" ending on a globular "head" which contains the binding sites for the ligand and subunit association. The transmembrane domain of each subunit is a single helix which spans across the membrane. The cytoplasmic domains are short and unstructured tails that mediate the assembly of signalling complexes that link the integrins to the cytoskeleton. Integrin structure is composed by modular domains and

flexible links which enable conformational changes. Changes in tertiary and quaternary structures allow the switch from bent or inactivated integrin to unbent/open and activated integrin (Hynes, 2002; Arnaout *et al*., 2005; Campbell and Humphries, 2011; Su *et al.*, 2016)

-Structure of the ectodomain

The ectodomain is composed by a ligand binding head piece ("head" and the upper legs) and the lower legs (Fig. 8) (Hynes, 2002; Arnaout *et al.*, 2005; Campbell and Humphries, 2011; Zhu *et al.*, 2013).

The head of the α5, αv and αIIb **α-subunits** is a β-propeller and is followed by the thigh and calf domains in the legs which have immunoglobulin-like β-sandwich folds. The link between the β-propeller and the thigh domain is a flexible interdomain. Between the thigh and calf domains there is also a flexible linker called "genu" or knee, which acts as a hinge, allowing the extension and bending of the legs.

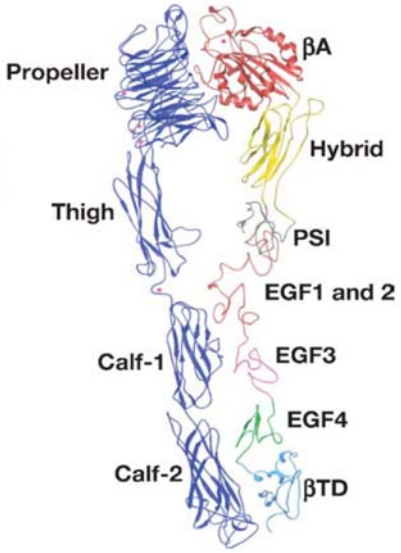

Figure 8. Structure of the integrin αvβ3 ectodomain. All the domains are labelled. From Arnaout *et al.* 2005.

The **β-subunit** of β1 and β3 integrins has seven domains with flexible links whose structure is complex (Arnaout *et al*., 2005; Campbell and Humphries, 2011). In the legs, the EGF-like region is relatively flexible and contains the knee linker between the EGF1 and 2, in proximity to the knee in the α-subunit, allowing also the bending. Moreover, other flexible connections in the β-subunit between the PSI and the hybrid domains and between the hybrid and the I-EGF domains, make this subunit rather plastic.

Ligand binding occurs in the β-propeller (α-subunit) and the βI interface (β-subunit), and it is dependent on divalent cations (Mg^{+2}, Ca^{+2}, and Mn^{+2}). There are three cation binding sites: the "metal ion-dependent adhesion" (MIDAS) flanked by the "adjacent to metal ion-dependent adhesion" site (ADMIDAS) and the "synergistic metal ion binding site" (SyMBS). Mg^{+2} binds to MIDAS to promote the integrin interaction with FN. Mn^{+2} binds to ADMIDAS and Ca^{+2} binds to ADMIDAS and SyMBS, regulating ligand binding. Binding of Ca^{+2} to SyMBS synergizes with suboptimal concentrations of Mg^{+2} to facilitate ligand binding. Contrary, Ca^{+2} binding to ADMIDAS has an inhibitory effect, and Mn^{+2} binding results in structural rearrangements which lead to an active integrin (Springer and Wang, 2004; Arnaout *et al.*, 2005; Campbell and Humphries, 2011; Zhang and Chen, 2012).

In integrin FN receptors, the FN-RGD is accommodated in a binding cleft at the α/β-subunit interface (Springer and Wang, 2004; Campbell and Humphries, 2011). Precisely, the aspartate residue coordinates directly with MIDAS-Mg^{+2} in the β-subunit while the arginine with the β-propeller domain in the α-subunit, anchoring the RGD to the binding cleft (Xiong *et al.*, 2002; Nagae *et al.*, 2012).

-Structure of the transmembrane domain

The integrin transmembrane (TM) domains are embedded in the cytoplasmic membrane and are generally represented as almost perpendicular to the long axis of the legs. The TM domains have been described to be involved in integrin transition from the resting to the active state. This is due to studies showing that there are interactions between the α and β subunit that take place at the TM domain and are only present in the resting state (Arnaout *et al*., 2005; Campbell and Humphries, 2011).

Most of the knowledge about the integrin TM structure is based on analysis with αIIbβ3, using either full-length or the TM with the cytoplasmic tail. NMR studies showed that TM domains of αIIb and β3 interact by glycines at the helix-helix interface in the resting state (Zhu *et al.*, 2009). In this inactive state, the β3 TM is tilted by interaction with the lipid membrane through a "snorkelling" lysine (Kim *et al.*, 2012). During integrin activation, these interactions are disassembled and therefore, the TM domains separate. Despite sequence similarities between β3 and β1 integrin TM domains, recent studies pointed that TM interactions might not be equal as the "snorkelling" lysine is not involved in the resting conformation of β1 (Lu *et al.*, 2016).

The TM association is favoured by the close proximity of the α and β subunit ectodomains in the inactive/bent conformation (Arnaout *et al*., 2005; Campbell and Humphries, 2011). The flexibility of the ectodomain-TM linkers is important and consistent with the model of integrin transition from resting to active state. The flexibility allows the changes of orientation of the TM to allow the respective changes in the ectodomain during this transition (Lau *et al.*, 2009)

- Structure of the cytoplasmic tail

Integrin cytoplasmic domains are really small compared to the ectodomains. Nevertheless, they are instrumental for integrin function as they contain the binding site for adaptor proteins that are involved in integrin activation and link the integrins to the cytoskeleton (Hynes, 2002).

The cytoplasmic tails (CT), according to many reports, are flexible and form transient structures in solution in absence of adaptor proteins or other binding partners (Spriner and Wang, 2004; Shattil *et al.,* 2010). Although it is not clear yet how the CT are organized, mutational analysis showed that β3 integrins lacking β tails fail to localize to focal adhesions, and have reduced ligand-binding activity and impaired activation of downstream signalling cascades (Liu *et al.*, 2000). As the integrin CT do not have enzymatic activity, its function relies on its interaction with cytoplasmic proteins which act as adaptors, recruiting other proteins to activate downstream signalling and to link the integrins to the cytoskeleton. Among protein interactions with the CT, PTB-containing proteins binding to a NPXY motif in the β-tails are especially important. Talin and kindlin can bind to these motifs and are essential to mediate integrin activation and signalling (Campbell and Humphries, 2011).

3.2 Integrin activation and conformational changes

Changes in integrin ligand-binding affinity or activation dictate cell adhesion to the ECM, migration, mechanotransduction or ECM assembly. Although the mechanism of integrin activation has been deeply studied in the past years, it is not fully understood yet. It is accepted that integrin activation consists of triggering events, resulting in the interaction of integrin tails with cytoplasmic proteins and rearrangement of integrin conformation to a ligand-binding affinity state (Adair *et al.*, 2005; Campbell and Humphries, 2011). Most of the activation mechanisms which have been hypothesised are based on EM or crystallographic studies with αvβ3 or αIIbβ3 integrins (Hynes, 2002). The bent conformation of inactive integrins impedes the interaction with the ligand as it orients the headpiece towards the cell membrane. Active integrins adopt an extended structure that exposes the binding site in the head piece, bringing them to a ligand-high affinity state (Xiong *et al.*, 2002; Arnaout *et al.*, 2005) (Fig. 9). This extended conformation confers accessibility to the ligand binding site in the headpiece (Springer and Wang, 2004; Arnaout *et al.*, 2005; Arnaout *et al.*, 2007; Shattil *et al.*, 2010; Campbell and Humphries, 2011). αvβ3 integrin EM analysis revealed that in addition to the bend/inactive and extended/active conformations, integrins might also have an intermediate state, consisting on an extended conformation with a closed headpiece (extended-closed conformation), (Fig. 9) (Takagi *et al.*, 2002).

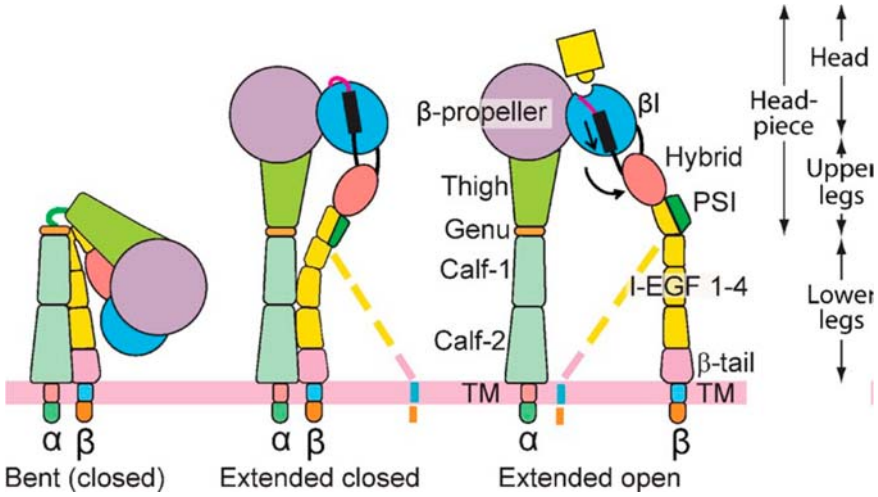

Figure 9. Integrin conformation in the different activation states. In the inactive state, integrins have the bent conformation which does not allow interaction with ligand. In the intermediate state they extend the legs and the head remains closed (extended-closed conformation), and when they are in an active state they acquire the extended open conformation which allows them to interact with the ligand. The dashed lines indicate the two lower leg conformations where the transmembrane domains are associated or separated. From Zhu et al. 2013.

Structural studies using antibodies and purified α5β1 ectodomains have suggested that this integrin might present these three conformational state, too (Su *et al.*, 2016). However, recent measurements of α5β1 conformational equilibria showed that energy is only required for transition from bend to extended conformation, and once the integrin extends, the open headpiece is prompted as it is energetically favoured (Li *et al.*, 2017). Therefore, the extension

of bent integrins seems to be the key regulatory event to activate integrins. Quantitative measurements have shown that force generated by the cytoskeleton and transmitted to integrins through adaptor proteins provides the energy needed to extend the bent integrins (Li and Springer, 2017) and to stabilise the open high-affinity conformation (Zhu *et al.*, 2008). This inside-out signalling is considered essential to transmit conformational changes towards the integrin ectodomain,activating them. Recently, it was found that talin and kindlin cooperatively work to switch integrin affinity to FN (Theodosiou *et al.*, 2016). Binding of these two adaptor proteins might separate the integrin tails and it is assumed that this generates the conformational changes that are transmitted across the membrane to the ectodomain to induce the high-affinity state (Arnaout *et al.*, 2005; Arnaout *et al.*, 2007). It is likely that different integrins are regulated differently. However, according to current findings, FN integrin receptors α5β1 and αvβ3 might be dependent on tensile force generated by the cytoskeleton to adopt the active state (Li and Springer, 2017, 2018; Li *et al.*, 2017).

4. The $FNIII_{7-10}$ cell binding region

The importance of the repetitions $FNIII_{7-10}$ for cell adhesion lays on the fact that it contains the major binding motif for the integrin receptor family: the RGD site (Pankov, 2002; Leiss *et al.*, 2008; Geiger and Yamada, 2011). In addition, the $FNIII_{7-10}$ cell binding region contains an extra motif for integrin interaction: the synergy site (Aota *et al.* , 1994; Bowditch *et al.*, 1994).

4.1. The RGD site

A RGD (Arginine-Glycine-Aspartate) motif located in $FNIII_{10}$ module was recognized as the minimal cell-binding sequence of FN in 1984 by Pierschbacher and colleagues (Pierschbacher and Ruoslahti, 1984). It is a highly conserved binding motif in FN (Redick *et al.*, 2000). Crystal structure of the $FNIII_{7-10}$ modules revealed that the RGD sequence is a flexible overhanging loop within the $FNIII_{10}$ (Fig. 10) (Leahy *et al.*, 1996), making it easily accessible for integrins. Integrin recognition of this tripeptide sequence is complex, and it also depends on flanking residues, as shown by adhesion studies using peptides with different sequences surrounding the RGD motif. Thus, cells adhere to an GRGDSP peptide with less affinity than to full-length or $FNIII_{7-10}$ (Ruoslahti, 1996). Another proof that the residues outside RGD as well as RGD three-dimensional presentation are relevant for specific ligand-receptor recognition is that several other proteins including vitronectin which binds αv-containing integrins, or fibrinogen (Fg) which binds αIIbβ3 integrins, have an RGD sequence, however not all of them share the same integrin receptors (Ruoslahti, 1996; Richard O. Hynes, 2002; Takagi, 2003, 2004b; Hynes, 2009).

Figure 10. A ribbon diagram of the FNIII10 structure with the RGD loop hanging over the β-sheet. Modified from Leahy *et al.* 1996.

Mutation of the FN RGD sequence into RGE causes embryonic lethality in homozygous mice at E10.5 (Takahashi *et al.*, 2007a; Girós *et al.*, 2011). The development of $FN^{RGE/RGE}$ embryos is interrupted at E9.0 and their number of somites is reduced to 13. The $FN^{RGE/RGE}$ mutation also shortens the posterior trunk and causes malformations in the presomitic mesoderm of embryos, hindering the completion of embryo turning (Girós *et al.*, 2011). These defects in $FN^{RGE/RGE}$ embryos are less severe than the ones in $FN^{-/-}$, but resemble the integrin $\alpha5^{-/-}$, indicating that integrity of the RGD site is essential for interaction with α5β1 integrins. The $FN^{RGE/RGE}$ embryos and cells assemble FN in a fibrillar matrix. It was suggested that αvβ3 integrins bind an NGR motif in the FN N-terminus (Curnis *et al.*, 2006; Takahashi *et al.*, 2007). However, later studies showed that this binding site is cryptic and cannot mediate FN fibrillogenesis (Xu *et al.*, 2010). In addition, unpublished results of our lab showed that the deletion of the three RGD amino acids in mouse (ΔRGD mutation) (*$Fn1^{\Delta RGD/\ \Delta RGD}$*) recapitulates the $FN^{-/-}$ mutation (Georges-Labouesse *et al.*, 1996) or integrin α5/αv double knock-out in mice (Yang *et al.*, 1999), lacking somites and arresting their development at E8.5. This suggests that αvβ3 could bind the mutated RGE site and assemble a fibrillar matrix. AFM measurements (unpublished results of our lab and Dr. Müller) show that αvβ3 integrins bind to an RGD mutated peptide ($FNIII_{7\text{-}10}^{RGE}$), proving that indeed integrin requirements for RGD recognition are different.

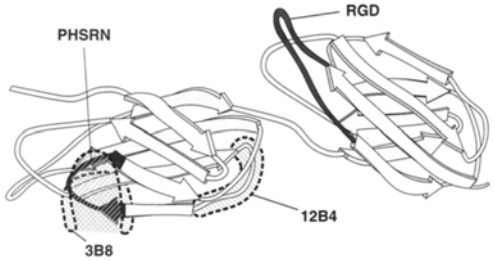

4.2. The FN synergy site

The synergy site is a 9-amino acid (DRVPPSRN in mice) sequence which was suggested to cooperate with the RGD motif for integrin binding. In contrast with the RGD site, the synergy site does not have adhesive activity by itself (Kimizuka *et al.*, 1991) and only binds to the α head of two integrins: α5β1 and αIIbβ3 (Aota *et al.* , 1994; Bowditch *et al.*, 1994). The residues which compose the synergy site of FN are highly conserved among different species (Fig. 11), with the exception of human that has an histidine instead of a proline in its sequence (DRVPHRNS) (Redick *et al.*, 2000).

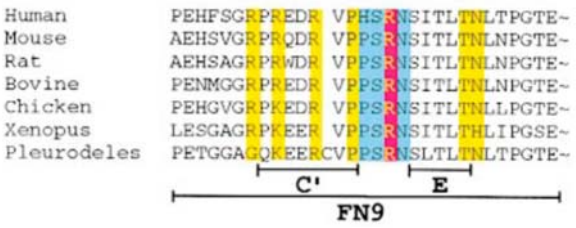

Figure 11. Conserved residues among species within the $FNIII_9$. Note that the synergy site DRVPPSRN is conserved. The relevant regions according to Redick et al. are underlined in different colours: in yellow are the residues which contribute to adhesion only together with the arginine in red. From Redick *et al.* 2000.

After identification of the RGD site, it was shown that flanking FNIII repeats could enhance its interaction with integrins and therefore, it was hypothesised the presence of synergistic regions within the $FNIII_{7\text{-}10}$ domains (Ruoslahti, 1996). Deletional studies of FN fragments identified potential synergistic integrin binding sites in $FNIII_9$ which could cooperate with the RGD motif in $FNIII_{10}$ to enhance cell spreading. In addition, it was observed that purified α5β1 and αIIbβ3 integrins could interact with 76 residues within the $FNIII_9$ repeat.

Later studies could restrict it to a sequence of 11 amino acids spanning from Asp[1373] to Thr[1383], located in a loop in between β-strands of the $FNIII_9$ module (Fig. 12) (Bowditch *et al.*, 1994; Leahy *et al.*, 1996). In addition, competition studies showed that the DRVPHSRNS human peptide could inhibit adhesion of purified αIIbβ3 and α5β1 integrins to full-length FN, while it did not have any effect on αvβ3 binding to FN (Aota *et al.*, 1994; Bowditch *et al.*, 1994). Aota and colleagues also determined that this sequence had a synergistic effect within the $FNIII_{7-10}$ domains and enhanced integrin adhesion. By site-direct mutagenesis in $FNIII_{7-10}$ fragment of FN, it was demonstrated that the R1379 in the PHSRN sequence was a critical component of the synergy site and that the nearby R1374 was also important for the synergistic binding activity in $FNIII_9$ (Aota et al., 1994; Redick *et al.*, 2000). Single mutation R1374A decreased adhesion slightly by itself and R1371A had minor effects on cell adhesion, while combination of R1374A- R1379A reduced dramatically cell adhesion to $FNIII_{7-10}$ fragment (Redick *et al.*, 2000). Mutation in these two arginines also affected platelet adhesion to $FNIII_{8-10}$ fragments. However, in this case, single mutation R1379A and double mutation R1371A-R1374A already reduced cell adhesion by 80% (Chada *et al.*, 2006).

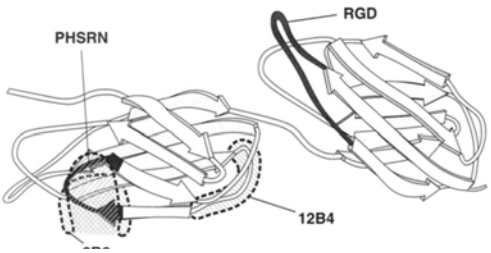

Figure 12. Model of the three-dimensional structure of the $FNIII_{9-10}$. The synergy and RGD loops are indicated in black. From Aota *et al.*

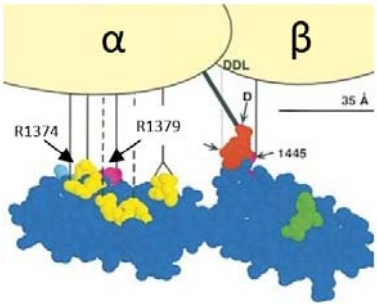

Figure 13. Model for the $FNIII_{9-10}$ interaction with α5β1 integrin, where α-subunit interacts with the synergy site and the D residue from the RGD. From Redick *et al.* 2000.

Crystallization of the $FNIII_{7-10}$ revealed that the interface between the $FNIII_9$ and $FNIII_{10}$ modules had distinctive properties than the rest of the interfaces between adjacent modules. The intermodular $FNIII_{9-10}$ region presents small rotation and tilt angles, making the $FNIII_{7-10}$ almost cylindrical and shortening the distance between the 9th and 10th modules. The small rotation places the RGD and the synergy site on the same face of the FN molecule. These properties also suggest that this junction is more flexible than others within $FNIII_{7-10}$, facilitating the interaction with integrins (Leahy *et al.*, 1996). The $FNIII_{7-10}$ structure also revealed that the synergy site is located 36 Å away from the RGD suggesting that integrins could interact with both motifs at the same time: the head domain of the α-subunit with the synergy site and the junction of α-β subunits with the RGD site (Fig. 13) (Bowditch *et al.*, 1994; Leahy *et al.*, 1996; Redick *et al.*, 2000), supporting the idea that the synergy site cooperates with the RGD site to mediate integrin α5β1 and αIIbβ3 interaction. Actually, structural studies have demonstrated that the α5 subunit stablishes an additional and specific interaction with FN, involving the residue R1379 within the synergy site and the D154 of the α5 subunit (Nagae *et al.*, 2012). Several protein and cell-based studies have been performed in order to elucidate the specific role and mechanism of the FN synergy site, which raised different hypothesis:

1. Structural and cellular analysis using FN peptides determined that the synergy site would modulate the initial FN-integrins interaction. It was shown that the synergy site was

only necessary for activating the integrin high-affinity state to promote interaction with the RGD site, and it was no longer required when integrins were previously activated with stimulatory antibodies like TS2/16 (Danen *et al.*, 1995). In the same lane, Sechler and colleagues described that activation of integrins by external factors (e.i. Mn^{+2}) supplied the need of the synergy site for initial FN matrix assembly (Sechler *et al.*, 1998). Structural studies pointed that the synergy motif might orient the RGD motif to maximize its exposure and facilitate the integrin binding (Altroff *et al.*, 2003; Takagi *et al.*, 2003). According to these studies, the synergy site was increasing the on-rate constant (K_{on}) of integrin binding to FN, and once integrins were bound to the RGD motif, interaction with the synergy site is no longer necessary (Takagi *et al.*, 2003).

2. The use of FRET sensors and theoretical approaches lead to the observation that conformational changes in FN could affect the accessibility of the FN synergy site, regulating the binding of FN to different integrin heterodimers (Grant *et al.*, 1997; Krammer *et al.*, 1999; Craig *et al.*, 2001; Krammer *et al.*, 2002; Mao and Jean E Schwarzbauer, 2006). This proposed hypothesis is based on the fact that αv-class of integrins only bind the RGD site while α5β1 binds both, the synergy and RGD sites. Simulations using steered molecular dynamics evidenced that mechanical stretching modifies $FNIII_{9\text{-}10}$ conformation, leading to changes in the distance between the synergy and the RGD sites (Craig *et al.*, 2001). Under low tension, FNIII is in a pre-stretched state and the distance between the RGD and the synergy site is 35 Å, allowing integrin interaction with both binding sites. High tension causes distortion in the RGD loop, disrupting any interaction with integrins through this motif (Grant *et al.*, 1997; Craig *et al.*, 2001; Krammer *et al.*, 2002). In addition, Craig and colleagues identified a third state: the decoupled state. This state is caused by moderate tension which will stretch the FN, increasing the distance synergy-RGD site by 20 Å (to 55 Å) as well as the rotational angle between $FNIII_9$ and $FNIII_{10}$. These changes provoke that the RGD and the synergy sites are not in the same face of the molecule and therefore, impedes a coordinate interaction of integrin with these two motifs. Since in this stretch state the RGD loop is unaltered, all integrins which do not interact with the synergy site could bind in a normal fashion to FN (Craig *et al.*, 2001; Krammer *et al.*, 2002). This hypothesis was supported by studies where it was observed that cells used preferentially αvβ3 integrin to bind and migrate on FN if the synergy site was mutated (Mao and Schwarzbauer, 2006).

3. Studies using a spinning-disk device to measure the strength of the integrin α5β1-FN bonds concluded that the interaction of integrins with the synergy site is necessary to tension these bonds increasing their life time upon mechanical forces (Friedland *et al.*, 2009). David Boettiger designed a spinning-disk device which subjects adherent cells to an external shear stress. These experiments allow evaluation of the integrin activation levels related to the strength of the bond. Boettiger group demonstrated that after the mechanical stress caused by the shear forces in the spinning-disk, α5β1 integrins presented a tensioned or activated status as different antibodies could bind regions that were cryptic in the partially activated integrin (García et al., 1998). It was proposed that integrins have two active binding states, correlated to the adhesion strength (García *et al.* , 1998; García *et al.*, 2002) and either extracellular or cytoskeletal forces could trigger integrin switch between relaxed and tensioned states (Friedland *et al.* , 2009). In addition, strengthening

the integrin-FN bonds generates different downstream signals that are dependent on integrin engagement and reinforcement of the bond, including FAK phosphorylation in the tyrosine 397 (Shi *et al.*, 2003; Friedland *et al.*, 2009; Seong *et al.*, 2013). It was suggested that the different integrin activation states are dependent on the different interaction with the RGD and synergy domains: the first integrin activation or relaxed state is from non-binding to a FN binding state and depends on integrin-RGD interaction; the second state is a higher binding or tensioned state and it depends on additional synergy region engagement. It was shown that while cells need to interact with the RGD site for binding the FN, this interaction serves only to activate and align the α5β1 integrin to FN interface and is non-coupled to force and strengthen of the bond. However, interaction with the synergy site provides the mechanical strength to the bond and induces the tensioned state of the integrin (García *et al.*, 2002; Friedland *et al.*, 2009).

5. FNIII$_{7\text{-}10}$ interaction with integrins

Integrin-RGD interactions are crucial for several cellular functions including focal adhesion formation and cytoskeleton arrangement, activation of several signalling pathways, cell migration and the assembly of FN in a fibrillar matrix (Pankov, 2002; Leiss *et al.*, 2008; Geiger and Yamada, 2011; Schwarzbauer and DeSimone, 2011).

5.1. Fibronectin fibrillogenesis

The assembly of FN in a fibrillar matrix is a complex process which involves secretion of newly synthetized FN, interaction with cell receptors, extension or unfolding of FN and interaction with other FN molecules (Fig. 14) (Singh *et al.*, 2010; Schwarzbauer and DeSimone, 2011). The FN fibrils composing the matrix are elastic as shown by FRET experiments (Baneyx *et al.*, 2001, 2002; Smith *et al.*, 2007). FN flexibility is in part due to the lack of intradomain disulphide bonds in the type III repeats and the presence of several hinge points along the molecule which allow rotation of individual repeats (Leahy *et al.*, 1996). Fibrils of FN form branched network surrounding the cells and connecting them. FN matrix is dynamic and constantly remodelled, serving as a reservoir for growth factors and fluid as well as niche for cells (Mao and Schwarzbauer, 2006; Singh *et al.*, 2010; Schwarzbauer and DeSimone, 2011). The assembly of FN matrix has been deeply studied, and can be monitored over time by cell immunostaining or by following FN conversion into a detergent deoxycholate (DOC) insoluble form (Wierzbicka-Patynowski, 2003; Mao and Schwarzbauer, 2005).

-FN binding to integrins and stretching

FN is secreted as a soluble dimer with a compact conformation mediated by intramolecular interactions (Mao and Schwarzbauer, 2005). Soluble and globular FN dimers are mechanically stretched during FN fibrillogenesis (Erickson, 2017) generating extended thin fibrils of about 3-5 nm of diameter, as observed in cell culture and EM images. An indication that FN gets extended during fibrillogenesis is that the diameter of thin FN fibrils has approximately the width of single type III repeats. Although molecular details of FN

fibrillogenesis are not fully understood (Singh *et al.*, 2010; Schwarzbauer and DeSimone, 2011), there is an accepted model of the process based on integrin-induced conversion of soluble FN to extended fibrils. Cytoskeletal forces generated by actin-myosin contraction and transmitted through integrins stretch and unfold the FN (Baneyx *et al.*, 2002; Lemmon *et al.*, 2009). Integrin cytoplasmic domains are associated with the actin cytoskeleton, acting as the link between the ECM and the intracellular space, and transducing the cytoskeletal forces to the FN and stretching it (Mao and Schwarzbauer, 2005; Singh *et al.,* 2010). Furthermore, the distribution of the traction forces generated by engaged integrins and cytoskeleton are also important for guiding the new forming FN fibrils. According to measurements of cell traction force, fibrillogenesis is directed by the spatial rearrangement of traction forces from the cell periphery toward the cell centre which may trigger the clustering of FN in these regions (Lemmon *et al.* , 2009).

It is well accepted that the first interaction between soluble FN and the cell occurs right after FN secretion and is mediated by binding of integrin α5β1 to the RGD site (Huveneers *et al.*, 2008). However, it has been seen that FN fibrillogenesis can be initiated by αvβ3 integrins in absence of α5β1 (Yang and Hynes, 1996) and that FN lacking a functional RGD site can be also assembled (Sechler *et al.*, 2000; Takahashi *et al.*, 2007). This RGD independent assembly can be initiated by binding of active α4β1 integrin to the alternative (V) spliced region (Sechler *et al.*, 2000). In addition, RGD mutation to RGE does not abolish FN fibrillogenesis by αvβ3 integrins in cell culture, nor in the mouse embryo (Takahashi *et al.*, 2007). It has been also proposed that the receptors syndecans, which are also linked to the cytoskeleton, are involved in FN matrix assembly, either independently or in cooperation with integrins (Xian *et al.*, 2010; Klass *et al.*, 2000; Stepp *et al.*, 2010). RhoA as well as myosin light chain kinase are essential for FN fibrillogenesis, and inhibiting their activity blocks FN matrix formation (Mao and Schwarzbauer, 2005), integrins and syndecans bound to FN stimulate Rho GTPase activity which in turn induces cytoskeleton contraction, facilitating FN matrix assembly (Huveneers *et al.*, 2008; Singh *et al.*, 2010).

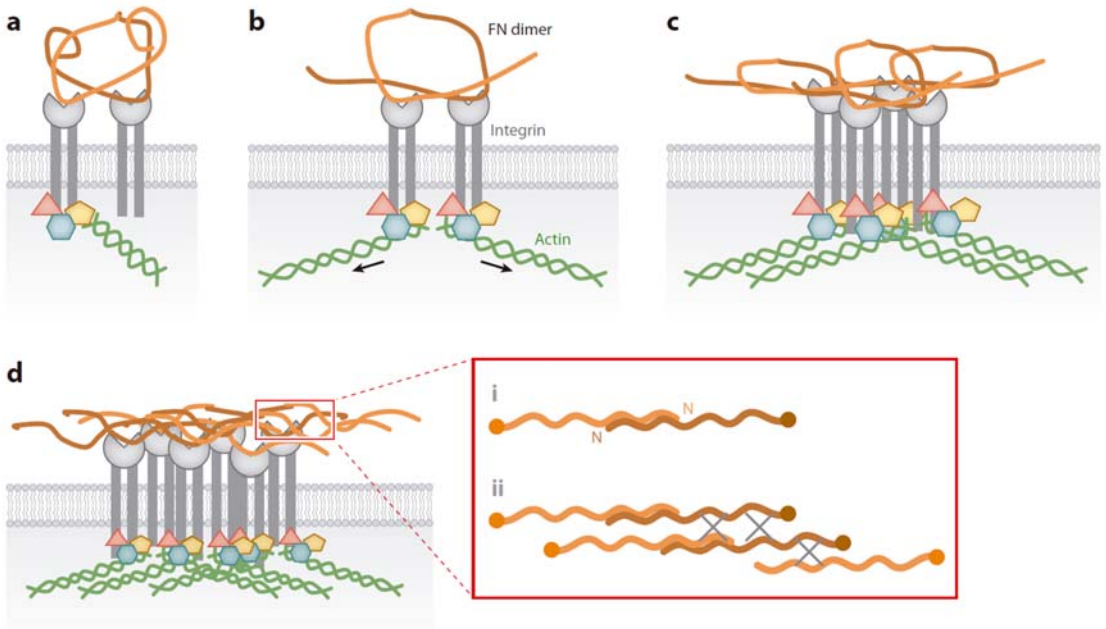

Figure 14. Major steps in FN matrix assembly, based in integrin induced-conversion of globular FN into extended fibrils. (a) FN is secreted as a globular and compact dimer (orange) which integrins (grey) can bind through the exposed RGD motif. (b) Upon FN-integrin binding, cytosolic adaptor proteins (pink, yellow and blue) are recruited to the integrin cytoplasmic tails and connect them to the actin cytoskeleton (green). Cytoskeletal contraction generates force that is transmitted across the integrins to the FN, inducing FN unfolding and making accessible the FN binding sites. (c) Integrin clustering brings together more unfolded FN molecules, promoting FN-FN interaction. (d) These events trigger formation of stable insoluble fibrillar matrix. The inset shows interactions between single subunits of FN dimers. (i) N indicates the N-terminus where the interaction between single FN fibrils forms. (ii) Later association between fibrils can take place by other FN-binding sites ($FNIII_{1-2}$ or $FNIII_{4-5}$). From Singh *et al*. 2010.

- **FN-FN interaction and matrix maturation**

In compact conformation, each FN monomer presents crossed-over arms in a pretzel-like shape, maintained by electrostatic interaction between $FNIII_{2-3}$ and $FNIII_{12-14}$ domains. In the FN compact conformation the FN binding sites for intermolecular interaction are cryptic, preventing spontaneous fibril formation in solution (Mao and Schwarzbauer, 2005; Lemmon *et al.*, 2011). This property is highly important to impede uncontrolled FN fibrillogenesis in body fluids including blood where it would have life threatening effects (Mao and Schwarzbauer, 2005; Singh *et al.*, 2010). Upon the FN binding to engaged integrins, FN is stretched, making available the FN-FN interactions sites, and therefore FN can stablish intermolecular interactions generating a complex fibrillar meshwork. Furthermore, integrin clustering upon FN binding brings the receptors and the bound FN close together, promoting FN-FN interactions (Mao and Schwarzbauer, 2005) and FN fibrils clustering together in bundels (Singh *et al.*, 2010).

FN-FN intermolecular interactions take place through the FNI_{1-5} (the 70-kDa fragment) $FNIII_{1-2}$, $FNIII_{4-5}$, $FNIII_{7}$ and $FNIII_{12-14}$ (Singh *et al.*, 2010). Several deletion and mutagenesis studies have shown that the 70-kDa fragment is essential to initiate FN fibrillogenesis as it binds to the other FN-FN binding sites (Sottile and Hocking, 2002). The major binding sites for 70-kDa fragment during fibrillogenesis are within the first two type III repeats, as mutational and competitive analysis with antibodies or FN fragments showed to block fibrillogenesis (Singh *et al.*, 2010). The $FNIII_{1-2}$ repeats have a longer linker in comparison to the other FNIII repeats. This feature confers it an unique structure which might facilitate the rotation and folding to promote FN intermolecular interactions (Leahy *et al.*, 1996; Mao and Schwarzbauer, 2005). The 70-kDa fragment binds also to the HepII ($FNIII_{12-14}$) site and the $FNIII_{4-5}$ repeats. However, these interactions are not involved in fibrillogenesis. Four hypotheses have been proposed to explain these additional interactions. One hypothesis is that multiple sites might need to interact between FN molecules to reduce the rate of dissociation of interacting FN dimers during fibrillogenesis. A second possibility is that additional intermolecular interactions along the FN molecule might enhance FN fibrils strength and stability, reducing fibril breakage. The third hypothesis proposes that different binding sites along FN subunits might act as zipper teeth, helping to keep aligned the FN dimers to facilitate the initial intermolecular interactions. The last hypothesis suggests that extra FN binding sites will promote fibril branching and therefore, contribute to the maturation of the FN matrix in a meshwork surrounding the cells (Singh *et al.*, 2010; Schwarzbauer and DeSimone, 2011).

The mature FN matrix contains fibrils which have grown in length and thickness and it becomes DOC insoluble. Although it was thought that the insolubility of the matrix was caused by the multiple intrachain disulphide bonds that FN dimer contains, now it is known that it is the result of the non-covalent intermolecular bonds stablished between the FN molecules (Singh *et al.*, 2010).

5.2. Integrin-FN adhesion complexes and signalling

The sites of integrin-FN adhesion connect the ECM to the cytoskeleton, maintaining cohesion and mediating mechanical and chemical signalling from the extracellular space to the cytoplasm (Schiller and Fässler, 2013). Active integrins aggregate and the bound proteins at their CTs are recruited at signalling-competent clusters, forming together with the FN-bound integrin adhesion complexes. Although it is not really clear how integrins cluster, clustering is observed with all integrin receptors and it stabilises the integrin-ligand adhesion as well as it increases the probability for dissociated integrin to rebind (Schiller and Fässler, 2013; Sun *et al.*, 2014). Integrin bound to physiological ligands such FN generates inside-out signalling by inducing additional structural rearrangements that promote interaction with other cytoplasmic proteins at their CTs, forming the so-called adhesome (Van Agthoven *et al.*, 2014). The adhesome is rather dynamic and involves assembly and disassembly of protein interactions which trigger cell spreading and migration (Schiller and Fässler, 2013; Sun *et al.*, 2014). The adhesome components were determined as a theoretical network of more than 200 proteins, based on in silico studies. This determined adhesome contains all the proteins that have been reported to locate to, or regulate, the adhesion complexes (Horton *et al.*, 2016). The vast amount of proteins contained in the adhesome, together with their recruitment dynamics and stoichiometry, makes it complicated to study and understand (Horton *et al.*, 2016; Schiller and Fässler, 2013). However, a consensus adhesome stablished paxillin, focal adhesion kinase (FAK), talin, vinculin and α-actinin as the essential proteins to regulate the adhesion complex function. These components are mostly adaptor proteins and actin regulators, which provide structural connection between integrins and actin, and mediate signalling (Horton *et al.*, 2016). The adaptor proteins connect directly or indirectly with the integrin tails, forming scaffolds within adhesions and eventually linking the integrin tails to the actin cytoskeleton (Geiger and Yamada, 2011). Signalling molecules at adhesion complexes include serine/threonine kinases and phosphatases, Rho-family GTPases and their regulators (GAPs and GEFs). They are recruited to the adhesion complexes via multiple docking sites in the scaffolding network of proteins (Geiger and Yamada, 2011). Super-resolution microscopy has revealed the organization of the proteins at the adhesion core in MEFs when adhered to FN. According to this study, upon binding to FN, the integrin adhesion complex shows an stratified architecture: a membrane-connected layer containing integrin CTs, FAK and paxillin, and intermediate force-transduction layer containing talin and vinculin, and an upper actin regulatory layer containing zyxin, VASP and α-actinin which links the adhesome to actin (Fig. 15) (Kanchanawong *et al.*, 2010).

The initial FN-integrin adhesion complexes form nascent adhesions (NAs) in cell protrusion that are unstable structures that can progress and mature into focal adhesions (FAs). NA are small FN-integrin adhesion with a high turnover and its formation is dependent on actin polymerization which causes cell protrusion. FA are larger and enduring FN-integrin clusters stabilized by the connection to the cytoskeleton (Arnaout *et al.*, 2007; Geiger and Yamada, 2011; Heisenberg and Fässler, 2012; Schiller and Fässler, 2013). The maturation from NA to FA relies on the stiffness of the ECM, the activity of myosin II-mediated cell contractility and the activity of formins on actin cytoskeleton (mDia). The recruitment of effectors like Rho-family of GTPases to the adhesome stimulate myosin II contractility as well as mDia-mediated actin stress fibres elongation. Balance between these two signalling pathways is fundamental for cells to adapt to the ECM stiffness and thus maturate and reinforce the FA or disassemble them (Schiller and Fässler, 2013). The distinct integrins, α5β1 and αv-containing integrins, play an important role in mediating cell adaptation to ECM stiffness (Schiller *et al.*, 2013). The α5β1 and αv-containing integrins, despite having some overlapping activities in FN assembly (Yang and Hynes, 1996), they also present specific functions as they distribute in FA and signal differently upon FN binding (Zaidel-Bar, 2013). At the molecular level, while α5β1 are responsible for stimulating myosin II contractility, αv-containing integrins signal to promote actin bundles formation through mDia (Schiller *et al.*, 2013). According to this, α5β1 is more mobile (Rossier *et al.*, 2012) and is responsible to generate force driven by the actin-myosin cytoskeleton within FN adhesions (Schiller *et al.*, 2013), whereas αvβ3-integrin is immobilized in large FA (Rossier *et al.*, 2012) and is important for cell stiffening on force application, providing structural support to cell adhesion (Schiller *et al.*, 2013). Therefore, it is important that these two integrin types cooperate to adapt the cell to the rigidity of the FN rich ECM (Schiller and Fässler, 2013; Zaidel-Bar, 2013).

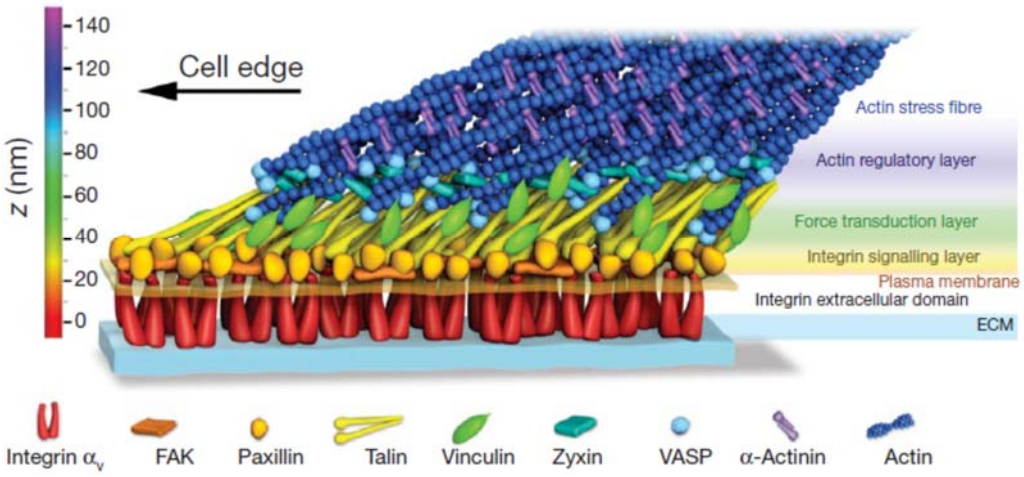

Figure 15. Model of FA molecular architecture showing the different layers where proteins distribute. Integrins are link to the ECM by the ectodomain, and adaptor proteins (integrin signalling and force transduction layer) are bound to their cytoplasmic tails linking them to the cytoskeleton. From Kanchanawong *et al.* 2010.

5.3. α5β1 interaction with the FN synergy and RGD sites

The integrin α5β1 presents some particularities in its interaction with FN, in comparison with other FN-RGD receptors. For example, it is the only one found in the fibrillar adhesions

which are formed in an additional step of integrin adhesion maturation. The name of this type of FN adhesion derives from fibrillogenesis, as they are associated with FN fibrils formation. Fibrillar adhesions are elongated and thin ECM contacts located at the centre of the cells and they are characterized by the presence of α5β1, tensin as adaptor protein and FN. α5β1-FN FA can translocate centripetally from the cell periphery to form the fibrillar adhesions, providing potentially forces to support formation of FN fibrils (Mao and Schwarzbauer, 2005). Moreover, the integrin α5β1 also interacts with the synergy site. Interactions outside the RGD site have been proposed to confer specificity to the integrin-FN adhesion since many of these receptors bind to the FN (Takagi, 2004). Therefore, the interaction between the integrin α-subunit and the synergy site might provide additional support or function to the classical integrin-RGD site bond (Bowditch *et al.*, 1994; Aota *et al.*, 1994; Danen *et al.*, 2002).

FN-α5β1 interaction presents a catch bond behaviour. This is also in line with findings that α5β1 integrin provides the force in FN adhesions (Schiller *et al.*, 2013) and that the FN-α5β1 bond can be tensioned through engagement with the synergy site (Friedland *et al*., 2009) (see section 4.2.). Catch bonds act as molecular hooks, holding firmly ligand and receptor when stretched by tensile forces. Thus, their lifetime increases when tensile force applied to the bond. *In vivo*, these tensile forces can be generated by the dragging motion imposed by fluids or by molecular motors (like actin-myosin), pulling on other proteins (Hertig and Vogel, 2012). Atomic force microscopy (AFM) experiments using purified α5β1 integrin ectodomain and FN fragments ($FNIII_{7\text{-}10}$) demonstrated that FN-α5β1 displays a triphasic force-dependent bond lifetimes (Kong *et al.*, 2009). Kong and colleagues observed that with forces ranging from 10–30 pN, FN-α5β1 formed catch bonds, as their life time was longer than with forces below or above this time (Fig. 16).

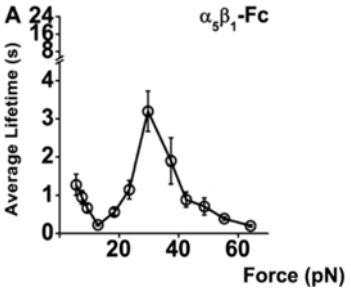

Figure 16. Plots of the α5β1 integrin-$FNIII_{7\text{-}10}$ bond lifetime versus force, measured by AFM. Note that the lifetime reaches it maximum around 30 pN, forming a catchbond, while below and above these range of forces it decreases. From Kong *et al.* 2009.

6. Fibronectin in plasma: its role in haemostasis

FN is a supportive factor in haemostasis. The role of FN in haemostasis is directly linked to its interaction with platelets, integrins and fibrin during thrombosis. Upon vascular injury, platelets form a plug to avoid haemorrhages and severe loss of blood. This plug consists of an aggregate of platelet sustained by a fibronectin-fibrin matrix (Furie and Furie, 2005; Cho and Mosher, 2006; Wang *et al.*, 2014). The FN contained in these plugs is pFN, and as *in vitro* experiments showed, platelets can assemble the pFN in a fibrillar matrix (Olorundare *et al.*, 2001; Cho and Mosher, 2006).

pFN was first found as a contaminant of purified Fg, which precipitated at temperatures below 4°C, and therefore it was called “cold-insoluble globulin” (Mosesson and Umfleet, 1970). pFN is exclusively synthetized by hepatocytes in the liver and circulates in the blood stream in its compact conformation. As explained before, pFN does not contain the FNIIIA and B extra

domains which are generated by alternative splicing, and one monomer lacks residues in the variable (IIICS) region, resulting in a natural mix of dimers (Singh *et al.,* 2010; Maurer *et al.,* 2015). The concentration of FN in plasma is between 200-600 µg/ml in humans and 100-400 µg/ml in mice. It has been postulated that due to the high concentrations in plasma, it is important that FN stays in its folded conformation to avoid fibril formation and consequent clotting. Plasma FN can be also isolated and purified from blood samples as it remains soluble in physiological saline concentrations (Maurer *et al.*, 2015).

Tissues take pFN up where it is incorporated in the fibrillar ECM along the synthesized cFN, as shown when cFN was deleted in mice and tissues contained pFN instead (Moretti *et al.*, 2007). However, mice expressing constitutively IIIA-FN (also referred as cFN) showed a decrease in the levels of FN in plasma and most tissues. Therefore, pFN can supply for the lack of cFN, but not vice versa. It has also been showed that platelets as well as fibroblasts efficiently assemble pFN in a fibrillar matrix *in vitro,* proving that pFN is as functional as cFN to constitute a matrix (Cho and Mosher, 2006).

6.1. FN receptors in platelets

Regulation of platelet activity and functions is critical for correct haemostasis and thrombosis. Platelets are small anucleate blood cells, derived from megakaryocytes that in physiological conditions remain in a steady state circulating in the blood stream. These resting platelets present a discoidal shape. Upon vessel injury, platelets are activated and become highly adhesive cells. Activated platelets change their shape, attach and accumulate at the damaged vessel and recruit more platelets, initiating blood clotting to avoid haemorrhages (Shattil, 2004; Stegner and Nieswandt, 2011; Vadasz *et al.*, 2015; Xu, Carrim, *et al.*, 2016; Xu, Zhang, *et al.*, 2016). The transition from resting to activated platelets needs to be finely tuned: platelets have to rapidly respond to vessel damage, but also they should not activate spontaneously as this might cause occluding thrombus in healthy vessels (Ma *et al.*, 2007; Stegner and Nieswandt, 2011).

During haemostasis and thrombosis, platelets adhere to the endothelium ECM and build an aggregate that is held by a fibronectin-fibrin matrix. Platelet receptors are indispensable for its adhesion and aggregation. The critical receptors for platelet thrombus formation are: are the glycoprotein VI (GPVI), the GPIb-IX-V complex and integrins. GPIb-IX-V complex is a leucine-rich repeat protein receptor for von Willebrand factor (vWF), which can bind also other molecules such as thrombospondin (platelet activator) and coagulation factors. The GPVI is a receptor for collagen and it also interacts with fibrin. Platelets express in their surface integrins α2β1 and α6β1 which bind to collagen and laminin respectively, and the fibronectin receptors α5β1 and αIIbβ3 (Denis and Wagner, 2007; Xu, Carrim, *et al.*, 2016). The integrin αIIbβ3 is only expressed in platelets and it also binds to Fg and vWF. Despite integrin α5β1 being a major receptor for FN, it has been described to have a rather secondary role in platelet adhesion (Grüner *et al.*, 2003; Xu, Carrim, *et al.*, 2016) while αIIbβ3 is thought to be the principal FN receptor in platelets. Moreover, proteomics data showed that murine platelets express about 131000 copies of αIIbβ3 and 1900 of α5β1 (Zeiler *et al.*, 2014). Deletion of the αIIbβ3 gene or mutations which abolish its function or activation, cause the haemorrhagic syndrome

Glanzmann thrombasthenia in both humans and mice (Hodivala-Dilke *et al.*, 1999; Tronik-Le Roux *et al.*, 2000; Moser *et al.*, 2008). Therefore, adhesion and aggregation of platelets depend, to a certain extent, on the correct activation and function of this integrin (Ma *et al.*, 2007).

6.2. First wave of haemostasis: the process of platelet thrombus formation

Thrombus formation involves different processes that have been divided in "first and second waves of haemostasis". The first wave of haemostasis comprises platelet tethering, firm adhesion, activation and aggregation. The second wave is mediated by the coagulation system. Exposure of tissue factor at the injured vessel wall activates the coagulation cascade, which enforces the first wave of haemostasis and assists the formation of a haemostatic fibrin clot (Stegner and Nieswandt, 2011; Vadasz *et al.*, 2015; Xu *et al.*, 2016). The process of platelet thrombus formation (first wave of haemostasis) is highly dynamic (Fig. 17), and as it is described below, comprises several distinct receptors and signalling cascades which cannot be totally isolated, and therefore, the division between the different single steps is not yet clear.

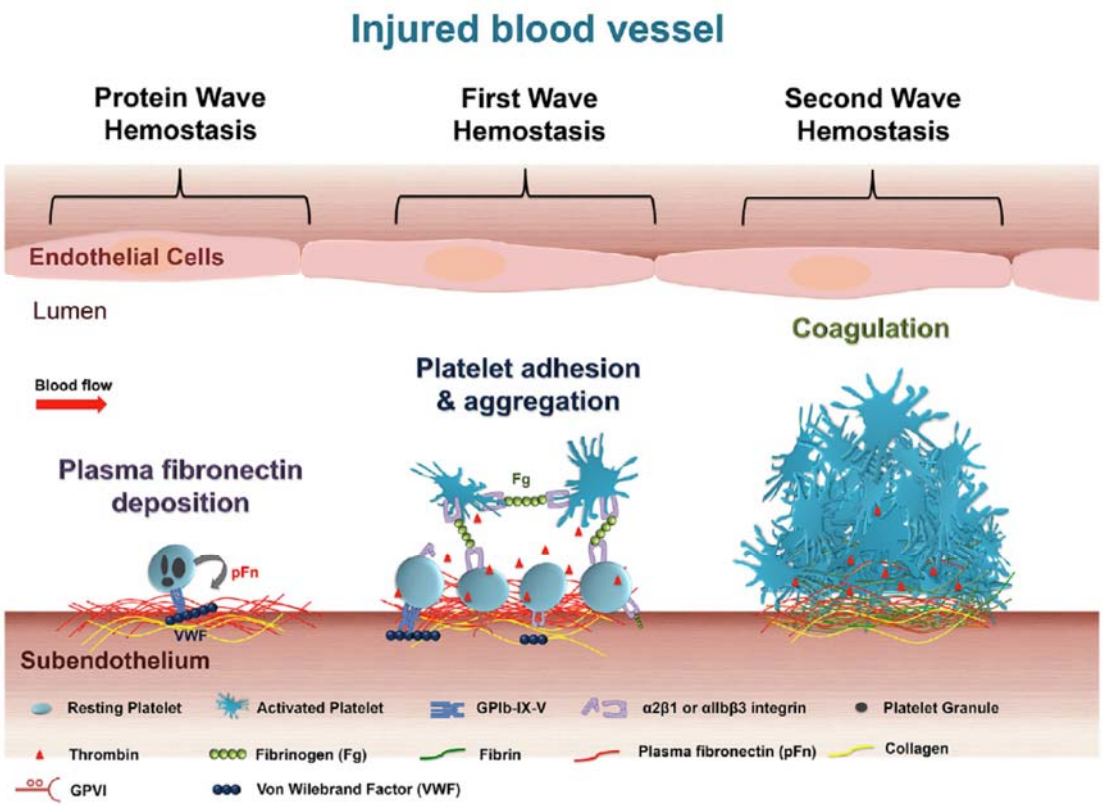

Figure 17. Platelet function in thrombosis. After vascular injury, plasma fibronectin quickly deposits onto the injured vessel wall. Platelets may also release their internalized plasma fibronectin from their granules. These plasma and platelet sources of fibronectin likely synergistically contribute to the protein wave of hemostasis. Platelet adhesion and aggregation are then initiated via platelet GP receptors and their ligands (collagen and vWF). Activated platelets also provide a negatively charge surface and mediate cell-based thrombin generation, which contributes to blood coagulation that is initiated following tissue damage (the second wave of hemostasis). In a growing hemostatic plug/thrombus, the fibrin and fibronectin matrix is usually formed in the interface between the injured vessel wall and platelet plug. From Vadasz *et al.* 2015.

Vessel injury exposes the endothelium ECM, making proteins such as collagens accessible to GPVI receptors in platelet which then, establish the first contacts with the endothelium. Circulating plasmatic vWF also binds to the exposed ECM, interacting directly with collagen fibrils in injured vessels, and with GPIb-IX-V receptors in platelets (Clemetson, 1999; Furie, 2005; Jackson, 2007; Varga-Szabo *et al.*, 2008). Platelet tethering to collagen and vWF constitutes the first wave of haemostasis and is important to retain the platelets (Jackson, 2007). The continuous shear forces generated by the blood flow drag platelets along and oppose its adhesion and aggregation. The magnitude of these forces are dependent on the diameter of the vessel in an inversely proportional relation (Varga-Szabo *et al.*, 2008). This force range from <500 s^{-1} in veins and venules, to 5000-40000 s^{-1} in arteries and arterioles (Stegner and Nieswandt, 2011). While initial interaction between collagen and GPVI can take place under low shear flow (forces below 1000 s^{-1}), vWF interaction with the GPIb subunit of the GPIb-IX-V complex can withstand high shear forces (Denis and Wagner, 2007; Andrews and Berndt, 2008).The GPIb-vWF interaction is characterized by fast association and dissociation rates, facilitating the initial platelet attachment to the endothelium (Denis and Wagner, 2007; Varga-Szabo *et al.* , 2008). Due to the short life-time of the GPIb-vWF bond, it supports platelet translocation to the vessel wall, but it does not mediate stable adhesion (Xu *et al.*, 2016). After platelet tethering and retention at the vessel wall, interaction with collagen activate them (Denis and Wagner, 2007). GPVI-collagen interaction triggers cell signalling to activate integrins and induces the release of the secondary mediators adenosine diphosphate (ADP) from the platelet granules to amplify platelet activation (Kato *et al.*, 2003; Stegner and Nieswandt, 2011).

The GPVI associates with the Fc γ chain receptor (FcγR) at the platelet membrane and after GPVI-collagen binding, FcRγ activates Src family kinases. Activation of Src kinases pathway leads to downstream events that elevate intracellular Ca^{+2} levels. Elevated intracellular Ca^{+2} levels triggers protein kinase C signalling and activation of Rap1b, which in turn can recruit the adaptor molecules riam, talin and kindlin3 to the plasma membrane to activate αIIbβ3 integrin (Denis and Wagner, 2007; Stegner and Nieswandt, 2011). Among them, talin is the most extensively studied. While in resting platelets talin is uniformly located, during platelet activation, it is recruited to the plasma membrane where it binds the integrin β3 cytoplasmic tail (Ma *et al.*, 2007). The binding site of talin in the β3 cytoplasmic TM overlaps with the interaction site for αIIb TM. Thus, talin binding to the β3 cytoplasmic tail destabilizes the β3 interaction with αIIb, dissociating the two integrin transmembrane domains and shifting the integrin to an extended conformation (Bennett, 2005; Mehrbod *et al.*, 2013; Coller, 2015) Thus, integrins αIIbβ3 and α5β1 are activated by “inside-out signalling” which is highly regulated to avoid spontaneous platelet aggregation, and can be mimicked by platelet activation agonists such as ADP or thrombin (Ma *et al.*, 2007). Activation of integrins leads to adhesion to Fg, vWF and FN, enabling platelet aggregation. Upon integrin-ligand interaction, the outside-in signaling also drives increments of intracellular Ca^{+2}, amplifying the activation process (Xu *et al.*, 2016). During platelet activation, the increase in intracellular Ca^{+2} also promotes the release of granules content, contributing also to platelet activation. Platelet granules contain a diverse assortment of molecules that are all involved in haemostasis:

transmembrane receptors (αIIbβ3 integrin), adhesive molecules (Fg, FN, vWF), coagulants (factors V, IX) or thrombin (Denis and Wagner, 2007; Xu *et al.*, 2016). Thrombin is a potent platelet activator that interacts with members of the protease-activated receptor (PAR-3 and PAR-4 in mice) at the platelet surface. The active form of thrombin is generated by the coagulation cascade. In addition to activate platelets, thrombin, as a serine protease, catalises the cleavage of Fg to fibrin (Stegner and Nieswandt, 2011). Fibrin generation is essential for the stabilization of the platelet thrombus. The persistence of a stable clot that resist the blood flow urges the adhesion and aggregation of more platelets and a close contact between them. This is achived by the generation of a fibrin network which allows the adhesion of more platelets and supports the growing thrombus (Denis and Wagner, 2007; Xu *et al.*, 2016). It is classically accepted that the conversion of Fg to fibrin during platelet aggregation is a sequencial process, which begins with the initial interaction αIIbβ3-Fg and is followed by its cleaveage to fibrin by thrombin and its polymerization, leading to platelet agreggation. However, recent studies showed that the probability of αIIbβ3-fibrin bond is higher and more stable than the αIIbβ3-Fg bond, suggesting that platelet adhesion to Fg and conversion to fibrin might be simultaneous. This is also supported by indications that αIIbβ3 binding sites on fibrin may be substantially different from Fg (Litvinov *et al.*, 2016).

6.3. FN role in haemostasis and platelet function

FN is packaged in platelet granules at a concentration of 1 μg per 3 x 10^8 platelets, and it is released upon platelet activation (Maurer *et al.* , 2010). Activated platelets assemble pFN by α5β1 and αIIbβ3 integrins, as blocking antibodies for these receptors blocked pFN assembly in platelets (Olorundare *et al.*, 2001). pFN is also a substrate for the coagulation factor FXIIIa and it becomes crosslinked and incorporated into fibrin clots (Mosher, 1975; Corbett *et al.*, 1997), by interaction of the N-terminal region of FN with the fibrin C-terminal region. As fibrin polymerizes the coagulation factor FXIII, transglutaminase covalently links glutamine residues of FN to the fibrin chains (Schwarzbauer and DeSimone, 2011).

Despite all the evidences for pFN function in haemostasis, specific deletion of pFN in mice did not cause longer haemorrhages or affected skin-wound healing, but it increased the infarction areas after cerebral ischemia (Sakai, 2001). However, further analysis of platelet aggregation concluded that, in fact, pFN contributes to the growth and stability of the thrombus. The pFN-deficient mice had about 98% of FN reduction in plasma and 88% in platelets. These mice displayed a delay in thrombus formation in a model of arterial injury. In mice lacking pFN, platelets adhered to the vessel wall. However, the thrombi grew slower, because platelets were continuously shedding from it, indicating that plasma FN is important for platelet clot cohesion (Ni *et al.*, 2003). Similar defects were found in $FN^{+/-}$ mouse model, in which pFN levels are half that of $FN^{+/+}$ mice (Matuskova *et al.*, 2006). In addition, this study also confirmed that the thrombotic effects of FN were due to pFN and not cFN, as deletion of FNIIIA or FNIIIB domains did not have any effect in platelet adhesion and aggregation (Matuskova *et al.*, 2006). Knocking-out Fg and vWF *in vivo* showed that these plasmatic proteins were also dispensable for haemostasis. Mice lacking Fg or vWF or lacking the two proteins formed thrombi after vessel injury, however, the platelets of these mice contained

higher levels of FN in their granules, suggesting that pFN was mediating the Fg/vWF independent platelet aggregation (Ni *et al.*, 2000). Contrary, later studies demonstrated that depletion of pFN in mice lacking both Fg and vW actually improved platelet aggregation and thrombus growth, and presence of soluble pFN inhibited platelet aggregation (Reheman *et al.*, 2009). To explain the inconsistency among distinct studies, Reheman and colleagues proposed that while soluble pFN has inhibitory effects in platelet aggregation, fibrilar pFN (bound to fibrin or fibrillary assembled) promotes platelet aggregation. Moreover in *in vitro* analysis it was found that insoluble pFN, either crosslinked with fibrin or assembled by platelets, enhances platelet thrombus formation (Cho *et al.*, 2006), and that fibrin is important for FN retention on platelet surface (Zhai *et al.*, 2007), supporting the hypothesis of a double function for pFN. Recently, a study using intravital microscopy technique confirmed that fibrin dictate the pro- and anti-thrombotic properties of pFN. This study determined that pFN acts as a regulator of platelet aggregation, and its role depends on its interactions with integrin αIIbβ3 and fibrin and its location within the thrombus. Thus, in the centre of the thrombi, containing fibrin, FN promotes platelet aggregation, whereas at the margins, with minimal fibrin, FN inhibits thrombus growth, preventing vessel occlusion (Wang *et al.*, 2014).

Wang and colleagues also observed that pFN, but not Fg or fibrin, is deposited in the vessel wound immediately after injury, before platelets adhere and independently of Fg or vWF deposition (Wang *et al.*, 2014). Since this early pFN deposition might precede the classical "first-wave" of haemostasis, the term of "protein-wave" was coined to name this step of the thrombus formation (Fig. 17). FN can bind to collagen, this interaction can be also covalently linked by factor XIIIa and this might favour a rapid incorporation of the pFN in the subendothelium (Wang and Ni, 2016). Blocking the collagen binding sites in FN impedes an initial enhancement of thrombus growth, supporting the idea that pFN is implicated in the beginning of thrombus formation (Cho and Mosher, 2006).

Altogether, it has been speculated that the deposited FN could be integrated into the sub-endothelial matrix and block the leak of blood and plasma (Wang and Ni, 2016). Arrival and attachment of platelets to the vessel wall might enrich the content of pFN. Adherent or activated platelets are able to assemble pFN at physiological shear rates (Cho and Mosher, 2006) and they can also deliver the pFN contained in their granules.

6.4. Non-haemostatic function of the platelet clot

Platelets are involved in physiological functions like tissue repair or immune response. Platelet aggregation, in addition to prevent blood loss, plays a role during development allowing formation of the lymphatic network (Uhrin *et al.*, 2010). During embryonic development, lymphatic endothelial cells (LECs), emerge from the anterior cardinal vein at E9.5 in mice, the emergent LECs migrate away from the cardinal vein to assemble the first lymphatic vessels, parallel to the blood vessels. This step is triggered by different specific signals including vascular endothelial growth factor-C (VEGF-C) (Planas-Paz and Lammert, 2013). After LEC sprouting from the cardinal vein, around E11.5-12.5, platelets adhere to the endothelial and lymphatic endotelial cells by binding podoplanin (Uhrin *et al.*, 2010). Podoplanin is a transmembrane glycoprotein at the surface of endothelial cells which interacts

with the platelet receptor C-type lectin-like receptor 2 (CLEC-2). Mice lacking podoplanin or CLEC-2 display the lymphatic vessels filled with blood due to impairment of the separation of lymphatic vessels from the blood vessels (Uhrin *et al.*, 2010; Herzog *et al.*, 2013) (Fig. 18 A-C). Moreover, deletion of the CLECL-2 downstream signalling proteins, Syk or SLP-76, in platelets or the endothelial loss of the T-synthase enzyme required for podoplanin synthesis, leads also to a phenocopy of the deletion of podoplanin or CLEC-2 in mice (Fig. 18 A) (Abtahian *et al.*, 2003; Fu *et al.*, 2008; Bertozzi *et al.*, 2010; Welsh *et al.*, 2016). Recently, it was proven that the platelets also keep the lympho-venous hemostasis through the adulthood by podoplanin-CLEC-2 activation and the formation of platelet-fibrin thrombi at the lymphatic duct-jugular vein junction (Fig. 18 B) (Hess *et al.*, 2014).

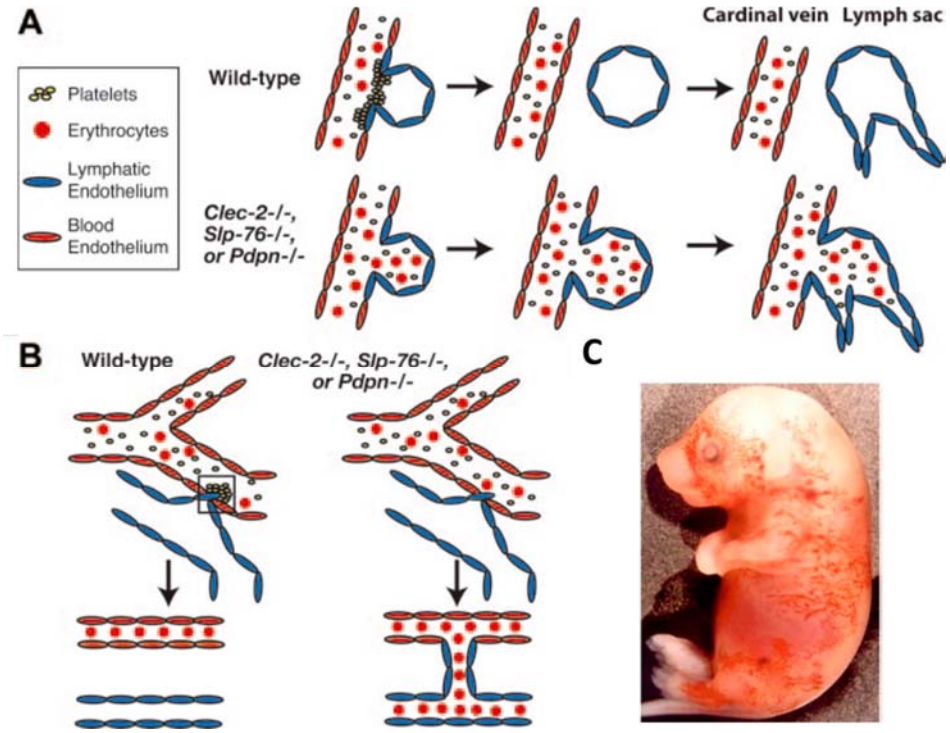

Figure 18. Lymphatic vascular development. (A) Lymphatic vessels rise from the cardinal vein. It begins at the cardinal vein in the embryo when the platelet aggregate triggers the first LECs differentiation to form the lymph sacs. In *Clec-2*$^{-/-}$, *Slp- 76*$^{-/-}$, and *Pdpn*$^{-/-}$ embryos there are primary missconections due to the lack of platelet aggregation on the vessel wall, and as consequence lymph sacs are filled with erythrocytes. (B) After lymphatic differenciation, platelets still maintain the blood and lymphatic vessels separation by forming microthrombi. Mutations like *Clec-2*$^{-/-}$, *Slp- 76*$^{-/-}$, and *Pdpn*$^{-/-}$ lead to vascular misconnections and blood infiltration in the lymphatic vessels. (C) E16.5 embryo suffering from haemorrhages and oedema caused by non-separation of the lymphatic vessels from the blood system. Modified from Bertozzi *et al.* 2010 (A-B) and Uhrin *et al.* 2010 (C).

II OBJECTIVES

II. OBJECTIVES

The aim of this PhD thesis was the functional analysis of the major integrin-binding site in FN, an RGD sequence located in the 10th type III module, from different perspectives. On one hand, to study the role of integrins-RGD interaction in fibrillogenesis. On the other hand, to study for the first time the *in vivo* function of the so-called synergy site in cooperation with the RGD motif. Each of these two major objectives entailed additional purposes.

a) Analysis of the role of integrin adhesion to RGD in FN fibrillogenesis:
   - FN fibril assembly by fibroblasts genetically engineered to express FN lacking the RGD motif (*Fn1*$^{\Delta RGD/\ \Delta RGD}$)
   - Influence of integrin activation by different ligands such as laminin, vitronectin, collagen or gelatine, in FN assembly in fibrils
   - Syndecan contribution to FN fibril assembly when FN lacks the RGD motif

b) Studies the FN synergy site function:
   - Analysis of mice expressing a mutated synergy site (*Fn1*$^{syn/syn}$) to unravel whether the synergy site of FN is important for tissue development and homeostasis
   - To investigate the implications of the FN synergy site in haemostasis after vessel injury and platelet function
   - To study the strength of the α5β1-FN bond and its capability to withstand shear forces as well as to form mature FA in the absence of the FN synergy site
   - To evaluate a possible compensatory effect by αv-class integrins: *in vitro* using cell lines lacking or expressing αv-class of integrins; and *in vivo,* by generating a double mutant *Fn1*$^{syn/syn}$*; Itgb3*$^{-/-}$ mouse strain that does not express β3-containing integrins and express FN with the synergy mutation

III MATERIALS AND METHODS

1. Mouse strains

Mice were housed in special pathogen free animal facilities and fed with standard mouse diet. The mice described in this study were kept in a mixed C57BL/6 x 129/Sv genetic background. All mouse work was performed in accordance with the Government of the Valencian community (Spain) guidelines (permission reference A1327395471346) and with the Government of Upper Bavaria.

1.1. *Fn1^{syn}* mouse strain

The knock-In mouse strain *Fn1*$^{syn/syn}$, that carries a mutation in the exon 28 of FN, which encodes the synergy motif, was generated in our laboratory. A 129/Sv mouse PAC clone was used to construct the targeting vector, which consisted of a 2.1 kb fragment containing exons 26 and 27, a neomycin cassette flanked by loxP sites, a 2.4 kb fragment containing the exon 28 carrying the mutated nucleotides, and a 3.5 kb fragment with the exons 29 to 32 (Fig. 19). The targeting construct was linearized with NotI and electroporated into R1 embryonic stem (ES) cells. Approximately 300 G418-resistant clones were isolated and screened by Southern blot for homologous recombination. The genomic DNAs were digested with SacI, XbaI or BstEII and probed with external probes 1 and 2. Two correctly targeted clones were injected into C57BL/6 host blastocysts to generate germline chimeras. The *Fn1*^{syn}-neo/+ mice were crossed with a deleter-Cre strain to eliminate the loxP flanked neomycin cassette. The elimination of neomycin was analysed by Southern blot with genomic DNA digested with Eco RI and probed with probe 3.

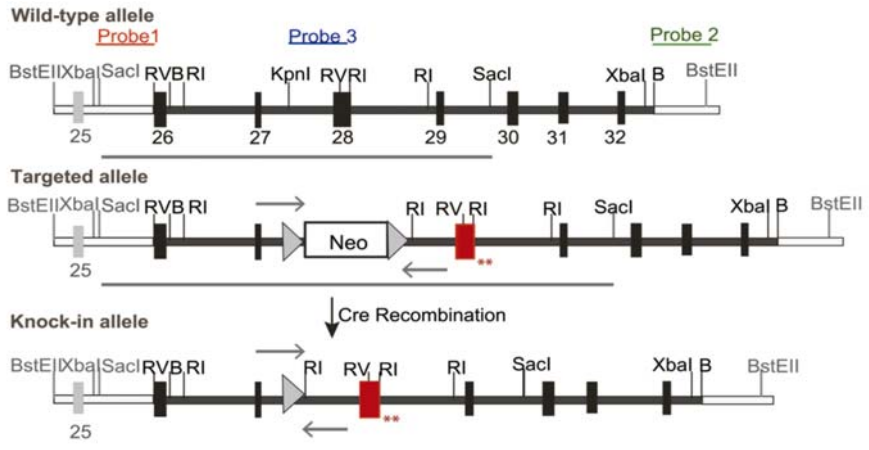

Figure 19. Strategy used to generate the *Fn1*$^{syn/syn}$. Mutations were introduced in the exon 28. Mutated exon 28 appears in red. Mutant *Fn1*$^{syn/syn}$ mice express the Knock-in allele without the Neo cassette. Probe 1-3 indicate the location of the probes used to analyse the construct by southern blot. Probe 3, which detected ERI-ERI fragment, was used as the internal probe to check mutant ES and mice. Grey arrows indicate the primers used to genotype the mutant mice.

The *Fn1*^{syn} mouse strain was kept in heterozygosis (*Fn1*$^{+/syn}$) or homozygosis (*Fn1*$^{syn/syn}$). Heterozygous mattings were done to obtain homozygous *Fn1*$^{syn/syn}$ and *Fn1*$^{+/+}$ littermates for experiments. Homozygous (*Fn1*$^{syn/syn}$x*Fn1*$^{syn/syn}$ or *Fn1*$^{+/+}$x *Fn1*$^{+/+}$) mattings were performed to obtain mice to extract blood plasma.

1.2. Generation of *Fn1*$^{syn/+}$; *Itgb3*$^{+/-}$ mice

To generate the compound *Fn1*$^{syn/+}$; *Itgb3*$^{+/-}$ mouse strain, *Fn1*$^{+/syn}$ and *Fn1*$^{syn/syn}$ were matted with *Itgb3*$^{+/-}$. The *Itgb3*$^{+/-}$ mouse strain was generated by Hodivala-Dilke (Hodivala-Dilke *et al.*, 1999). Double heterozygous (*Fn1*$^{syn/+}$; *Itgb3*$^{+/-}$) mattings were done to keep the strain. For experiments, time-mattings *Fn1*$^{syn/+}$; *Itgb3*$^{+/-}$x *Fn1*$^{syn/+}$; *Itgb3*$^{+/-}$ or *Fn1*$^{syn/syn}$; *Itgb3*$^{+/-}$x *Fn1*$^{syn/syn}$; *Itgb3*$^{+/-}$ were planned and caesarean were practiced extracting embryos at different embryonic stages from E11.5 till E18.5.

1.3. Genotyping

Mice were genotyped by polymerase chain reaction (PCR) of genomic DNA. To genotype adult mice, tail biopsies were collected at weaning age (P21) and digested in 500 µl of DNA lysis buffer at 55°C over-night, shaking. On the next day, tail lysates were spin during 5 minutes at 13000 rpm. The supernatant was mixed with isopropanol (1:1) and centrifuged 5 minutes at 13000 rpm. Pellet was washed with 500 µl of 70% ethanol (% vol:vol in H_2O) and centrifuged. The last pellet was resuspended in 50-100 µl of sterile Milli-Q water and dissolved during 1 h at 55°C.

To genotype embryos, collected yolk sacs were digested with 25-75 µl of 25 mM NaOH/0.2 mM EDTA at 98°C for 30 minutes. Samples were cooled at 4°C for 15 minutes, spin down in a microcentrifuge and neutralized with equal volume (25-75 µl) of 40 mM Tris HCl (pH 5.5).

Once the genomic DNA was isolated, 1-2 µl were used for PCR. The PCR primers and conditions are in tables 1 and 2. The total volume (50 µl) of PCR products were mixed with 6x loading buffer (0.2% Orange G w:v, 60% Glycerol v:v in 0.5 M EDTA) and loaded in a 2% agarose gel with TAE buffer (40 mM Tris-Acetate, 1 mM EDTA) containing 0.5 µg/ml of ethidium bromide. The electrophoresis was run at 120-150 V and visualized in a UV transilluminator at 365 nm.

Table 1. Protocol for genotyping the knock-in mutation in the synergy site of FN. Details of primers and PCR conditions.

FN^{syn} PCR	
Foward Primer 5'-CCCGTTTTCACTCTCGTCAT-3´	
Reverse Primer 5'-TCACAAGGAAACCAGGGAAC-3'	
PCR Products Wild-type band: 300 bp Mutant band: 400 bp	
PCR mix	PCR protocol
1x Taq Buffer	(1) 5 min 95°C
20 pmol each primer	(2) 30 secs 95°C ⎫
0.25 mM dNTPs	(3) 30 secs 58°C ⎬ 35 cycles
1 unit Taq polymerase	(4) 45 secs 72°C ⎭
1-2 µl gDNA	(5) 5 min 72°C
water up to 50 µl	(6) Hold 4 °C

Table 2. Protocol for genotyping the deletion of integrin β3 gene. Details of Primers and PCR conditions.

Itgβ3 PCR	
Foward Primer (p1) 5'- CTTAGACACCTGCTACGGGC-3'	
Reverse Primer (p2) 5'-TCACAAGGAAACCAGGGAAC-3' Reverse Primer (p3) 5´-CCTGCCTGAGGCTGAGTG-3´	
PCR Products Wild-type band (p1+p2): 446 bp Mutant band (p1+p3): 583 bp	
PCR mix	PCR protocol
1x Taq Buffer	(1) 5 min 95°C
50 pmol each primer	(2) 30 secs 95°C ⎫
0.5 mM dNTPs	(3) 30 secs 58°C ⎬ 35 cycles
1 unit Taq polymerase	(4) 45 secs 72°C ⎭
1-2 µl gDNA	(5) 5 min 72°C
water up to 50 µl	(6) Hold 4 °C

2. Fibroblasts cell lines

The *Fn1*$^{\Delta RGD/\Delta RGD}$, *Fn1*$^{wt/wt}$ and *Fn1*$^{RGE/RGE}$ fibroblast were derived from mouse embryonic stem cells (ESC). The ESCs, were isolated from 3.5 days-old embryos. They were cultured in suspension and differentiated into fibroblasts with 1% DMSO. After 1 week they were

transformed and consequently immortalized with SV40 large T antigen (SV40-TL), as described below. The mouse *Fn1*-Knockout (*Fn1*-KO) cell line and the integrin pan-Knockout fibroblast lines (pKO) were isolated from mouse kidney and immortalized by retroviral delivery of the SV40-TL antigen. To generate *Fn1*-KO cells, the *Fn1* gene was deleted from $Fn1^{flox/flox}$ with the adenoviral transduction of the Cre recombinase. Integrin pKO fibroblasts were provided by Reinhard Fässler and generated as described by Schiller *et al.* (2013).

All fibroblasts cell lines, including NIH3T3 and HT1080 (human fibrosarcoma), were maintained in culture using DMEM (Dulbecco's Modified Eagle's medium, Gibco), 10% (v:v) FBS (fetal bovine serum, Gibco) and 1% (v:v) penicillin-streptomycin and splited using trypsin-EDTA (Gibco) when cultures were confluent. Washes were done using a swing rotor centrifuge at 280-350 x g for 5 min at room temperature (RT). Before doing experiments, cells were cultured for 12-24 h in starving medium: 9% serum replacement medium (SRM), composed of 46.5% AIM-V (Life Technologies), 5% RPMI (Life Technologies) and 1% NEAA (Non-Essential Amino Acid Solution, Sigma-Aldrich), supplemented with 1% FN depleted-FBS and 1% Penicillin/Streptomycin (Pen/Strep; Gibco) in DMEM. When preparing the cells for experiments detachment was done with 0.02 mM EDTA in PBS and during experiments cells were cultured in DMEM, 9% SRM-DMEM or in SRM. All cells were grown at 37°C and 5% CO_2.

2.1. Fibroblast isolation from mouse kidney

Kidneys from 2-3 months old $Fn1^{flox/flox}$ mice were dissected in a laminar flow hood under sterile conditions. Kidneys were washed carefully with PBS. Ducts were cut off and kidneys opened longitudinally and placed in 2.5 mg/ml trypsin dissolved in DMEM. Kidneys were cut in small pieces while being immersed in the trypsin solution. This preparation was incubated for 45 min at 37°C and aspirated up and down with a pipette every 10 minutes to separate better the cells. Later, cells were centrifuged 5 min at 500 rpm and the supernatant was removed. The pellet containing the isolated cells was resuspended in 10% FBS-DMEM, washed twice by centrifugation and finally resuspended in 10 ml of 10% FBS-DMEM and plated in a 25 cm^2 tissue culture flask. After 24 h, 100 µl of Pen/Strep was added to the medium. Cells were kept in culture and medium changed every day. After 5 days in culture, cells were immortalized by retroviral delivery of the SV40-TL and kept about 1 week in culture. Then, they were plated at low density (around 500 cells in 150 mm tissue dish) to pick clones. Clones were visible after 5-8 days and those with fibroblast morphology were picked up with a cylinder. After 1 week growing one clone was selected to delete the FN gene from $Fn1^{flox/flox}$ by Cre recombinase delivery.

2.2. Primary fibroblast immortalization with SV40 large T antigen

NIH3T3 fibroblast expressing SV40 T Large antigen cDNA sequence packed in recombinant murine retroviruses (Brown *et al.*, 1986) were used to immortalize the isolated fibroblasts. To that purpose NIH3T3 were cultured in 10% FBS-DMEM with 1% Pen/Strep. Medium was collected from subclonfluent NIH3T3, cultured for 24 h. This medium was centrifuged to pellet down possible cell debris and filtered with 0.22 µm. This medium containing the SV40 T Large antigen was diluted 1:1 in 10% FBS-DMEM with 1% Pen/Strep. The medium from the isolated

primary fibroblasts was exchanged by the medium containing the SV40 T Large antigen. After 8 h, the process was repeated. SV40 T Large antigen inactivates tumour suppressor genes like *p53* or *Rb* and can induce telomerase activity, immortalizing the infected cells (Ahuja *et al.* , 2005).

2.3. Syndecans 1-4 knock-down

Syndecans mRNA translation was blocked in *Fn1*$^{\Delta RGD/\Delta RGD}$ cells by gene silencing with siRNA. Predesigned siRNA pools (SMARTpool, Dharmacon) against syndecan 1 (Sdc1) and 4 (Sdc4) were delivered in subconfluent fibroblast culture with the aid of lipofectamine 3000 (Invitrogen). Before siRNA transfection, cells were starved overnight in 1% FN depleted medium. Then 50,000 fibroblasts were seeded on laminin-coated 12 well-dish or 12 mm glass coverslips in SRM during 3 h before transfection. 150 nM of each siRNA (Sdc1 and Sdc4) were transfected with 2 µl of lipofectamine 300 and 100 µl Optimem, following manufacturer´s instructions. Briefly, siRNA was mixed with 50 µl Optimem (solution A) and 2 µl lipofectamin with 50 µl Optimem (solution B) for 5 min. Next, solutions A and B were mixed for 20 min at room temperature and added to the cell culture. The SRM was replaced 12 h post-transfection and cells were incubated for 96 h. Syndecan levels were analysed by westernblot to check gene silencing and compared to cells transfected with siRNA contained a scrambled sequence. To study the effect of syndecan knock-down in FN assembly, cells seeded on laminin-coated coverslips were immunostained after the 96 h post-transfection.

3. Standard Techniques for Biochemistry, Molecular and Cell Biology

3.1. Bacterial transformation

Omnimax or DH5α *E. coli* (50-100 µl) were transformed with 50-100 ng of plasmid DNA and incubated 30 min on ice. Next, a heat shock of 42 secs at 42 °C followed by 2 min on ice was done. Luria Bertani (LB) broth (900 µl) was added and cells were incubated at 37 °C for 1 h shaking. Different volumes of the transformation were plated in LB Agar containing 100 µg/ml ampicillin. Colonies were grown for 12 h, pick and inoculated for miniprep DNA isolation with QIAprep spin kit (Quiagen) following manufacturer's instructions.

3.2. Quantitative gene expression analysis by qPCR

- RNA extraction and cDNA synthesis

Cells were trypsinized from a regular culture and after washing the trypsin, resuspended in PBS and spin down. RNA was extracted with RNeasy Kit (Quiagen) following manufacturer´s instructions. RNA was eluted in RNase free water and concentration was measured with a Nanodrop ND1000 spectrophotometer. For RNA reverse transcription into cDNA, 500 ng of RNA were used together with 4 µl of 5x iScript reaction mix and 1 µl of iScript reverse transcriptase (BioRad), to a final volume of 20 µl in nuclease free water. The manufacturer´s suggested reaction for retrotranscription was employed:

Priming	5 min	25°C
Transcription	25 min	46°C
RT Inactivation	1 min	95°C

- Quantitative PCR (qPCR)

The retrotranscribed cDNA was diluted 1:10 in water for the qPCR. For each reaction: 5 µl of cDNA dilution was mixed with 10 µl of iQ SYBR Green Supermix (BioRad) and 0.5 µM of forward and reverse primers. The sequence of primers was obtained from former publications and are in table 3. The PCR was run in a LightCycler 480 Instrument (Roche) following the protocol in table 4. GAPDH was used as housekeeping gene to normalize the expression levels of the analysed genes.

Table 3. Primer sequences used for qPCR.

Gene	Forward Primer	Reverse Primer	Reference
Fn1	5' TACCAAGGTCAATCCACACCCC 3'	5'CAGATGGCAAAAGAAAGCAGAGG 3'	Sakai et al. 2003
Sdc1	5'GTGGCGGCACTTCTGTCATC 3'	5' GCACCTGTGGCTCCTTCGTC 3'	Zhang et al. 2013
Sdc2	5' TGTGTCCGCAGAGACGAGAA 3´	5' GGAATCAGTTGGGATGTTGTCA 3'	Zhang et al. 2013
Sdc3	5' ATACTGGAGCGGAAGGAGGT 3'	5' TTTCTGGTACGTGACGCTTG 3'	Zhang et al. 2013
Sdc4	5' AACCACATCCCTGAGAATGC 3´	5' AGGAAAACGGCAAAGAGGAT 3´	Zhang et al. 2013
Gapdh	5´AGGTCGGTGTGAACGGATTTG 3´	5´GGGGTCGTTGATGGCAACA 3´	Zhang et al. 2013

Table 4. Protocol used for qPCR of each gene.

STEP	TEMPERATURE	TIME
Denature	95°C	3 min
PCR	95°C 60°C	30 secs ┐ 40 1 min ┘ cycles
Cooling	4 °C	Hold

3.3. Protein electrophoresis and coomassie staining

Protein samples were mixed with Laemmli buffer, boiled for 5 min and loaded in an 8-12% SDS-PAGE. Electrophoresis was always run in denaturing conditions at 80-120 V. After electrophoresis, the gel was stained with Coomassie blue stain for 30 min at RT shaking; and rinsed with destain solution twice. To clear the gel, it was kept in destain solution overnight shaking.

3.4. Western blots

Protein samples, either from cell lysates or from purified FN, were mixed with Laemmli buffer and boil for 5 min, loaded in SDS-PAGE for electrophoresis. Next, for Western-blotting the gel was transferred to a Polyvinylidene difluoride (PVDF) membrane. The membranes were blocked with 5% BSA or milk powder in TBST during 1h at RT and incubated overnight with

primary antibodies (Table 5) diluted in blocking buffer at 4°C. On the next day, membranes were washed three times in TBST, incubated with secondary antibodies (table 5) diluted in blocking buffer at RT for 1 h. Then, membranes were washed three times with TBST and developed with horseradish peroxidase (HRP) chemiluminescent substrate Immobilon (Millipore). Protein levels were analysed using ImageJ and normalized to a loading control.

Table 5. Primary and Secondary antibodies used for western blots. Dilutions were done in blocking buffer.

Primary Antibody	Secondary Antibody
rabbit anti- FN (sc-12765, Abcam); Dilution 1:2000	Goat anti-rabbit conjugated with HRP (172–1019, Bio-Rad) Dilution 1:10000
mouse anti- syndecan 1 (sc-12765, Santa Cruz Biotechnology); Dilution 1:2000	Goat anti-mouse conjugated with HRP (172–6516, Bio-Rad) Dilution 1:10000
mouse anti- syndecan 2 (sc-376160, Santa Cruz Biotechnology); Dilution 1:2000	Goat anti-mouse conjugated with HRP (172–6516, Bio-Rad) Dilution 1:10000
mouse anti- syndecan 3 (sc-398194, Santa Cruz Biotechnology); Dilution 1:2000	Goat anti-mouse conjugated with HRP (172–6516, Bio-Rad) Dilution 1:10000
mouse anti- syndecan 4 (sc-12766, Santa Cruz Biotechnology); Dilution 1:2000	Goat anti-mouse conjugated with HRP (172–6516, Bio-Rad) Dilution 1:10000
Rat anti- tubulin (MAB1318, Millipore) Dilution 1:3000	Donkey anti-rat conjugated with HRP (5204-2504, Bio-Rad) Dilution 1:10000
Rabbit anti- RhoA (67B9, Cell Signalling) Dilution 1:2000	Goat anti-rabbit conjugated with HRP (172–1019, Bio-Rad) Dilution 1:10000
Rat anti- tubulin (MAB1318, Millipore) Dilution 1:3000	Donkey anti-rat conjugated with HRP (5204-2504, Bio-Rad) Dilution 1:10000
Mouse anti-gamma chain fibrinogen (ab119948, Abcam) Dilution 1:2000	Donkey anti-mouse conjugated with HRP (172-1011, Bio-Rad) Dilution 1:10000
Rabbit anti-pTyr397FAK (44–624G, Biosource) Dilution 1:1000	Goat anti-rabbit conjugated with HRP (172–1019, Bio-Rad) Dilution 1:10000
Rabbit anti-pTyr861FAK (44–626G, Biosource) Dilution 1:1000	Goat anti-rabbit conjugated with HRP (172–1019, Bio-Rad) Dilution 1:10000
Rabbit anti-mouse FAK (06–543, Millipore) Dilution 1:1000	Goat anti-rabbit conjugated with HRP (172–1019, Bio-Rad) Dilution 1:10000
Mouse anti- vinculin (V9131, Sigma-Aldrich) Dilution 1:1000	Donkey anti-mouse conjugated with HRP (172-1011, Bio-Rad) Dilution 1:10000

- Cell lysates preparation

About 0.3-0.5 x 10^6 cells were seeded on 6 well-plates in regular culture conditions. After 24 h, the cells were lysed with RIPA buffer during 10 min on ice. Cell lysates were sonicated for 30 secs and spin for 5 min at 10000 rpm in a table centrifuge at 4°C. Protein concentration was measured with Pierce BCA Protein Assay Kit (Thermo Scientific) following manufacturer´s instructions and using different concentrations of BSA as standard. The same quantity of protein (30-50 µg) of each sample was loaded on a 12% SDS-PAGE for electrophoresis followed by Western-blotting. The levels of the protein of interest were analysed using ImageJ and normalized using tubulin or GAPDH as a loading control.

3.5. Cell immunostaining and microscopical analysis

For cell immunostaining, the cells were fixed after the indicated incubation times. Fixation was carried out with 2 or 4% paraformaldehyde (w:v in PBS) during 10 minutes at RT. Cells were washed thoroughly with PBS three times (5 minutes, shaking) and permeabilized with 0.1% Triton X-100 (Merck) in PBS, 10 min at RT. After washing three times with PBS, coverslips were blocked with 3% BSA in PBS for 1h at RT and incubated over night at 4°C with primary antibodies (table 6) diluted in blocking solution. Integrin β1 was stained without previous permeabilization. For that, after fixation and washing, coverslips were blocked and incubated 1 h at RT with the integrin β1 antibody dilution. After washing out the unbound antibody, coverslips were permeabilized, blocked and stained overnight with the rest of primary antibodies. On the next day, primary antibody solution was washed with PBS three times and coverslips incubated 1 h at RT with secondary antibodies (table 6) and TRITC-labelled phalloidin (Sigma-Aldrich) (diluted 1:400) in blocking solution. Secondary antibody solution was washed three times with PBS and nuclei were stained with DAPI (1:10000 dilution in PBS) for 7 min at RT, washed three times with PBS and mounted with elvanol. Images of the preparations were taken with a Confocal Laser Scanning Microscope Zeiss 780LSM and analysed with ImageJ.

Table 6. Primary and Secondary antibodies used for cell immunostaining. Dilutions were done in blocking buffer.

Primary Antibody	Secondary Antibody
Rabbit anti-mouse Fibronectin (AB2033, Millipore) Dilution 1:500	Goat anti-rabbit conjugated with Alexa488 (A11008, Invitrogen) Dilution 1:400
Mouse anti-mouse Paxillin (BD Transduction Laboratories TM) Dilution 1:300	Donkey anti-mouse conjugated with A647 (A31571, Invitrogen) Dilution 1:500
Rabbit anti-mouse integrin β1 Gift from R.Fässler Dilution 1:500	Goat anti-rabbit conjugated with Alexa488 (A11008, Invitrogen) Dilution 1:400

3.6. Surface integrin analysis by flow cytometry

Cells were detached with trypsin and trypsinization was stop with 100 µg/ml trypsin inhibitor (Calbiochem). Cells were washed with PBS and finally resuspended in FACS buffer. Cells were counted, and about 5 x 10^5 cells were distributed in rounded bottom wells of 96-well plate or in a corning falcon round-bottom polystyrene tube, spin down and resuspended in primary antibody or isotypes control dilution (1:200) in FACS buffer (table 7). Cells were stained for 30 min on ice and followed by two cycles of centrifugation and resuspension in FACS buffer to wash out the unbound antibody. When non-labelled antibodies were used, an extra incubation step with labelled secondary antibody diluted 1:200 in FACS buffer was done (30 min on ice), followed of 2 cycles of washes. Stained cells were then resuspended in 300 µl of FACS Buffer and analysed in a FACSCanto (BD Bioscience). During analysis, the same settings of forward scatter (FSC) and side scatter (SSC) were used to select size and granularity for each cell line, which were established using and non-labelled sample of each cell line. These settings were maintained among in replicates and experiments. Also, for comparison of different cell lines, the same laser and detector settings were used. Data was evaluated using FlowJob (BD Bioscience) and fluorescence intensity measurements were normalized using the intensity values of the isotope control for each antibody. Experiments were done 3 times with technical triplicates in each experiment.

Table 7. Primary and Secondary antibodies used for flow cytometry. Dilutions were done in blocking buffer.

Antibody	Isotype Control
Phycoerythrin (PE) Hamster anti- β1 integrin (102207, BioLegend)	PE Armenian Hamster IgG (400907, BioLegend)
PE rat anti-α5 integrin (557447, PharMingen)	PE Rat IgG2a, κ (553930), PharMingen)
PE hamster anti-β3 integrin (12–0611, BD Bioscience)	PE Armenian Hamster IgG (400907, BioLegend)
PE rat anti-αv integrin (551187, PharMingen)	PE Rat IgG1, κ (553925, PharMingen)
PE rat anti- α4 integrin (557420, PharMingen)	PE Rat IgG2a, κ (553930, PharMingen)
rat anti- syndecan-4 (550350, PharMigen) Secondary: mouse anti-rat-FITC (10094D, PharMigen)	FITC Rat IgG2a, κ (554688, PharMingen)

4. Activated RhoA detection

Rho GTPases are bound to GTP in their active form. To identify them, Ren and colleagues designed a protocol based in the specificity of the protein Rhotekin to bind only GTP-Rho

GTPases (Ren, Kiosses and Schwartz, 1999). Rhotekin contains a Rho binding domain (RBD) which has been cloned in vectors for protein expression linked to a GST tag. By performing pull-downs with purified GST-RBD it is possible to quantify the cellular levels of active RhoA.

- Preparation of GST-RBD beads

A pGEX plasmid containing the RBD (pGEX-GST-RBD, Adgene) tagged to GST was used to transform DH5α competent *E. coli.* (for cloning steps see above in 3.3.1.). A transformed colony was inoculated in a 50 ml LB broth with 50 µg/ml ampicillin (Sigma-Aldrich) and grown over night at 37°C. This culture was diluted into 450 ml LB-Ampicillin and let grow for 30 min at 37°C. To induce protein expression, 100 µM Isopropyl B-D-thiogalactopyranoside (IPTG) was added to the culture and grown for about 20-24 h at 25°C. The bacterial culture was centrifuged at 4000 x g for 15 min and the pellet frozen. The pellet was resuspended in Rho-lysis buffer supplemented with 1 mM Phenylmethylsulfonyl fluoride (PMSF), 1 mM Dithiothreitol (DTT) and 200 µM Na_3VO_4 and sonicated for 1 min on ice. The cell lysates were clarified by centrifuging at 27000 x g, 15 min at 4°C. The supernatant was mixed with 50% solution of Glutathione Sepharose beads (GE Healthcare Life Science) in lysis buffer and incubated for 1h at 4°C, rotating. Next, the mixture was centrifuged in a swing rotor at 500 x g for 5 min at 4°C and washed twice with HBS buffer supplemented with 1 mM DTT. After the last wash, the slurry was mix with HBS buffer with 1 mM DTT, in a 1:1 relation.

To quantify the concentration of the beads preparation, 10 µl of it together with BSA standards for comparison were run in an electrophoresis and stained with Coomassie blue. The BSA standards contained 20, 10 and 5 µg of protein. Aliquots containing 60 µg protein in HBS: glycerol in a 3: 1 ratio were snap frozen and stored at -80°C.

-GTP bound RhoA pull-down

Fn1$^{\Delta RGD/\Delta RGD}$, *Fn1*$^{RGE/RGE}$ and *Fn1*$^{+/+}$ cells were pre-starved overnight with 9% serum replacement medium (SRM) supplemented with 1% FN-depleted FBS. Tissue culture dishes (100 mm) were coated with 10 µg/ml of laminin (from Engelbreth-Holm-Swarm murine sarcoma basement membrane, Sigma-Aldrich) or 0.01% of poly-L-lysine solution (Sigma-Aldrich) for 1 h at room temperature. About 2.5 x 10^6 cells were seeded and incubated in SRM for 24h. On the next day, SRM was aspirated and plates washed with HBS buffer, working always on ice. Cells were lysed with 1 ml of Rho-Lysis buffer containing 1 mM PMSF, protease inhibitors (cOmplete, Roche) and a phosphatase inhibitors cocktail (P2 and P3, Sigma-Aldrich) following manufacturer´s instructions, for 5 min on ice. Plates were scraped to collect lysates and lysates were spin in a table centrifuge at 15000 x g for 5 min and the supernatant placed in a new tube and kept for experiments. Protein concentration was measured with Bradford Protein Assay (Thermo Scientific) following manufacturer´s instructions and using different concentrations of BSA as standard. Next, volumes and protein concentration of each sample were equalized to obtain 0.5-1.5 mg/ml in 1-1.5 ml. 100 µl were taken from each sample and kept as the input. After two rounds of washing the GST-RBD beads with HBS buffer, 20 µg of the beads were added to each sample of protein lysate and incubated for 45 min at 4°C rotating. Afterwards, samples were spin at 6800 x g, 10 secs at 4°C and washed three times

with Rho-lysis buffer. The final pellet as well as the input fraction were resuspended in Laemmli buffer and boiled for 5 min. Both, pull-down and input samples were loaded in a 12% SDS-PAGE for western-blotting. Activated RhoA levels were referred to the total RhoA (input) and normalized using tubulin as a loading control.

5. Analysis of FN matrix assembly by fibroblasts

Cells were pre-starved overnight with 9% serum replacement medium (SRM) supplemented with 1% FN depleted FBS. Glass coverslips (8 mm diameter) or 12 well dishes were coated with 50-200 µl of a 10 µg/ml solution of different substrates: laminin (from Engelbreth-Holm-Swarm murine sarcoma basement membrane, Sigma-Aldrich), vitronectin (Vitronectin XF^{TM}, Stem cell), collagen type I (PureCol, Advanced BioMatrix) or gelatine (Sigma-Aldrich) during 1 h at RT. After washing with PBS, coverslips/dishes were blocked 1h with 1% BSA in PBS (w:v). Cells were detached with 2 mM EDTA in PBS and the same number of each cell line was seeded onto the coverslips/dish and incubated during indicated times in SRM.

For blocking the heparin binding sites, cells were let adhere for 3 hours, then the SRM was exchanged by SRM containing 0.1 mg/ml heparin (Sigma-Aldrich) and cells were incubated in culture for 24 or 72 h. For activating integrins with manganese, after 24h of incubation with or without heparin, 100 µM of $MnCl_2$ was added to the medium during 3h. FN matrix was analysed by immunofluorescence.

- Quantification of FN synthesis and secretion

Three fractions of FN were analysed: secreted soluble FN in the medium, the intracellular soluble FN and the fibrillar crosslinked FN. For analysing the levels of secreted FN, the same number of cells were starved and seeded on laminin coated 12-well dishes as explained above, treated or not with heparin or/and manganese. After 24, 72 or 120 h medium was collected and centrifuged 5 minutes at 350 x g to pellet down possible cellular debris. The same volume of each sample was loaded in an 8% SDS-PAGE for western-blotting. To analyse the fibrillar fraction of FN, the same cell preparation on 12 well-dishes were washed with PBS twice after collecting the medium and lysed with 100 µl of DOC buffer 10 min on ice. Cell lysates were collected with the help of a scraper, passed through a 25 gauges syringe and centrifuged at 14000 rpm for 20 min. Supernatant was collected and kept as the soluble FN, and the pellet was washed with DOC buffer and centrifuged again. The final pellet contained the fibrillar (DOC insoluble) FN and was resuspended in 60 µl of solubilization buffer. Protein concentration in DOC-soluble fractions was estimated using Pierce BCA protein assay (kit from ThermoFisher) and used to normalize protein concentration in the corresponding DOC-insoluble fraction. In an 8% SDS-PAGE gel, 30-50 µg of DOC soluble and 50% of the total volume of DOC insoluble were loaded for western-blotting. Fibrillar FN levels were normalized to soluble FN and soluble FN and secreted FN were normalized using tubulin as a loading control.

6. Histological analysis

6.1. Paraffin embedding and tissue staining

Adult mice were perfused post-mortem with 4% parafolmaldehyde (PFA) in PBS or tissue pieces and embryos were fixed overnight with 4% PFA at 4˚C. Fixed tissues were dehydrated in graded alcohol series (50, 70, 80, 90 and 100% ethanol), cleared two times in xylene and embedded in paraffin (Paraplast X-tra, Sigma-Aldrich). Paraffin blocks were cut into 8 µm thick sections and stained with Haematoxylin-Eosin (H-E) or immunostained.

- Haematoxylin-Eosin staining

First paraffin was removed by washes with xylene and tissue was rehydrated with an inverse graded ethanol series (100, 95, 80, 70 and 50%), washed with water and PBS. For staining the nucleus with haematoxylin, the sections were immersed for 3 min in Mayer (Merck) solution (1:5 (v:v) in water). After washing out the unspecific staining with running water, sections were counterstained for 1 min with 0.2% eosin solution (0.2% eosin-Y (w:v) and 80% Ethanol). Then, the sections were washed with water, dehydrated in ethanol 90% and 100% and cleared with xylene twice and slides were mounted with water-free solution Entellan (Merck).

- Immunostaining

For tissue immunofluorescence, paraffin was removed as above (see H-E). Sections were unmasked by heating in citrate buffer for 10 min, washed in PBS and blocked for 1 h with 3% BSA in PBS at RT and incubated overnight with the primary antibody (table 8) diluted in blocking buffer. On the next day, glass slides were washed and incubated with secondary antibodies (table 8) diluted in blocking buffer for 1 h at room temperature, washed in PBS, DAPI stained (1:10000 in PBS, 7 min) and mounted on glass coverslips with elvanol.

Table 8. Primary and Secondary antibodies used for tissue immunostaining. Dilutions were done in blocking buffer.

Primary Antibody	Secondary Antibody
Rabbit anti-mouse Fibronectin (AB2033, Millipore) Dilution 1:300	Goat anti-rabbit conjugated with Alexa488 or Alexa546 (A11008 or A11010 Invitrogen) Dilution 1:400
Rabbit anti-mouse Lyve1 (ab14914, Abcam) Dilution IF 1:300, WM 1:100	Donkey anti-mouse conjugated with Alexa488 or Alexa546 (A21202 or A10036, Invitrogen) Dilution 1:400
Rat anti-mouse Ter119 (09082D, PharMingen) Dilution IF 1:400, WM 1:100	Goat anti-rat conjugated with A647 (A21247, Invitrogen) Dilution 1:400
Rabbit anti-mouse Collagen IV (2150–1470, Bio-Rad) Dilution WM 1:100	Goat anti-rabbit conjugated with Alexa488 or Alexa546 (A11008 or A11010, Invitrogen) Dilution 1:400

Mouse anti-smooth muscle actin conjugated with Cy3 (A2547, Sigma-Aldrich) Dilution IF 1:500, WM 1:200	
Rabbit anti-NG2 chondroitin sulfate proteoglycan (AB5320, Merck Millipore) Dilution WM 1:100	Goat anti-rabbit conjugated with Alexa488 or Alexa546 (A11008 or A11010, Invitrogen) Dilution 1:400
Rabbit anti-laminin-1 (L9393, Sigma-Aldrich) Dilution WM 1:100	Goat anti-rabbit conjugated with Alexa488 or Alexa546 (A11008 or A11010, Invitrogen) Dilution 1:400

6.2. Whole-mount (WM) preparation and staining

Embryos were isolated from pregnant mothers at the stages of E11.5, E15.5 and E16.5 and fixed overnight at 4˚C with Dent´s fixative consisting of 80% Methanol, 20% DMSO. The skin was dissected after fixation from the E15.5 and E16.5 embryos, washed 3 times with 100% methanol (5 min) and kept at -20˚C in 100% methanol. In the case of adult mice, a small piece of the ear was dissected post-mortem and fixed overnight at 4˚C with DENT´s fixative. After fixation, the ear was open longitudinally in halves and washed three times with 100% methanol for storage or staining.

For staining, fixed pieces of skin, ear or whole E11.5 embryos were hydrated in decreasing (75, 50 and 25%) methanol series, diluted in PBS supplemented with 0.1% Tween20 (PBST) and blocked for 2 h at RT with 3% BSA in PBST. Incubations with primary and secondary antibodies (table 8) were done overnight at 4˚C with gentle rocking and after washing with PBST, tissues were mounted with elvanol.

7. Purification of plasmatic FN and depletion of FN in fetal bovine serum

7.1. Plasma isolation

Blood was extracted (permission ref 2016/VSC/PEA/00215) from *Fn1*$^{+/+}$ and *Fn1*$^{syn/syn}$ mice to isolate the plasma for FN purification. Mice were anesthetized with Isoflurane and blood was taken retro-orbitally with non-heparinized capillaries. Collected blood was mixed with 0.5 M EDTA (1:100) as anticoagulant and centrifuged at 3000 rpm for 20 min in a table centrifuge. Supernatant was placed in a new microcentrifuge tube and centrifuged again to eliminate possible remaining blood cells. The last supernatant (plasma) was kept at -80°C for experiments. All samples of plasma had yellowish colour, these where haemolysis happened presented red colour and were discarded.

7.2. FN purification

To purify FN from plasma (pFN) a protocol from Retta, Ferraris and Tarone, 1999 was adapted to mouse plasma samples. Gelatin-Sepharose (GE Healthcare Life Science) was packed

in minicolumns (Poly-Prep, Bio-Rad) for affinity chromatography. About 1 ml of gelatin-Sepharose was used per 3 ml of mouse plasma. A peristaltic pump (Pharmatia) was used to ensure a constant flow-through. After equilibrating the column with TBS mouse plasma was incubated with the Gelatin-Sepharose overnight at 4°C rotating at 3 rpm. Next, columns were washed with 0.5 NaCl in 10 mM Tris-HCl pH 7.4 and TBS till no protein was detected by spectrophotometry (absorbance 280 nm). Columns were incubated with a bed volume of 2 M urea in TBS for 1 h rotating at RT and 3 rpm. FN was eluted and collected in 0.5-1 ml fractions, and their absorbance measured at 280 nm. Urea (2 M) was continuously added and protein concentration of each fraction measured till an absorbance of zero at 280 nm was reached. The eluates were loaded in an 8% SDS-PAGE gel and stained with Coomassie to check their purity. Samples with only a clear 250 kDa band were picked up for dialysis and further experiments. The selected FN fractions from the elution were placed in dialysis membranes (VISKING dialysis tubing, SERVA) and dialyzed against TBS at 4°C with soft stirring for 18 h with two buffer changes. Afterwards, FN concentration was measured by spectrophotometry in NanoDrop and checked the protein by western blot, aliquoted and snap frozen. Frozen aliquots were stored at -80°C for experiments.

7.3. FN characterization

The purity of the eluted FN was checked by Coomassie staining before dialysis. Only those samples without contamination of other proteins were selected for dialysis. Dialyzed samples were tested for degradation and fibrinogen contamination by western blot. To discard any differences between plasma purified FN^{wt} and FN^{syn} in its ability for coating glass we tested the protein glass adsorption by ELISA.

- pFN adsorption to glass

- GLASS TREATMENT

To ensure a good adsorption of purified pFN onto glass, glass coverslips were poly-maleic anhydride-1-octadecene (POMA; Polysciences Inc)-treated which binds covalently to the C-terminus of FN molecule (Prewitz *et al.*, 2013). Glass coverslips were aminosilanized by submerging them 1 h at RT with a mixture of 1 part of 30% H_2O_2 and 4 parts of H_2SO_4. After thoroughly rinsing with water, coverslips were sonicated for 5-10 min in water twice. Next, washed twice with methanol and incubated for 1 h in 3-aminopropyl trimethoxy-silane diluted in methanol in a 1:50 relation. A solution of 0,16% POMA in tetrahydrofuran was transferred to the coverslip by dip coating with constant velocity equal to 48 mm min^{-1}. Immediately after dip-coating with POMA, coverslips were coated with purified pFN.

- ELISA

To test mouse purified pFN adsorption to glass, coverslips were coated with 0.1–10 µg/ml of protein during 1 h at RT, followed by a blocking step of 1 h using 1% BSA in PBS. To quantify the adsorbed FN, the coverslips were then incubated for 2 h at RT with anti-FN antibody (Ab; diluted 1/300 in blocking solution), washed, incubated with anti-rabbit HRP-conjugated (diluted 1/500 in blocking solution) 1 h at RT and finally treated with 50 ml of 2,2'-azino-bis(3-ethylbenzthiazoline-6-sulfonic acid (ABTS; Peroxidase substrate kit, Vector SK-4500) for 30 min

in the dark. The ABTS-containing solution was collected in ELISA microplates, and the absorbance was measured at 405 nm.

7.4. FN depletion in serum

To eliminate FN from the FBS used in cell culture, 5 ml of Gelatin-Sepharose were packed in chromatography minicolumns and equilibrated with TBS. Columns were disassembled, mixed with 50 ml of FBS and incubated overnight at 4°C rotating at 3 rpm. On the next day, the FBS was eluted and collected. A small volume of the elution was diluted in Laemmli buffer and analyzed in western blot for checking presence of FN. If the eluted FBS contained some FN, the process was repeated as many times as necessary to eliminate all the FN.

8. Plasma FN assembly

Fn1-KO fibroblasts were starved overnight in 9% SRM supplemented with 1% FN-depleted serum, detached with 2 mM EDTA in PBS and transferred into 8-well Lab-Tek chambers (Thermo Scientific) in 9% SRM without serum. The Lab-Tek chambers had been previously coated for 1 h with a solution of 20 mg/ml of Laminin (Roche) at RT and blocked for 30 min with 1% BSA in PBS. After 3 h of cell adhesion, the 9% SRM was supplemented with 1% mouse plasma and cells were incubated for 24, 48, 72 and 96 h, fixed with 4% PFA and prepared for immunofluorescence staining. After fixation, PFA was washed out with PBS and the preparation was blocked with 3% BSA-PBS. Staining was done by the method already describe in section 2.2.

9. Generation of FNIII7-10 fragments

We used human cDNA encoding the FNIII7-10 fragment and subcloned in the expression vector pET-15b (Takahashi et al., 2007). To generate the FNIII7-10^{syn} we mutated by site-directed mutagenesis the two arginines in the synergy sequence: DRVPHSRN>DAVPHSAN. We performed two rounds of PCR using the following primers: 5´-GATGCGGTGCCCCACTCTCGGAAT-3´ (forward) and 5´-GATGCGGTGCCCCACTCTGCGAAT-3´ (forward) and the complementary reverse primers. PCR protocol using *Pfu Ultra* (Quickchange, Aligent) are in table 9. The PCR products were digested with DpnI for 1 h at 37°C to eliminate the template DNA and keep only the PCR products. After the first PCR, omnimax competent cells (Thermo Scientific) were transformed and 10-15 colonies were picked for sequencing to confirm the mutagenesis. A selected colony was inoculated into LB broth with 50 µg/ml ampicillin, grown for 8-12 h and pellet down. Plasmid DNA was isolated with MiniPrep Kit (Quiagen), following manufacturer's instructions. Two positive clones were used to carry out the second mutagenesis, following the same steps. A clone containing the two mutations was picked for protein expression.

Table 9. FN synergy mutagenesis protocol

PCR mix	PCR protocol
1x Pfu Buffer	(1) 1 min 95°C
125 ng each primer	(2) 1 min 95°C ⎫
0.5 mM dNTPs	(3) 1 min 55°C ⎬ 30 cycles
2.5 unit *Pfu* polymerase	(4) 14 min 65°C ⎭
50 ng DNA	(5) 15 min 68°C
water up to 25 µl	(6) Hold 4 °C

-Protein Expression

The expression of recombinant FN fragments was done in the E. coli strain Rosetta T1R. Purification was performed using TALON Metal Affinity chromatography (Clontech, Saint Germain en Laye, France). Finally, the protein was obtained by gel filtration chromatography using Superdex 200 10/300 GL columns (GE Healthcare) and Superdex Size Exclusion Media (GE Healthcare) and eluted in PBS.

10. Fibroblast adhesion studies

Adhesion and spreading of different fibroblast cell lines to pFN^{syn} in comparison to pFN^{wt} was analysed using different methods.

10.1 Static cell adhesion assay

Fibroblast were starved during 12-24 h as described in section 3.2. 96 well plates were coated with 10 µg/ml of either pFN, poly-lysine (Sigma-Aldrich) or 3% BSA in PBS during 1 h at RT, followed by a blocking step of 30 min using 3% BSA in PBS. The same number of cells (5 x 10^4) were plated with DMEM, allowed to adhere for the indicated times and medium was removed by shaking the dishes. The wells were washed three times with PBS by immersing and shaking the plates. The adhered cells were stained with crystal violet (20% Methanol, 0.1% Crystal Violet) overnight at 4˚C, washed and incubated for 2 h at RT with 0.1% triton X-100 in PBS. Absorbance was measured at 595 nm. Three replicates were done per condition in each experiment to average the absorbances.

10.2. Initial adhesion: time-lapse microscopy

Tissue culture µ-Slide eight well chambers (Ibidi) were coated with 10 µg/ml of pFN during 1 h (RT) and blocked with 3% BSA in PBS for 30 min. Starved cells (10^4) were seeded in the chambers and immediately imaged with frame rates of 90 s in a Zeiss Axiovert microscope using the VisiView (Visitron) software.

10.3. Spreading and focal adhesion analysis

Glass coverslips were POMA treated, coated with purified pFN for 1 h at RT and blocked with 3% BSA in PBS for 30 min. After washing, 2 x 10^4 starved cells were seeded on the pFN

coated coverslips for 15, 30, 60 and 120 min. After each time point in the spreading course, cells were fixed and stained for paxillin, integrin β1 and actin as described in section 3.

10.4. Adhesion in shear stress by spinning-disk

Assaying fibroblasts adhesion under shear stress with a spinning-disk device (Fig. 20) allow calculation of the adhesion strength. The spinning-disk instrument was designed by David Boettiger (Boettiger, 2007). To this end, POMA-treated rounded glass coverslips of 25 mm diameter were coated with 400 µl of 10 µg/ml purified pFN during 1 h at RT and afterwards blocked 1 h with 1% BSA in PBS. The cells were starved overnight and detached with 2 mM EDTA, washed and resuspended in DMEM. When cells were heparin treated, 0.1 mg/ml heparin was dissolved in DMEM and this solution was used for the experiment. The same number of cells (7 x 10^5) were seeded and allowed to adhere onto the FN coated coverslips for 1 h. Next, coverslips were placed on the support of the spinning-disk device, immersed in Dulbecco´s PBS, supplemented with 80 mM $CaCl_2$ and 80 mM $MgCl_2$, and spun for 5 min at 6,000 rpm. After spinning, cells were fixed with 4% PFA for 10 min at RT and nuclei stained with DAPI. The nuclei were counted with a Zeiss Axiovert (objective 10x) controlled by MetaMorph software (Molecular Devices), with an automated motorized stage which allows taking images at determined positions. Number of nuclei were normalized to the counts at the coverslip centre (force zero). The resulting data were analysed as described (Boettiger, 2007) using MATLAB. Briefly, the detachment profile for each experiment (Fig. 45 A) was fitted to a sigmoid curve: $f = 1/\{1 + exp[b(\tau - \tau_{50}]\}$. We calculated for each condition the τ_{50}, which is the force for 50% cell detachment.

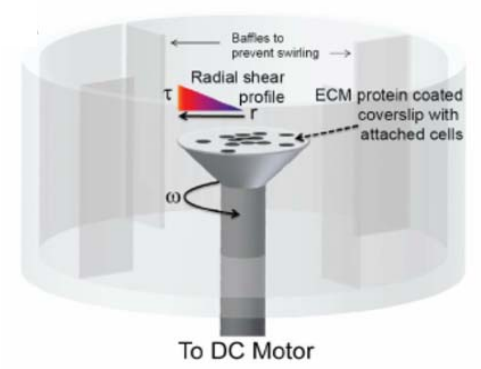

Figure 20. Scheme of the spinning-disk device used to measure the strength of the bond. The motor makes the platform rotate. On top of the platform the cover-slip with the adherent cells is attached by vacuum.

10.5. Integrin cross-linked to FN

7 x 10^5 cells were seeded onto pFN-coated glass coverslips following the spinning-disk protocol. Spun and non-spun cells were incubated with 1 mM 3,3'-dithiobis (sulfosuccinimidyl propionate) (DTSSP; Thermo Scientific) during 15 min at 4˚C. Quenching was carried out with 50 mM Tris, pH 7.4 for 15 min at RT and cells were extracted with crosslinking lysis buffer. Cell

lysates were collected, and coverslips were thoroughly washed with crosslinking washing buffer followed by incubation reducing buffer for 1 h at 37˚C to break the crosslinks. The whole crosslinked fractions and the cell lysates were separated by 10% SDS-PAGE and transferred to a PVDF (for protocol see above). Western-blots were analysed with ImageJ and the levels of crosslinked integrins were calculated as the relation between the crosslinked and the total integrin fractions (cell lysates + crosslinked fraction).

10.6. Adhesion on different stiffness

Softgel dishes made with polyacrylamide gels of 0.4, 4 and 50 kPa (Matrigen easy coat, Softwell) were coated with 400 µl of 10 µg/ml purified pFN during 1 h at RT and blocked 1 h with 1% BSA in PBS. An equal number of 7 x 10^5 fibroblasts were seeded on the coated softgels for 1 h, and the course of spreading was followed at 15, 30 and 60 min. For that purpose, pictures were taken with a Zeiss Axiovert microscope at these time points. In each experiment, 12 pictures were taken per condition. The number of cells in each field (picture) and their spreading area were quantified with ImageJ.

10.7. Focal Adhesion Kinase phosphorylation analysis

7 x 10^5 fibroblasts were plated on pFN-coated glass coverslips or polyacrylamide gels in DMEM for 1 h. After 1h of adhesion in the different substrates, cells were lysed in RIPA buffer (50 mM Tris, pH 7.4; 1% NP-40; 0.5% Na-Deoxycolate; 0.1% SDS; 2 mM EDTA) supplemented with proteinase inhibitors (Complete Proteinase Inhibitor Cocktail tablet, Roche), phosphatase inhibitors (Protease Inhibitors Cocktail 2 Aqueous Solution and Cocktail 3, Sigma-Aldrich), 1 mM Na_3VO_4 and 5 mM NaF for 10 min on ice, and sonicated for 1 min. The protein concentrations were quantified using the Pierce BCA Protein Assay Kit (Thermo Scientific) assay and 30–50 µg of protein was separated by 10% SDS-PAGE gel, transferred to nitrocellulose membranes and hybridized with specific antibodies (table 6). Western-blots were analysed with ImageJ and the levels of phospho-Tyr397- FAK or phospho-Tyr861FAK were referred to the total FAK content.

11. Haemostasis and platelets studies

11.1. Platelet isolation and quantification

To isolate platelets, heparinized blood extracted from *Itgb3*$^{+/+}$ or *Itgb3*$^{-/-}$ mice was centrifuged at 70 x g for 10 min at RT, the platelet enriched upper phase was then centrifuged at 800 x g for 10 min and the platelet pellet was finally washed twice with Tyrodes buffer pH 6.5. Washed platelets were resuspended in Tyrodes buffer pH 7.4 and counted using a ProCyte Hematology Analyzer (IDEXX Laboratories). For experiments, platelet numbers were adjusted to equivalent concentrations with Tyrodes buffer pH 7.4 complemented with 1 mM $CaCl_2$, 1 mM $MgCl_2$.

11.2. FN and fibrinogen quantification in isolated platelets and blood plasma

Platelets were isolated from *Fn1*$^{+/+}$and *Fn1*$^{syn/syn}$ heparinized blood as described above. About 5 x 10^6 platelets were lysed with 0,1% Triton in TBS with proteinase inhibitors (Complete

Proteinase Inhibitor Cocktail tablet, Roche) during 10 min on ice. After centrifugation at 13000 rpm, the supernatant was run in an 8% SDS-PAGE under reducing conditions, transferred to nitrocellulose membranes and incubated with anti-FN and anti-Fg antibodies (table 5). To quantify the plasma content of FN and fibrinogen, 2 ml of plasma were loaded onto the 8% SDS-PAGE. As a reference, human pFN (Calbiochem) and human fibrinogen (Sigma-Aldrich) were used. Western-blots were analysed with ImageJ. To know the FN levels in platelets derived from the different mouse genotypes the FN levels were related to their vinculin contents.

11.3. Whole blood platelet count

Blood from *Fn1*$^{syn/syn}$ or *Fn1*$^{+/+}$ mice was collected in heparinized Microvette CB 300 LH tubes (Sarstedt) and platelets were counted using a ProCyte Hematology Analyzer (IDEXX Laboratories, Ludwigsburg, Germany).

11.4. Microvascular thrombus formation and Intravital microscopy and tail bleeding assays

The analysis of thrombus formation *in vivo* by intravital microscopy and tail-bleeding assays were performed in the laboratory of Prof. C. Reichel.

- Analysis of microvascular thrombus

The surgical preparation of the mouse cremaster muscle was performed as described (Baez, 1973). Mice were anesthetized using a mixture of 100 mg/kg ketamine and 10 mg/kg xylazin. The left femoral artery was cannulated in a retrograde manner to administer FITC-labelled dextran (MW 150 kDa; Sigma-Aldrich). The right cremaster muscle was exposed through a ventral incision of the scrotum. The muscle was opened ventrally in a relatively avascular zone and spread over the pedestal of a custom-made microscopy stage. Epididymis and testicle were detached from the cremaster muscle and placed into the abdominal cavity. Throughout the surgical procedure and in vivo microscopy, the muscle was superfused with warm saline solution. At the end of each experiment, blood samples were collected by cardiac puncture to determine systemic cell counts using a haematology analysis system (ProCyte DX, IDEXX Laboratories).

Microvascular thrombus formation was induced by phototoxic injury as described (Rumbaut *et al.*, 2005) with slight modifications. Briefly, after surgical preparation of the cremaster muscle, 4 ml/kg body weight of a 2.5% solution of FITC-dextran was infused intraarterially and the exposed the vessel segment under investigation was continuously epi-illuminated with a wavelength of 488 nm (Polychrome II, TILL Photonics). An Olympus water immersion lens (60x /NA 0.9) in an upright microscope (BX50; Olympus Microscopy) was used to focus the light onto the cremaster muscle and to visualize the microvascular thrombus formation in real-time. Thrombus formation was induced in one arteriole (25–35 mm) per experiment by analysing the time until the first platelet adhesion to the vessel wall (defined as the onset of thrombus formation) occurred and the time until blood flow ceased (defined as the complete occlusion of the vessel).

- Tail bleeding assay

Using anesthetized mice directly after the analysis of microvascular thrombus formation. For this purpose, the distal 2 mm segment of the tail was cut with a scalpel. Bleeding was monitored by absorbing the bead of blood with a filter paper in 30 secs intervals without touching the wound. Tail bleeding time was defined as the time until haemorrhage ceased.

11.5. *In vitro* platelet aggregation

Platelet aggregation was measured with 1 x 10^8 washed platelets stimulated with 0.5 U/ml thrombin (Sigma-Aldrich) or 5 mg/ml fibrillar type I collagen (Nycomed) in the presence of 10 µg/ml pFN isolated either from *Fn1*$^{+/+}$ or *Fn1*$^{syn/syn}$ mice. For platelet aggregation with 20 mM ADP, platelet rich plasma (PRP) was isolated. The mouse blood was collected with 3.8% sodium citrate buffer (1:9, buffer:blood), centrifuged at 110 x g and the supernatant (PRP) was collected. A volume of 225 ml of PRP containing 6.75 x 10^7 platelets was used for each experiment adding 20 mM ADP. Light transmission was recorded with a ChronoLog aggregometer over 15 min as arbitrary units with the transmission through buffer defined as 100% transmission.

11.6. Platelet adhesion in static conditions

To study platelet spreading, glass bottom dishes were coated with 10 µg/ml of pFN^{wt}, pFN^{syn}, fibrinogen (Sigma-Aldrich) or soluble collagen type I (PureCol, Advanced Biomatrix) at RT for 1 h and blocked with 1% BSA in PBS. Washed platelets (0.5–1 x 10^6) were added to the dishes in a final volume of 1 ml and activated with 0.01% thrombin (Sigma-Aldrich). Images were taken after 15, 30 and 60 min under a differential interference contrast microscopy (Zeiss Axiovert 200M microscope with a Plan-NEOFLUAR, x 100, 1.45 oil objective; Zeiss) using the MetaMorph software (Molecular Devices). The platelet spreading area was analysed using the ImageJ software.

11.7. Platelet adhesion under flow

Flow chamber experiments were carried out as described previously (Schulz et al., 2009) using the air-driven continuous flow pump system from Ibidi (Fig. 21). Briefly, platelets were isolated, fluorescently labelled with 5 mM carboxyfluorescein succinimidyl ester (CFSE; Invitrogen) in Tyrodes buffer pH 6.5 for 15 min and then washed. To achieve near-physiological conditions during perfusion of the coated flow chamber slides, 2 ml of washed platelets with a platelet count of 1 x 10^7 were combined with 1 ml of human erythrocytes isolated from the blood of a healthy volunteer (see below). For each experiment, 4 channels of a flow chamber slide (µ-Slide VI 0.1 ibiTreat, Ibidi) were coated with 10 µg/ml fibrillar collagen, fibrinogen, pFN^{wt} or pFN^{syn} over night at 4˚C and blocked with 1% BSA the following day. The coated channels of one µ-slide were connected in series with connector tubing for simultaneous perfusion. The platelet suspension was filled in one reservoir of a Perfusion Set Black (Ibidi) and the pump was started with unidirectional flow at the highest possible pressure (100 mbar) until all channels were filled with the blood-like fluid. Then, the experiment was started by adjusting the shear rate to approximately 1000/s. The channels were perfused for 10 min and

subsequently washed by perfusing Tyrode´s buffer for another 10 min. Platelets were imaged after performing the perfusion with a Zeiss Apotome microscope and platelet surface coverage per field was analysed using ImageJ.

- Erythrocytes isolated from human blood

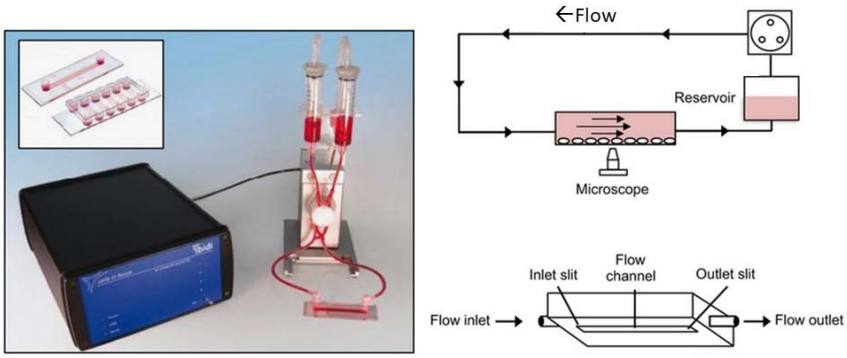

Figure 21. Scheme of flow-chamber. Platelets and erythrocytes are placed in the reservoirs (syringes) and the pump pulse them through the tubing to the chamber. In the chamber the sample circulates across the channel and it can be visualized with a microscope. The sample leaves one of the reservoirs and returns to the other.

Blood was collected in 10% EDTA (0.5 M). To separate the plasma and blood cells from the erythrocytes, whole blood was centrifuged at 500 x g for 10 min at 4 °C and supernatant was aspirated. Next, Tyrode´s was added to wash the erythrocyte pellet (in a 2:1, buffer:pellet ratio) and erythrocytes were again centrifuged. Two additional washes were done to reach a haematocrit of 70-80% for adhesion experiments in flow chambers.

12. Statistics

Data are represented as the average of the different experiments performed together with the standard deviation of the mean (SEM). All experiments were performed at least three times. The sample size is indicated in the results or figure legend. In every experiment, control and treatment (or wild-type and mutant) were handled in parallel to obtain paired samples. To calculate the significance of differences among conditions or between mutant and wild-type, t-student test was employed considering a normal distribution of the sample. Differences were considered as statistically significant when p-value<0.05 (*p<0.05, **p<0.01 and ***p<0.001).

ANNEX I

Buffers and Medium

DNA lysis buffer: 20 mM NaCl, 100 mM Tris-HCl pH 7.6, 5 mM EDTA, 0.2% SDS and 100 µg/ml of proteinase K

DNA 6x loading buffer: 0.2% Orange G w:v, 60% Glycerol v:v in 0.5 M EDTA

TAE buffer: 40 mM Tris-Acetate, 1 mM EDTA

PBS: 137 mM NaCl, 2.7 mM KCl, 8 mM Na_2HPO_4, and 2 mM KH_2PO_4

TBS: 0.15 M NaCl in 10 mM Tris-HCl, pH 7.4

FACS buffer: 3% BSA (bovine serum albumin; Pan Biotech) in TBS

RIPA buffer: 50 mM Tris, pH 7.4; 1% NP-40; 0.5% Na-Deoxycolate; 0.1% SDS; 2 mM EDTA supplemented with proteinase inhibitors (cOmplete Proteinase Inhibitor Cocktail tablet, Roche)

Rho-lysis buffer: 20 mM Hepes, 150 mM NaCl, 1% Triton X-100, 5 mM $MgCl_2$

HBS buffer: 20 mM Hepes, 150 mM NaCl, 5 mM $MgCl_2$

Regular cell medium: DMEM (Dulbecco's Modified Eagle's medium, Gibco), 10% (v:v) FBS (fetal bovine serum, Gibco) and 1% (v:v) penicillin-streptomycin and split using trypsin-EDTA (Gibco)

SRM: 6.5% AIM-V (Life Technologies), 5% RPMI (Life Technologies) and 1% NEAA (Non-Essential Amino Acid Solution, Sigma-Aldrich)

Luria-Bertani (LB) broth: 1% Triptona, 0.5% Yeast extract and 1% NaCl (w:v)

Laemmli buffer: 60 mM Tris-HCl pH 6.8, 2% SDS, 5% Glycine, 0.01% Bromophenol blue and 2% β-mercaptoethanol

Comassie Blue stain solution: 0.125% Coomasie blue (w:v), 50% Methanol (v:v), 10% Acetic Acid (v:v)

Comassie Blue destain solution: 40% Methanol (v:v), 10% Acetic Acid (v:v)

Protein Electrophoresis Buffer: 250 mM Glycine, 25 mM Tris-HCl, 1% SDS

Blotting buffer: 250 mM Glycine, 25 mM Tris-HCl, 20% MetOH

TBST: 0.1% Tween20 in TBS; v:v

DOC buffer: 2% Sodium Deoxycolate, 2 mM Tris-HCl pH8.8, 2 mM EDTA, supplemented with proteinase inhibitors (cOmplete Proteinase Inhibitor Cocktail tablet, Roche)

DOC solubilization buffer: 1% SDS in 2mM Tris-HCl pH8.8, 2mM EDTA, supplemented with proteinase inhibitors (cOmplete Proteinase Inhibitor Cocktail tablet, Roche)

Citrate buffer: 10 mM $Na_3C_6H_5O_7$ pH 6, and 0,01% Tween

DENT´s fixative: 80% Methanol, 20% DMSO

FN purification washing buffer: 0.5 NaCl in 10 mM Tris-HCl pH7.4

Quenching buffer: 50 mM Tris-HCl, pH 7.4

Crosslinking lysis buffer: 20 mM Tris-HCl, pH 7.4, 0.1% SDS and proteinase inhibitors (cOmplete cocktail)

Crosslinking washing buffer: 20 mM Tris-HCl, pH 8.5

Reducing buffer: 20 mM Tris-HCl, pH 8.5, 0.1% SDS and 25 mM DTT

RIPA buffer (50 mM Tris, pH 7.4; 1% NP-40; 0.5% Na-Deoxycolate; 0.1% SDS; 2 mM EDTA) supplemented with proteinase inhibitors (Complete Proteinase Inhibitor Cocktail tablet, Roche),

Tyrodes buffer:134 mM NaCl, 2.9 mM KCl, 12 mM $NaHCO_3$, 10 mM N-2-hydroxyethylpiperazine-N-2-ethanesulfonic acid, 5 mM glucose, 0.35% BSA

IV RESULTS

Chapter I. Analysis of the role of the RGD motif in FN fibrillogenesis

Chapter II. Study the FN synergy site function

IV RESULTS

Chapter I. Analysis of the role of the RGD motif in FN fibrillogenesis

1. Characterization of *Fn1*$^{\Delta RGD/\Delta RGD}$ fibroblasts

To investigate the function of the RGD motif of the FNIII10 module in fibrillogenesis, three cell lines of fibroblast were used. Wild-type fibroblasts (*Fn1*$^{+/+}$), fibroblasts which lack the RGD sequence (*Fn1*$^{\Delta RGD/\Delta RGD}$), and fibroblasts with a substitution RGD>RGE (*Fn1*$^{RGE/RGE}$). The last described in Takahashi *et al.*, 2007 and proved able to assemble FN matrix by interaction through αv integrins. In the initial cell-fibronectin interaction and posterior fibrillogenesis, there are two major cell components involved: cell receptors and the actin-myosin cytoskeleton (Schwarzbauer and DeSimone, 2011). Therefore, the expression of major FN receptors (integrins and syndecans) as well as the activity of an important actin-myosin regulator (RhoA) were initially analysed.

1.1. Integrin expression on cell surface

Fibroblasts express different integrin receptors on their surface to bind distinct ligands. The most important integrins for this study are those which bind and assemble FN: α5β1, αvβ3 and α4β1 (Leiss *et al.*, 2008). To determine which integrins are expressed and to compare their levels at the surface on each cell line, cells were analysed by flow cytometry. Single staining showed that the three cell lines presented similar levels of α5, β1 and β3 (Fig. 22). Unexpectedly, the *Fn1*$^{RGE/RGE}$ had lower levels of integrin αv compared to *Fn1*$^{\Delta RGD/\Delta RGD}$ and *Fn1*$^{+/+}$, and none of the fibroblasts expressed appreciable levels of α4 integrins. Therefore, FN binding and assembly through integrins in the three cell lines cannot by produced by α4β1/β7 but they can use α5β1, αvβ3 and probably other αv-class integrins.

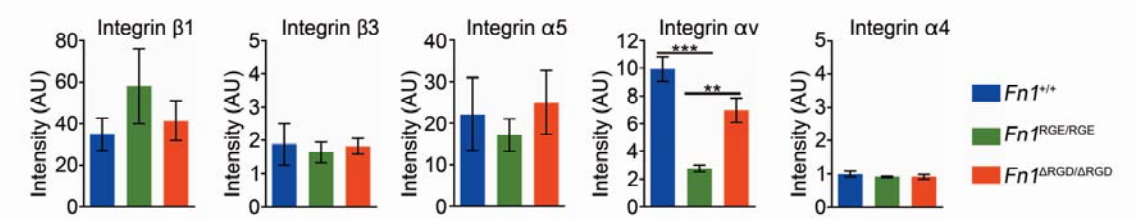

Figure 22. Quantification of the integrin levels at the surface of the *Fn1*$^{+/+}$, *Fn1*$^{RGE/RGE}$ and *Fn1*$^{\Delta RGD/\Delta RGD}$ fibroblasts. All the intensities obtained with the antibodies labelling were relativized to the intensity of the isotype control for each of them, therefore intensities values near 1 mean that the antibody and the isotype control are similar. N=3 experiments; 10,000 cells analyzed per experiment

1.2. Syndecans expression

Syndecans are a family of 4 transmembrane heparin/chondroitin sulphate proteoglycans, which can have different expression patterns. While syndecan-4 is broadly expressed, syndecan-1 is predominant in epithelial cells, syndecan-2 in mesenchymal derived cells and syndecan-3 is early in development widespread and later primarily found in neuronal tissues (Xian *et al.*, 2010). Considering this different expression pattern and that the three cell lines were derived from embryonic stem cells, the expression of syndecans was first analysed by quantitative PCR (qPCR). The same amount of isolated mRNA from the three cell lines, was

retrotranscribed to cDNA to quantify the expression levels of the 4 syndecans (sdc1-4). The normalized results of qPCR showed that, although at different levels, the three cell lines expressed all 4 syndecans (Fig. 23).

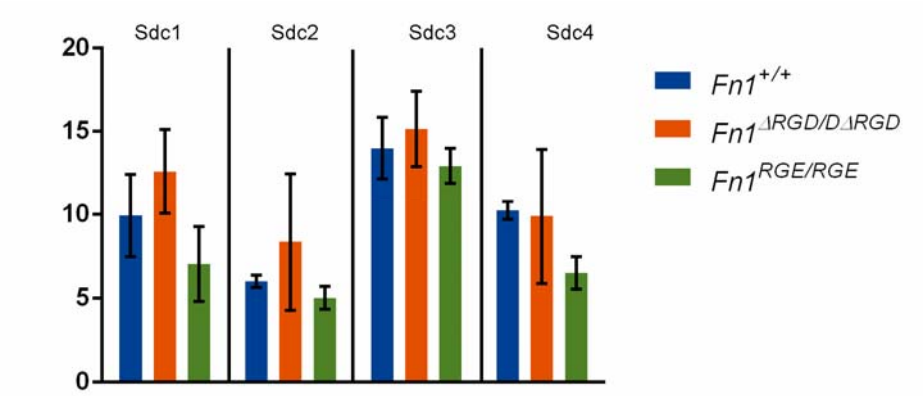

Figure 23. Analysis of the syndecan expression in *Fn1*$^{+/+}$, *Fn1*$^{RGE/RGE}$ and *Fn1*$^{\Delta RGD/\Delta RGD}$ fibroblasts by qPCR. Syndecan expression was relativized to mRNA of the housekeeping gene *gapdh*. Bars represent the average of 4 technical replicates of the same experiment

To corroborate that syndecan mRNAs were also translated into proteins, cell lysates were used to analyse syndecan levels by western blot (Fig. 22). The relative level of syndecan-1 was higher in *Fn1*$^{\Delta RGD/\Delta RGD}$ (6 folds) and *Fn1*$^{RGE/RGE}$ (3 folds) fibroblasts compared to wild-type cells. Syndecans-2, 3 and 4 levels were also 3, 1.5 and 3.6 folds higher in *Fn1*$^{\Delta RGD/\Delta RGD}$ cells, respectively, in comparison to *Fn1*$^{+/+}$. The *Fn1*$^{RGE/RGE}$ fibroblasts expressed higher levels of syndecans-2, 3 and 4 (2, 1 and 2.7 folds respectively) than *Fn1*$^{+/+}$cells. Still *Fn1*$^{\Delta RGD/\Delta RGD}$ cells expressed higher levels of syndecans than *Fn1*$^{+/+}$ and *Fn1*$^{RGE/RGE}$ (Fig. 24).

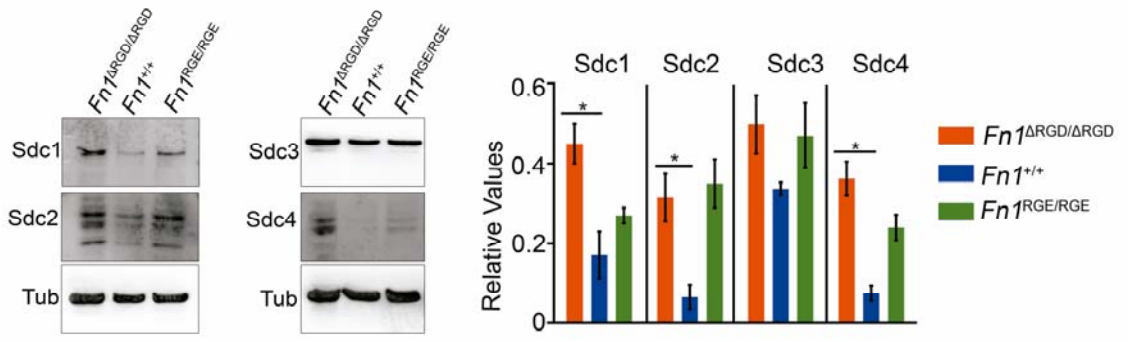

Figure 24. Analysis of the protein expression syndecan 1-4 in *Fn1*$^{+/+}$, *Fn1*$^{RGE/RGE}$ and *Fn1*$^{\Delta RGD/\Delta RGD}$ fibroblasts by western blot, is shown a reperentative experiment. Syndecan expression was relativized to tubulin levels. Histogram: mean values and signification of sdcs 1-4 expression. 3 independent experiments.

Syndecan-4 was additionally, analysed by FACS, to confirm its surface levels, and we observed that *Fn1*$^{\Delta RGD/\Delta RGD}$ cells present this receptor in its surface at 2-fold higher levels than *Fn1*$^{+/+}$ fibroblast (Fig. 25).

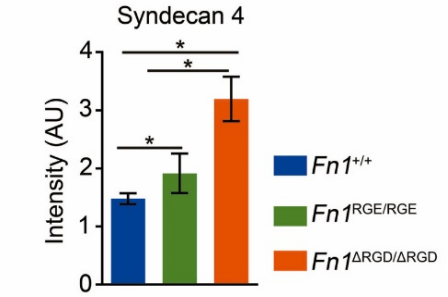

Figure 25. Analysis of syndecan 4 levels at the surface of the *Fn1*$^{+/+}$, *Fn1*$^{RGE/RGE}$ and *Fn1*$^{\Delta RGD/\Delta RGD}$ fibroblasts. All the intensities obtained were relativized to the intensity of the isotype. N=3 experiments; 10000 cells analyzed per experiment.

1.3. RhoA activity

Actin-myosin cytoskeleton contraction is important for FN fibrillogenesis to transmit force through the FN receptors to unfold the FN and assemble it into fibrils (Baneyx *et al.*, 2002; Mao and Schwarzbauer, 2005). RhoGTPases regulate actin cytoskeletal dynamics and RhoA specifically is implicated in stress fibres arrangement (Danen *et al.*, 2002). As RhoA activity is important for FN matrix assembly, levels of active (GTP-bound) RhoA were measured to test whether RhoA was equally functional in *Fn1*$^{\Delta RGD/\Delta RGD}$, *Fn1*$^{RGE/RGE}$ and *Fn1*$^{+/+}$ fibroblasts. For that purpose cells were seeded on laminin coated surfaces and GTP-bound RhoA was pull-down with RBD (Rho Binding Domain) of Rhotekin (Ren, *et al.* 1999). Activated RhoA was identified in the RBD-pull-down fraction by western blot and normalized to total RhoA and tubulin levels; and no major differences were observed between the three cell lines (Fig. 26). Cells bind laminin through integrins which could activate RhoA, so fibroblasts were seeded on polylysine to test whether RhoA could be activated by the ECM secreted by themselves. Polylysine is positively-charged and mediates electrostatic interactions with the negative charged ions of the cell membrane. Thus, the measured activated RhoA in this case is unspecific of the coating used but specific of the ECM secreted by each cell line. Levels of relative GTP-bound RhoA in the three cell lines were similar. These results confirmed that *Fn1*$^{\Delta RGD/\Delta RGD}$, *Fn1*$^{RGE/RGE}$ and *Fn1*$^{+/+}$ fibroblasts activate RhoA in the same levels (Fig. 26).

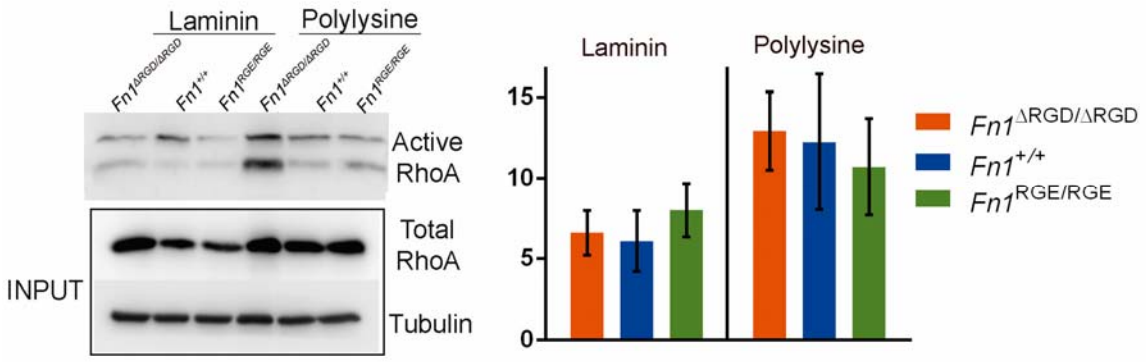

Figure 26. RhoA active (GTP-bound) levels in *Fn1*$^{+/+}$, *Fn1*$^{RGE/RGE}$ and *Fn1*$^{\Delta RGD/\Delta RGD}$ fibroblasts when seeded on laminin or polylysine. Values of active RhoA were relativized to tubulin and total RhoA in the input. Graphs represents average and SEM; N=3.

2. Deletion of the RGD sequence does not abolish FN fibrillogenesis

Embryos expressing FN that lacks the RGD sequence die at E9.5 an stage similar to FN-null mice. However, surprisingly, FN fibrils were visible in their tissues. To decipher how $FN^{\Delta RGD}$ fibrillogenesis takes place, several FN matrix assembly analyses were done *in vitro*. For that purpose, the matrix assembled by fibroblast expressing $FN^{\Delta RGD}$ ($Fn1^{\Delta RGD/\Delta RGD}$) was compared to the one assembled by wild-type and by $Fn1^{RGE/RGE}$ (expressing mutant FN^{RGE}) fibroblasts.

To initially study $FN^{\Delta RGD}$ fibrillogenesis, the three cell lines were seeded onto glass coverslips coated with different ECM proteins: laminin, vitronectin, collagen I and gelatine, and the process of assembly was analysed after 24, 72 and 120 h by immunofluorescence to detect FN (green), actin (red) and paxillin (white), protein that is recruited to focal adhesions (FA). Different proteins were used to coat the glass in order to roll out whether this would affect FN assembly since they are ligands of distinct integrins. Hence, fibroblasts bind predominantly laminin via α6β1 integrin, vitronectin by αvβ3/5, collagen I via α1β1 and gelatine via αvβ3 (Davis, 1992; Taubenberger *et al.*, 2010).

2.1. FN matrix assembly on laminin

When wild-type cells adhered to laminin (Fig. 27 A-C), reorganized the actin cytoskeleton in stress fibres from the first day, and the paxillin was located both at the tip of the FAs at the cell centre of the cell forming fibrillar adhesions. The first FN^{wt} fibrils were thin and short and localized at the centre of the cell after 24 h of plating cells on laminin. This FN network became denser in the following hours, consisting of long and thin fibrils almost parallel to the actin fibres and surrounding the cells (Fig. 27 A). The $Fn1^{RGE/RGE}$ fibroblasts, as it has been described (Takahashi *et al.*, 2007), elaborated a fibrillar FN matrix in the periphery of the cell, composed by shorter and thicker fibrils (Fig. 27 B). Contrary to $Fn1^{\Delta RGD/\Delta RGD}$ fibroblast, the $Fn1^{RGE/RGE}$ cells assembled elongated FA and most of the cells contained stress fibres across the cell body. The $Fn1^{\Delta RGD/\Delta RGD}$ fibroblast (Fig. 27 C) adhered well to laminin although they arranged less stress fibres across the cell and most of the actin was in the periphery of the cell. The $Fn1^{\Delta RGD/\Delta RGD}$ fibroblast assembled FA that were wide and with a fan shape instead of the typical thin and elongated observed in wild type fibroblasts, and most lacked paxillin. Interestingly, most of the paxillin remained diffusely distributed in the cytosol and was incorporated into the FAs at later times. In $Fn1^{\Delta RGD/\Delta RGD}$ fibroblast FN was principally located inside the cell during the first 24h, and in few short fibrils at the tips of the cells. In the following hours the matrix slightly increased in complexity, but the FN fibrils remained short and thick at the tips of the cells, never at the centre.

2.2. FN matrix assembly on vitronectin

On vitronectin, where fibroblasts adhere by αvβ3 or αvβ5 integrins, $Fn1^{\Delta RGD/\Delta RGD}$, $Fn1^{RGE/RGE}$ cells as well as the wild type could nicely adhere, form stress fibres and incorporate paxillin into FAs and fibrillar adhesions (Fig. 27 D-E). However, the FN matrix produced by $Fn1^{\Delta RGD/\Delta RGD}$ cells was again abnormal consisting of few heterogeneous thick and short fibrils (Fig. 27 F). This result suggested that $FN^{\Delta RGD}$ fibrillogenesis process is uncoupled from the

traction forces generated by the stress fibres which cannot be used to pull efficiently the FN dimers.

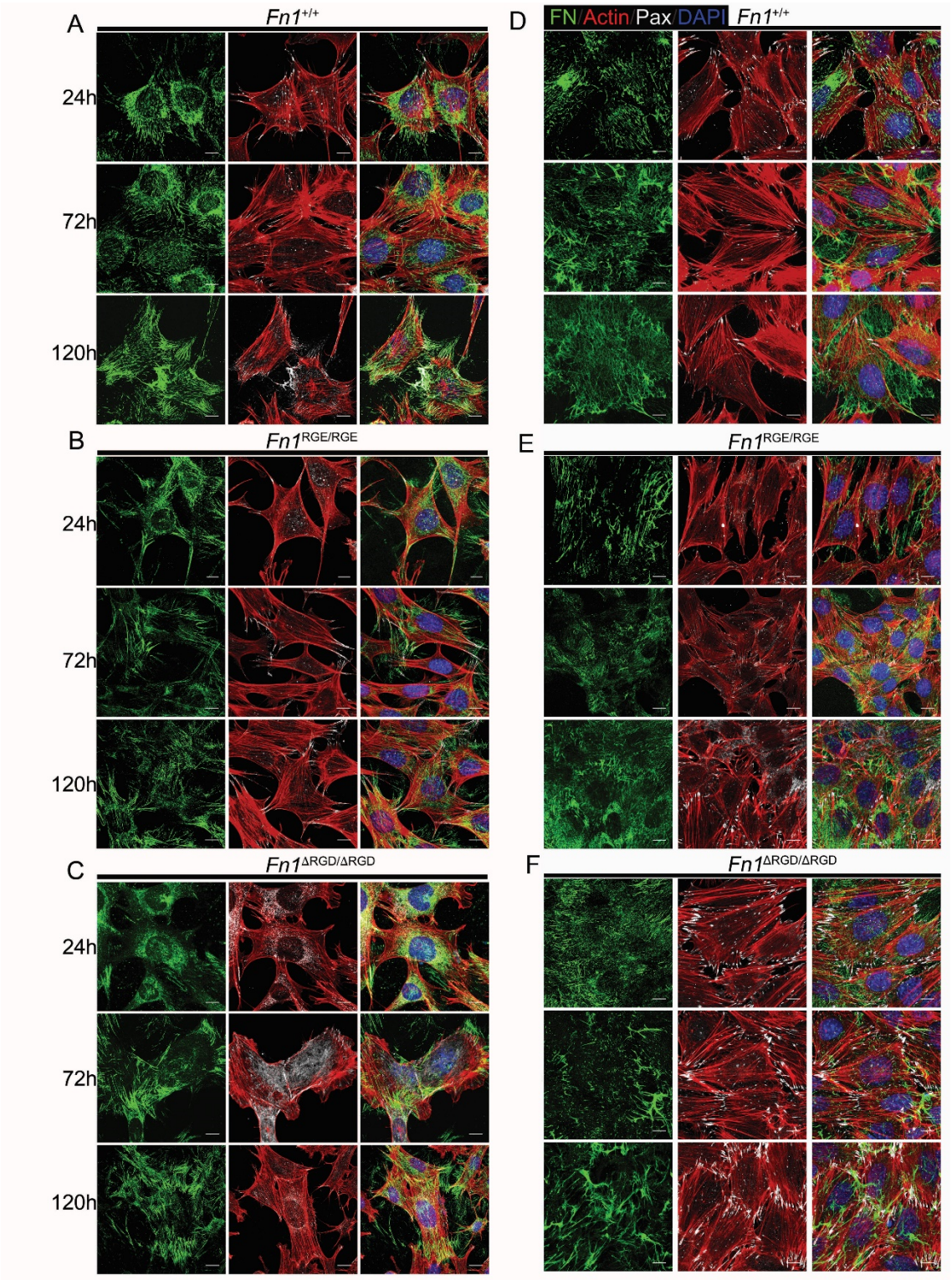

Figure 27. The deletion of the RGD site in FN does not abolish fibril assembly on laminin (A-C) or vitronectin (D-F). (**A** and **D**) Wild-type fibroblasts assemble an organized and dense fibrillary matrix of FN (in green) over the time-course studied (24, 72 and 120h). FN fibrils are in the centre of the cell aligned with the actin cytoskeleton (stained as phalloidin in green) as well as in the periphery of the cell where focal adhesions (paxillin positive; in white) are located. (**B** and **E**) The RGE mutation allows the formation of a fibrillar matrix exclusively in the periphery of the cell, characteristic of fibrillogenesis carried out by αv-integrin. (**C** and **F**) Fibroblasts containing the ΔRGD mutation are able to secrete and assemble the mutated FN. However, at 24h there are still lot of intracellular $FN^{\Delta RGD}$. The $FN^{\Delta RGD}$ fibrils are thicker and the matrix form by these cells looks disorganized. Staining: fibronectin in green; actin stain as phalloidin in red; paxillin in white and dapi in blue. Scale bar: 10µm.

2.3. FN matrix assembly on collagen type I and gelatine

On collagen type I and gelatine, *Fn1*$^{+/+}$ as well as *Fn1*$^{RGE/RGE}$ cells formed structured FN fibrils like in the other substrates (Fig. 28 A-B), however *Fn1*$^{RGE/RGE}$ cells on gelatine do not assemble robust FN fibrils till 72 h in comparison to *Fn1*$^{+/+}$. *Fn1*$^{\Delta RGD/\Delta RGD}$ needed longer time to spread on collagen type I and gelatine and form the first FN fibrils compared to *Fn1*$^{+/+}$ or *Fn1*$^{RGE/RGE}$ cells. After extended culture (120 h) FN$^{\Delta RGD}$ formed irregular networks with thick and short fibrils (Fig. 28 A-B). This suggests that the cytoskeleton cannot be rearranged and exert enough pulling forces to extend and assemble the FN when *Fn1*$^{\Delta RGD/\Delta RGD}$ adhered to collagen or gelatine. Significantly, on gelatine the *Fn1*$^{\Delta RGD/\Delta RGD}$ cells could not spread and formed few FN fibrils that were thick and formed clumps (Fig. 28 B). Gelatine is collagen I denatured that offers RGD motifs that were cryptic in the native conformation allowing αvβ3 binding but no α5β1 binding (Davis, 1992; Taubenberger *et al.*, 2010), as vitronectin. However, we observed that while on vitronectin the *Fn1*$^{+/+}$ and *Fn1*$^{RGE/RGE}$ assembled big stress fibres and FA and a complex FN matrix after 24 h, on gelatine they needed more time and these structures were evident after 72 h. In addition, *Fn1*$^{\Delta RGD/\Delta RGD}$ on gelatine did not spread well after 72 h, whereas on vitronectin they could spread already at 24 h. These observations suggest that αvβ3 interaction with the exposed RGD in the collagen does not activate integrins to trigger signalling and further actin polymerization as fast or as efficiently as interaction with vitronectin does.

Altogether, these data indicate that, independently of the substrate and despite the differences in cell spreading, the FN$^{\Delta RGD}$ fibrils are assembled more slowly than the wild type FN and form abnormal networks that are less dense with shorter and irregular fibrils.

2.4. Quantification of FN fibrils by western blot

Since the *Fn1*$^{\Delta RGD/\Delta RGD}$ fibroblasts appear to form less fibrils and those were assembled in less structured and complex matrix, we wanted to quantify the proportion of insoluble matrix formed on each condition. To this end, FN precipitation with deoxycholate (DOC) was employed to measure the amount of fibrillar FN (Sottile and Hocking, 2002). The three cell lines were seeded on laminin and cultured during 24, 72 and 120 h and lysated with the DOC buffer to precipitate and hence separate the fibrillar from the soluble (intracellular) FN. As shown in figure 29 quantification of FN by western blot demonstrated that the levels of fibrillar FN$^{\Delta RGD}$ were reduced by 30-40% in all studied time points in comparison to FN^{WT} and FN^{RGE} (Fig. 29 A-B, D-E, G-H). Nevertheless, the intracellular FN levels were similar in the three cell lines (Fig. 29 C, F, I). It is worth noting that while levels of fibrillar FN augmented with time, the amount of intracellular decreased in the three cell lines, suggesting that either the secretion of FN is more efficient with the time or the biosynthesis decreases after the cell forms its matrix. The second option is however in contradiction with the fact in Fn*1*$^{\Delta RGD/\Delta RGD}$ there is a similar reduction although their FN matrix is smaller than in wild type fibroblasts.

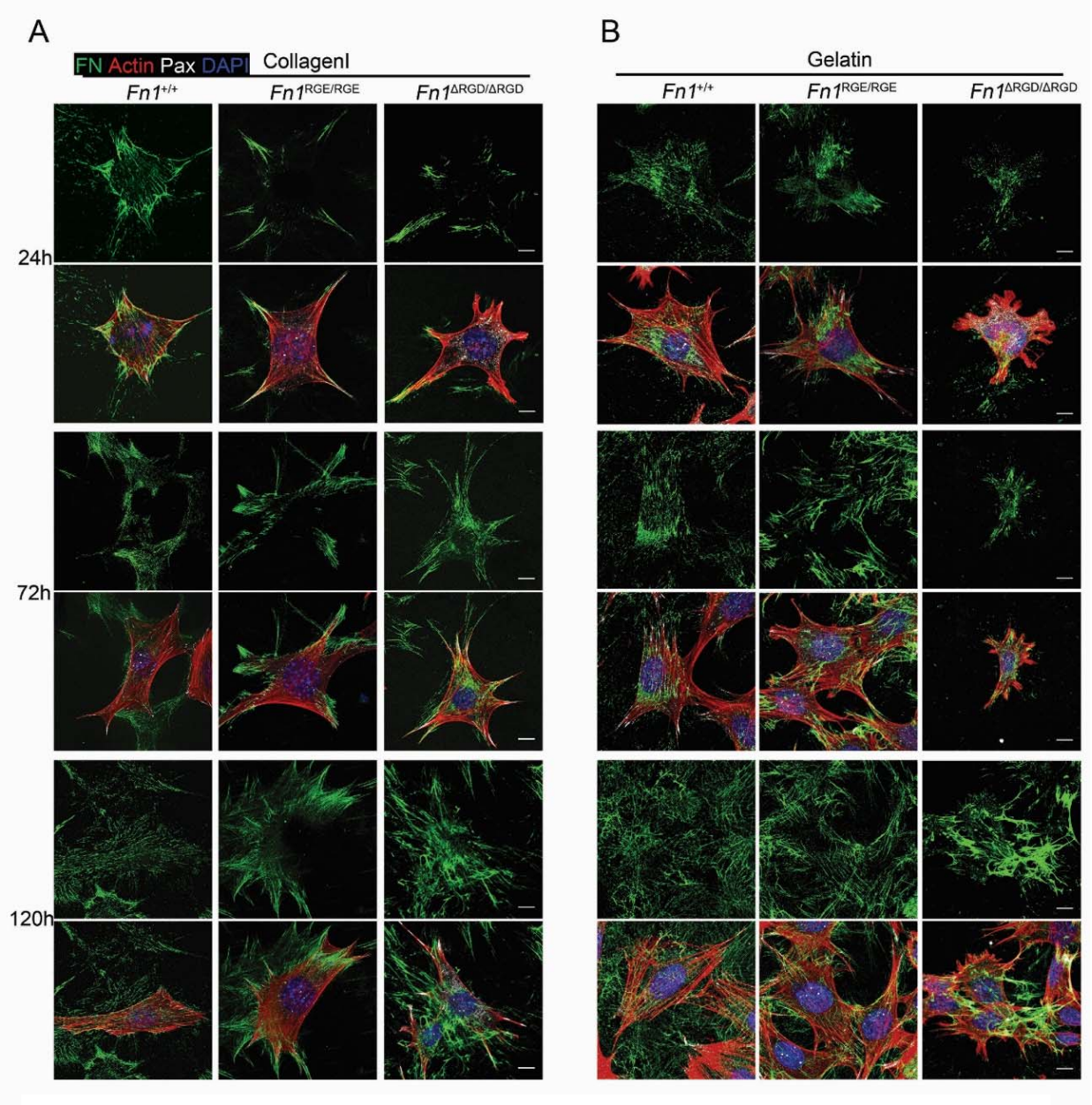

Figure 28. The deletion of the RGD site in FN does not abolish fibril assembly on collagen I (A) or gelatine (B). **(A)** FN matrix assembly by *Fn1*$^{+/+}$, *Fn1*$^{\Delta RGD/\Delta RGD}$ and *Fn1*$^{RGE/RGE}$ on collagen I. **(B)** FN matrix assembly by *Fn1*$^{+/+}$, *Fn1*$^{\Delta RGD/\Delta RGD}$ and *Fn1*$^{RGE/RGE}$ on gelatin. Staining: fibronectin in green; actin stain as phalloidin in red; paxillin in white and dapi in blue. Scale bar: 10µm.

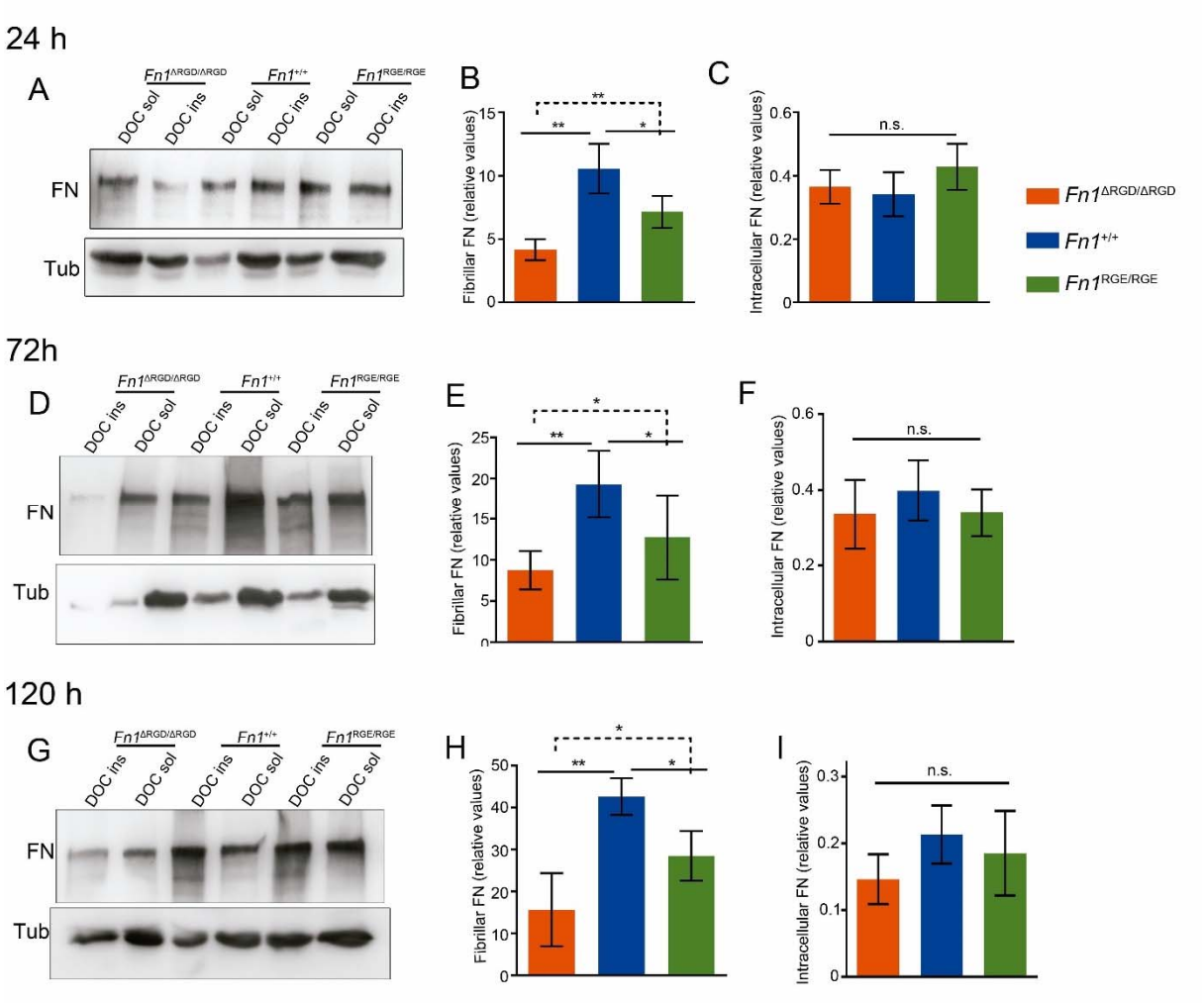

Figure 29. Quantification of fibrillar FN in cell culture. Fibrillar FN precipitated with DOC and soluble FN after 24 h (**A**), 72 h (**D**) and 120 h (**G**) of cell culture. Quantification of the levels of fibrillar FN after 24 h (**B**), 72 h (**E**) and 120 h (**H**) relativized to soluble FN. (**C**) Levels of cellular soluble FN after 24 h (**C**), 72 h (**F**) and 120 h (**I**), relativized to tubulin. Represented average and SEM; N=8 for 24 h, and N=3 for 72 and 120 h.

2.5. Quantification of secreted FN by western blot

To analyse whether the reduced FN matrix assembled by *Fn1*$^{\Delta RGD/\Delta RGD}$ fibroblasts was owed to a reduced secretion of FN, the levels of FN in the medium conditioned by the cells were measured by western blot. Soluble FN was significantly elevated in the conditioned medium by *Fn1*$^{\Delta RGD/\Delta RGD}$ and *Fn1*$^{RGE/RGE}$ cells in all time points, while there was almost no appreciable soluble FN in the medium from *Fn1*$^{+/+}$ fibroblasts over the studied time-course (Fig. 30 A-FC). The amount of soluble FN in the medium from conditioned *Fn1*$^{\Delta RGD/\Delta RGD}$ fibroblasts was already high after 24 h in comparison to *Fn1*$^{+/+}$ and *Fn1*$^{RGE/RGE}$ cells (Fig. 30 A). These results indicate that FN is secreted but not efficiently assembled into a fibrillar matrix in *Fn1*$^{\Delta RGD/\Delta RGD}$ fibroblasts and that *Fn1*$^{RGE/RGE}$ cells are in an intermediate situation.

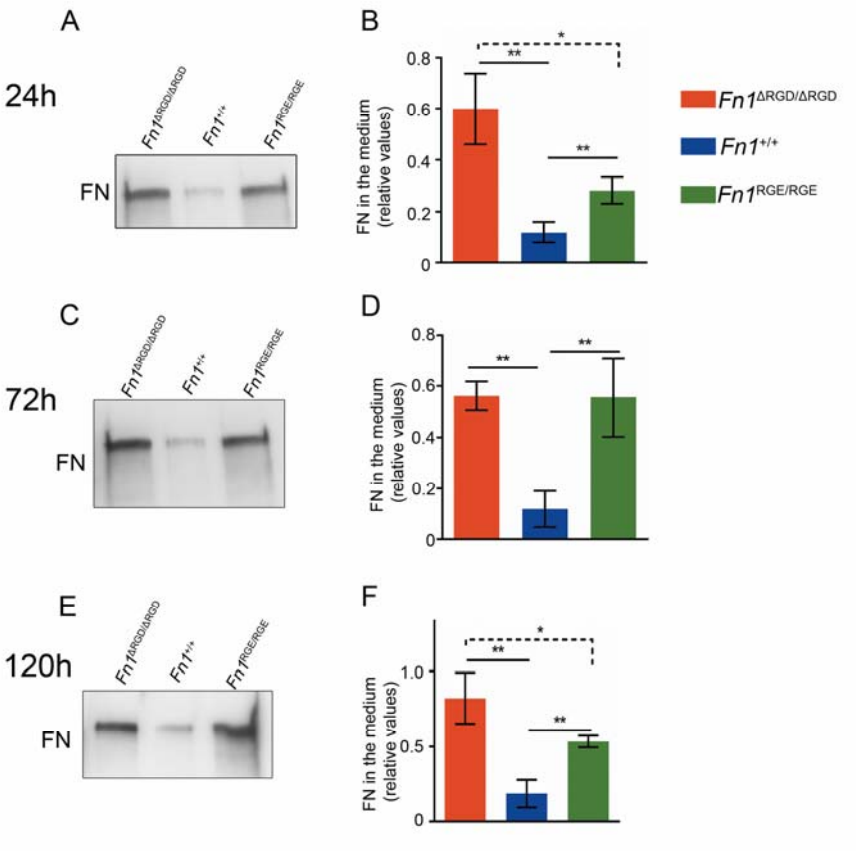

Figure 30. Soluble FN levels in the medium conditioned by fibroblasts *Fn1*$^{\Delta RGD/\Delta RGD}$, *Fn1*$^{+/+}$ or *Fn1*$^{RGE/RGE}$. FN found in the medium after 24 h (**A, B**), 72 h (**C, D**) and 120 (**E, F**) of cell culture and its quantification. FN levels were normalized (relative) to tubulin levels in figure 27. Represented average and SEM; N=8 for 24 h, and N=3 for 72 and 120 h.

3. FNIII$_{12\text{-}14}$ motif is involved FN$^{\Delta RGD}$ fibrillogenesis

FN fibrillogenesis has been described as a cell driven process mediated by cellular receptors (Singh *et al.,* 2010). The analysis of the integrin profile in *Fn1*$^{\Delta RGD/\Delta RGD}$ fibroblasts by FACS showed that these cells lack α4 integrins on their surface (Fig. 22), therefore this receptor is not responsible of the RGD-independent FN assembly (Sechler *et al.*, 2000) in the *Fn1*$^{\Delta RGD/\Delta RGD}$ fibroblasts. However, we demonstrated that *Fn1*$^{\Delta RGD/\Delta RGD}$ fibroblasts express syndecans 1-4 and in higher levels than wild type cells (Fig. 24). Syndecans have been shown to co-localize with integrins in the periphery of focal adhesions (Morgan *et al.*, 2007). Syndecan-4 was shown to cooperate with α5β1 integrins in mediating FN signalling and cytoskeleton reassembly (Simons and Horowitz, 2001; Morgan *et al.*, 2007). The syndecans have also been described as mediating FN fibril assembly in cooperation with integrins (Morgan, Humphries and Bass, 2007; Choi *et al.*, 2011). Syndecans bind to FN by their heparin sulphate lateral chains. To study whether these receptors are involved in FN$^{\Delta RGD}$ fibrillogenesis, we used heparin to block in the FN molecule the sites of syndecan binding and performed matrix assembling experiments.

3.1. FN matrix assembly blocking the heparin binding sites

To analyse whether syndecans are mediating $FN^{\Delta RGD}$ fibrillogenesis, assembly assay was performed in the presence of heparin (0.1 mg/ml). The 3 cell lines (*Fn1*$^{+/+}$, *Fn1*$^{RGE/RGE}$ and *Fn1*$^{\Delta RGD/\Delta RGD}$) were seeded on laminin for 3 h and then heparin was added to the medium. After 24 h *Fn1*$^{+/+}$ cells formed a nice and dense FN network similar to the produced without heparin (Fig. 31 A). The heparin treatment did not affect FN^{RGE} fibrillogenesis as well and *Fn1*$^{RGE/RGE}$ fibroblasts could form FN fibrils after 24 h in a similar manner than the non-treated *Fn1*$^{RGE/RGE}$ cells (Fig. 31 B). However, the heparin treatment blocked completely the FN network assembly in *Fn1*$^{\Delta RGD/\Delta RGD}$ fibroblasts and only some FN was visible in the cell cytosol. Moreover, the *Fn1*$^{\Delta RGD/\Delta RGD}$ cells could not fully spread in the presence of heparin (Fig. 31 C). To discard that $FN^{\Delta RGD}$ fibrillogenesis was impaired in presence of heparin due to spreading defects, identical experiments with *Fn1*$^{+/+}$, *Fn1*$^{RGE/RGE}$ and *Fn1*$^{\Delta RGD/\Delta RGD}$ cells were done using other substrates to coat the cover-slips. The effect of heparin on collagen I or gelatine was similar: after 24 h in presence of heparin fibrillogenesis was not affecting *Fn1*$^{+/+}$ cells whereas heparin impaired fibril formation in *Fn1*$^{\Delta RGD/\Delta RGD}$ fibroblasts (Fig. 31 D-E). In addition, on these two substrates *Fn1*$^{\Delta RGD/\Delta RGD}$ fibroblasts had also problems to spread when heparin was added. Contrary, on vitronectin the three cell lines could nicely spread, form stress fibres and FA when treated with heparin (Fig. 31 F), yet *Fn1*$^{\Delta RGD/\Delta RGD}$ fibroblasts did not assemble a fibrillar matrix of FN whereas *Fn1*$^{+/+}$ did. Thus, heparin blocked $FN^{\Delta RGD}$ fibrillogenesis but did not affect FN matrix assembly by *Fn1*$^{+/+}$ or *Fn1*$^{RGE/RGE}$.

3.2. Quantification of FN fibrils and secreted FN with heparin treatment by western blot

We confirmed the heparin effect in fibrillogenesis by western blot. FN fibrils were precipitated with DOC in *Fn1*$^{\Delta RGD/\Delta RGD}$, *Fn1*$^{+/+}$ and *Fn1*$^{RGE/RGE}$ cell lysates and quantified. As above, cells were seeded on laminin coated dishes and after 3 h of adhesion heparin was added (0.1 mg/ml) and incubated for 24 h. Treatment with heparin reduced by 52.8% the levels of DOC insoluble FN in *Fn1*$^{\Delta RGD/\Delta RGD}$ fibroblast and did not affect the fibrillar levels of FN^{WT} and FN^{RGE} (Fig. 32 A-B). The levels of fibrillar FN generated by *Fn1*$^{\Delta RGD/\Delta RGD}$ fibroblasts with or without heparin treatment were still reduced compared to the levels of fibrillar FN generated by *Fn1*$^{+/+}$ and *Fn1*$^{RGE/RGE}$ cells (Fig. 32 A-B). We could also confirm that heparin treatment did not affected the intracellular levels of FN in any of the three cell lines (Fig. 32 C)

Furthermore, FN was analysed in the conditioned medium from *Fn1*$^{\Delta RGD/\Delta RGD}$ fibroblast showing that it had higher levels than the medium from the other two cell lines and contained similar quantities of FN with heparin than without heparin. In the medium conditioned by *Fn1*$^{+/+}$ and *Fn1*$^{RGE/RGE}$ without heparin the amount of FN was not altered in comparison with the medium conditioned by these cell lines treated with heparin (Fig. 32 D-E). Hence, heparin did not affect the amount of secreted FN in any of the cell lines. All together these results confirm that heparin blocks the FN fibrillogenesis mediated by *Fn1*$^{\Delta RGD/\Delta RGD}$ fibroblasts.

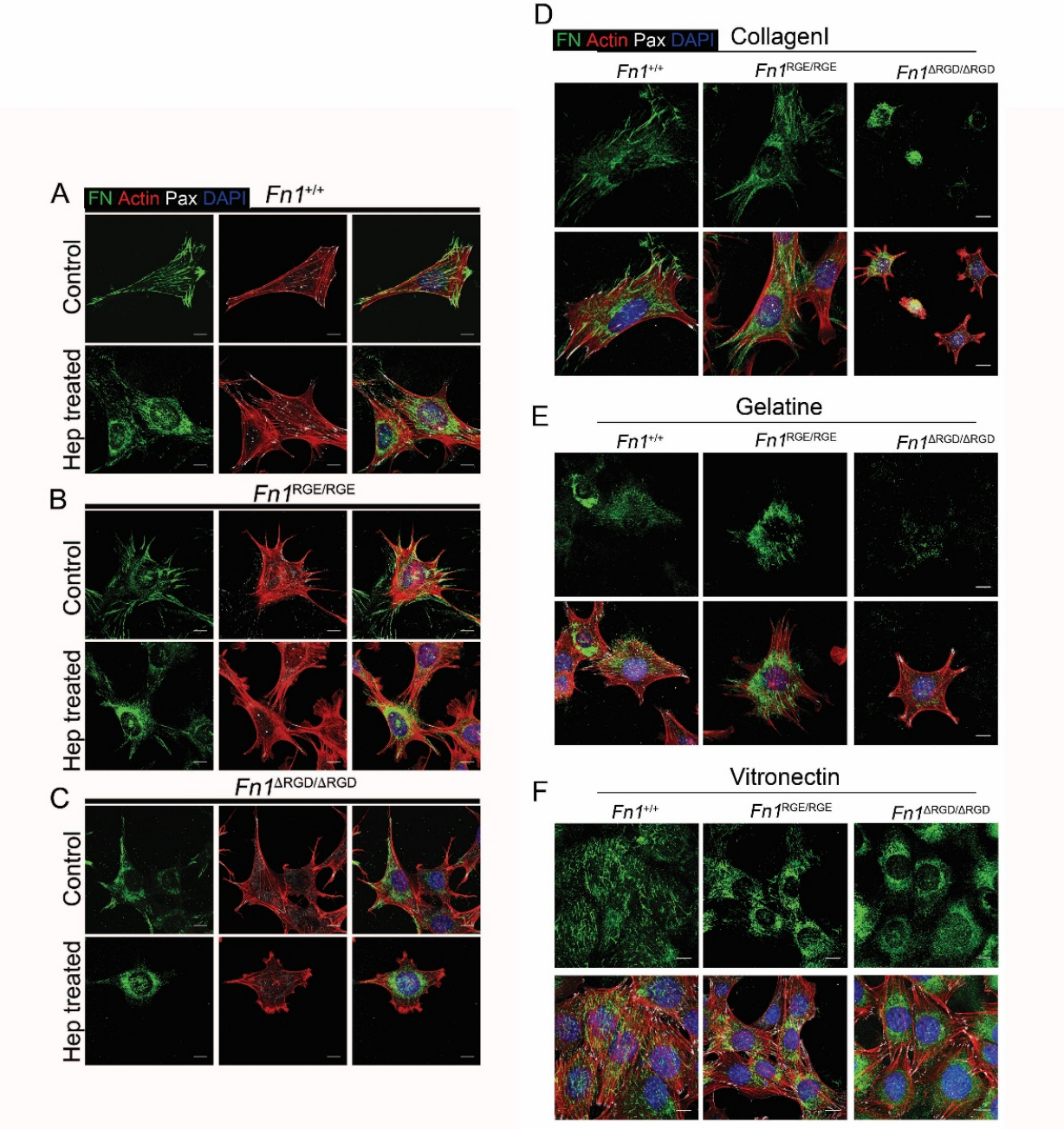

Figure 31. Blocking the HepII cell binding site hampers $FN^{\Delta RGD}$ secretion and consequent assembly. (A-C) FN matrix assembly during 24 h in presence of heparin. After 24 h of heparin treatment, $Fn1^{+/+}$ (A) and $Fn1^{RGE/RGE}$ (B) fibroblasts have assembled a matrix on laminin which is comparable to the non-treated fibroblasts. Heparin treatment in $Fn1^{\Delta RGD/\Delta RGD}$ fibroblasts (C) impedes fibrillogenesis. (D) FN matrix assembly by $Fn1^{+/+}$, $Fn1^{RGE/RGE}$ and $Fn1^{\Delta RGD/\Delta RGD}$ on collagen I treated with heparin. (E) FN matrix assembly by $Fn1^{+/+}$, $Fn1^{RGE/RGE}$ and $Fn1^{\Delta RGD/\Delta RGD}$ on gelatine treated with heparin. (F) FN matrix assembly by $Fn1^{+/+}$, $Fn1^{RGE/RGE}$ and $Fn1^{\Delta RGD/\Delta RGD}$ on vitronectin treated with heparin. Note how $Fn1^{\Delta RGD/\Delta RGD}$ do not form FN fibrils despite presenting FA and stress fibres. Staining: fibronectin in green; actin stain as phalloidin in red; paxillin in white and dapi in blue. Scale bar: 10µm.

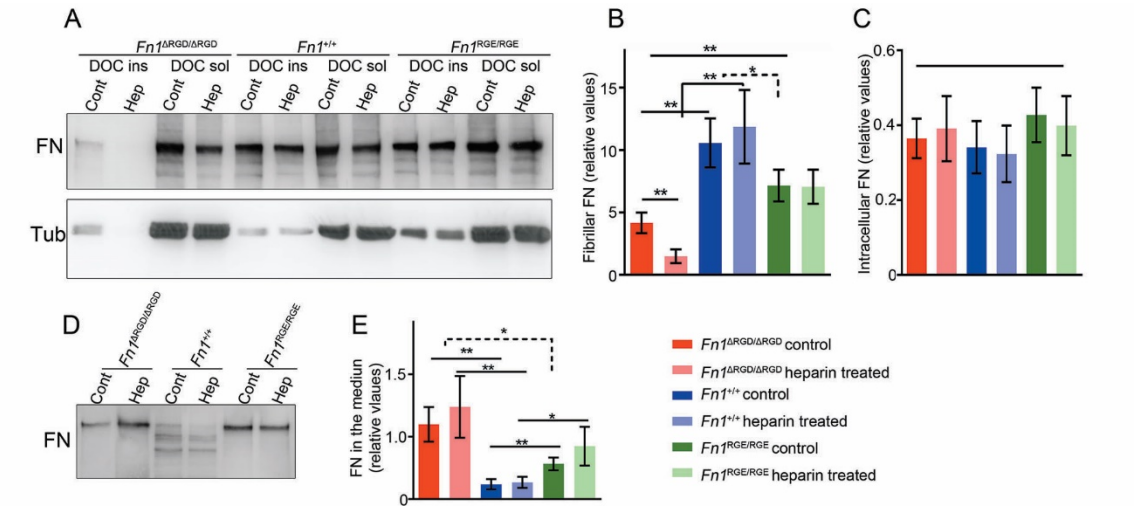

Figure 32. Quantification of fibrillar and soluble FN in fibroblast cultures. (A) Fibrillar FN precipitated with DOC after 24h of cell culture with and without heparin treatment. (B) Quantification of the levels of fibrillar FN after 24h relativized to soluble FN and (C) of cellular soluble FN after 24h with or without heparin treatment. (D) FN found in the medium with or without heparin after 24h and (E) its quantification. Represented average and SEM; n=8

4. FN$^{\Delta RGD}$ is assembled in an integrin independent manner

The FN matrix assembly experiments indicate that cells do not spread and arrange the cytoskeleton equally well onto the different substrates used. We observed that in laminin and vitronectin, where *Fn1*$^{\Delta RGD/\Delta RGD}$ fibroblasts spread more and formed more prominent FA, FN assembly was favoured. Since integrin receptors mediate cell adhesion and spreading to those substrates, we hypothesised that integrin activation might influence FN$^{\Delta RGD}$ fibrillogenesis. To evaluate the effect of integrin activation on FN$^{\Delta RGD}$ fibrillogenesis, matrix assembly assays were performed adding $MgCl_2$.

4.1. FN$^{\Delta RGD}$ matrix assembly after activating integrins

It is well demonstrated that $MnCl_2$ is an integrin activator (Mould *et al.* , 1995). Mn^{+2} binds the MIDAS motif in the β-I domain of the integrin β subunit inducing conformational changes which stabilise their unbent or active conformation (Plow *et al.*, 2000; Mould *et al.*, 2003). Unlike ECM proteins or antibodies, Mn^{+2} is an activator unspecific of integrin dimers. Thus, $MnCl_2$ was used to induce integrin activation in *Fn1*$^{\Delta RGD/\Delta RGD}$ fibroblast and evaluate whether it improves FN$^{\Delta RGD}$ fibrillogenesis or it occurs in an integrin independent manner. The three lines of fibroblasts were seeded on laminin-coated coverslips for 24 h and next 100 µM $MnCl_2$ was added for 3 h. FN fibrils were analysed both by immunostaining and by DOC precipitation and western blot. Upon addition of $MnCl_2$, immunostaining showed that the three lines arranged stress fibres and focal adhesions (Fig. 33). However, while upon $MnCl_2$ treatment *Fn1*$^{+/+}$ cells contained more fibrillar FN in their surroundings and the DOC insoluble fraction was significantly higher (Fig. 34 A-B), in *Fn1*$^{\Delta RGD/\Delta RGD}$ fibroblast no increment of FN fibrillogenesis was detected neither in the immunostainings nor in the insoluble DOC FN fraction in western blots (Fig. 34). Treatment with manganese seemed to increase FN^{RGE} fibrillogenesis in the immunostainings, although the insoluble DOC fraction increment was not significative. By

analysing FN intracellular levels and FN in the medium, we could discard that the treatment with manganese had affected either to FN expression or secretion in any of the three cell lines as there were no differences. Thus, integrin activation favours actin rearrangement, FA formation and enhances only $FN^{+/+}$ and FN^{RGE} fibrillogenesis, but not $FN^{\Delta RGD}$.

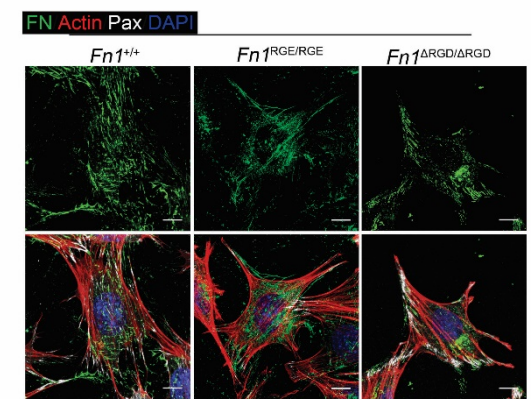

Figure 33. Activations of integrins does not improve $FN^{\Delta RGD}$. *Fn1*$^{+/+}$, *Fn1*$^{RGE/RGE}$ and *Fn1*$^{\Delta RGD/\Delta RGD}$ fibroblast on laminin treated with $MnCl_2$ during 3h. Staining: fibronectin in green; actin stain as phalloidin in red; paxillin in white and dapi in blue. Scale bar: 10µm.

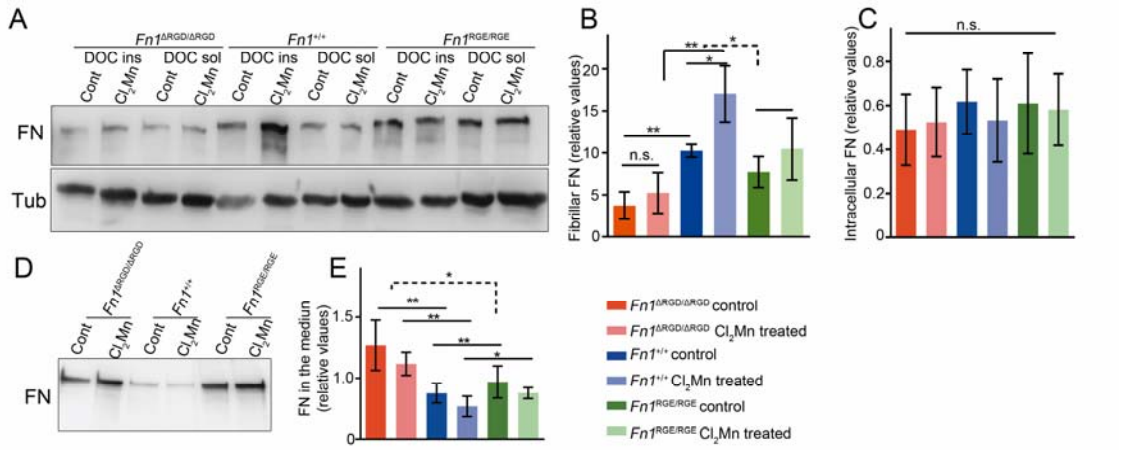

Figure 34. Quantification of fibrillar and soluble FN in fibroblast cultures. (A) Fibrillar FN precipitated with DOC after 24 h of cell culture with and without manganese treatment. (B) Quantification of the levels of fibrillar FN after 24 h relativized to soluble FN and (C) of cellular soluble FN after 24 h with or without manganese treatment. (D) FN found in the medium with or without manganese after 24h and (E) its quantification. Represented average and SEM; n=4.

4.2. $FN^{\Delta RGD}$ is assembled by heparin sites engagement and independently of integrins

To confirm that the $FN^{\Delta RGD}$ is assembled by the heparin site, independently of integrins, FN matrix assembly was assayed in presence of heparin and Mn^{+2} by immunostaining and DOC precipitation. Cells were plated on laminin coated coverslips and treated heparin for 24 h to block the FNIII12-14 motif and $MnCl_2$ during 3h to activate integrins. As shown in figure 35, in

the three cell types seeded on laminin, stress fibres and FA were formed when treated with heparin and $MnCl_2$ together. FN fibrillogenesis in $FN^{+/+}$ and FN^{RGE} were not affected by adding together heparin and $MnCl_2$ (Fig. 35) in comparison of single treatment with $MnCl_2$ (Fig. 33) and levels of DOC insoluble FN were like the controls (Fig. 36). The *Fn1*$^{\Delta RGD/\Delta RGD}$ fibroblasts treated with Mn^{+2} in presence of heparin in the medium could not form FN fibrils, confirming that its fibrillogenesis is independent of integrins and heparin-binding regions dependent (Fig. 35). Fibrillar FN precipitation with DOC was reduced by 51% when *Fn1*$^{\Delta RGD/\Delta RGD}$ fibroblasts were treated with heparin and with Mn^{+2} together, corroborating the previous observations (Fig. 36).

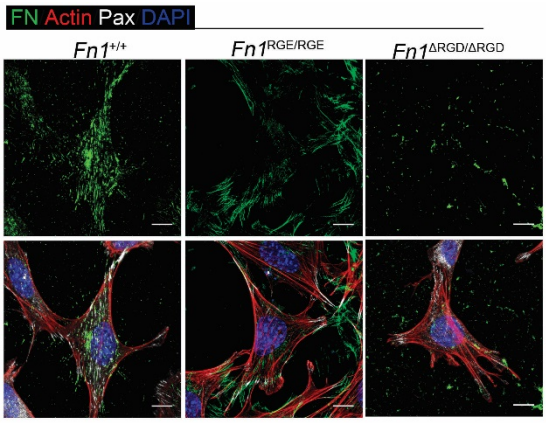

Figure 35. Activations of integrins does not recover $FN^{\Delta RGD}$ fibrillogenesis blockage by heparin. *Fn1*$^{+/+}$, *Fn1*$^{RGE/RGE}$ and *Fn1*$^{\Delta RGD/\Delta RGD}$ fibroblast on laminin treated with $MnCl_2$ during 3h. Staining: fibronectin in green; actin stain as phalloidin in red; paxillin in white and dapi in blue. Scale bar: 10µm.

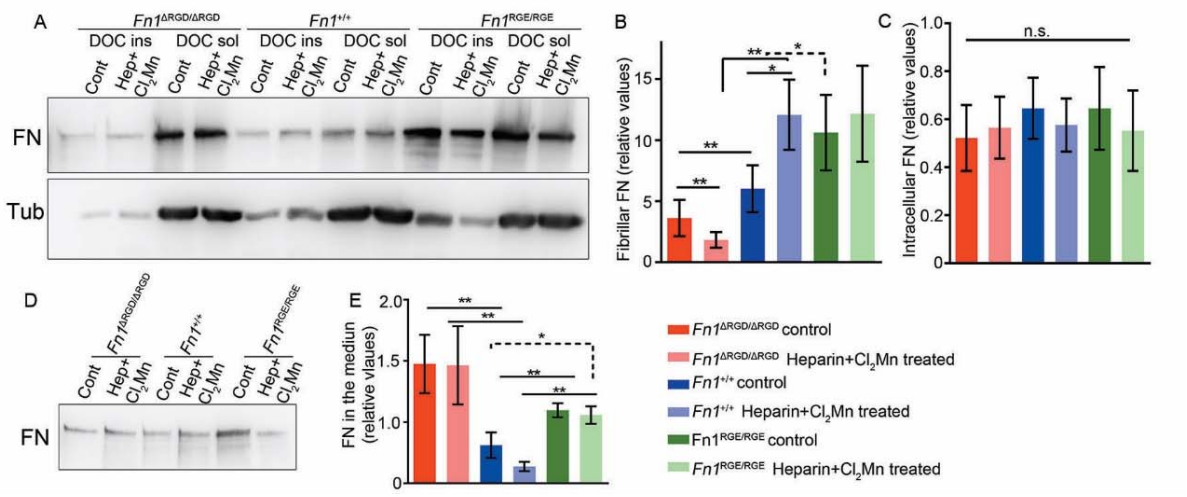

Figure 36. Quantification of fibrillary and soluble FN in fibroblast cultures. (A) Fibrillar FN precipitated with DOC after 24h of cell culture with and without heparin and manganese treatment. (B) Quantification of the levels of fibrillary FN after 24h relativized to soluble FN and (C) of cellular soluble FN after 24h with or without heparin and manganese treatment. (D) FN found in the medium with or without heparin and manganese after 24h and (E) its quantification. Represented average and SEM; N=4.

5. FN$^{\Delta RGD}$ is assembled by syndecans

To directly address whether syndecans are involved in FN$^{\Delta RGD}$ matrix assembly, syndecan translation was blocked in *Fn1*$^{\Delta RGD/\Delta RGD}$ fibroblasts using interference RNA (siRNA). Since the *Fn1*$^{\Delta RGD/\Delta RGD}$ fibroblasts express the 4 members of the syndecan family, initially, we tried to knock-down the expression of the four of them. For that, we combined 4 different siRNA against syndecans 1, 2, 3 and 4. Transfection of the 4 different siRNA together resulted toxic for the cells, and they died after 24 h. So next, we assayed silencing each syndecan (1-4) individually transfecting independently siRNA against each syndecan in *Fn1*$^{\Delta RGD/\Delta RGD}$ fibroblasts, and analysed how it affected the expression levels of the four syndecans. siRNA against syndecan 1 (*sdc1*) reduced levels of *sdc1* and *sdc3*; and siRNA against syndecan 4 (*sdc4*) reduced levels of *sdc2* and *sdc4*. To silence the four syndecans, we co-transfected siRNA against *sdc1* and *sdc4*. Combination of siRNA against syndecan 1 (*sdc1*) and 4 (*sdc4*) generated partial knock-downs for syndecans 1, 2, 3 and 4 in *Fn1*$^{\Delta RGD/\Delta RGD}$ and *Fn1*$^{+/+}$ fibroblasts. *Fn1*$^{\Delta RGD/\Delta RGD}$ and *Fn1*$^{+/+}$ syndecan knock-down (*Fn1*$^{\Delta RGD/\Delta RGD}$*-sdc-KD; Fn1*$^{+/+}$*-sdc-KD*) was achieved after 96 h by siRNA transfection delivered with lipofectamine. The siRNA (150 pmol) reduced the protein level of syndecan 1 by 30%; syndecan 2 by 70%; syndecan 3 by 30% and syndecan 4 by 70% in *Fn1*$^{\Delta RGD/\Delta RGD}$*-sdc-KD* (Fig. 37A-C), while transfection with scrambled siRNA did not alter syndecan protein levels (Fig. 37A-C), indicating the specificity of the treatment. In the case of *Fn1*$^{+/+}$ fibroblasts, transfection of the combination of siRNA reduced the reduced the protein level of syndecan 1 by 87%; syndecan 2 by 78%; syndecan 3 by 86% and syndecan 4 by 78% in *Fn1*$^{+/+}$*-sdc-KD;* while transfection with scrambled siRNA did not affected the syndecan expression (Fig. 37A-C). FN$^{\Delta RGD}$ assembly was assayed in *Fn1*$^{\Delta RGD/\Delta RGD}$*-sdc-KD* after 96 h by immunostaining. While *Fn1*$^{\Delta RGD/\Delta RGD}$ transfected with scrambled siRNA (*Fn1*$^{\Delta RGD/\Delta RGD}$-scr) assembled FN$^{\Delta RGD}$, syndecan knock-down, despite partial, hindered FN$^{\Delta RGD}$ matrix assembly (Fig. 37 D). Contrary, FN assembly was not altered in *Fn1*$^{+/+}$*-sdc-KD* (Fig. 37 D). The defect in *Fn1*$^{\Delta RGD/\Delta RGD}$-sdc-KD cells to assemble FN in a fibrillar matrix confirmed that FN$^{\Delta RGD}$ fibrillogenesis takes place through the FNIII$_{12\text{-}14}$ engagement by syndecans.

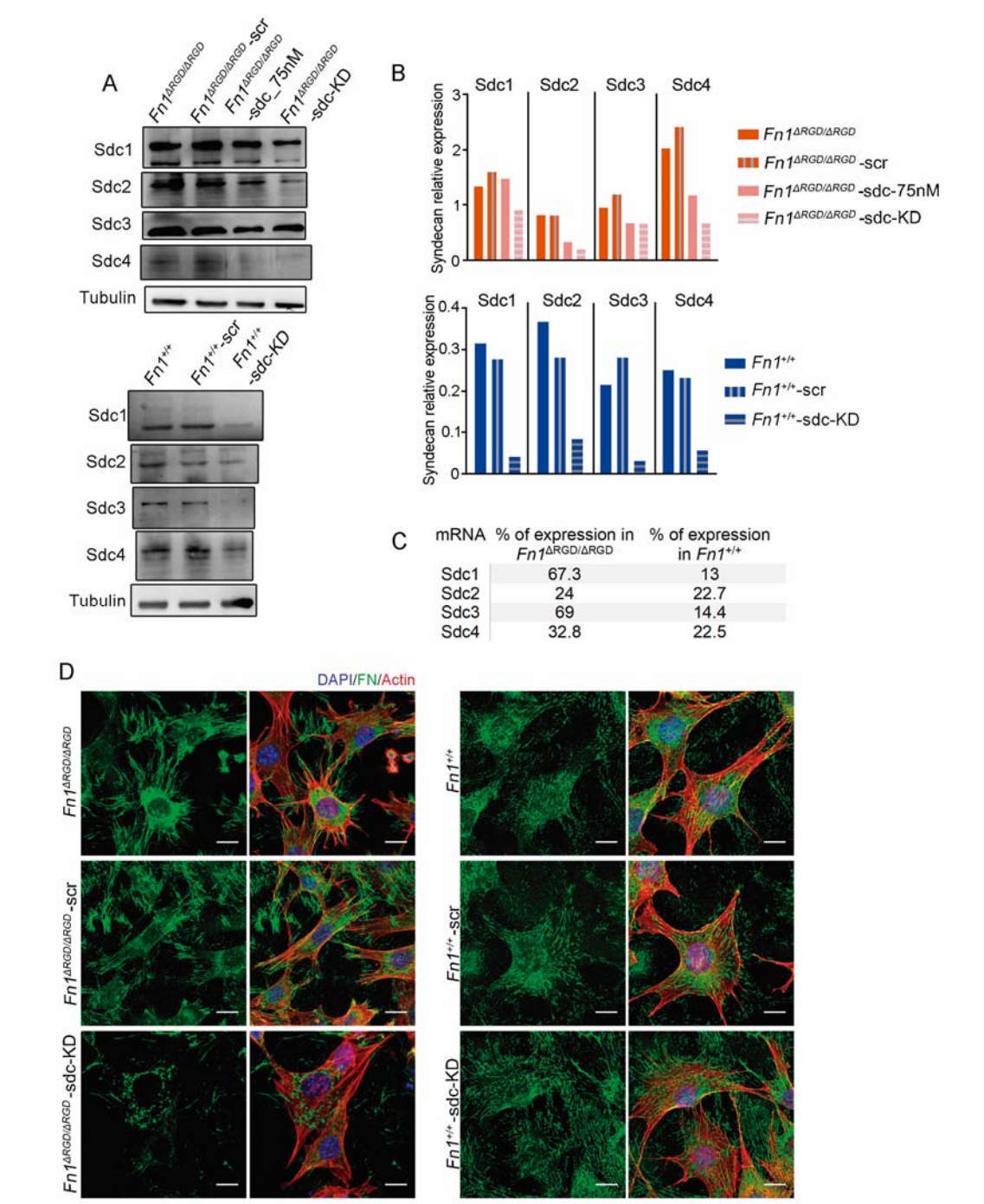

Figure 37. Syndecan knock-down abolish $FN^{\Delta RGD}$ matrix assembly. (A) Western blot and (B) quantification of syndecans 1-4 protein levels 96 h post-transfection. Protein level of syndecans (sdc) were normalized to tubulin. Two amounts of siRNA were transfected (75 nM and 150 nM), and the one reducing more the protein levels (150 nM) was chosen for studying matrix assembly. (C) Percentage of protein reduction when cells are transfected with 150 nM siRNA in comparison with *Fn1*$^{\Delta RGD/\Delta RGD}$ and *Fn1*$^{+/+}$cells. (D) Matrix assembly in *Fn1*$^{\Delta RGD/\Delta RGD}$*-sdc-KD*, compared to *Fn1*$^{\Delta RGD/\Delta RGD}$ and *Fn1*$^{\Delta RGD/\Delta RGD}$*-scr,* and to *Fn1*$^{+/+}$*, Fn1*$^{+/+}$*-scr, Fn1*$^{+/+}$*-sdc-KD* . Staining: fibronectin in green; actin stain as phalloidin in red and dapi in blue.

IV RESULTS

Chapter II. Study of the FN synergy site function

1. The *Fn1*$^{syn/syn}$ mice

To directly test the *in vivo* role(s) of the FN synergy site, we analysed tissues and haemostasia in mice carrying a knock-in mutation in this motif (*Fn1*^{syn}) which annulates the synergy site function. These mice present the two arginines (R1374 and R1379) of the synergy motif (DRVPPSRN) in the FN-III9 module substituted by alanines (Fig. 38 A). The R>A substitution was described as critical to eliminate the synergy site function in fibroblasts and platelet adhered to FN (Aota *et al.*, 1994; Redick *et al.*, 2000; Chada *et al.* , 2006; Friedland *et al.*, 2009). Therefore, these amino acids were selected to design the *Fn1*^{syn} knock-in mouse (see construction in Fig. 19; material and methods). Heterozygous mice (*Fn1*$^{+/syn}$), which showed no apparent phenotype, were matted and generated homozygous offspring (*Fn1*$^{syn/syn}$) in a normal Mendelian ratio, before and after weaning (Fig. 38 B). Mice were genotyped by PCR as shown in figure 38 C. The *Fn1*$^{syn/syn}$ mice were fertile and had a normal life span compared with their wild-type litter mates.

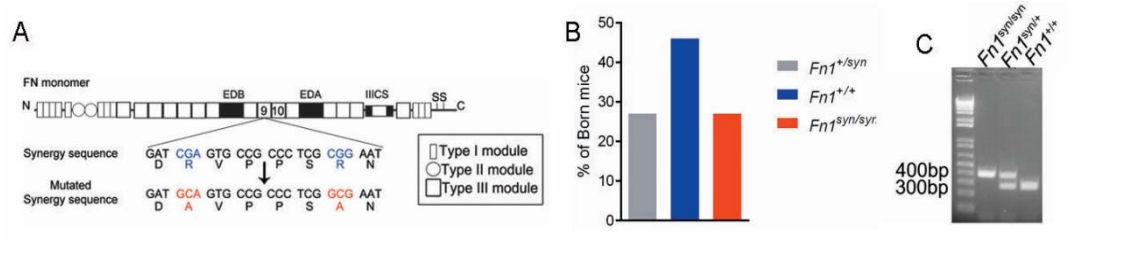

Figure 38. (A) Cartoon of FN and the nucleotide point mutations disrupting the function of the synergy site. (B) Percentage of born mice from *Fn1*$^{+/syn}$ mattings (88 litters, 457 mice).

1.1. Tissue Analysis of *Fn1*$^{syn/syn}$ mice

To deeply characterize the mice carrying the mutation in the synergy site, the morphology and FN distribution in several tissues were examined. Heart, liver, kidney, and lung were dissected from 3-month-old mice, fixed and paraffin embedded for haematoxylin-eosin and immunostainings. FN and α5 integrin-FN interaction are critical for heart and blood vessel morphogenesis and maintenance (George *et al.*, 1993; George, Baldwin and Hynes, 1997; van der Flier *et al.*, 2010; Turner *et al.*, 2014), however analysis of heart and blood vessel showed no abnormalities in *Fn1*$^{syn/syn}$ mice compared with *Fn1*$^{+/+}$ littermates (Fig. 39 A). As shown, heart morphology and FN distribution were apparently normal in *Fn1*$^{syn/syn}$ mice. Blood vessel organization was analysed in whole mount ear samples with anti-PECAM-1 and anti-αSMA immunostainings to label endothelial and mural cells respectively, revealing no abnormalities in the endothelium (Fig. 39 B). The subendothelial matrix visualized with antibodies to laminin-1, collagen IV and FN, was also normally organized in *Fn1*$^{syn/syn}$ mice (Fig. 39 C). Furthermore, we discarded problems of blood leakage by immunostaining the erythrocytes with anti-Ter119 and the endothelial cells with anti-PECAM-1 (Fig. 39 C, right bottom panel). Kidneys, lungs and liver were also analysed and both, morphology and FN distribution were indistinguishable between *Fn1*$^{syn/syn}$ and control littermates (Fig. 39 C).

Altogether, these data indicate that the FN synergy site is dispensable for development and postnatal tissue homeostasis.

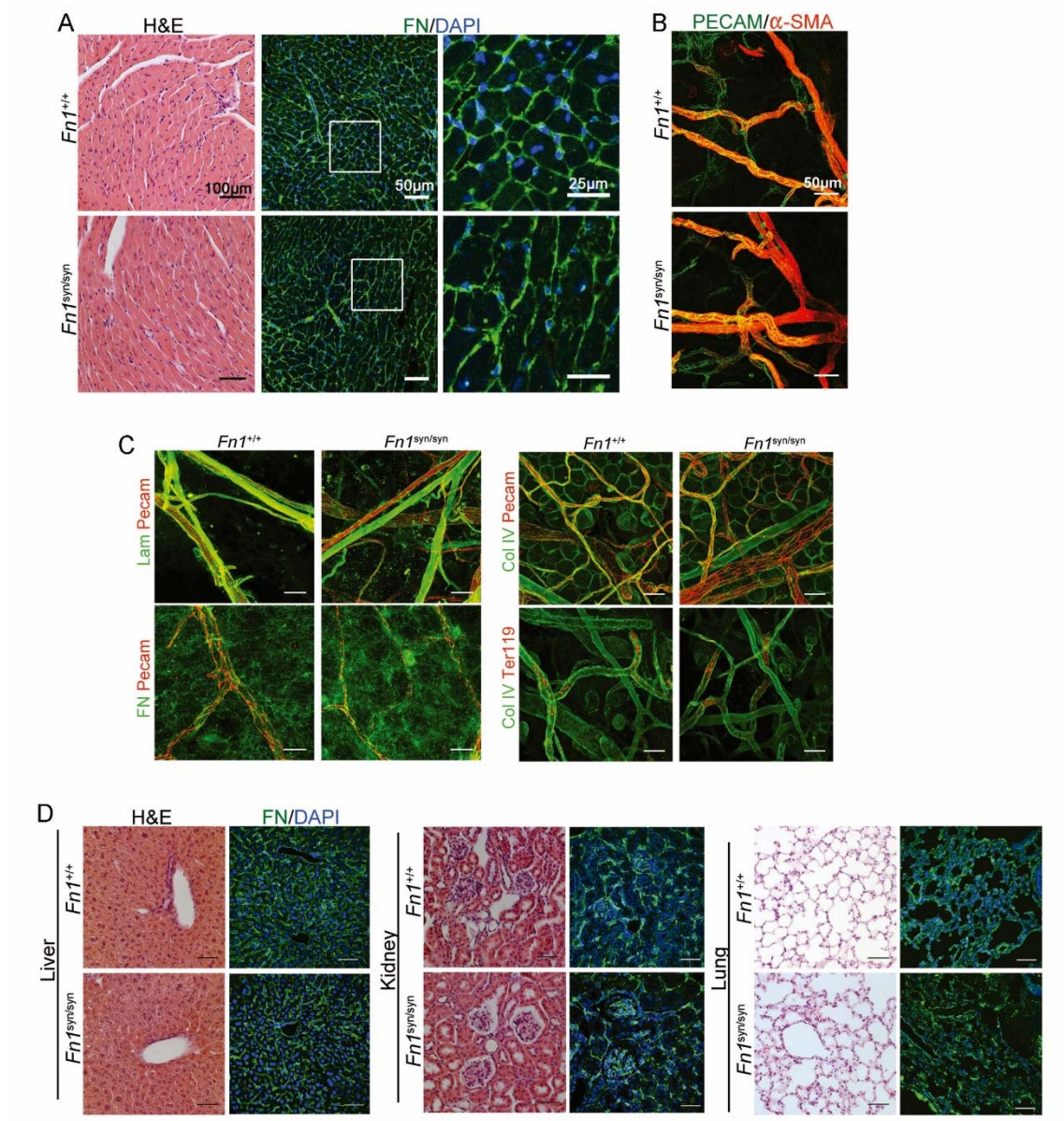

Figure 39. Normal tissue morphology in *Fn1*$^{syn/syn}$ mice. (A) Representative images of 3-months-old *Fn1*$^{+/+}$ and *Fn1*$^{syn/syn}$ heart sections stained with H and E and immunostained for FN. (B) Confocal images of ear whole-mounts from 3 months-old mice immunostained with anti-PECAM-1 and anti-aSMA to visualize the dermal endothelial cell tubes and smooth muscle cells. (C) Confocal images of ear whole-mounts from 3 months-old mice immunostained with anti-PECAM-1 and Laminin, FN and ColIV to visualize the basement membrane, or immunostained with anti-PECAM-1 and Ter119 to corroborate that there is no blood leaking. (D) Representative images of 3-months-old *Fn1*$^{+/+}$ and *Fn1*$^{syn/syn}$ heart sections stained with H and E and immunostained for FN. Scale bars: 100 µm in H and E; 50 µm in immunostainings.

1.2. Haemostasis analysis of *Fn1*$^{syn/syn}$ mice

Plasma (p) FN is required for platelets to aggregate and for the stability of blood clots (Ni *et al.*, 2003; Wang *et al.*, 2014). Moreover, platelets contain the two integrins which bind to the FN synergy site, α5β1 and αIIbβ3 (Chada *et al.* , 2006; Zeiler *et al.,*2014). To test the influence of the synergy site in platelet function, several experiments were performed. In vivo,

tail bleeding time was measured after tail biopsy (Fig. 40 A). The bleeding time was significantly longer in *Fn1*$^{syn/syn}$ (7.27 ± 1.71 min; mean ± SD) compared to *Fn1*$^{+/+}$ (4.64 ± 1.50 min) mice. Importantly, blood platelet counts were normal in *Fn1*$^{syn/syn}$ mice in comparison to the wild-type littermates (Fig. 40 B). Western-blot of plasma showed that levels of pFN were similar in *Fn1*$^{+/+}$ (318.7 ± 24.1 mg/ml) and *Fn1*$^{syn/syn}$ (316.1 ± 31.0 mg/ml) mice (Figure 40 C).

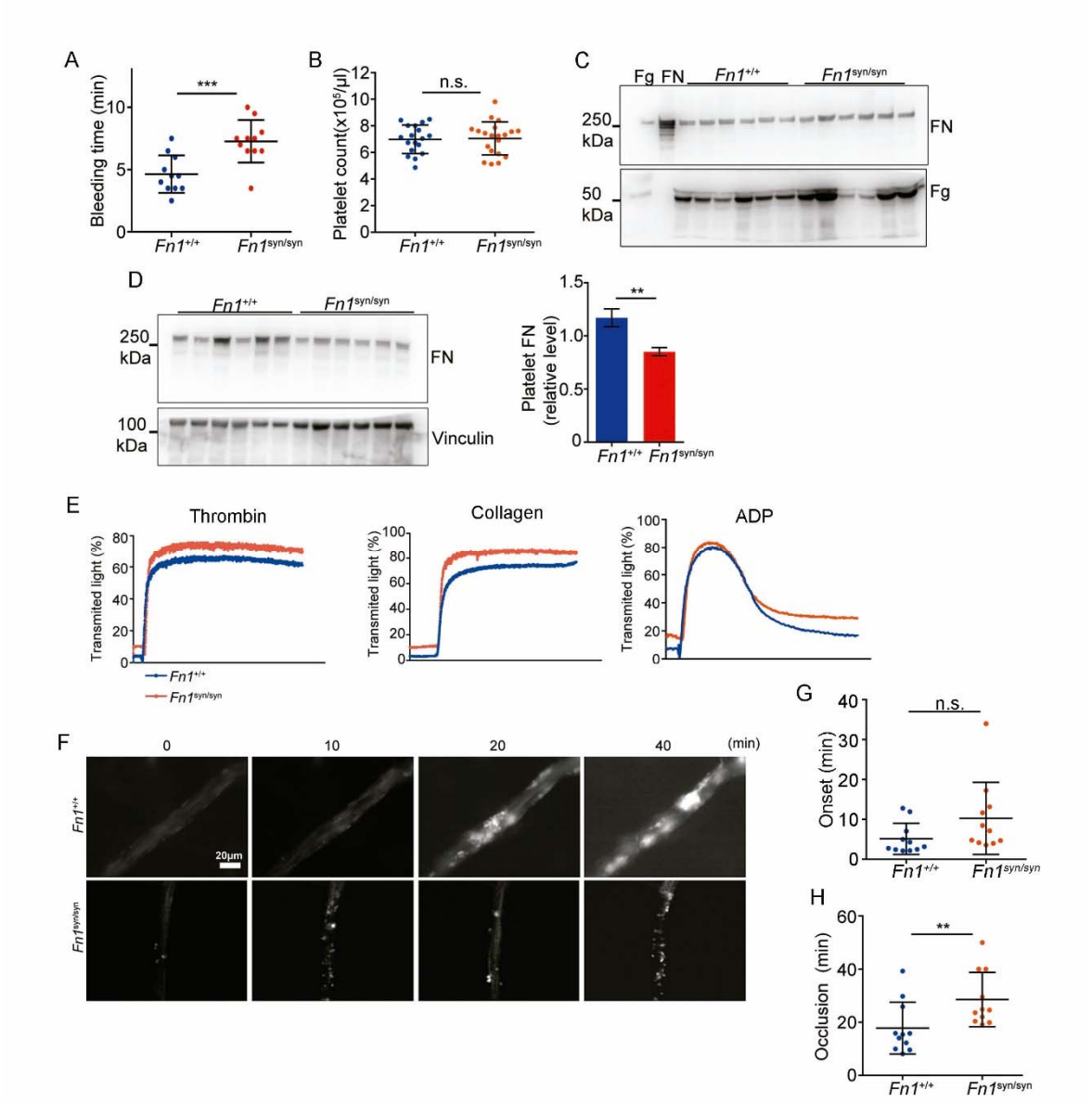

Figure 40. Hemostasis in *Fn1*$^{syn/syn}$ mice. (A) Bleeding time of 3-months-old *Fn1*$^{+/+}$ (n= 11) and *Fn1*$^{syn/syn}$ (n= 11) mice. (B) Platelet counts in blood samples of *Fn1*$^{+/+}$ (n= 18) and *Fn1*$^{syn/syn}$ (n= 19) mice. (C) FN content in platelets derived from *Fn1*$^{+/+}$ (n= 6) and *Fn1*$^{syn/syn}$ (n= 6) mice. (D) Quantification of FN content in platelets relative to their vinculin levels. (E) Washed platelets aggregation *in vitro* using thrombin or collagen and PPR aggregation using ADP. (F) Representative still images of the arteriolar occlusion (white:platelets). (G) Onset time of platelet aggregates in injured arterioles. (H) Occlusion time of injured arterioles in the cremaster muscle of 3-months-old *Fn1*$^{+/+}$ (n= 11) and *Fn1*$^{syn/syn}$ (n= 11) mice. Values are shown as mean ± SD; statistical significances were calculated using the Student t-test; **p<0.01 and ***p<0.001.

Importantly, plasma levels of fibrinogen were also similar in *Fn1*$^{+/+}$ (2.10 ± 0.17 mg/ml) and *Fn1*$^{syn/syn}$ (2.08 ± 0.07 mg/ml) mice. Since αIIbβ3 integrins mediate the uptake of pFN into platelet α-granules (Ni et al., 2003a), western-blotting with lysates from washed platelets were performed and found that the FN content was significantly reduced to 70% in platelets from *Fn1*$^{syn/syn}$ mice (Fig. 40 D). Therefore, we concluded that the integrin αIIbβ3 is less efficient to internalize FN. To study *in vitro* aggregation of washed platelets, it was induced with either collagen I, thrombin or PRP aggregation with ADP. In all conditions platelets from *Fn1*$^{syn/syn}$ mice achieved normal shape changes and aggregations compared to *Fn1*$^{+/+}$ (Fig. 40 E), indicating that under these conditions isolated and washed platelet of *Fn1*$^{syn/syn}$ mice were functional. To quantitatively study the velocity of thrombus formation in vivo, thrombi induction was measured by intravital microscopy, in the arterioles of the cremaster muscle upon vessel injury. The experiments revealed a small delay in the onset of thrombus formation in the *Fn1*$^{syn/syn}$ mice (10.29 ± 9.04 min) that, however, was not significantly different compared to the *Fn1*$^{+/+}$ littermates (5.13 ± 3.89 min). In contrast, the time required for arteriole occlusion was significantly increased in *Fn1*$^{syn/syn}$ mice (28.56 ± 10.24 min) compared to *Fn1*$^{+/+}$ mice (17.82 ± 9.74 min) (Fig. 40 F-G). Notably, in 3 out of 11 *Fn1*$^{syn/syn}$ mice no total occlusion was observed after 40 min (Fig. 40 F and H), a defect that was never observed in control mice. These results demonstrate that the synergy site is dispensable for development and postnatal tissue homeostasis but is required to stabilize platelet clots in vivo and to prevent prolonged bleeding times.

2. FN^{syn} matrix assembly and fibroblasts adhesion to purified FN^{syn}

FN-deficient (*Fn1*-KO) fibroblasts, which do not express FN, were used for adhesion experiments in order to exclude the influence of the secreted FN. To corroborate that the cells express the integrins of interest (α5β1 and αvβ3), their surface levels were analysed by Flow Cytometry (FACS). Integrin profile showed that *Fn1*-KO cells presented α5, αv, β1 and β3 integrins on their surface (Fig. 41).

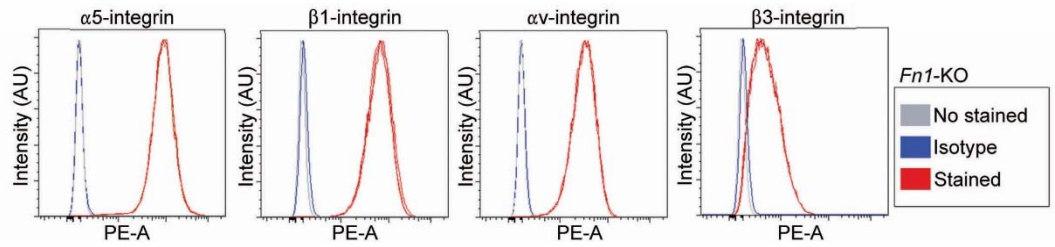

Figure 41. Integrin levels in the surface of *Fn1*-KO fibroblasts.

2.1. FN^{syn} fibrillar matrix assembly

Although FN fibrillogenesis can happen in absence of α5β1 integrin, appropriate FN assembly into a fibrillar network depends on α5β1 binding to FN (Fogerty *et al*., 1990). To test whether FN assembly proceeds normally in the absence of the synergy site, *Fn1*-KO fibroblasts were seeded on laminin and incubated over 96 h with blood plasma extracted from either

Fn1$^{+/+}$ or *Fn1*$^{syn/syn}$ mice. Every 24 h cells were fixed and stained to check the FN matrix assembly progression. In line with FN tissue immunostaining of *Fn1*$^{syn/syn}$ mice, *Fn1*-KO cells assembled fibrillar FN networks with plasma from *Fn1*$^{syn/syn}$ mice of similar complexity, fibril diameter and length than with plasma from *Fn1*$^{+/+}$mice (Fig. 42).

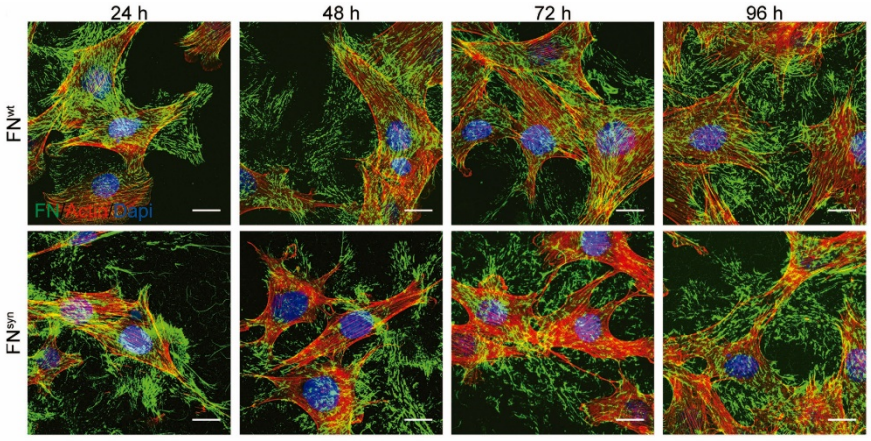

Figure 42. The FN synergy site is dispensable for FN fibrillogenesis. *Fn1-KO* fibroblasts grown in 1% plasma derived from either *Fn1*$^{+/+}$ or *Fn1*$^{syn/syn}$ mice, fixed at the indicated times and stained for FN (green), F-actin stain (with Phalloidin; red) and nuclei (with DAPI; blue). Scale bar: 10 µm.

2.2. Characterization of purified plasmatic FN

In all adhesion experiments, the glass coverslips or plastic 96 well microplates were coated with plasma FN (pFN) purified from *Fn1*$^{+/+}$ or *Fn1*$^{syn/syn}$ mice. After purification, the pFN was analysed for purity and integrity by Coomassie staining and western blotting (Fig. 43 A-B). The presence of only one band of 250 kDa was a sign of lack of degradation and purity (Fig. 43 A). In addition, we confirmed by western blotting that the 250 kDa band was FN and that there was no contamination by fibrinogen (Fig. 43 C). We tested the pFN adsorption to glass by ELISA and demonstrated that both, pFN^{wt} and pFN^{syn}, coat glass surfaces equally at a concentration of 10 µg/ml (Fig. 43 D). Thus, 10 µg/ml was the chosen concentration to use in all experiments.

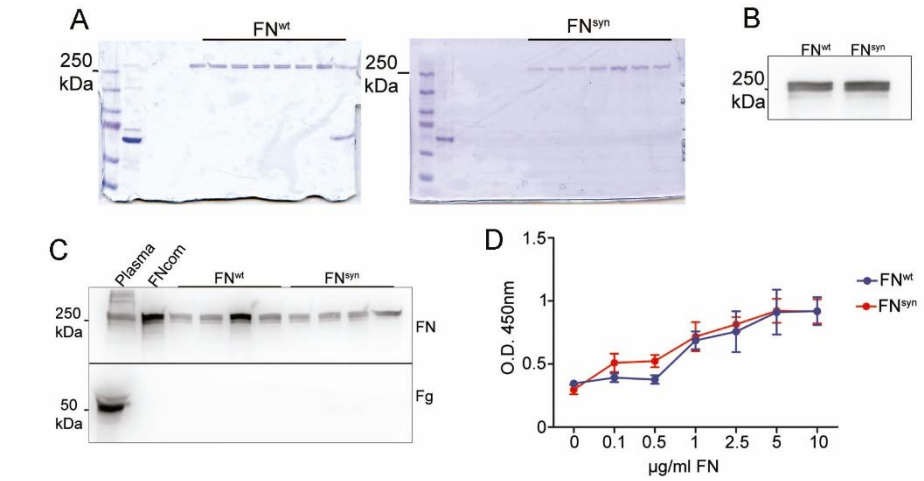

Figure 43. Characterization of purified plasmatic FN. (A) Electrophoresis and Coomassie staining of urea eluted purified pFN. (B) Western blot of dialyzed purified pFN. (C) Western blot of purified pFN samples to check possible fibrinogen contamination. FNcom indicates human commercial FN. Plasma was isolated from mice. (D) purified pFN absorbance to glass, measured by Elisa.

2.3. Fibroblasts adhesion and spreading on FN^{syn}

The adhesion of *Fn1*-KO fibroblasts was analyzed on 96-well plates coated with FN^{wt} and FN^{syn}. Fibroblasts adhesion to FN began around 3 min after cell seeding and increased with time without noticeable differences between FN^{wt} and FN^{syn} in 60 min (Fig. 44 A). Immunostaining of spreading *Fn1*-KO fibroblasts at different time points showed that while the formation of nascent adhesions (NAs) was similar on FN^{wt} and FN^{syn} (Fig. 44 B), the number of adhesions as well as percentage of paxillin-positive focal adhesions (FAs) linked to stress fibres were significantly reduced in *Fn1*-KO fibroblasts seeded for 30 min on FN^{syn} (Fig. 44 B, D-E) and indicating that the transition from NAs to mature, stress fibre-anchored FAs is delayed on FN^{syn}. Furthermore, cell spreading, determined as cell area at different time points after cell seeding onto FN^{syn}-coated substrates, was also delayed in the first 30 min (Fig. 44 C). Time-lapse video microscopy confirmed the delayed cell spreading on FN^{syn} and revealed unstable adhesions consisting of several cycles of binding and release from the substrate (video capture images in Fig. 45). These findings indicate that, although the synergy site is dispensable for FA formation, it promotes the transition from NAs to FAs.

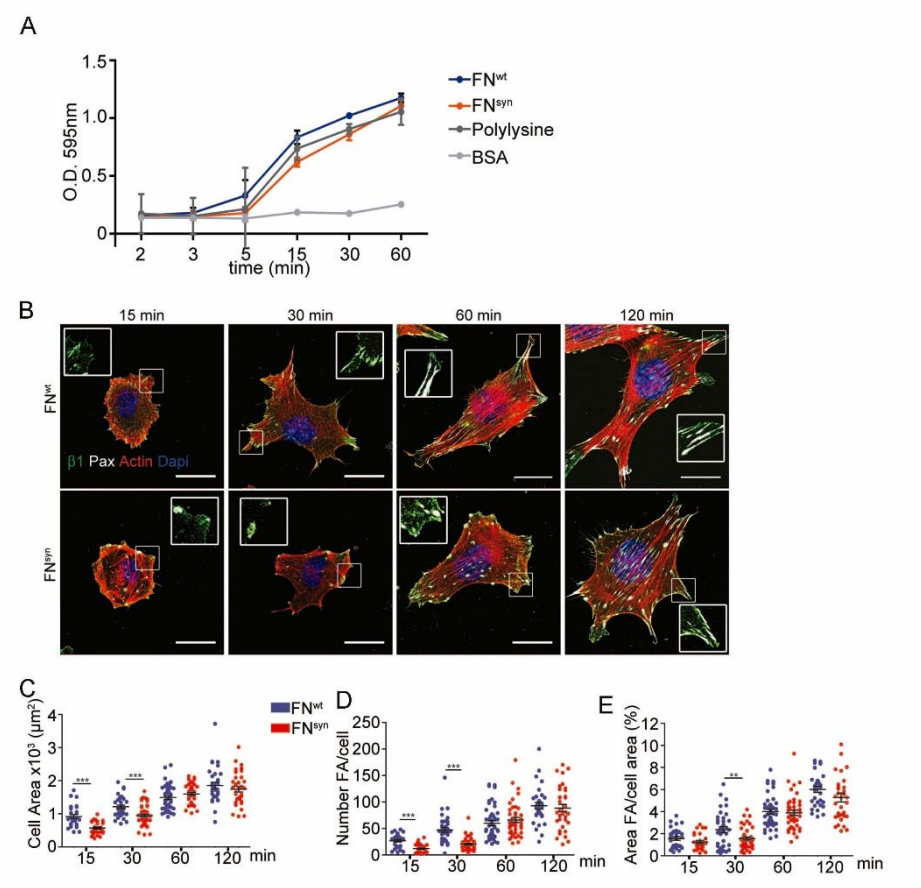

Figure 44. The FN synergy site is dispensable for cell adhesion and spreading. (A) *Fn1*-Knock-Out (*Fn1*-KO) adhered to pFN^{wt} or pFN^{syn} during a 60 min time-course. Adhered cells were fixed, stained with crystal violet and measured with by spectrophotometry (n= 4 independent experiments). (B) *Fn1*-KO cells seeded on pFN^{wt} or pFN^{syn}, fixed at the indicated times and stained for F-actin (red), paxillin (white) and total b1 integrin (green). Scale bar, 20 µm. (C–E) Cell size (C), number of FAs per cell (D) and percentage coverage by FAs (paxillin-positive) (E) were quantified (n=25 cells assessed from three independent experiments; mean ± sem).

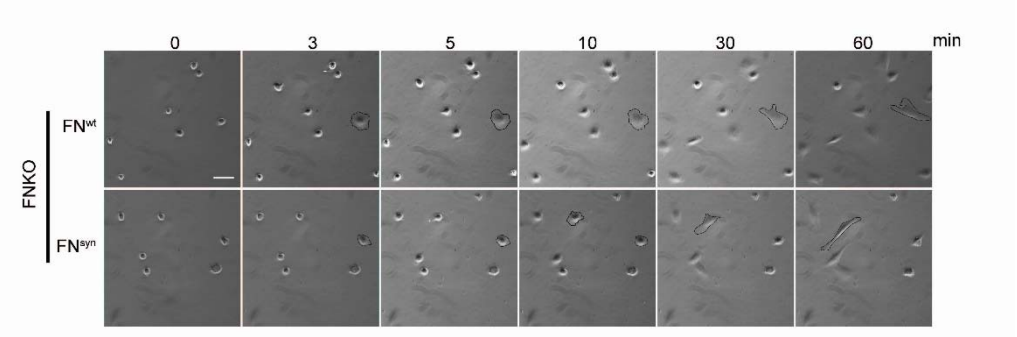

Figure 45. Captures of life-time microscopy videos of *Fn1*-KO fibroblasts spreading on pFN^{wt} or pFN^{syn}. Cell area is defined with black line.

2.4. Strength of the integrin α5-FN^{syn} bond

Friedland et al., 2009 reported that HT1080 cells seeded on the FNIII7-10 fragment, reinforce the adhesion strength to FN upon force application, such as shear forces. We wanted to know whether the synergy site was critical in this reinforcement. To this end, we made adhesion experiments under shear stress with a spinning-disk device. Overnight-starved *Fn1*-KO fibroblasts were seeded for 1 h onto glass coated with FN^{wt} or FN^{syn} and recombinant FNIII7-10^{wt} or FNIII7-10^{syn} polypeptides and applied a hydrodynamic shear force (Garcia, 1998). The number of *Fn1*-KO fibroblasts adhering to FN^{wt}-coated coverslips and spun for 5 min decreases non-linearly with the applied force following a sigmoidal curve (Fig. 46 A), whose inflection point (τ50) corresponds to the mean shear stress for 50% detachment, and hence to a quantitative measure of adhesion strength. The τ50 values of *Fn1*-KO cells decreased on full-length pFN^{syn} by 16% compared to pFN^{wt} (Fig. 46 B), and by 43% on FNIII7-10^{syn} fragment compared to FNIII7-10^{wt} (Fig. 46 C), indicating that cells adhere less strongly to the synergy site-deficient FN and that higher adhesion strengths arise on full-length FN compared to FNIII7-10 fragments. The differences between full-length FN and the fragment could indicate that other FN receptors, such as syndecans, could contribute to strength the bond. To test whether syndecans contribute to the strength of the bond, cells were adhered for 1 h on FN-coated coverslips in presence of 0.1 mg/ml heparin. When cells were treated with heparin, the strength of the bond reduced 19% when cells adhered to FN^{wt} and 15% when cells adhered to FN^{syn} in comparison to non-treated fibroblasts (Fig. 46 D). However, the differences in the τ50 values between cells adhered to full-length FN^{syn} and to FN^{wt} were mantained (reduction of 18%) in presence of heparin. Quantification of number of cells adhered in static (pre-spin) conditions showed that heparin treatment affected cell adhesion to FN as 18-20% less cells adhered to both FNs in presence of heparin (Fig. 46 E). Hence, syndecans do not compensate the lack of a functional synergy site or contribute to the strength of the bond but rather influence cell adhesion to FN.

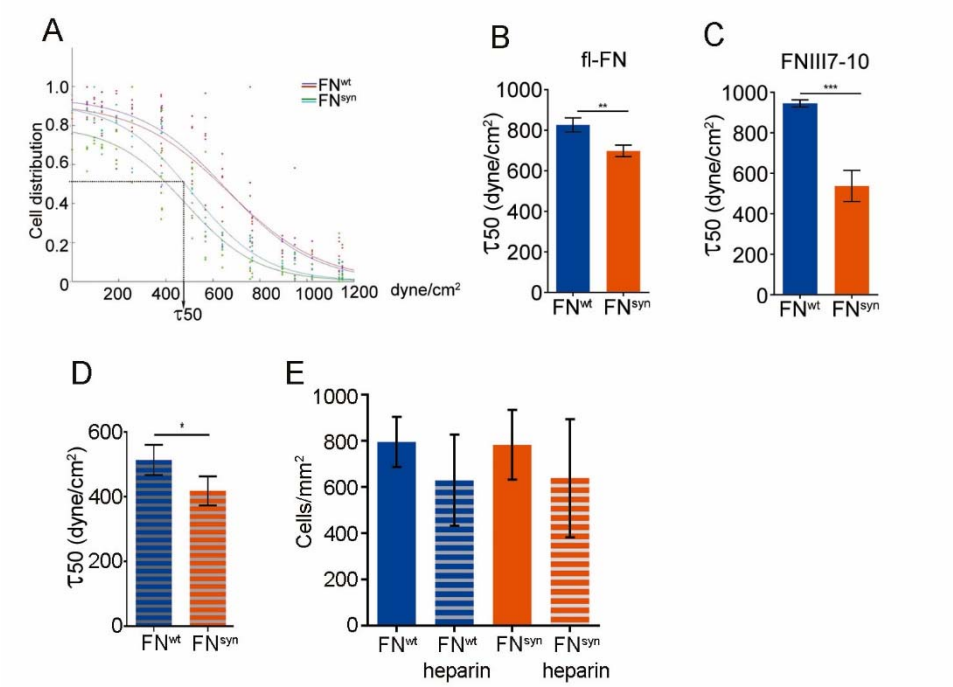

Figure 46. The FN synergy site is required to strengthen the FN-α5β1 bonds. (A) Representative spinning disk experiment showing the cell distribution profile against the shear force. (B-C) Quantification of adhesion strength. 7 x 10^5 *Fn1*-KO cells attached onto (A) purified, full-length (fl) pFN^{wt} or pFN^{syn} or (B) $FNIII7\text{-}10^{wt}$ or $FNIII7\text{-}10^{syn}$ and spun with a spinning disk device (N=7 independent experiments with fl-FN; n=3 independent experiments with FNIII7-10; mean ± sem). (D) Quantification of adhesion strength. Heparin treated *Fn1*-KO cells attached onto purified, full-length (fl) pFN^{wt} or pFN^{syn} (n=3 independent experiments). (E) Quantification of adhered *Fn1*-KO cells to purified, full-length (fl) pFN^{wt} or pFN^{syn} when treated with heparin in comparison with non-treated cells (n=3 independent experiments; mean ± sem).

To address whether the significant but slight reduction in the strength of the bond when *Fn1*-KO cells adhered to full-length pFN^{syn} was exclusive of this cell line, the experiments were repeated using HT1080 cells (Fig. 47). This cell line expresses also α5β1 and αvβ3 although they strength the FN bond by α5β1 (Engler *et al.*, 2009). The HT1080 cells reduced a 33% the τ50 when they adhered to full-length FN^{syn} in comparison to FN^{wt} (Fig. 47 A). In this case the reduction when cells adhered to $FNIII7\text{-}10^{syn}$ fragment was of 30% compared to $FNIII7\text{-}10^{wt}$ (Fig. 47 B). This indicates that the function of the synergy site in bond strengthening is not exclusive of a cell line and is highly relevant to strength the integrin α5β1-FN bond.

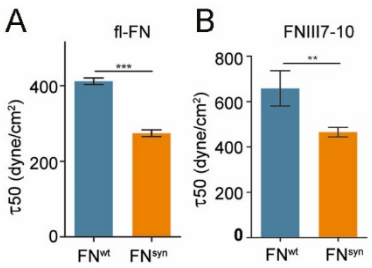

Figure 47. The FN synergy site strengthens the FN-α5β1 bonds in human cells. Quantification of adhesion strength. 7 x 10^5 *Fn1*-KO cells attached onto (A) purified, full-length (fl) pFN^{wt} or pFN^{syn} or (B) $FNIII7\text{-}10^{wt}$ or $FNIII7\text{-}10^{syn}$ and spun with a spinning disk device (N=3 independent experiments; mean ± sem).

2.5. Catch bond formation between integrin α5 and FN^{syn}

Simultaneous engagement of the RGD motif and the synergy site was suggested to enable α5β1 and αIIbβ3 integrins to induce tensioned bonds (catch bonds). Catch bonds cause receptor and ligand to be in close proximity. Therefore, to quantify catch bonds they can be chemically cross-linked with a linker of 8-atoms length (Shi and Boettiger, 2003). Moreover, it has been shown that application of an external force can promote bonds to tension and form catch bonds (Friedland et al., 2009). To test the extent of bond tensioning on FN^{syn}, serum-starved *Fn1*-KO fibroblasts were seeded (15, 30 and 60 min) onto FN^{wt}- and FN^{syn}-coated glass, respectively, spun and treated with 3,3'-dithiobis (sulfosuccinimidyl propionate) (DTSSP) to crosslink extracellular secondary amines of the ligand and receptor that are within 1.2 nm proximity to each other when bonds are tensioned. The amount of α5 integrins crosslinked to FN in *Fn1*-KO fibroblasts was reduced to 60% on FN^{syn} compared with FN^{wt} (Fig. 48). Upon spinning, *Fn1*-KO cells increased the proportion of α5 integrins crosslinked to FN^{wt}. Importantly, in cells on FN^{syn}, the external tension exerted by the spinning-disk was unable to increase the number of crosslinked bonds and their numbers remained at the same levels as before spinning (Fig. 48). Altogether indicates that the shear force strengthens α5β1-mediated adhesion to FN in a synergy site-dependent manner promoting catch bond formation.

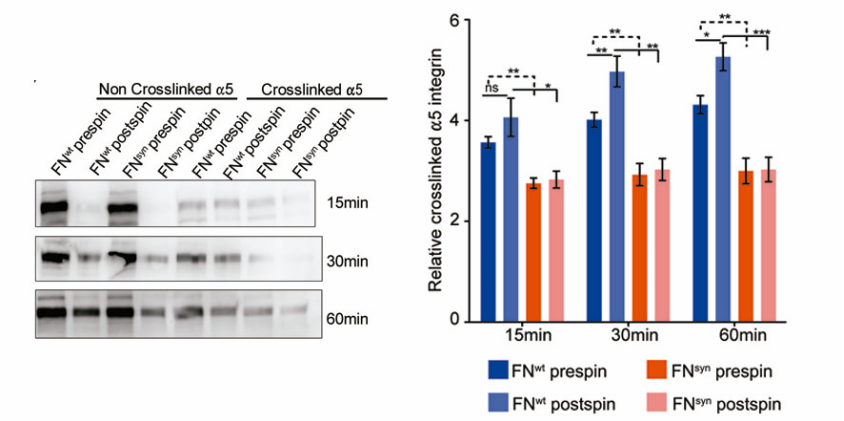

Figure 48. The FN synergy is important for stablishing FN-α5β1 catch bonds. Western-blot analysis (left) and quantification (right) of cross-linked α5 integrins to pFN^{wt} or pFN^{syn} before and after applying shear forces (n=6 independent experiments; mean ± sem).

2.6. Signalling downstream integrin α5-FN^{syn} bond: FAK phosphorylation

It was reported that the conversion of FN-α5β1 bonds from a relaxed to a tensioned state induces phosphorylation of focal adhesion kinase (FAK) on the tyrosine 397 (Y397) (Guan *et al.*, 1991; Kornberg *et al.*, 1992) (Fig. 49 A). To test whether the mutation in the synergy site affects phosphorylation of Y397-FAK, cells were plated for 1 h on FN^{syn} or FN^{wt}. Levels of pY397-FAK were reduced to 54% when cells adhered to FN^{syn} compared to FN^{wt} (Fig. 49 B). Importantly, phosphorylation in the Y861-FAK, which depends on substrate binding but is independent of tension in the bond (Shi and Boettiger, 2003), was indistinguishable in cells seeded on FN^{wt} or FN^{syn} (Fig. 49 B). Since the intensity of FAK Y397 phosphorylation somehow

operates as a sensor for ECM rigidity (Seong *et al*., 2013), according to our results, *Fn1*-KO fibroblasts attached to FN^{syn} cannot perceive substrate stiffness.

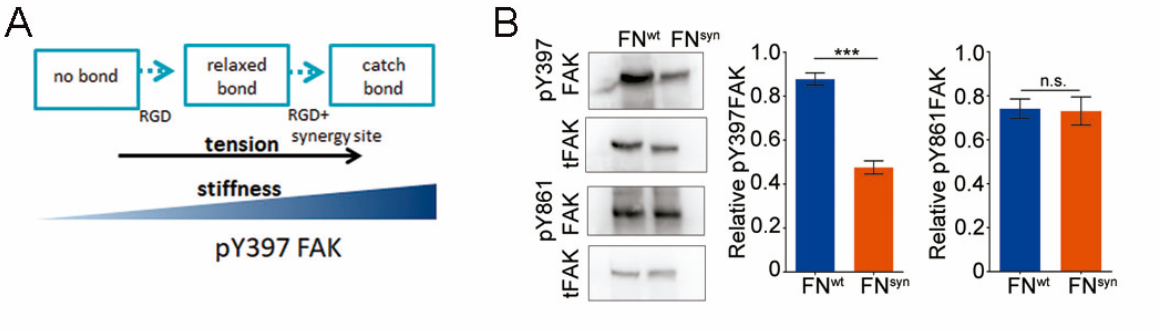

Figure 49. The FN synergy site is required to establish tensioned FN-α5β1 bonds. (A) Bond conversion to catch bond dependent to the stiffness and tension and its relationship with FAK phosphorylation. (B) Western blot analysis (left) and quantification (right) of pY397- and pY861-FAK levels in *Fn1*-KO cells plated on pFN^{wt} or pFN^{syn} (n=6 independent experiments; mean ± sem).

2.7. Adhesion and signalling on FN^{syn}-coated gels of different stiffness

Cells sense mechanical properties of their microenvironment (Butcher *et al.*, 2009) and, in turn, transmit forces to it, adapting to different mechanical microenvironments by signalling (Seong *et al.*, 2013). We tested the capability of *Fn1*-KO fibroblasts to adapt to FN^{syn} ECM of different rigidities. For that purpose, *Fn1*-KO fibroblasts were seeded for 1 h on polyacrylamide gels of different stiffness (0.4, 4 and 50 kPa) coated with FN^{wt} or FN^{syn} and cell spreading was analysed after 15, 30 and 60 min (Fig. 50 A-C). Cells detect rigidity, and thereby modulate their behaviour, exerting more force on high stiffness. To exert more force, integrins strengthen the bond and actin polymerizes (Elosegui-Artola *et al.*, 2014). *Fn1*-KO fibroblasts adhered to FN^{wt}-coated gels increment their spreading area with the stiffness of the substrate as consequence of strengthening the bond. However, as shown in figure 50 B, less cells adhered to FN^{syn} than to FN^{wt}-coated gels of 0.4, 4 and 50 kPa (all softer than glass). Furthermore, cells seeded on FN^{syn}-coated gel surfaces showed less spreading areas in all time-points and stiffness analysed in comparison to FN^{wt}-coated gels (Fig. 50 C), indicating that integrin engagement to the synergy site is essential to strengthen the bond and adapt to the stiffness of the FN ECM. To analyse whether signalling was also altered under these conditions, after 60 min of adhesion, levels of pY397FAK were checked by western blotting (Fig. 50 D). While cells on FN^{wt}-coated gels experimented a slight increase in Y397-FAK phosphorylation on higher stiffness, on FN^{syn}-coated gels phosphorylation of FAK was heavily reduced regardless the stiffness of the substrate. All these results together confirmed that cells are less sensible to changes in the mechanical properties of their environment when the synergy site is mutated.

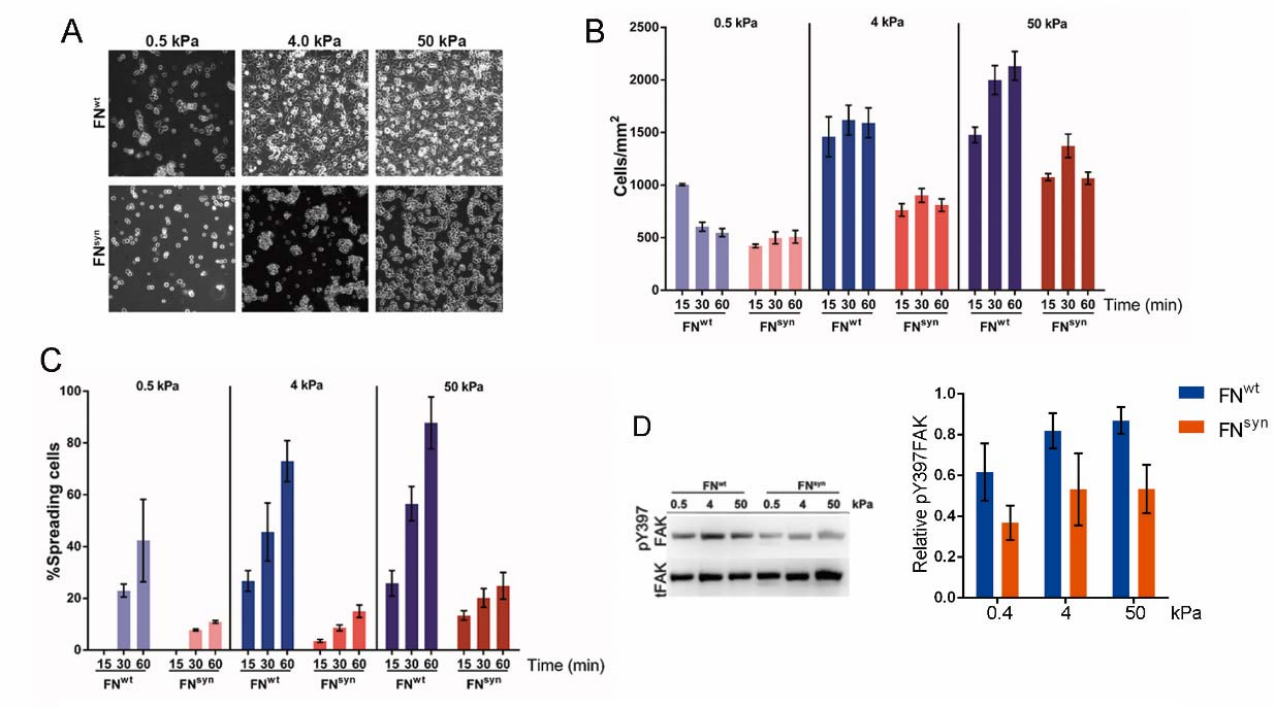

Figure 50. The FN synergy site modulates adaptation to different rigidities. (A) Representative images of *Fn1*-KO adhered to pFN^{wt} or pFN^{syn}-coated soft gels of different stiffness (0.4, 4 and 50 kPa) during 60 min. (B-C) Measurements of (B) cell area and (C) cell spreading of *Fn1*-KO adhered to pFN^{wt} or pFN^{syn}-coated different stiffness soft gels over a time-course (n=3 independent experiments; 15 fields measure per experiment and condition). (D) Western blot analysis (left) and quantification (right) of pY397-FAK levels in *Fn1*-KO cells plated on pFN^{wt} or pFN^{syn}-coated gels of different rigidities (n=7 independent experiments; mean ± sem).

3. Influence of αv-class integrins in cell adhesion to FN^{syn}

Fn1-KO cells express high levels of αv-class integrins, which do not bind the synergy site and therefore could, at least in part, compensate for the absence of the synergy site. To test this hypothesis, adhesion and spreading to FN^{wt} and FN^{syn}-coated substrates was studied with pan-integrin-null fibroblasts (pKO) expressing specific integrins. The pKO fibroblasts were genetically engineered to no present integrins on their surfaces and subsequently were reconstituted with single integrins generating three cell lines: pKO-β1 which only express α5β1 integrin, pKO-αv which contain αvβ3 and αvβ5 integrins, and pKO-αv/β1 with both sets of integrins (α5β1, αvβ3 and αvβ5) (Schiller et al., 2013).

3.1. Adhesion and spreading of pKO-β1, pKO-αv and pKO-αv/β1 to FN^{syn}

For the three lines (pKO-β1, pKO-αv and pKO-αv/β1) cell adhesion was evaluated on FN^{syn} over a time-course (15, 30 and 60 min) and compared to FN^{wt} (Fig. 50 A). The number of adhered cells increased over time in the three lines, regardless the substrate. Although pKO-αv cells adhered less than pKO-β1 or pKO-αv/β1 over the time course, the mutation in the FN synergy site did not affect pKO-αv cell adhesion. The mutation of the syngergy site did not affect neither pKO-αv/β1 fibroblast adhesion too. However, FN pKO-β1 cells exhibited reduced adhesion on FN^{syn} compared to FN^{wt} at all analysed time points (Fig. 51 B) indicating that αv integrins could compensate the absence of synergy site. To analyse cell spreading and FA formation, pKO-β1, pKO-αv and pKO-αv/β1 fibroblasts were seeded on FN-coated cover-slips for 15, 30 and 60 min and immunostained for paxillin and actin. From the three cell lines, pKO-

β1 spreading on FN^{syn} was significantly reduced compared to FN^{wt} (Fig. 51 B–F). Moreover, pKO-β1 cells displayed different morphology on FN^{syn} than on FN^{wt}, most of the actin remained cortical and fewer stress fibres formed. A detailed analysis of pKO-β1 fibroblasts FA showed that these fibroblasts had significantly fewer FAs and the areas of FAs determined with paxillin and β1 integrin stainings were significantly reduced on FN^{syn} compared to FN^{wt} (Fig. 51 G, H), which altogether suggests that FN^{syn}-bound α5β1 integrins fail to organize functional adhesion sites and to induce contractile stress fibres required for cell spreading. pKO-αv cells adhered and spread similarly on FN^{wt} and FN^{syn}, and developed comparably large, paxillin-positive FAs that were anchored to thick stress fibers (Fig. 51 B, D). Importantly, pKO-αv/β1 cells also showed the same adhesion and spreading behaviour and developed similar density of FAs on FN^{syn}, indicating that αv-containing integrins compensate for the absence of a functional synergy site (Fig. 51 B, E). Interestingly, the pKO-αv/β1 cells do not show a delay in the transition from NAs to mature FAs on FN^{syn}, as we observed with *Fn1*-KO cells. Integrin profile by FACS analysis (Fig. 51 I) showed that, as expected, pKO-β1, pKO-αv and pKO-αv/β1 has different αv and β1 integrin levels. The pKO-αv/β1 cells had significantly higher β3 and lower α5 integrin cell surface levels compared to *Fn1*-KO cells, which could explain that pKO-αv/β1 fibroblasts do not experience a delay in FA maturation.

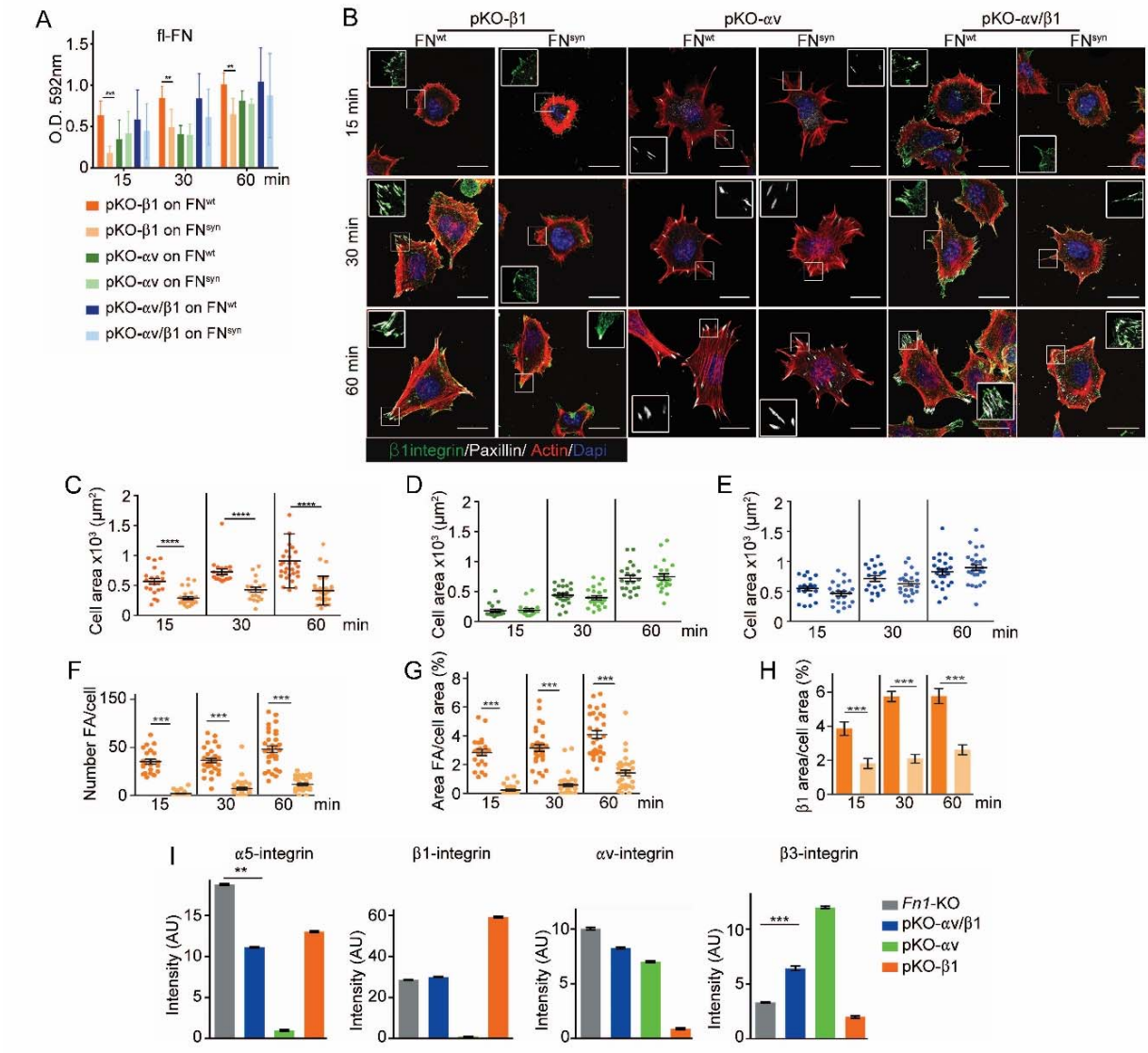

Figure 51. α5β1 integrins require the synergy site in FN to induce cell spreading. (A) Adhesion of pKO-β1, pKO-αv and pKO-αv/β1 fibroblasts seeded on pFN^{wt} or pFN^{syn} for indicated times (n=3 independent experiments; mean ± sem). (B) of pKO-β1, pKO-αv and pKO-αv/β1 fibroblasts were seeded on pFN^{wt} or pFN^{syn}, fixed at the indicated times and stained for total b1 integrin (green), paxillin (white) and F-actin (red). Scale bar, 50 mm. (C–E) Quantification of cell area of pKO-β1 (C), pKO-αv (D) and pKO-αv/β1 (E) cells seeded on pFN^{wt} or pFN^{syn} for indicated times. (F–H) Quantification of the number of FAs (F), the percentage of FA coverage measured as paxillin-positive area (G) and the percentage of b1 integrin-positive areas referred to the total cell area (H) in pKO-b1 cells (n = 25 cells for each measurement and three independent experiments; mean ± sem).(I) Integrin levels on pKO-β1, pKO-αv and pKO-αv/β1 fibroblasts surface.

4. Compensation by αv-class integrins *in vivo*

To test whether integrin αvβ3 can also compensate for the loss of FN synergy site *in vivo*, we crossed mice carrying the *Fn1*^{syn} mutation with the mouse strain *Itgb3*-null (Hodivala-Dilke et al., 1999). The *Itgb3*-null (*Itgb3*$^{-/-}$) mice cannot express β3 integrins and fail to assemble the widely expressed αvβ3 integrin receptor and the platelet-specific αIIbβ3 integrin. The *Itgb3*$^{-/-}$ mice suffer from a bleeding disorder resembling human Glanzmann thrombasthenia, which implies that around the 87% of *Itgb3*$^{-/-}$ mice are born but only 40% of them survive the first year of life (Hodivala-Dilke et al., 1999). To test how the *Fn1*^{syn} mutation affect development and survival of *Itgb*3$^{-/-}$ mice, *Fn1*$^{syn/+}$;*Itgb*3$^{+/-}$ as well as *Fn1*$^{syn/syn}$;*Itgb*3$^{+/-}$ mice were intercrossed obtaining a total of 245 and 90 live offspring at P21, respectively (Annexe II, Tables 1 and 2). Out of the 335 offspring altogether, only one, instead of the expected 38 homozygous *Fn1*$^{syn/syn}$;*Itgb*3$^{-/-}$ mice, survived to P21. The survivor died at the age of 5 months from excessive bleeding. Thus, we can conclude that the compound of mutations is embryonic lethal. To determine the embryonic day of lethality, embryos were collected at different gestation times and genotyped (Annexe II, Tables 1 and 2). Homozygous *Fn1*$^{syn/syn}$;*Itgb*3$^{-/-}$ embryos were present at the expected Mendelian distribution until E15.5, but no live embryos were present at E16.5 or later. *Fn1*$^{syn/syn}$;*Itgb*3$^{+/-}$ were normally distributed, indicating that one β3 integrin allele is sufficient to compensate for normal development.

4.1. Study of *Fn1*$^{syn/syn}$; *Itgb*3$^{-/-}$ lethality and vascular system

The *Fn1*$^{syn/syn}$;*Itgb*3$^{-/-}$ embryos presented multiple haemorrhages observable in the skin (Fig. 52 A). It is well known that FN is involved in heart and vessel morphogenesis (George *et al*., 1997). To test whether the haemorrhages were caused by defects in heart development or morphogenesis, hearts from E15.5 embryos were analysed. Histological analysis with H&E showed that the hearts from *Fn1*$^{syn/syn}$;*Itgb*3$^{-/-}$ embryos were similar to hearts from control littermates (Fig. 52 B), discarding deficiencies in heart morphogenesis to cause the haemorrhages. It has been shown that the absence of α5β1 integrin leads to vascular defects (Abraham *et al.*, 2008). To test whether vascular abnormalities due to an impaired α5β1 function contribute to the severe bleeds and the lethality of *Fn1*$^{syn/syn}$;*Itgb*3$^{-/-}$ embryos, skin whole mounts from E15.5 embryos were immunostained with epithelial (PECAM-1) and mural cell (α-smooth muscle acctin, α-SMA) markers. The arteries and veins of the dermal vasculature of E15.5 *Fn1*$^{syn/syn}$;*Itgb*3$^{-/-}$ embryos were more tortuous and irregularly covered with α-SMA-positive cells compared with wild-type littermates (Fig. 52 C). In addition, the

vascular network was less intricate and had significantly fewer branching points in *Fn1*$^{syn/syn}$;*Itgb3*$^{-/-}$ embryos compared to the control littermates (Fig. 52 D).

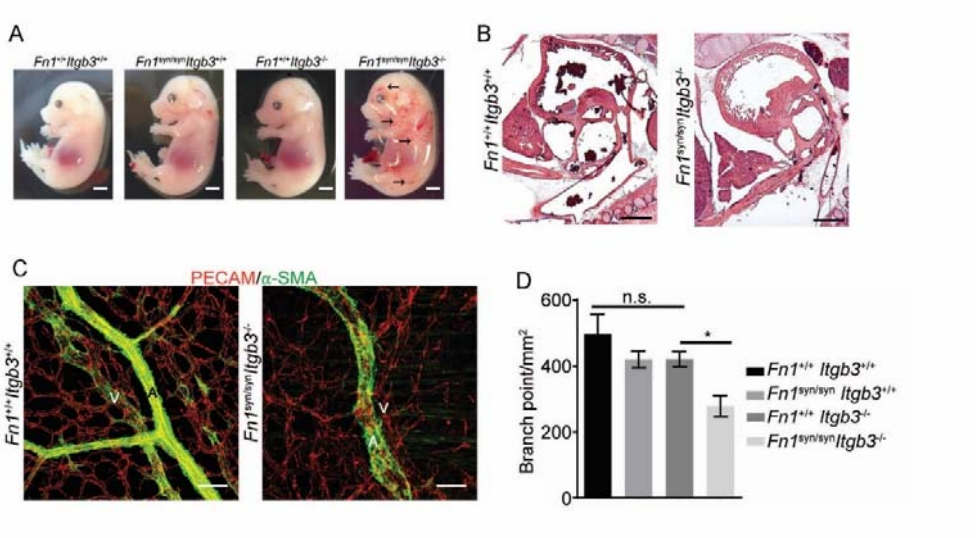

Figure 52. *Fn1*$^{syn/syn}$;*Itgb3*$^{-/-}$ mice suffer from severe haemorrhages and malformed vessels. (A) Representative images from E15.5 littermates embryos resulting from *Fn1*$^{syn/+}$;*Itgb3*$^{-/-}$ intercrossed. Compound *Fn1*$^{syn/syn}$;*Itgb3*$^{-/-}$ embryos display cutaneous oedema (arrowhead) and abundant skin haemorrhages (arrows); scale bars, 50 mm. (B) Representative images of E15.5 heart sections. Scale bar 100 µm. (C) PECAM-positive endothelial cells (red) and a-SMA-positive smooth muscle cells (green) in dermal whole mounts from E15.5 *Fn1*$^{+/+}$;*Itgb3*$^{+/+}$ and *Fn1*$^{syn/syn}$;*Itgb3*$^{-/-}$ littermate embryos indicate veins (V) and arteries (A). Scale bar 50 µm. (D) Quantification of the number of branching points (n = 10–15 images of 2–3 embryos; mean ± sem)

Reduced vasculature density could be caused by either a defect in new vessels formation (sprouting) or in vessel stability. Sprouting can be analysed in the trunk of embryos at E10-11.5, where it is possible to observe the ramifications or sprouts which the endothelial cells produce in order to form new vessels. Whole mount immunostaining of E11.5 embryos with an anti-PECAM-1 revealed that the vessels in the trunk of *Fn1*$^{syn/syn}$;*Itgb*3$^{-/-}$ embryos had normal sprouting in comparison to their control littermates (Fig. 53 A-B) discarding a defect in vessel formation.

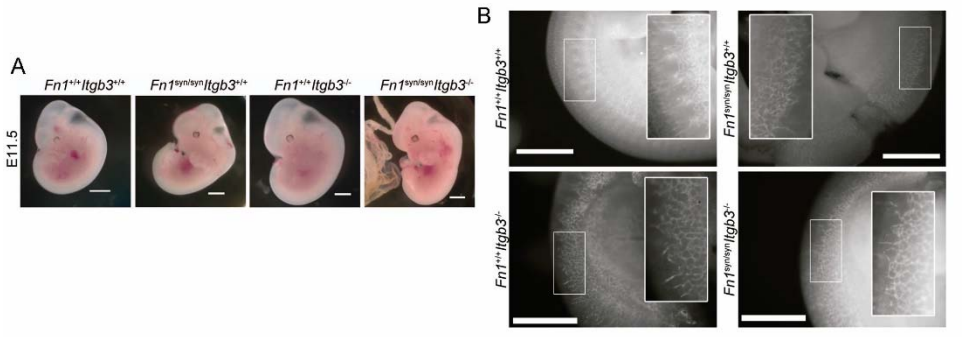

Figure 53. *Fn1*$^{syn/syn}$;*Itgb3*$^{-/-}$ mice do not display sprouting defects. (A) Images of E11.5 embryos from *Fn1*$^{syn/+}$;*Itgb3*$^{+/-}$ mattings. Scale bar, 2 mm (B) E11.5 whole mount embryos of indicated genotype stained with PECAM. High magnifications indicate that *Fn1*$^{syn/syn}$;*Itgb3*$^{-/-}$ embryos have normal angiogenesis. Scale bar, 1 mm.

A sign of vascular instability is the presence of vessels undergoing retraction, which is due to deficient cell-cell or cell-matrix adhesion. This event is observed as vessels (endothelial cells) without lumen and later as basal membrane lacking endothelial cells (Yamamoto *et al.*, 2015). The analysis of the blood vessels (PECAM-1 labelled) and its basal membrane (collagen IV labelled) in *Fn1*$^{syn/syn}$;*Itgb3*$^{-/-}$ embryos at E15.5 showed that many blood vessels were retracting (arrows, fig. 54 A), and in comparison to *Itgb3*$^{-/-}$ or wild-type littermates the number of retracted vessel per area was significantly higher (Fig. 54 B). In addition, areas with vessels under retraction in *Fn1*$^{syn/syn}$;*Itgb3*$^{-/-}$ were coincident with regions of haemorrhages (Fig. 54 C), suggesting that these events could cause vessel leaking. To examine the mural cells, which protect the endothelium, pericytes were marked with NG2 proteoglycan (NG2). Small vessels of in *Fn1*$^{syn/syn}$;*Itgb3*$^{-/-}$ embryos were often less covered by pericytes (Fig. 53 D). Indeed, pericytes seemed to detach from the endothelium in some points and also to aggregate in some branching areas (arrow heads in Fig. 54 D). Altogether, these observations pointed that vessel wall coverage and stability are reduced in *Fn1*$^{syn/syn}$;*Itgb3*$^{-/-}$ embryos and probably contribute to their severe haemorrhages.

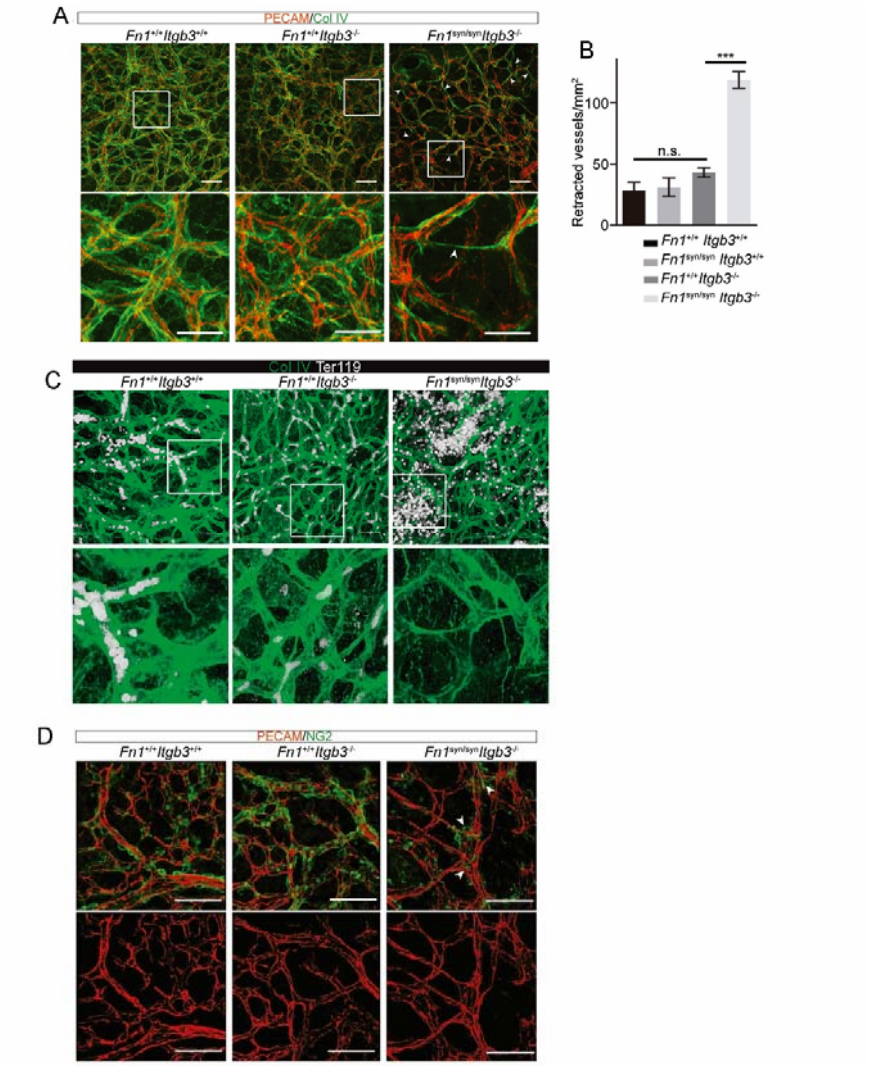

Figure 54. *Fn1*$^{syn/syn}$;*Itgb3*$^{-/-}$ present malformed vessels. (A) Vascular basement membranes in dermal whole mounts from E15.5 *Fn1*$^{+/+}$;*Itgb3*$^{+/+}$, *Fn1*$^{+/+}$;*Itgb3*$^{-/-}$ and *Fn1*$^{syn/syn}$;*Itgb3*$^{-/-}$ littermate embryos stained for type IV collagen (green) and PECAM-positive endothelial cells (red). Arrowheads show small vessels lacking lumen. (B) Quantification of retracted vessels (n = 14–23 from 4–7 embryos; mean ± sem). (C) Dermal whole mounts stained with anti-collagen IV (basal membrane) and anti-ter119 (erythrocytes) to analyse blood leakage and haemorrhages in E15.5 *Fn1*$^{+/+}$;*Itgb3*$^{+/+}$, *Fn1*$^{+/+}$;*Itgb3*$^{-/-}$ and *Fn1*$^{syn/syn}$;*Itgb3*$^{-/-}$ littermate embryos. (D) PECAM-positive endothelial cells (red) and NG2-positive pericytes (green) in dermal whole-mounts from E15.5 *Fn1*$^{+/+}$;*Itgb3*$^{+/+}$, *Fn1*$^{+/+}$;*Itgb3*$^{-/-}$ and *Fn1*$^{syn/syn}$;*Itgb3*$^{-/-}$ littermate embryos. Note pericytes are sparse, absent or aggregate on mutant vessels (arrowheads). Scale bars, 50 µm.

4.2. *Fn1*$^{syn/syn}$; *Itgb3*$^{-/-}$ lymphatic phenotype

The *Fn1*$^{syn/syn}$; *Itgb3*$^{-/-}$ embryos displayed multiple cutaneous haemorrhages and oedema, which were first visible at E11.5-12.5 (Fig. 55 A) and then spread over the whole body at E15.5 (Fig. 52 A). Interestingly, at E12.5 the bleeds were only located at two specific sites: the subclavian and the jugular veins (arrowheads in Fig. 55 A). These two veins are connected to the main lymphatic ducts, which drain the lymph back to the blood. The process of separating the lymphatic vessels from the blood system at E11-13, and its failure causes the blood infiltration in the lymphatic vessels (Carramolino *et al.*, 2010).

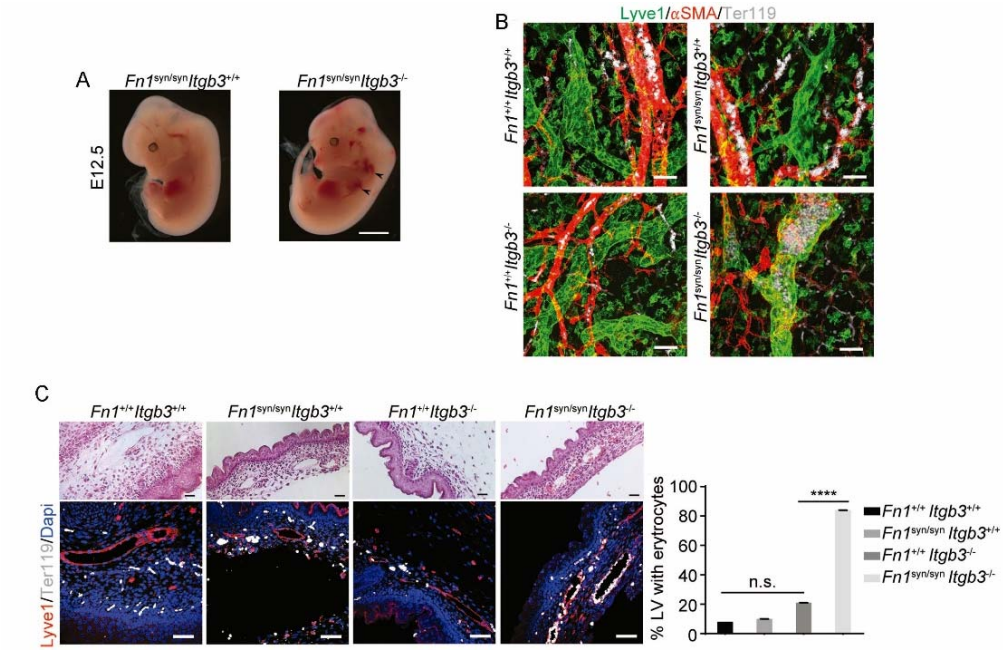

Figure 55. *Fn1*$^{syn/syn}$;*Itgb3*$^{-/-}$ suffer from severe hemorrhages and fail to separate the blood and lymphatic vasculatures. (A) E12.5 *Fn1*$^{syn/syn}$;*Itgb3*$^{-/-}$ embryos display hemorrhages in the jugular and axilar areas in the left side (arrowheads). Scale bar, 50 mm. (B) Skin whole-mount from E15.5 embryos showing Lyve1-positive lymphatic vessels (green), αSMA-positive blood vessels (red) and Terr119-positive erythrocytes (white). The lymphatic vessels of compound *Fn1*$^{syn/syn}$;*Itgb3*$^{-/-}$embryos are dilated, covered by ectopic αSMA-positive cells and filled with erythrocytes. Scale bar, 50 µm. (D) Representative images of skin sections tained with H and E (upper panel) and Lyve1 and Terr119 (lower panel) showing erythrocytes in lymphatic vessels. Scale bar, 50 µm. (E) Quantification of the percentage of lymphatic vessels filled with Ter119-positive erythrocytes (n = 40 vessels counted per embryo, in two embryos per each genotype; mean ± sem).

To address whether the *Fn1*$^{syn/syn}$; *Itgb3*$^{-/-}$ embryos suffered from deficiencies in lymphatic vessel segregation, whole mounts of skin were immunostained to mark lymphatic vessels (Lyve-1), smooth muscle cells (α-smooth muscle actin, α-SMA) and erythrocytes (Ter119) (Fig. 55 B). Staining with Lyve-1 showed that at E15.5 lymphatic vessels in the skin of *Fn1*$^{syn/syn}$; *Itgb3*$^{-/-}$ appeared distended or hyperplasic. In addition, they contained some ectopic α-SMA positive cells surrounding the lymphatic endothelium and were filled of erythrocytes, contrary to *Itgb3*$^{-/-}$ embryos or wild-type littermates whose lymphatic vessels lacked Ter119-positive cells and were not surrounded with α-SMA-positive cells. To confirm this observation, embryo paraffin sections were immunostained with Lyve-1 and Ter119 and the number of dermal lymphatic vessels infiltrated with erythrocytes were counted (Fig. 55 C-D). Whereas in *Fn1*$^{syn/syn}$; *Itgb3*$^{-/-}$ embryos the 80% of the lymphatic vessels were infiltrated with erythrocytes, only the 20% of *Itgb3*$^{-/-}$ and none of *Fn1*$^{syn/syn}$ or wild-type lymphatic vessels had erythrocytes. These results together indicate that the mutation in the synergy site impedes lymphatic vessel separation from blood vessels when the integrin β3 is absent.

5. *Itgb3*$^{-/-}$ platelet function in *Fn1*$^{syn/syn}$ background

The separation of the primary lymphatic sac from the cardinal vein is driven by platelet adhesion to and aggregation at the endothelium (Carramolino et al., 2010; Uhrin et al., 2010). The platelets from *Fn1*$^{syn/syn}$;*Itgb3*$^{-/-}$ embryos lack the αIIbβ3 integrin receptor and cannot bind fibrinogen, but remains the capability to strengthen adhesion to FN using α5β1 integrin receptors. Thus, the defect in lymphatic system separation could be due to a defect in platelet adhesion to FN. To address if platelet function was more compromised in *Fn1*$^{syn/syn}$;*Itgb3*$^{-/-}$ embryos than in *Fn1*$^{+/+}$;*Itgb3*$^{-/-}$, cell adhesion was assayed in static and under flow conditions.

5.1. Static platelet adhesion

Platelets are activated by agonists, which enables them to bind to different plasma and ECM proteins (Jackson, 2007). To assay adhesion, washed *Itgb3*$^{-/-}$ and *Itgb3*$^{+/+}$ platelets were seeded on fibrinogen, collagen, FN^{wt} or FN^{syn}, ligands which are bound by distinct receptors (Fig. 56 A). Platelet spreading area was measured after 15, 30 or 60 min of adhesion (Fig. 56 B-C). Both, *Itgb3*$^{-/-}$ and *Itgb3*$^{+/+}$ platelets spread on collagen in a similar way. As expected, *Itgb3*$^{-/-}$ platelets failed to spread on fibrinogen (mean spreading area of 4.6 mm^2) while *Itgb3*$^{+/+}$ platelets acquired a mean spreading area of 14 mm^2 already after 15 min. *Itgb3*$^{-/-}$ platelets attached and spread on FN^{wt} although they had a smaller spreading area (8.9 mm^2) than *Itgb3*$^{+/+}$ (14 mm^2) after 60 min. Importantly, while *Itgb3*$^{+/+}$ had similar spreading area on FN^{syn} (14 mm^2) than on FN^{wt}, *Itgb3*$^{-/-}$ platelets could not spread on FN^{syn}, similarly to the situation with fibrinogen substrate (3.8 mm^2). This indicates that platelets lacking the integrin αIIbβ3, although express α5β1 failed to adhere to FN^{syn}.

5.2. Platelet adhesion under flow

To study platelet adhesion under more physiological conditions, washed *Itgb3*$^{-/-}$ and *Itgb3*$^{+/+}$ platelets were subjected to shear flow in specialized chambers. The chambers were coated with fibrinogen, collagen, FN^{wt} or FN^{syn}. A mixture of washed platelets and erythrocytes

was let run through the coated chambers and afterwards the amount of adhered platelets was measured as % of platelet coverage (Fig. 56 D-E). As in static conditions, *Itgb3*$^{-/-}$ and *Itgb3*$^{+/+}$ platelets adhered to collagen and *Itgb3*$^{-/-}$ platelets did not bind fibrinogen. In this case, both *Itgb3*$^{-/-}$ and *Itgb3*$^{+/+}$ bind similarly to FN^{wt}. Interestingly, application of shear flow reduced adhesion of wild-type platelets to FN^{syn} by 10-fold compared to FN^{wt} and adhesion of *Itgb3*$^{-/-}$ platelets was lost on FN^{syn} as well as on fibrinogen (Fig. 56 D, E). These *in vitro* experiments demonstrate that adhesion of αIIbβ3-deficient platelets to wild-type FN is partially compensated by α5β1 integrins in a FN synergy site-dependent manner, and that α5β1 as well as αIIbβ3 integrins require the FN synergy site to reinforce platelet adhesion to FN, under physiological conditions.

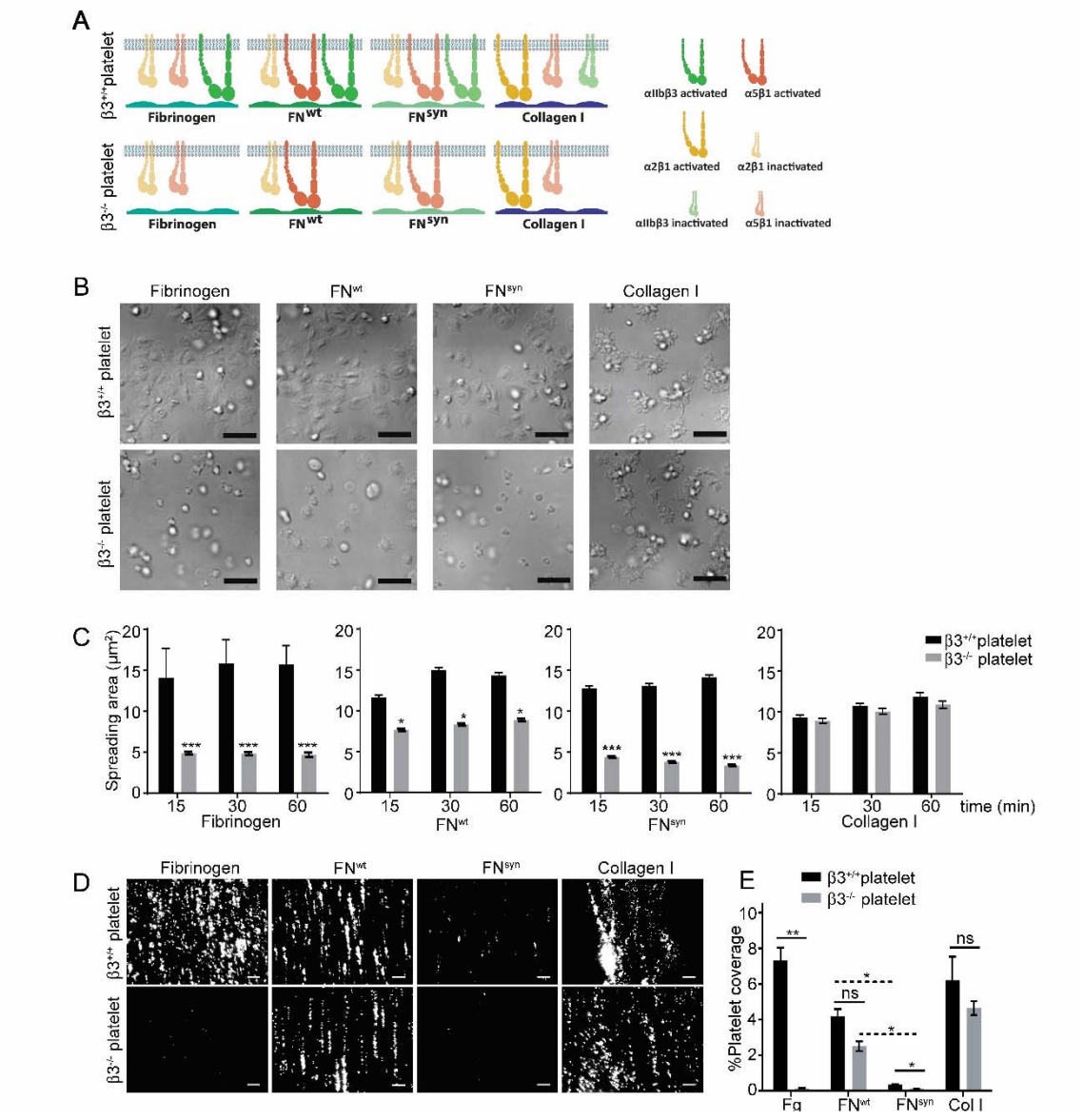

Figure 56. Shear flow exposed platelets fail to adhere to pFN^{syn}. (A) Cartoon showing the platelet integrins that can be ligated to the different substrates used in the experiments. The color intensity of the integrin denotes whether the integrin is active or inactive. (B) Spreading of *Itgb3*$^{+/+}$ and *Itgb3*$^{-/-}$ platelets after 1 h on fibrinogen, pFN^{wt}, pFN^{syn} and type I collagen. Scale bars, 10 μm. (C) Quantification of the platelet area at indicated times (n = 100 platelets per each condition in three independent experiments; mean ± sem). (D) Representative figures of fluorescently labeled *Itgb3*$^{+/+}$ or *Itgb3*$^{-/-}$ platelets seeded on indicated substrates and exposed to shear flow. Scale bar, 40 μm. (E) Platelet coverage after 10 min shear flow of 1000 s^{-1}. (n = 10 pictures per experiment, four independent experiments for each condition; mean ± sem).

Table 1. Progeny of *Fn1*$^{syn/+}$*;Itgb3*$^{+/-}$ x *Fn1* $^{syn/+}$*;Itgb3*$^{+/-}$ intercrosses.

Age	Num.	*Fn1*$^{syn/syn}$ *Itg*b3$^{+/-}$	*Fn1*$^{syn/syn}$ *Itg*b3$^{+/+}$	*Fn1*$^{syn/syn}$ *Itg*b3$^{-/-}$	*Fn1*$^{+/syn}$ *Itg*b3$^{+/-}$	*Fn1*$^{+/syn}$ *Itg*b3$^{+/+}$	*Fn1*$^{+/syn}$ *Itg*b3$^{-/-}$	*Fn1*$^{+/+}$ *Itg*b3$^{+/-}$	*Fn1*$^{+/+}$ *Itg*b3$^{+/+}$	*Fn1*$^{+/+}$ *Itg*b3$^{-/-}$
E11.5	36	6 (16.7%)	1 (2.8%)	1 (2.8%)	10 (27.8%)	6 (16.7%)	4 (11.1%)	5 (13.9%)	2 (5.6%)	1 (2.8%)
E14.5	23	2 (8.7%)	2 (8.7%)	2 (8.7%)	5 (21.7%)	5 (21.7%)	1 (4.3%)	1 (4.3%)	4 (17.3%)	1 (4.3%)
E15.5	121	12 (9.9%)	5 (4.1%)	3 (2.5%)	39 (32.2%)	5 (15.4%)	12 (9.9%)	14 (11.6%)	17 (14%)	4 (3.3%)
E16.5	16	2 (12.5%)	1 (6.25%)	0	5 (31.5%)	1 (6.25%)	1 (6.25%)	3 (37.5%)	1 (6.25%)	2 (12.5%)
E17.5	16	2 (12.5%)	0	0	6 (23%)	3 (19%)	2 (12.5%)	2 (12.5%)	1 (8%)	0
P 21	245	33 (13.5%)	32 (13%)	0	57 (23%)	46 (18.7%)	13 (5.3%)	35 (14.4%)	17 (3.9%)	12 (4.9%)
Mendelian Distribution	100	12.5%	6.25%	6.25%	25%	12.5%	12.5%	12.5%	6.25%	6.25%

Table 2. Progeny of *Fn1*$^{syn/syn}$*;Itgb3*$^{+/-}$ x *Fn1*$^{syn/syn}$*;Itgb3*$^{+/-}$ intercrosses.

Age	Num.	*Fn1*$^{syn/sy}$ ^{n}*Itg3*$^{+/-}$	*Fn1*$^{syn/sy}$ ^{n}*Itg3*$^{+/+}$	*Fn1*$^{syn/sy}$ ^{n}*Itg3*$^{-/-}$
E11.5	13	4 (31%)	6 (46%)	3 (23%)
E14.5	31	7 (22.6%)	14 (45.2%)	10 (32.2%)
E15.5	9	3 (33%)	3 (33%)	3 (33%)
E16.5	31	8 (26%)	19 (61%)	4 (13%)
P 21	90	25 (27.7%)	64 (71%)	1 (1.1%)
Mendelian Distribution	100	25%	50%	25%

V DISCUSSION

Chapter I. Analysis of the role of the RGD motif in FN fibrillogenesis

Chapter II. Study the FN synergy site function

V DISCUSSION

Chapter I. Analysis of the role of the RGD motif in FN fibrillogenesis

The RGD motif of FN has been considered essential for FN fibrillogenesis as it binds α5β1 integrins. It is well accepted that FN fibrillogenesis is a cell driven process started by cellular receptors that activate cytoskeletal contraction (Schwarzbauer, 1991; Mao and Schwarzbauer, 2005). According to this model, integrin activation and the actin force transmitted through them is essential to unfold the soluble secreted FN, allowing intermolecular interactions and formation of a fibrillar meshwork (Schwarzbauer and DeSimone, 2011). The α5β1 integrin has been pointed as the principal receptor to mediate FN fibrillogenesis for different reasons: (1) this receptor was considered the major receptor for FN as FN is its only ligand, and their interaction is essential for development (Schwarzbauer and DeSimone, 2011); (2) the α5β1 integrin is the only one found in the denominated fibrillar adhesions associated to FN fibrillogenesis (Mao and Schwarzbauer, 2005); (3) α5β1 was shown to bind more efficiently folded soluble FN than αvβ3 (Huveneers *et al.*, 2008). However, other integrins, such αv-class or α4 have been shown to form FN fibrils in absence of α5β1 *in vitro* (Wu *et al.*, 1996; Yang and Hynes, 1996) and, more interesting, *in vivo* (Takahashi *et al.*, 2007a). Specifically, the mice expressing FN with the mutation RGD>RGE, despite dying at E9.5, contained FN fibrils in their tissues (Takahashi *et al.*, 2007a). The $FN^{RGE/RGE}$ embryos have a phenotype similar to α5-null embryos (Girós *et al.*, 2011a). The α5-null embryos die as well at E9.5, and its phenotype is not as severe as the phenotype of FN-null mice (Yang *et al*., 1993; Georges-Labouesse *et al.*, 1996), although the deletion of both α5 and αv integrins *in vivo* resembles the phenotype of FN-null mice (Yang *et al.*, 1999).This suggested that the RGE mutation abolished only integrin α5β1 binding to FN. In addition, *in vitro* experiments pointed that αvβ3 integrin could interact with a region outside the RGD motif (Takahashi *et al.*, 2007a), suggesting that no integrin could interact with the mutated RGE motif. Our lab generated mice lacking the RGD site (*Fn1*$^{\Delta RGD/\Delta RGD}$) and demonstrated that the mice with the ΔRGD mutation had a phenotype that resembled the FN-null mice (unpublished results from my lab). This result excluded that alternative regions could mediate α5β1 or αvβ3 integrin binding to FN. However, we found that the lack of the RGD motif does not abolish FN fibrillogenesis in the embryo (unpublished results from my lab) and in fibroblasts in culture. Our aim was to unravel the mechanism to assemble $FN^{\Delta RGD}$ fibrils.

It has been described that α4 integrins engage the FN by binding different domains and can assemble a FN fibrillar matrix in cell culture in an RGD-independent manner (Sechler *et al.*, 2000). However, we excluded the α4β1/β7 contribution to $FN^{\Delta RGD}$ fibrillogenesis due to the lack of α4 expression in *Fn1*$^{\Delta RGD/\Delta RGD}$ fibroblasts.

Alternatively, the Heparin II binding site in the FN has been reported to be important for unfolding compact globular FN (Mitsi *et al.*, 2008) and mediating FN-FN interactions (Raitman *et al.*, 2017). Precisely, it was shown that heparin can catalyse transition from folded FN to unfolded by interacting with the HepII binding region and inducing conformational changes that extend the FN molecule(Mitsi *et al.*, 2008). Moreover, Raitman and colleagues (2017) also found that FN-heparin and FN-heparan sulphate-mimetic favoured FN matrix assembly in cells lacking heparan sulphate receptors by interacting through the HepII region. They proposed that heparin and heparan-sulphate could bind two or more HepII sites, bringing together FN molecules and facilitating the matrix assembly. We found that blocking with heparin the FN heparin-binding sites inhibits the $FN^{\Delta RGD}$ fibrillogenesis in *Fn1*$^{\Delta RGD/\Delta RGD}$ fibroblasts. The added

heparin competes with the syndecan (heparan sulphate) receptors to bind heparin binding sites within FN. Since the ΔRGD mutation abolish integrin binding, the fact that heparin blocks the $FN^{\Delta RGD}$ fibrillogenesis indicate the involvement of heparan sulphate receptors in this process. It has been described that heparin can bind fibronectin to the $FNIII_{1-2}$ (HepI), the $FNIII_{13-14}$ (HepII) and $FNIII_{4-6}$ (Hep III) (Xian *et al.*, 2010; Raitman *et al.*, 2017). Out of these 3 binding sites, the HepII motif has been defined as a binding site for the heparan sulphate chains of syndecans (Sekiguchi *et al.*, 1983; Benecky *et al.*, 1988; Ingham *et al.*, 1990). Syndecans are involved in cell adhesion, signalling and matrix assembly in cooperation with integrins (Klass *et al.*, 2000; Morgan, Humphries and Bass, 2007; Stepp *et al.*, 2010; Kwon *et al.*, 2012; Van Agthoven *et al.*, 2014). Syndecan interaction with FN activates signalling through protein kinase C and Rac1, reorganizing the actin cytoskeleton and promoting lamella formation and focal adhesions (Bass *et al.*, 2007; Choi *et al.*, 2011). Moreover, syndecans have been shown to cooperate with integrins in ECM signalling. Among the syndecan family, syndecan-1 has been described to cooperate with integrins αvβ3/β5 in FN and vitronectin adhesion (Xian *et al*., 2010); and syndecans 2 and 4 are described to cooperate with α5β1 integrin in mediating adhesion to FN, FN signalling, cytoskeleton reassembly and FN fibrillogenesis (Klass *et al.* , 2000; Munesue *et al.*, 2002; Whiteford *et al.*, 2007; Wang *et al.*, 2010). The $Fn1^{\Delta RGD/\Delta RGD}$ fibroblasts express all 4 syndecans classes in higher levels compared with wild-type fibroblasts, suggesting that they might have a more relevant function in those cells. We could demonstrate that $FN^{\Delta RGD}$ fibril formation was abolished after syndecan gene silencing using siRNA against Sdc1, Sdc2, Sdc3 and Sdc4. Levels of syndecan expression reduced to 30% for Sdc1 and 3, and to 70% for Sdc2 and 4 in $Fn1^{\Delta RGD/\Delta RGD}$ fibroblasts impaired totally FN fibrillation. Therefore, we can conclude that syndecans induce an RGD-independent FN fibrillogenesis. However, the $FN^{\Delta RGD}$ fibrils are disorganized and tend to clump, and the matrices that they form are not as dense as the FN^{wt} or FN^{RGE}, suggesting that to develop a fully structured FN matrix is necessary cooperation with integrins.

We explored two possibilities of generating cytoskeleton pulling forces in an α5β1 integrin-independent manner: first seeding the cells on specific substrates which are ligand of specific integrin classes; and second by external activation of integrins with manganese ($MnCl_2$). α6β1 integrin binds to laminin, αvβ3/5 to vitronectin, α1β1 to collagen I and αvβ3 to gelatine. In none of these cases integrin binding contributed to improve $FN^{\Delta RGD}$ fibrillogenesis. As consequence, $FN^{\Delta RGD}$ matrix was disorganized, composed by thick fibrils which seem to clamp together. Significantly, this feature was observable even with $Fn1^{\Delta RGD/\Delta RGD}$ cells on vitronectin, which binds αvβ3 or αvβ5 integrins and form evident stress fibers (Schiller *et al.*, 2013) and incorporate paxillin into FAs and fibrillar adhesions, comparable to $Fn1^{wt/wt}$. Moreover, RhoA activation in $Fn1^{\Delta RGD/\Delta RGD}$ fibroblasts is comparable to $Fn1^{wt/wt}$. RhoA activity has been reported to be essential for mediating FN matrix assembly through regulation of the actin cytoskeleton polymerization (Danen *et al.*, 2002), as the stress fibres transmit directly the adequate pulling force to the FN dimers via α5β1 integrins bound to the RGD motif. We also demonstrated that integrins activation by an external factor, such as manganese does not improve $FN^{\Delta RGD}$ fibril assembly. We conclude therefore, that certain $FN^{\Delta RGD}$ fibrillogenesis is produced by syndecan-HepII interaction but this process requires α5β1 integrin-FN adhesion to be functional.

V DISCUSSION

Chapter II. Study the FN synergy site function

The synergy site of FN was described as a second but critical binding site for α5β1 (Aota *et al.*, 1994) and platelet αIIbβ3 (Bowditch *et al.*, 1994) integrins. Since then, several *in vitro* studies argued its importance in cell adhesion (Takagi *et al.*, 2003; Mao and Schwarzbauer, 2006), strength of the bond between α5β1-FN (Danen *et al.*, 1995; Friedland *et al.*, 2009) or αIIbβ3-FN or even FN fibrillogenesis (Sechler *et al.*, 1998). Despite these *in vitro* studies, there was neither a consensus nor an *in vivo* evidence for the function of the FN synergy site. In addition, all these publications employed fragments of FN instead of the full-length protein, omitting potential conformational changes of the protein or compensatory effects with other cell-binding sites, which could influence the *in vivo* function of the synergy site. To address these questions, a mouse containing the FN synergy site mutated (*Fn1*^{syn}) was generated to analyse its function and to produce soluble full-length protein from mouse plasma, allowing complementary *in vitro* analysis.

1. The function in the synergy site in FN-integrin interaction

Previous studies suggested the importance of the synergy site for integrin α5β1 binding to FN, implying that it could be essential *in vivo* for α5β1 function. Two principal functions were attributed to the synergy site of FN: on one hand, it was suggested that the synergy site could facilitate the initial encounter between integrins and FN (Takagi *et al.*, 2003); on the other hand, it was proposed that the synergy site could strength the FN-α5β bond producing the so call catch bonds (Friedland *et al.*, 2009). The first would imply that mutations impairing the synergy site function would abrogate α5β1 integrin binding to FN, leading to a reduced α5β1 integrin function which would affect *Fn1*$^{syn/syn}$ mice development. The α5-null mice die at E9.5 with defects in the mesoderm which arrests somitogenesis (Yang *et al.*, 1993). However, contrary to expectations, the *Fn1*$^{syn/syn}$ mice were born in mendelian proportion, their size and lifespan were normal. Furthermore, histological analysis of the heart, lungs, kidney, liver and blood vessels showed that the *Fn1*$^{syn/syn}$ mice did not display apparent developmental defects. Altogether, indicated that the synergy site is dispensable for organogenesis and tissue homeostasis. Ablation of the *Fn1* gene in mice, as well as the simultaneous ablations of the *Itgα5* and *Itgav* integrin genes in mice arrests development at embryonic day 8.5 (E8.5) due to defects in the formation of mesoderm and mesoderm-derived structures (George *et al.*, 1993; Yang *et al.*, 1999). As mentioned before, the replacement of the FNIII10 RGD motif with RGE in mice also affects mesoderm development, although it is less severe and restricted to the vascular system and to the posterior body axis of the developing embryo (Takahashi *et al.*, 2007b; Girós *et al.*, 2011b). Interestingly, these defects resemble those observed in *Itgα5*-deficient mice indicating that the RGE mutation is sufficient to abrogate α5β1 integrin function and that the synergy site cannot compensate for a dysfunctional RGD motif. Therefore, the normal development of *Fn1*$^{syn/syn}$ mice excludes an essential role of the synergy site for α5 integrin function during development and tissue homeostasis (Grant et al., 1997; Krammer et al., 2002).

The absence of obvious 'α5β1-loss-of-function defects' (Yang et al., 1993) in *Fn1*$^{syn/syn}$ mice indicate that the synergy site is probably dispensable to promote integrin-FN binding. Fibroblast experiments using purified plasma FN as a substrate demonstrated that in fact cells adhere and spread on FN^{syn}. However, when cells are adhered to FN^{syn} they delay maturation

of NA into FA and experiment rapid cycles of binding and detaching compared to cells adhered to FN^{wt}, indicating that cells are less efficient to reinforce the α5β1 integrin-FN bond. We measured the strength of the bond by exposing cells to shear forces with a spinning-disk device. These experiments showed that the mutation of the FN synergy site reduced the force that cells can withstand, so we concluded that the synergy site contribution is important for α5β1 integrin to strengthen the FN bond. Moreover, the reduction of the strength of the bond when the FN synergy was mutated affected to two cell lines, *Fn1*-KO mouse fibroblasts and human HT1080 cells, suggesting that it is a general function of the synergy site rather than an isolate property of a single cell line. Interestingly, the HT1080 cells suffered a higher reduction in the strength of the bond (33%) than the *Fn1*-KO fibroblasts (16%) when adhered to full-length FN^{syn}. HT1080 cells, despite expressing different FN receptors, have been described to only strengthen the FN bond via α5β1 (Shi and Boettiger, 2003). This could explain their higher sensibility to the synergy mutation. Other explanation is the different origin of the HT1080 cells (human) and the FN^{syn} (purified from mouse plasma). The mouse synergy site (DRVPPSRN) and the human one (DRVPHSRN) sequence differ in one amino acid, and we cannot discard that this affects to the affinity between the integrin and the FN, and therefore affect to the strengthen of the bond. In addition, we also used fragments ($FNIII_{7\text{-}10}$) of human origin, which hence contain the human sequence of the synergy site. When using these fragments, the *Fn1*-KO adhered to $FNIII_{7\text{-}10}{}^{syn}$ suffered a higher reduction in bond strengthening (43%), compared to the reduction on full-length FN. This differences in adhesion strength could not be explained by additional binding to other motifs outside $FNIII_{7\text{-}10,}$ like syndecan adhesion to HepII. Hence, it is possible that the organism origin of the FN or $FNIII_{7\text{-}10}$ affects the integrin affinity to FN synergy site, and hence the strengthening of the bond. Catch bonds are defined as bonds whose lifetime is prolonged by tensile mechanical forces. The catch bond between α5β1 integrin and FN was proved by AFM using purified integrin ectodomain and the $FNIII_{7\text{-}10}$ fragment (Kong *et al.*, 2009). Catch bonds can be quantified in whole cells by chemical crosslinking using a water-soluble crosslinker of 8-atoms length (Shi and Boettiger, 2003; Legate *et al.*, 2011). In the present study we could prove by chemical crosslinking that the mutated synergy site hinders catch bond formation between FN and α5β1 integrins. Therefore, the synergy site of FN is critical for strengthening the α5β1 integrin-FN bond and its consequent progression into catch bonds.

We demonstrated that impairing the FN synergy site affects α5β1 integrin-FN downstream signalling, measured as phosphorylation of FAK in tyrosine 397. FAK phosphorylation in Y397 has been shown to be a read out of the tension transmitted through α5β1 integrin-FN adhesion and to increase with ECM stiffness (Shi, 2003; Provenzano *et al.*, 2009; Elosegui-Artola *et al.*, 2016). When the cells were plated on synergy site-mutated FN, they reduced their levels of pY397FAK and the phosphorylation did not increase with substrate stiffness.

The ECM, integrins, adaptor proteins and the actomyosin cytoskeleton, form a mechanical link known as a 'molecular clutch' which sense and respond to rigidity (Elosegui-Artola *et al.*, 2014). Cells adapt to substrate stiffness by regulating the loading force which ultimately depends on actin rearward flow and the integrin interaction with its ligand and adaptors. Higher rigidities require larger mechanical loading forces exerted by the molecular

clutch and bonds between FN-integrin need to be reinforced so that the K_{off} of the bond increases enough to prevail over the K_{on}, in the same manner that FN-integrin bonds need to be reinforced to withstand external tension. We observed that when cells adhered to either soft (0.4-4 kPa) or stiff (50 kPa or glass) FN^{syn} matrices, they present reduced levels of pY397FAK and phosphorylation does not increase with stiffness. Higher stiffness promote cell spreading and FA formation, and when cells adhered to FN^{wt} coated gels their spreading area increased with stiffness. However, cells adhered to FN^{syn}–coated gels did not respond to increased stiffness and their areas were always between 75% (on 0.5 kPa) and 90% (on 4 and 50 kPa) smaller after 60 min than cells adhered to FN^{wt} coated gels of the same stiffness, suggesting that cells adhered to FN^{syn} matrices do not sense changes in stiffness in comparison with cells adhered to FN^{wt}. Schiller and colleagues (Schiller *et al.*, 2013) demonstrated that cells adapt to the environment stiffness by an interplay between α5 and αv integrins. Therefore, despite cells can adhere to FN^{syn}, we observe that α5 cannot reinforce the bond through the synergy site and the cell cannot adapt to different rigidities, suggesting a defect in this interplay.

According to the results of the present work, the synergy site mediates the reinforcement in α5β1 integrin-FN bonds, permitting the molecular clutch to respond to mechanical changes in the environment such as shear forces or changes in the ECM rigidity.

Platelet express α5β1 and αIIbβ3 integrins, both receptors of the synergy site. It is well known that platelet adhesion to pFN is mediated by αIIbβ3 with contributions from α5β1 in mice, and plays a critical role for haemostasis (Ni and Freedman, 2003; Wang *et al.*, 2014). However, the role of FN in haemostasis and thrombosis is very complex and not fully understood. According to most of the reports, FN is involved in the first wave of haemostasis, and its function for thrombus formation can be compensated by fibrinogen or von Willebrand factor (Maurer *et al.*, 2010; Wang *et al.*, 2014) although, it is critical for thrombus growth or stability (Ni *et al.*, 2003). When $Fn1^{syn/syn}$ mice were exposed to stress such as tail bleeding or arteriole injury they presented longer bleeding times than $Fn1^{wt/wt}$ mice in both tail bleeding assay and arteriole injury, suggesting that mutations in the synergy site cause platelet adhesion defects in these stress situations. In addition, we observed that $Fn1^{syn/syn}$ platelets contain less intracellular FN and this could affect platelet aggregation in $Fn1^{syn/syn}$ mice. Platelets uptake extracellular pFN using integrin receptors α5β1 and αIIbβ3, and this FN is later retained in their α-granules to be released upon platelet activation (Ni *et al.*, 2000). Therefore, the reduced FN in the α-granules indicates that platelets bind inefficiently to FN^{syn}, and the defective FN uptake could be the consequence of weakened or absence of FN-integrin binding. We could not demonstrate defects in *in vitro* platelet aggregation. Ni et al. 2003 also reported that depletion of FN did not cause alterations in thrombus formation *in vitro* and concluded that involvement of FN in platelet aggregation was shear dependent. We observed that the onset of platelet aggregation and the thrombus occlusion in venules were not disturbed by synergy mutation, but it was delayed in arterioles, indicating that the synergy site of FN is essential to resist the higher shear flow in arterioles, which can be up to 2000 s^{-1}. This indicates that indeed the synergy site mediates platelet-FN bond strengthening and become important in platelet aggregation under stress situations.

2. Compensatory effects counteract the lack of a functional synergy site

Only the integrin receptors α5β1 or αIIbβ3 use the synergy sequence to reinforce its adhesion to the FN-RGD motif, thus other FN receptors could compensate the lack of a fully functional synergy site. Specifically, αv-class of integrins compensate partially α5β1 functions in absence of this integrin (Yang and Hynes, 1996), although the two integrin classes signal differently upon FN binding (Danen *et al.*, 2002; Schiller *et al.*, 2013). In the present study experiments with fibroblasts expressing either α5β1 or αvβ3/β5 integrins demonstrated that effectively, in the absence of other integrins, cells expressing αv integrins could adhere and spread independently of the synergy site. Yet, the FN synergy site was essential for α5β1 mediated cell spreading, as we proved that although cells only expressing α5β1 can bind FN^{syn}, the lack of α5β1-synergy site engagement lead to poor recruitment of this integrin in FAs and reduced stress fibres organization. This confirmed that αv class of integrins compensate for the lack of a functional synergy site during adhesion and spreading *in vitro*. It is remarkable the slight differences in the spreading between *Fn1*-KO and pKO-αv/β1 fibroblast lines. Despite both cell lines experience compensation by αv integrin, pKO-αv/β1 fibroblasts do not delay FA maturation, like *Fn1*-KO do. This could be explained because pKO-αv/β1 fibroblasts contain significantly higher cell surface levels of β3 integrin than *Fn1-KO* cells, suggesting that certain threshold of αvβ3 integrin expression could overcome the deficient synergy site.

To confirm *in vivo* the αvβ3 compensation, we intercrossed the $Fn1^{syn/syn}$ mice with $Itgb3^{-/-}$ mice. The *in vivo* ablation of β3 integrin in the $Fn1^{syn/syn}$ mice leads to embryonic lethality at E15.5. The $Fn1^{syn/syn}$*; *$Itgb3^{-/-}$ embryos depict a haemorrhagic phenotype starting at E12.5. This phenotype is more severe than the haemorrhagic phenotype presented by $Itgb3^{-/-}$ mice, confirming that integrins αvβ3 and αIIbβ3 compensate a non-functional synergy site. This compensation can be the result of two different mechanisms: (1) αvβ3 integrin overcomes the lack of the synergy site in mesenchymal cells, giving support in adhesion of this cells; (2) the interaction between αIIbβ3 and fibrinogen can counteract for the absence or reduction of platelet adhesion to FN^{syn}. These different mechanisms are not exclusive, and they can act in conjunction. We could establish that the double mutant $Fn1^{syn/syn}$*; *$Itgb3^{-/-}$ mice display two types of defects. On one hand, the $Fn1^{syn/syn}$*; *$Itgb3^{-/-}$ present alteration in vessel development; and on the other hand, in platelet function. This demonstrates that both β3-containing integrins, αvβ3 expressed in mesenchymal cells and αIIbβ3 present in platelets, are compensating for the lack of a functional synergy site *in vivo*.

The lack of αvβ3 integrin expression has not been described to alter vessel formation and homeostasis (Hodivala-Dilke *et al.*, 1999). However, its absence in the $Fn1^{syn/syn}$ mice causes vessel instability characterized by poor coverage by mural cells and endothelial cells detachment from the basal membrane, and consequent vessel retraction. Mural cells, which include vascular smooth muscle cells (VSMCs) and pericytes, are important in blood vessel maintenance. Abnormal interaction of these two cell types with the endothelial cells or the subendothelial ECM causes haemorrhages and vessel hyperplasia, leading in some cases to severe cardiovascular diseases which lead to embryonic lethality (Armulik *et al.*, 2005). Mural and endothelial cells (ECs) express α5β1 and αvβ3 integrins to bind FN in the subendothelium (van der Flier *et al.*, 2010). Integrin β1 is critical for mural cell function, and despite its ablation reduces cell spreading compromising the support to ECs, it does not abolish adhesion to the

endothelium or the surrounding ECM (Abraham *et al.*, 2008), probably because other integrins, like αv-class, can still bind to FN. We evidenced that mural cells adhere poorly to the endothelium in *Fn1*$^{syn/syn}$*; Itgb3*$^{-/-}$ blood vessels and were absent in many areas of the *Fn1*$^{syn/syn}$*; Itgb3*$^{-/-}$ vessel surface. Interestingly, these defects in mural cells coverage and function in compound *Fn1*$^{syn/syn}$*; Itgb3*$^{-/-}$ mice are observed starting at E15.0, when blood pressure increases more than 5 folds in the embryo (Le *et al.*, 2012). Mural cells are highly contractile, and possibly need strong adhesions to withstand cytoskeletal forces and, it is likely that this blood pressure increment in the embryo also exerts (shear) forces in the vessels sensed by the endothelial and mural cells. We conclude that the defects in *Fn1*$^{syn/syn}$*; Itgb3*$^{-/-}$ vasculature are due to the combined lack of αvβ3 integrins and defective α5β1-FN^{syn} interaction, which causes that mural cells cannot reinforce the α5β1-FN bond without the contribution of the synergy site and they detach from the endothelium. As consequence, the endothelial cells (ECs) are unprotected and therefore capillaries, veins and arteries become more fragile.

The *Fn1*$^{syn/syn}$ mice present a mild platelet defect which causes prolonged bleeding after injury, however *Fn1*$^{syn/syn}$*; Itgb3*$^{-/-}$ embryos present abundant cutaneous haemorrhages. These haemorrhages are caused by blood leaking because of vascular instability and infiltration of erythrocytes in the lymphatic vessels. The presence of erythrocytes in the lymphatic vessels was an indicator of a defect in lymphatic vessel development. We could demonstrate that the mutant *Fn1*$^{syn/syn}$*; Itgb3*$^{-/-}$ embryos do not separate the lymphatic vessels from the blood vessels because a defect in platelet function. As platelets adhere to pFN by αIIbβ3 and α5β1 (Ni and Freedman, 2003; Wang *et al.*, 2014), we aimed to deep in the implications of the synergy site for platelet adhesion and function. We analysed the platelet adhesion to pFN in static conditions and proved that, when platelets lack integrin αIIbβ3, adhesion to mutant FN^{syn} is completely abrogated. Interestingly, when the shear force in a flow chamber was applied to study platelet adhesion to FN, the synergy site is crucial for wild-type platelets to adhere to FN. These results demonstrate that the synergy site plays a central role in platelet adhesion as soon as force is applied to the bonds between FN and platelet integrins. This force-dependent requirement of the synergy site for platelet adhesion is consistent with the delayed thrombus formation observed in the adult *Fn1*$^{syn/syn}$. However, this effect was less severe than expected, considering the effect observed in our flow chamber experiments. Thrombus formation is a highly compensated process, and depletion of von Willebrand factor and fibrinogen together or fibrinogen and pFN together does not dismiss it (Ni *et al.*, 2000; Reheman *et al.*, 2009). Therefore, it is no unexpected that even though platelets need the FN synergy site to mediate a tight and stable thrombus, presence of other plasma proteins *in vivo* compensates for it. We confirmed this aspect, in the compound *Fn1*$^{syn/syn}$*; Itgb3*$^{-/-}$ embryos that do not separate the lymphatic vessels from the blood vessels. The fact that integrin β3 genetic ablation dismisses platelet adhesion to mutant synergy FN causing insufficient platelet-mediated separation of the lymphatic vessels from the cardinal vein in the *Fn1*$^{syn/syn}$*; Itgb3*$^{-/-}$ embryos, confirms the compensatory effects by this integrin binding to fibrinogen.

In the platelet adhesion assays we also observed that α5β1 integrin mediates interaction with FN^{wt} in *Intgb3*$^{-/-}$ under shear stress conditions. Taking into account that platelets contain around 100 times less α5β1 than αIIbβ3 integrins (Zeiler *et al.*, 2014), this result emphasise the

fundamental role of the adhesion strengthening property of the FN synergy site, which is important for both, mesenchymal-derived cells and platelets (Fig. 57).

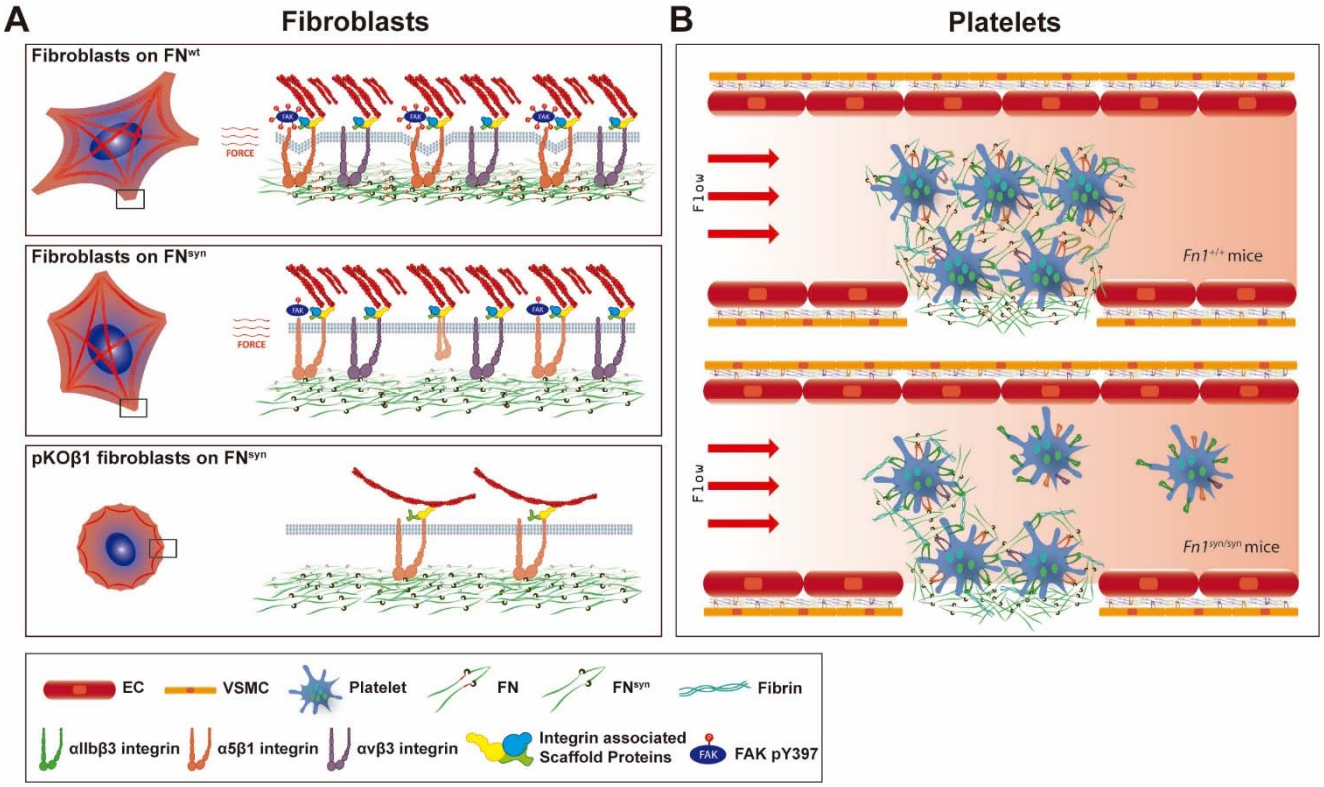

Figure 57. The major role of the FN synergy site is to re-enforce cell adhesion. (A) Hydrodynamic shear force-exposed fibroblasts seeded on a FN^{wt}- coated surface form catch-bonds that strengthen α5β1 integrin-mediated adhesions to FN and trigger phosphorylation of Y397-FAK (upper image). On FN^{syn}-coated surfaces, the αvβ3 integrins compensate for the absent synergy site allowing fibroblast adhesion and the reduced a5b1 binding strength leads to diminished phosphorylation of pY397-FAK (middle image). The elimination of αv-class integrins decreases cell adhesion on FN^{syn}-coated surfaces, reduces cell spreading and delays the maturation of FA and fibrillar adhesions (lower image). (B) Platelets in *Fn1*$^{+/+}$ mice form tight aggregates on injured vessel walls that withstand the shear forces of the blood flow (upper image), while platelets in an injured vessel in *Fn1*$^{syn/syn}$ mice fail to withstand the blood flow leading to a delayed thrombus formation (lower image). Endothelial cells (EC); vascular smooth muscle cells (VSMC).

VI CONCLUSIONS

The two major binding sites for the integrin α5β1 have been analysed, the RGD and the synergy site, with different aims and approaches. For the RGD site we put the focus in FN fibrillogenesis. For the FN synergy site, we unravelled its role *in vivo.*

1. We demonstrate with fibroblasts in culture that the deletion of RGD sequence does not abolish FN fibrillogenesis, although $FN^{\Delta RGD}$ fibrils present a different morphology than FN^{wt}, suggesting that RGD motif is essential for a well-structured FN matrix.
2. The process of $FN^{\Delta RGD}$ fibrillogenesis is produced after engagement of the FN heparin sites by syndecan receptors.
3. The R>A mutation of the FN synergy sequence does not affect mouse development neither adult tissue homeostasis.
4. The mice expressing FN with mutant synergy site have prolonged bleeding times and delayed thrombus formation when stress is induced by vascular injury, compared to wild type mice, indicating a defect in platelet function. Flow chamber experiments confirm that although in static conditions platelets can bind to FN^{syn}, under shear flow their adhesion to FN^{syn} is abolished.
5. Cells adhere to FN^{syn} protein and can assemble normal FN fibrils, however the maturation of nascent adhesions to focal adhesions is delayed on FN^{syn}.
6. The strength of the α5β1-FN bond is reduced under shear forces and cells form significantly less catch bonds between α5β1 integrin and the mutated FN^{syn}. This effect is observed in different cell lines from mouse (*Fn1*-KO) and human (HT1080).
7. FAK phosphorylation in the tyrosine 397, a marker of integrin tension, is reduced in cells adhered to FN^{syn}-coated surfaces and not altered by the substrate stiffness
8. The phenotype of the $Fn1^{syn/syn}$ mice becomes embryonic lethal when the expression of β3 integrins is annulated, pointing compensatory effects by integrin αvβ3 and by the plasmatic protein fibrinogen.
9. In cells in culture αvβ3 integrin expression allows cell spreading, stress fibre formation and FA assembly on FN^{syn}-coated surfaces.
10. In the embryo, the lack of αvβ3 expression together with the synergy site inactivation impairs blood vessel stability, caused by an altered adhesion of mural and endothelial cells to their ECM.
11. In platelets, the lack of synergy site function is partially compensated by fibrinogen that binds αIIbβ3 integrins. This is evidenced in the $Fn1^{syn/syn}$*;* $Itgb3^{-/-}$ double mutant mice that depict lack of separation between lymphatic and blood vasculatures, a developmental defect caused by severe deficiencies in platelet adhesion.
12. Altogether our results indicate that the synergy site is important for reinforcing the integrin-FN bond under stress situations and that αv-containing integrins can partially compensate its absence.

BIBLIOGRAPHY

BIBLIOGRAPHY

Abraham, S. *et al.* (2008) 'Integrin 1 Subunit Controls Mural Cell Adhesion, Spreading, and Blood Vessel Wall Stability', *Circulation Research*, 102(5), p. 562. doi: 10.1161/circresaha.107.167908.

Abtahian, F. *et al.* (2003) 'Regulation of blood and lymphatic vascular separation by signaling proteins SLP-76 and Syk', *Science*. NIH Public Access, 299(5604), pp. 247–251. doi: 10.1126/science.1079477.

Adair, B. D. *et al.* (2005) 'Three-dimensional EM structure of the ectodomain of integrin ??V??3 in a complex with fibronectin', *Journal of Cell Biology*, 168(7), pp. 1109–1118. doi: 10.1083/jcb.200410068.

Adams, R. H. and Alitalo, K. (2007) 'Molecular regulation of angiogenesis and lymphangiogenesis', *Nat Rev Mol Cell Biol*, 8(6), pp. 464–478. doi: 10.1038/nrm2183.

Van Agthoven, J. F. *et al.* (2014) 'Structural basis for pure antagonism of integrin αVβ3 by a high-affinity form of fibronectin.', *Nature structural & molecular biology*, 21(4), pp. 383–8. doi: 10.1038/nsmb.2797.

Ahuja, D., Sáenz-Robles, M. T. and Pipas, J. M. (2005) 'SV40 large T antigen targets multiple cellular pathways to elicit cellular transformation', *Oncogene*. Nature Publishing Group, 24(52), pp. 7729–7745. doi: 10.1038/sj.onc.1209046.

Altroff, H., Choulier, L. and Mardon, H. J. (2003) 'Synergistic activity of the ninth and tenth FIII domains of human fibronectin depends upon structural stability.', *The Journal of biological chemistry*. American Society for Biochemistry and Molecular Biology, 278(1), pp. 491–7. doi: 10.1074/jbc.M209992200.

Andrews, R. K. and Berndt, M. C. (2008) 'Platelet adhesion: A game of catch and release', *Journal of Clinical Investigation*. American Society for Clinical Investigation, pp. 3009–3011. doi: 10.1172/JCI36883.

Aota, S. I., Nomizu, M. and Yamada, K. M. (1994) 'The short amino acid sequence Pro-His-Ser-Arg-Asn in human fibronectin enhances cell-adhesive function', *Journal of Biological Chemistry*, 269(40), pp. 24756–24761.

Armulik, A. (2005) 'Endothelial/Pericyte Interactions', *Circulation Research*. American Heart Association, Inc., 97(6), pp. 512–523. doi: 10.1161/01.RES.0000182903.16652.d7.

Arnaout, M. A., Mahalingam, B. and Xiong, J.-P. (2005) 'Integrin Structure, Allostery, and Bidirectional Signaling', *Annual Review of Cell and Developmental Biology*, 21(1), pp. 381–410. doi: 10.1146/annurev.cellbio.21.090704.151217.

Arnaout, M. A., Goodman, S. L. and Xiong, J. P. (2007) 'Structure and mechanics of integrin-based cell adhesion', *Current Opinion in Cell Biology*, pp. 495–507. doi: 10.1016/j.ceb.2007.08.002.

Astrof, S., Crowley, D. and Hynes, R. O. (2007) 'Multiple cardiovascular defects caused by the absence of alternatively spliced segments of fibronectin', *Developmental Biology*. Academic Press, 311(1), pp. 11–24. doi: 10.1016/J.YDBIO.2007.07.005.

Bader, B. L. *et al.* (1998) 'Extensive vasculogenesis, angiogenesis, and organogenesis precede lethality in mice lacking all alpha v integrins.', *Cell*, 95(4), pp. 507–519. doi: 10.1016/S0092-8674(00)81618-9.

Baez, S. (1973) ‘An open cremaster muscle preparation for the study of blood vessels by in vivo microscopy.’, *Microvascular research*, 5(3), pp. 384–94.

Baneyx, G., Baugh, L. and Vogel, V. (2001) ‘Coexisting conformations of fibronectin in cell culture imaged using fluorescence resonance energy transfer.’, *Proceedings of the National Academy of Sciences of the United States of America*, 98(25), pp. 14464–8. doi: 10.1073/pnas.251422998.

Baneyx, G., Baugh, L. and Vogel, V. (2002a) ‘Fibronectin extension and unfolding within cell matrix fibrils controlled by cytoskeletal tension.’, *Proceedings of the National Academy of Sciences of the United States of America*, 99(8), pp. 5139–5143. doi: 10.1073/pnas.072650799.

Barkalow, F. J. and Schwarzbauer, J. E. (1991) ‘Localization of the major heparin-binding site in fibronectin.’, *The Journal of biological chemistry*, 266(12), pp. 7812–8. Available at: http://www.jbc.org/content/266/12/7812.full.pdf (Accessed: 21 March 2018).

Bass, M. D., Morgan, M. R. and Humphries, M. J. (2007) ‘Integrins and syndecan-4 make distinct, but critical, contributions to adhesion contact formation.’, *Soft matter*, 3(3), pp. 372–376. doi: 10.1039/b614610d.

Beauvais, D. M. *et al.* (2009) ‘Syndecan-1 regulates alphavbeta3 and alphavbeta5 integrin activation during angiogenesis and is blocked by synstatin, a novel peptide inhibitor.’, *The Journal of experimental medicine*, 206(3), pp. 691–705. doi: 10.1084/jem.20081278.

Bencharit, S. *et al.* (2007) ‘Structural Insights into Fibronectin Type III Domain-mediated Signaling’, *Journal of Molecular Biology*, 367(2), pp. 303–309. doi: 10.1016/j.jmb.2006.10.017.

Benecky, M. J. *et al.* (1988) ‘Evidence that binding to the carboxyl-terminal heparin-binding domain (Hep II) dominates the interaction between plasma fibronectin and heparin.’, *Biochemistry*, 27(19), pp. 7565–71. doi: 10.1021/bi00419a058.

Bennett, J. S. (2005) ‘Structure and function of the platelet integrin IIb 3’, *Journal of Clinical Investigation*, 115(12), pp. 3363–3369. doi: 10.1172/JCI26989.

Bergmeier, W. *et al.* (2006) ‘The role of platelet adhesion receptor GPIb far exceeds that of its main ligand, von Willebrand factor, in arterial thrombosis’, *Proceedings of the National Academy of Sciences*. National Academy of Sciences, 103(45), pp. 16900–16905. doi: 10.1073/pnas.0608207103.

Bertozzi, C. C. *et al.* (2010) ‘Platelets regulate lymphatic vascular development through CLEC-2-SLP-76 signaling’, *Blood*. American Society of Hematology, 116(4), pp. 661–670. doi: 10.1182/blood-2010-02-270876.

Bertozzi, C. C., Hess, P. R. and Kahn, M. L. (2010) ‘Platelets: Covert regulators of lymphatic development’, *Arteriosclerosis, Thrombosis, and Vascular Biology*. American Heart Association, Inc., 30(12), pp. 2368–2371. doi: 10.1161/ATVBAHA.110.217281.

Bharadwaj, M. *et al.* (2017) ‘αV-class integrins exert dual roles on α5β1 integrins to strengthen adhesion to fibronectin.’, *Nature communications*. Nature Publishing Group, 8, p. 14348. doi: 10.1038/ncomms14348.

Bingham, R. J. and Potts, J. R. (2010) ‘Fibronectin Structure: A New Piece of the Puzzle Emerges’. doi: 10.1016/j.str.2010.05.003.

Bowditch, R. D. *et al.* (1994) ‘Identification of a Novel Integrin Binding Site in Fibronectin’, *The Journal of biological chemistry*, 269(14), pp. 10856–10863.

Brown, M. *et al.* (1986) ‘A Recombinant Murine Retrovirus for Simian Virus 40 Large T cDNA

Transforms Mouse Fibroblasts to Anchorage- Independent Growth', *JOURNAL OF VIROLOGY*, 60(1), pp. 290–293.

Busby, T. F. *et al.* (1995) 'Heparin binding by fibronectin module III-13 involves six discontinuous basic residues brought together to form a cationic cradle', *Journal of Biological Chemistry*. American Society for Biochemistry and Molecular Biology, 270(31), pp. 18558–18562. doi: 10.1074/jbc.270.31.18558.

Butcher, D. T., Alliston, T. and Weaver, V. M. (2009) 'A tense situation: forcing tumour progression', *Nature Reviews Cancer*. Nature Publishing Group, 9(2), pp. 108–122. doi: 10.1038/nrc2544.

Campbell, I. D. and Humphries, M. J. (2011) 'Integrin structure, activation, and interactions', *Cold Spring Harbor Perspectives in Biology*. Cold Spring Harbor Laboratory Press, pp. 1–14. doi: 10.1101/cshperspect.a004994.

Castelletti, F. *et al.* (2008) 'Mutations in FN1 cause glomerulopathy with fibronectin deposits.', *Proceedings of the National Academy of Sciences of the United States of America*, 105(7), pp. 2538–2543. doi: 10.1073/pnas.0707730105.

Carramolino, L. *et al.* (2010) 'Platelets Play an Essential Role in Separating the Blood and Lymphatic Vasculatures During Embryonic Angiogenesis', *Circulation Research*. American Heart Association, Inc., 106(7), pp. 1197–1201. doi: 10.1161/CIRCRESAHA.110.218073.

Chada, D., Mather, T. and Nollert, M. U. (2006) 'The Synergy Site of Fibronectin Is Required for Strong Interaction with the Platelet Integrin αIIbβ3', *Annals of Biomedical Engineering*. Kluwer Academic Publishers-Plenum Publishers, 34(10), pp. 1542–1552. doi: 10.1007/s10439-006-9161-1.

Cho, J. and Mosher, D. F. (2006a) 'Enhancement of thrombogenesis by plasma fibronectin cross-linked to fibrin and assembled in platelet thrombi', *Blood*. American Society of Hematology, 107(9), pp. 3555–3563. doi: 10.1182/blood-2005-10-4168.

Cho, J. and Mosher, D. F. (2006b) 'Impact of fibronectin assembly on platelet thrombus formation in response to type I collagen and von Willebrand factor', *Blood*, 108(7), pp. 2229–2236. doi: 10.1182/blood-2006-02-002063.

CHO, J. and MOSHER, D. F. (2006) 'Role of fibronectin assembly in platelet thrombus formation', *Journal of Thrombosis and Haemostasis*, 4(7), pp. 1461–1469. doi: 10.1111/j.1538-7836.2006.01943.x.

Choi, Y. *et al.* (2011) 'Syndecans as cell surface receptors: Unique structure equates with functional diversity.', *Matrix biology : journal of the International Society for Matrix Biology*. International Society of Matrix Biology, 30(2), pp. 93–9. doi: 10.1016/j.matbio.2010.10.006.

Chon, J. H. and Chaikof, E. L. (2002) 'A von Willebrand factor-derived heparin-binding peptide regulates cell–substrate adhesive strength and chemokinesis behavior', *Biochimica et Biophysica Acta (BBA) - Molecular Cell Research*. Elsevier, 1542(1–3), pp. 195–208. doi: 10.1016/S0167-4889(01)00181-1.

Clemetson, K. J. (1999) 'Primary haemostasis: Sticky fingers cement the relationship', *Current Biology*, 9(3), pp. 110–112. doi: 10.1016/S0960-9822(99)80063-3.

Coller, B. S. (2015) 'αIIbβ3: Structure and function', *Journal of Thrombosis and Haemostasis*. NIH Public Access, pp. S17–S25. doi: 10.1111/jth.12915.

Corbett, S. A. *et al.* (1997) 'Covalent Cross-linking of Fibronectin to Fibrin Is Required for Maximal

Cell Adhesion to a Fibronectin-Fibrin Matrix', *Journal of Biological Chemistry*, 272(40), pp. 24999–25005. doi: 10.1074/jbc.272.40.24999.

Craig, D. *et al.* (2001) 'Comparison of the early stages of forced unfolding for fibronectin type III modules.', *Proceedings of the National Academy of Sciences of the United States of America*, 98(10), pp. 5590–5595. doi: 10.1073/pnas.101582198.

Danen, E. H. J. *et al.* (1995) 'Requirement for the Synergy Site for Cell Adhesion to Fibronectin Depends on the Activation State of Integrin 5 1', *Journal of Biological Chemistry*, 270(37), pp. 21612–21618. doi: 10.1074/jbc.270.37.21612.

Danen, E. H. J. *et al.* (2002) 'The fibronectin-binding integrins α5β1 and αvβ3 differentially modulate RhoA-GTP loading, organization of cell matrix adhesions, and fibronectin fibrillogenesis', *Journal of Cell Biology*, 159(6), pp. 1071–1086. doi: 10.1083/jcb.200205014.

Davis, G. E. (1992) 'Affinity of integrins for damaged extracellular matrix: αvβ3 binds to denatured collagen type I through RGD sites', *Biochemical and Biophysical Research Communications*, 182(3), pp. 1025–1031. doi: 10.1016/0006-291X(92)91834-D.

Denis, C. *et al.* (1998) 'A mouse model of severe von Willebrand disease: defects in hemostasis and thrombosis.', *Proceedings of the National Academy of Sciences of the United States of America*. National Academy of Sciences, 95(16), pp. 9524–9. doi: 10.1073/PNAS.95.16.9524.

Denis, C. V. and Wagner, D. D. (2007) 'Platelet adhesion receptors and their ligands in mouse models of thrombosis', *Arteriosclerosis, Thrombosis, and Vascular Biology*, 27(4), pp. 728–739. doi: 10.1161/01.ATV.0000259359.52265.62.

Elosegui-Artola, A. *et al.* (2014) 'Rigidity sensing and adaptation through regulation of integrin types', *Nature Materials*, 13(6), pp. 631–7. doi: 10.1038/nmat3960.

Elosegui-Artola, A. *et al.* (2016) 'Mechanical regulation of a molecular clutch defines force transmission and transduction in response to matrix rigidity', *Nature Cell Biology*. Nature Publishing Group, 18(5), pp. 540–548. doi: 10.1038/ncb3336.

Elosegui-Artola, A., Trepat, X. and Roca-Cusachs, P. (2018) 'Control of Mechanotransduction by Molecular Clutch Dynamics', *Trends in Cell Biology*. Elsevier Current Trends. doi: 10.1016/J.TCB.2018.01.008.

Engler, A. J. *et al.* (2009) 'A novel mode of cell detachment from fibrillar fibronectin matrix under shear', *Journal of Cell Science*, 122(10), pp. 1647–1653. doi: 10.1242/jcs.040824.

Erickson, H. P. (1994) 'Reversible unfolding of fibronectin type III and immunoglobulin domains provides the structural basis for stretch and elasticity of titin and fibronectin.', *Proceedings of the National Academy of Sciences*. National Academy of Sciences, 91(21), pp. 10114–10118. doi: 10.1073/pnas.91.21.10114.

Erickson, H. P. (2002) 'Stretching fibronectin', *Journal of Muscle Research and Cell Motility*, pp. 575–580. doi: 10.1023/A:1023427026818.

Erickson, H. P. (2017) 'Protein unfolding under isometric tension-what force can integrins generate, and can it unfold FNIII domains?', *Current opinion in structural biology*. NIH Public Access, 42, pp. 98–105. doi: 10.1016/j.sbi.2016.12.002.

Erikson, H. P., Carrell, N. and McDonagh, J. (1981) 'Fibronectin molecule visualized in electron microscopy: A long, thin, flexible strand', *Journal of Cell Biology*, 91(3 I), pp. 673–678. doi: 10.1083/jcb.91.3.673.

van der Flier, A. *et al.* (2010) 'Endothelial 5 and v integrins cooperate in remodeling of the

vasculature during development', *Development*, 137(14), pp. 2439–2449. doi: 10.1242/dev.049551.

Fong, K. P. *et al.* (2016) 'Directly Activating the Integrin αIIbβ3 Initiates Outside-In Signaling by Causing αIIbβ3 Clustering', *Journal of Biological Chemistry*. American Society for Biochemistry and Molecular Biology, 291(22), pp. 11706–11716. doi: 10.1074/jbc.M116.716613.

Friedland, J. C., Lee, M. H. and Boettiger, D. (2009) 'Mechanically activated integrin switch controls alpha5beta1 function.', *Science (New York, N.Y.)*, 323(5914), pp. 642–644. doi: 10.1126/science.1168441.

Fu, J. *et al.* (2008) 'Endothelial cell O-glycan deficiency causes blood/lymphatic misconnections and consequent fatty liver disease in mice', *Journal of Clinical Investigation*. American Society for Clinical Investigation, 118(11), pp. 3725–3737. doi: 10.1172/JCI36077.

Furie, B. (2005) 'Thrombus formation in vivo', *Journal of Clinical Investigation*, 115(12), pp. 3355–3362. doi: 10.1172/JCI26987.

Furie, B. B. C. and Furie, B. B. C. (2005) 'Review series Thrombus formation in vivo', *The Journal of Clincial Investigation*. American Society for Clinical Investigation, 115(12), pp. 3355–3362. doi: 10.1172/JCI26987.trical.

García, A. J., Schwarzbauer, J. E. and Boettiger, D. (2002) 'Distinct Activation States of α5β1 Integrin Show Differential Binding to RGD and Synergy Domains of Fibronectin †', *Biochemistry*, 41(29), pp. 9063–9069. doi: 10.1021/bi025752f.

García, A. J., Takagi, J. and Boettiger, D. (1998) 'Two-stage activation for alpha5beta1 integrin binding to surface-adsorbed fibronectin.', *The Journal of biological chemistry*. American Society for Biochemistry and Molecular Biology, 273(52), pp. 34710–5. doi: 10.1074/jbc.273.52.34710.

Geiger, B. and Yamada, K. M. (2011) 'Molecular architecture and function of matrix adhesions', *Cold Spring Harbor Perspectives in Biology*, 3(5), pp. 1–21. doi: 10.1101/cshperspect.a005033.

Geiger, B. and Yamada, K. M. (2011) 'Molecular Architecture and Function of Matrix Adhesions', *Cold Spring Harbor Perspectives in Biology*, 3(5), pp. a005033–a005033. doi: 10.1101/cshperspect.a005033.

George, E. L. *et al.* (1993) 'Defects in mesoderm, neural tube and vascular development in mouse embryos lacking fibronectin.', *Development (Cambridge, England)*, 119(4), pp. 1079–91. doi: 10.1083/jcb.200107107.

George, E. L., Baldwin, H. S. and Hynes, R. O. (1997) 'Fibronectins are essential for heart and blood vessel morphogenesis but are dispensable for initial specification of precursor cells.', *Blood*, 90(8), pp. 3073–81.

Georges-Labouesse, E. N. *et al.* (1996) 'Mesodermal development in mouse embryos mutant for fibronectin', *Developmental Dynamics*, 207(2), pp. 145–156. doi: 10.1002/(SICI)1097-0177(199610)207:2<145::AID-AJA3>3.0.CO;2-H.

Girós, A. *et al.* (2011) 'α5β1 integrin-mediated adhesion to fibronectin is required for axis elongation and somitogenesis in mice', *PLoS ONE*. Edited by D. Gullberg. Public Library of Science, 6(7), p. e22002. doi: 10.1371/journal.pone.0022002.

Goossens, K. *et al.* (2009) 'Quantification of Fibronectin 1 (FN1) splice variants, including two novel ones, and analysis of integrins as candidate FN1 receptors in bovine preimplantation embryos', *BMC Developmental Biology*, 9(1), p. 1. doi: 10.1186/1471-213X-9-1.

Grant, R. P. *et al.* (1997) 'Structural requirements for biological activity of the ninth and tenth

FIII domains of human fibronectin', *Journal of Biological Chemistry*. American Society for Biochemistry and Molecular Biology, 272(10), pp. 6159–6166. doi: 10.1074/jbc.272.10.6159.

Grüner, S. *et al.* (2003) 'Multiple integrin-ligand interactions synergize in shear-resistant platelet adhesion at sites of arterial injury in vivo', *Blood*, 102(12), pp. 4021–4027. doi: 10.1182/blood-2003-05-1391.

Guan, J. L. and Hynes, R. O. (1990) 'Lymphoid cells recognize an alternatively spliced segment of fibronectin via the integrin receptor alpha 4 beta 1.', *Cell*. Cell Press, 60(1), pp. 53–61. doi: 0092-8674(90)90715-Q [pii].

Hautanen, A. *et al.* (1989) 'Effects of modifications of the RGD sequence and its context on recognition by the fibronectin receptor.', *The Journal of biological chemistry*, 264(3), pp. 1437–42. Available at: http://www.ncbi.nlm.nih.gov/pubmed/2521482.

Heisenberg, C. P. and Fässler, R. (2012) 'Cell-cell adhesion and extracellular matrix: diversity counts', *Current Opinion in Cell Biology*, 24(5), pp. 559–561. doi: 10.1016/j.ceb.2012.09.002.

Henderson, B. *et al.* (2011) 'Fibronectin: A multidomain host adhesin targeted by bacterial fibronectin-binding proteins', *FEMS Microbiology Reviews*. Blackwell Publishing Ltd, 35(1), pp. 147–200. doi: 10.1111/j.1574-6976.2010.00243.x.

Hertig, S. and Vogel, V. (2012) 'Catch bonds', *Current Biology*. Elsevier, 22(19), pp. R823–R825. doi: 10.1016/j.cub.2012.08.035.

Herzog, B. H. *et al.* (2013) 'Podoplanin maintains high endothelial venule integrity by interacting with platelet CLEC-2', *Nature*. Nature Publishing Group, 502(7469), pp. 105–109. doi: 10.1038/nature12501.

Hess, P. R. *et al.* (2014) 'Platelets mediate lymphovenous hemostasis to maintain blood-lymphatic separation throughout life', *Journal of Clinical Investigation*. American Society for Clinical Investigation, 124(1), pp. 273–284. doi: 10.1172/JCI70422.

Hodivala-Dilke, K. M. *et al.* (1999) 'β3-integrin–deficient mice are a model for Glanzmann thrombasthenia showing placental defects and reduced survival', *Journal of Clinical Investigation*, 103(2), pp. 229–238. doi: 10.1172/JCI5487.

Horton, E. R. *et al.* (2016) 'The integrin adhesome network at a glance', *Journal of Cell Science*, 129(22), pp. 4159–4163. doi: 10.1242/jcs.192054.

Hughes, P. E. *et al.* (1996) 'Breaking the integrin hinge: A defined structural constraint regulates integrin signaling', *Journal of Biological Chemistry*. American Society for Biochemistry and Molecular Biology, 271(12), pp. 6571–6574. doi: 10.1074/jbc.271.12.6571.

Huveneers, S. *et al.* (2008) 'Binding of soluble fibronectin to integrin alpha5 beta1 - link to focal adhesion redistribution and contractile shape.', *Journal of cell science*, 121(Pt 15), pp. 2452–2462. doi: 10.1242/jcs.033001.

Hynes, R. O. (2002) 'Integrins: bidirectional, allosteric signaling machines.', *Cell*. Elsevier, 110(6), pp. 673–87. doi: 10.1016/S0092-8674(02)00971-6.

Hynes, R. O. (2002) 'Integrins: Bidirectional, allosteric signaling machines', *Cell*, 110(6), pp. 673–687. doi: 10.1016/S0092-8674(02)00971-6.

Hynes, R. O. (2009) 'The extracellular matrix: not just pretty fibrils.', *Science (New York, N.Y.)*. American Association for the Advancement of Science, 326(5957), pp. 1216–9. doi: 10.1126/science.1176009.

Hynes, R. O. and Yamada, K. M. (1982) 'Fibronectins: multifunctional modular glycoproteins.', *The Journal of cell biology*. Rockefeller University Press, 95(2 Pt 1), pp. 369–77. doi: 10.1083/JCB.95.2.369.

Ingber, D. E. (2006) 'Cellular mechanotransduction: putting all the pieces together again', *The FASEB Journal*, 20(7), pp. 811–827. doi: 10.1096/fj.05-5424rev.

Ingham, K. C., Brew, S. A. and Atha, D. H. (1990) 'Interaction of heparin with fibronectin and isolated fibronectin domains.', *The Biochemical journal*, 272(3), pp. 605–11. doi: 10.1042/bj2720605.

Jackson, S. P. (2007) 'The growing complexity of platelet aggregation.', *Blood*. American Society of Hematology, 109(12), pp. 5087–95. doi: 10.1182/blood-2006-12-027698.

Jessen, J. R. (2015) 'Recent advances in the study of zebrafish extracellular matrix proteins', *Developmental Biology*. Academic Press, 401(1), pp. 110–121. doi: 10.1016/J.YDBIO.2014.12.022.

Kadler, K. E., Hill, A. and Canty-Laird, E. G. (2008) 'Collagen fibrillogenesis: fibronectin, integrins, and minor collagens as organizers and nucleators.', *Current opinion in cell biology*, 20(5), pp. 495–501. doi: 10.1016/j.ceb.2008.06.008.

Kanchanawong, P. *et al.* (2010) 'Nanoscale architecture of integrin-based cell adhesions', *Nature*. Nature Publishing Group, 468(7323), pp. 580–584. doi: 10.1038/nature09621.

Kato, K. *et al.* (2003) 'The contribution of glycoprotein VI to stable platelet adhesion and thrombus formation illustrated by targeted gene deletion', *Blood*. American Society of Hematology, 102(5), pp. 1701–1707. doi: 10.1182/blood-2003-03-0717.

Kim, C. *et al.* (2012) 'Basic amino-acid side chains regulate transmembrane integrin signalling', *Nature*. NIH Public Access, 481(7380), pp. 209–214. doi: 10.1038/nature10697.

Kim, N. G. and Gumbiner, B. M. (2015) 'Adhesion to fibronectin regulates Hippo signaling via the FAK-Src-PI3K pathway', *Journal of Cell Biology*. Rockefeller University Press, 210(3), pp. 503–515. doi: 10.1083/jcb.201501025.

Kimizuka, F. *et al.* (1991) 'Role of type III homology repeats in cell adhesive function within the cell-binding domain of fibronectin', *Journal of Biological Chemistry*, 266(5), pp. 3045–3051.

Klass, C. M., Couchman, J. R. and Woods, A. (2000) 'Control of extracellular matrix assembly by syndecan-2 proteoglycan', 113(3), pp. 493–506.

Kong, F. *et al.* (2009) 'Demonstration of catch bonds between an integrin and its ligand', *The Journal of Cell Biology*, 185(7), pp. 1275–1284. doi: 10.1083/jcb.200810002.

Krammer, A. *et al.* (1999) 'Forced unfolding of the fibronectin type III module reveals a tensile molecular recognition switch', *Proceedings of the National Academy of Sciences*, 96(4), pp. 1351–1356. doi: 10.1073/pnas.96.4.1351.

Krammer, A. *et al.* (2002) 'A structural model for force regulated integrin binding to fibronectin's RGD-synergy site', *Matrix Biology*. Elsevier, 21(2), pp. 139–147. doi: 10.1016/S0945-053X(01)00197-4.

Kornberg, L. *et al.* (1992) 'Cell adhesion or integrin clustering increases phosphorylation of a focal adhesion-associated tyrosine kinase.', *The Journal of biological chemistry*, 267(33), pp. 23439–42. Available at: http://www.ncbi.nlm.nih.gov/pubmed/1429685 (Accessed: 23 January 2018).

Kubow, K. E. *et al.* (2015) 'Mechanical forces regulate the interactions of fibronectin and collagen I in extracellular matrix.', *Nature communications*. Nature Publishing Group, 6, p. 8026. doi: 10.1038/ncomms9026.

Kwon, M. J. *et al.* (2012) 'Syndecans play dual roles as cell adhesion receptors and docking receptors', *FEBS Letters*. Federation of European Biochemical Societies, 586(16), pp. 2207–2211. doi: 10.1016/j.febslet.2012.05.037.

Lau, T.-L. *et al.* (2009) 'The structure of the integrin αIIbβ3 transmembrane complex explains integrin transmembrane signalling', *The EMBO Journal*, 28(9), pp. 1351–1361. doi: 10.1038/emboj.2009.63.

Le, V. P., Kovacs, A. and Wagenseil, J. E. (2012) 'Measuring left ventricular pressure in late embryonic and neonatal mice.', *Journal of visualized experiments: JoVE*. MyJoVE Corporation, (60). doi: 10.3791/3756.

Legate, K. R. *et al.* (2011) 'Integrin adhesion and force coupling are independently regulated by localized PtdIns(4,5)2 synthesis', *The EMBO Journal*, 30(22), pp. 4539–4553. doi: 10.1038/emboj.2011.332.

Leahy, D. J., Aukhil, I. and Erickson, H. P. (1996) '2.0 Å Crystal Structure of a Four-Domain Segment of Human Fibronectin Encompassing the RGD Loop and Synergy Region', *Cell*. Cell Press, 84(1), pp. 155–164. doi: 10.1016/S0092-8674(00)81002-8.

Leiss, M. *et al.* (2008) 'The role of integrin binding sites in fibronectin matrix assembly in vivo', *Current Opinion in Cell Biology*, 20(5), pp. 502–507. doi: 10.1016/j.ceb.2008.06.001.

Lemmon, C. A., Chen, C. S. and Romer, L. H. (2009) 'Cell traction forces direct fibronectin matrix assembly', *Biophysical Journal*. Elsevier, 96(2), pp. 729–738. doi: 10.1016/j.bpj.2008.10.009.

Lemmon, C. A., Ohashi, T. and Erickson, H. P. (2011) 'Probing the Folded State of Fibronectin Type III Domains in Stretched Fibrils by Measuring Buried Cysteine Accessibility', *Journal of Biological Chemistry*. in Press, 286(30), pp. 26375–26382. doi: 10.1074/jbc.M111.240028.

Li, J. *et al.* (2017) 'Conformational equilibria and intrinsic affinities define integrin activation', *The EMBO Journal*. EMBO Press, 36(5), pp. 629–645. doi: 10.15252/embj.201695803.

Li, J. and Springer, T. A. (2017) 'Integrin extension enables ultrasensitive regulation by cytoskeletal force', *Proceedings of the National Academy of Sciences*. National Academy of Sciences, 114(18), pp. 4685–4690. doi: 10.1073/pnas.1704171114.

Li, J. and Springer, T. A. (2018) 'Energy landscape differences among integrins establish the framework for understanding activation', *The Journal of Cell Biology*, 217(1), pp. 397–412. doi: 10.1083/jcb.201701169.

Litvinov, R. I. *et al.* (2016) 'The platelet integrin ??IIb??3 differentially interacts with fibrin versus fibrinogen', *Journal of Biological Chemistry*, 291(15), pp. 7858–7867. doi: 10.1074/jbc.M115.706861.

Liu, S., Calderwood, D. a and Ginsberg, M. H. (2000) 'Integrin cytoplasmic domain-binding proteins.', *Journal of cell science*, 113 (Pt 2, pp. 3563–3571.

Lu, Z. *et al.* (2016) 'Implications of the differing roles of the β1 and β3 transmembrane and cytosplasmic domains for integrin function', *eLife*. eLife Sciences Publications Limited, 5(DECEMBER2016), p. e18633. doi: 10.7554/eLife.18633.

Ma, Y.-Q., Qin, J. and Plow, E. F. (2007) 'Platelet integrin alpha(IIb)beta(3): activation

mechanisms.', *Journal of thrombosis and haemostasis : JTH*. Wiley/Blackwell (10.1111), 5(7), pp. 1345–52. doi: 10.1111/j.1538-7836.2007.02537.x.

Mahalingam, Y., Gallagher, J. T. and Couchman, J. R. (2007) 'Cellular adhesion responses to the heparin-binding (HepII) domain of fibronectin require heparan sulfate with specific properties.', *The Journal of biological chemistry*. American Society for Biochemistry and Molecular Biology, 282(5), pp. 3221–30. doi: 10.1074/jbc.M604938200.

Mao, Y. and Schwarzbauer, J. E. (2005) 'Fibronectin fibrillogenesis, a cell-mediated matrix assembly process', *Matrix Biology*, 24(6), pp. 389–399. doi: 10.1016/j.matbio.2005.06.008.

Mao, Y. and Schwarzbauer, J. E. (2006) 'Accessibility to the Fibronectin Synergy Site in a 3D Matrix Regulates Engagement of α 5β 1 versus α vβ 3 Integrin Receptors', *Cell Communication & Adhesion*. Taylor & Francis, 13(5–6), pp. 267–277. doi: 10.1080/15419060601072215.

Marjenberg, Z. R. *et al.* (2011) 'Cooperative binding and activation of fibronectin by a bacterial surface protein.', *The Journal of biological chemistry*. American Society for Biochemistry and Molecular Biology, 286(3), pp. 1884–94. doi: 10.1074/jbc.M110.183053.

Marsden, M. and DeSimone, D. W. (2001) 'Regulation of cell polarity, radial intercalation and epiboly in Xenopus: novel roles for integrin and fibronectin', *Development*, 128(18).

Matuskova, J. *et al.* (2006) 'Decreased Plasma Fibronectin Leads to Delayed Thrombus Growth in Injured Arterioles', *Arteriosclerosis, Thrombosis, and Vascular Biology*, 26(6), pp. 1391–1396. doi: 10.1161/01.ATV.0000216282.58291.c6.

Maurer, L. M. *et al.* (2012) 'Ligation of the fibrin-binding domain by ??-strand addition is sufficient for expansion of soluble fibronectin', *Journal of Biological Chemistry*, 287(16), pp. 13303–13312. doi: 10.1074/jbc.M111.294041.

Maurer, L. M., Ma, W. and Mosher, D. F. (2015) 'Dynamic structure of plasma fibronectin.', *Critical reviews in biochemistry and molecular biology*. NIH Public Access, 51(4), pp. 213–27. doi: 10.1080/10409238.2016.1184224.

Maurer, L. M., Tomasini-Johansson, B. R. and Mosher, D. F. (2010) 'Emerging roles of fibronectin in thrombosis', *Thrombosis Research*. Elsevier Ltd, 125(4), pp. 287–291. doi: 10.1016/j.thromres.2009.12.017.

Mehrbod, M., Trisno, S. and Mofrad, M. R. K. (2013) 'On the activation of integrin αIIbβ3: Outside-in and inside-out pathways', *Biophysical Journal*. The Biophysical Society, 105(6), pp. 1304–1315. doi: 10.1016/j.bpj.2013.07.055.

Mitsi, M. *et al.* (2008) 'A catalytic role of heparin within the extracellular matrix', *Journal of Biological Chemistry*, 283(50), pp. 34796–34807. doi: 10.1074/jbc.M806692200.

Morgan, M. R., Humphries, M. J. and Bass, M. D. (2007) 'Synergistic control of cell adhesion by integrins and syndecans.', *Nature reviews. Molecular cell biology*, 8(12), pp. 957–69. doi: 10.1038/nrm2289.

Moretti, F. A. *et al.* (2007) 'A major fraction of fibronectin present in the extracellular matrix of tissues is plasma-derived', *Journal of Biological Chemistry*. American Society for Biochemistry and Molecular Biology, 282(38), pp. 28057–28062. doi: 10.1074/jbc.M611315200.

Moser, M. *et al.* (2008) 'Kindlin-3 is essential for integrin activation and platelet aggregation', *Nature Medicine*. Nature Publishing Group, 14(3), pp. 325–330. doi: 10.1038/nm1722.

Mosesson, M. W. and Umfleet, R. A. (1970) 'The cold-insoluble globulin of human plasma. I. Purification, primary characterization, and relationship to fibrinogen and other cold-insoluble

fraction components.', *The Journal of biological chemistry*, 245(21), pp. 5728–36.

Mosher, D. F. (1975) 'Cross-linking of cold-insoluble globulin by fibrin-stabilizing factor.', *The Journal of biological chemistry*, 250(16), pp. 6614–21.

Mould, A. P. *et al.* (2003) 'Structure of an integrin-ligand complex deduced from solution X-ray scattering and site-directed mutagenesis', *Journal of Biological Chemistry*, 278(41), pp. 39993–39999. doi: 10.1074/jbc.M304627200.

Mould, A. P., Akiyama, S. K. and Humphries, M. J. (1995) 'Regulation of Integrin 5 1-Fibronectin Interactions by Divalent Cations: EVIDENCE FOR DISTINCT CLASSES OF BINDING SITES FOR Mn2+, Mg2+, AND Ca2+', *Journal of Biological Chemistry*, 270(44), pp. 26270–26277. doi: 10.1074/jbc.270.44.26270.

Moulisová, V. *et al.* (2017) 'Engineered microenvironments for synergistic VEGF - Integrin signalling during vascularization.', *Biomaterials*. Elsevier, 126, pp. 61–74. doi: 10.1016/j.biomaterials.2017.02.024.

Nagae, M. *et al.* (2012) 'Crystal structure of α5β1 integrin ectodomain: Atomic details of the fibronectin receptor', *The Journal of Cell Biology*, 197(1), pp. 131–140. doi: 10.1083/jcb.201111077.

Napper, C. E., Drickamer, K. and Taylor, M. E. (2006) 'Collagen binding by the mannose receptor mediated through the fibronectin type II domain', *Biochem. J*, 395, pp. 579–586. doi: 10.1042/BJ20052027.

Ni, H. *et al.* (2000) 'Persistence of platelet thrombus formation in arterioles of mice lacking both von Willebrand factor and fibrinogen', *Journal of Clinical Investigation*, 106(3), pp. 385–392. doi: 10.1172/JCI9896.

Ni, H. *et al.* (2003) 'Plasma fibronectin promotes thrombus growth and stability in injured arterioles.', *Proceedings of the National Academy of Sciences of the United States of America*, 100(5), pp. 2415–9. doi: 10.1073/pnas.2628067100.

Ni, H. and Freedman, J. (2003) 'Platelets in hemostasis and thrombosis: role of integrins and their ligands', *Transfusion and Apheresis Science*, 28(3), pp. 257–264. doi: 10.1016/S1473-0502(03)00044-2.

Nieswandt, B. *et al.* (2001) 'Glycoprotein VI but not alpha2beta1 integrin is essential for platelet interaction with collagen.', *The EMBO journal*. European Molecular Biology Organization, 20(9), pp. 2120–30. doi: 10.1093/emboj/20.9.2120.

Oberhauser, A. F. *et al.* (2002) 'The mechanical hierarchies of fibronectin observed with single-molecule AFM', *Journal of Molecular Biology*, 319(2), pp. 433–447. doi: 10.1016/S0022-2836(02)00306-6.

Olorundare, O. E. *et al.* (2001) 'Assembly of a fibronectin matrix by adherent platelets stimulated by lysophosphatidic acid and other agonists', *Blood*. American Society of Hematology, 98(1), pp. 117–124. doi: 10.1182/blood.V98.1.117.

Pankov, R. *et al.* (2000) 'Integrin dynamics and matrix assembly: Tensin-dependent translocation of ??5??1 integrins promotes early fibronectin fibrillogenesis', *Journal of Cell Biology*, 148(5), pp. 1075–1090. doi: 10.1083/jcb.148.5.1075.

Pankov, R. (2002) 'Fibronectin at a glance', *Journal of Cell Science*. The Company of Biologists Ltd, 115(20), pp. 3861–3863. doi: 10.1242/jcs.00059.

Patterson, K. C. *et al.* (2013) 'Measurement of cationic and intracellular modulation of integrin binding affinity by AFM-based nanorobot.', *Biophysical journal*. Elsevier, 105(1), pp. 40–7. doi: 10.1016/j.bpj.2013.05.052.

Pickford, A. R. *et al.* (1997) 'Solution structure of a type 2 module from fibronectin: implications for the structure and function of the gelatin-binding domain', *Structure*. Cell Press, 5(3), pp. 359–370. doi: 10.1016/S0969-2126(97)00193-7.

Pierschbacher, M. D. and Ruoslahti, E. (1984) 'Cell attachment activity of fibronectin can be duplicated by small synthetic fragments of the molecule', *Nature*, 309(5963), pp. 30–33. doi: 10.1038/309030a0.

Planas-Paz, L. and Lammert, E. (2013) 'Mechanical forces in lymphatic vascular development and disease', *Cellular and Molecular Life Sciences*, 70(22), pp. 4341–4354. doi: 10.1007/s00018-013-1358-5.

Plow, E. F. *et al.* (2000) 'Ligand binding to integrins', *Journal of Biological Chemistry*, 275(29), pp. 21785–21788. doi: 10.1074/jbc.R000003200.

Potts, J. R. and Campbell, I. D. (1996) 'Structure and function of fibronectin modules', *Matrix Biology*. Elsevier, 15(5), pp. 313–320. doi: 10.1016/S0945-053X(96)90133-X.

Poulter, N. S. *et al.* (2017) 'Clustering of glycoprotein VI (GPVI) dimers upon adhesion to collagen as a mechanism to regulate GPVI signaling in platelets', *Journal of Thrombosis and Haemostasis*. Wiley/Blackwell (10.1111), 15(3), pp. 549–564. doi: 10.1111/jth.13613.

Prewitz, M. C. *et al.* (2013) 'Tightly anchored tissue-mimetic matrices as instructive stem cell microenvironments', *Nature Methods*. Nature Publishing Group, 10(8), pp. 788–794. doi: 10.1038/nmeth.2523.

Provenzano, P. P. *et al.* (2009) 'Matrix density-induced mechanoregulation of breast cell phenotype, signaling and gene expression through a FAK–ERK linkage', *Oncogene*. Nature Publishing Group, 28(49), pp. 4326–4343. doi: 10.1038/onc.2009.299.

Ramanathan, A. and Karuri, N. (2014) 'Fibronectin alters the rate of formation and structure of the fibrin matrix', *Biochemical and Biophysical Research Communications*. Elsevier Inc., 443(2), pp. 395–399. doi: 10.1016/j.bbrc.2013.11.090.

Raitman, I. *et al.* (2017) 'Heparin-fibronectin interactions in the development of extracellular matrix insolubility.', *Matrix biology: journal of the International Society for Matrix Biology*. International Society of Matrix Biology. doi: 10.1016/j.matbio.2017.11.012.

Redick, S. D. *et al.* (2000) 'Defining Fibronectin ' s Cell Adhesion Synergy Site by Site-directed Mutagenesis', *The Journal of cell biology*, 149(2), pp. 521–527. doi: 10.1083/jcb.149.2.521.

Reheman, A. *et al.* (2009) 'Plasma fibronectin depletion enhances platelet aggregation and thrombus formation in mice lacking fibrinogen and von Willebrand factor', *Blood*, 113(8), pp. 1809–1817. doi: 10.1182/blood-2008-04-148361.

Ren, X., B.kiosses, W. and Schwartz, M. A. (1999) 'Regulation of the small GTP-binding protein Rho by cell adhesion and the cytoskeleton', *Stress: The International Journal on the Biology of Stress*, 18(3), pp. 578–585.

Retta, S. F., Ferraris, P. and Tarone, G. (1999) 'Purification of Fibronectin from Human Plasma', in *Adhesion Protein Protocols*. New Jersey: Humana Press, pp. 119–124. doi: 10.1385/1-59259-258-9:119.

Rossier, O. *et al.* (2012) 'Integrins β1 and β3 exhibit distinct dynamic nanoscale organizations inside focal adhesions', *Nature Cell Biology*. Nature Publishing Group, 14(10), pp. 1057–1067. doi: 10.1038/ncb2588.

Rumbaut, R. E., Slaff, D. W. and Burns, A. E. (2005) 'Microvascular Thrombosis Models in Venules and Arterioles *In Vivo*', *Microcirculation*. Wiley/Blackwell (10.1111), 12(3), pp. 259–274. doi: 10.1080/10739680590925664.

Ruoslahti, E. (1996) 'RGD AND OTHER RECOGNITION SEQUENCES FOR INTEGRINS', *Annual Review of Cell and Developmental Biology*. Annual Reviews 4139 El Camino Way, P.O. Box 10139, Palo Alto, CA 94303-0139, USA, 12(1), pp. 697–715. doi: 10.1146/annurev.cellbio.12.1.697.

Sakai, T. (2001) 'Plasma fibronectin supports neuronal survival and reduces brain injury following transient focal cerebral ischemia but is not essential for skin-wound healing and hemostasis', *Nature Med.*

Schiller, H. B. *et al.* (2013) 'β1- and αv-class integrins cooperate to regulate myosin II during rigidity sensing of fibronectin-based microenvironments', *Nature Cell Biology*, 15(6), pp. 625–636. doi: 10.1038/ncb2747.

Schiller, H. B. and Fässler, R. (2013) 'Mechanosensitivity and compositional dynamics of cell-matrix adhesions', *EMBO Reports*. European Molecular Biology Organization, pp. 509–519. doi: 10.1038/embor.2013.49.

Schwarzbauer, J. E. (1991) 'Identification of the Fibronectin Sequences Required for Assembly of a Fibrillar Matrix', *Cell*, 113(6), pp. 1463–1473.

Schwarzbauer, J. E. and DeSimone, D. W. (2011) 'Fibronectins, Their Fibrillogenesis, and In Vivo Functions', *Cold Spring Harbor Perspectives in Biology*, 3(7), pp. a005041–a005041. doi: 10.1101/cshperspect.a005041.

Sechler, J. L. *et al.* (1998) 'Modulation of cell-extracellular matrix interactions.', *Annals of the New York Academy of Sciences*, 857, pp. 143–154.

Sechler, J. L. *et al.* (2000) 'A novel RGD-independent fibronectin assembly pathway initiated by α4β1 integrin binding to the alternatively spliced V region', *Journal of Cell Science*, 113, pp. 1491–1498.

Sekiguchi, K. *et al.* (1983) 'Binding of fibronectin and its proteolytic fragments to glycosaminoglycans. Exposure of cryptic glycosaminoglycan-binding domains upon limited proteolysis', *Journal of Biological Chemistry*, 258(23), pp. 14359–14365.

Seong, J. *et al.* (2013) 'Distinct biophysical mechanisms of focal adhesion kinase mechanoactivation by different extracellular matrix proteins.', *Proceedings of the National Academy of Sciences of the United States of America*, 110(48), pp. 19372–7. doi: 10.1073/pnas.1307405110.

Shah, R. *et al.* (2017b) 'Spontaneous unfolding-refolding of fibronectin type III domains assayed by thiol exchange: Thermodynamic stability correlates with rates of unfolding rather than folding', *Journal of Biological Chemistry*. American Society for Biochemistry and Molecular Biology, 292(3), pp. 955–966. doi: 10.1074/jbc.M116.760371.

Sharma, A. (1999) 'Crystal structure of a heparin-and integrin-binding segment of human fibronectin', *The EMBO Journal*, 18(6), pp. 1468–1479. doi: 10.1093/emboj/18.6.1468.

Shattil, S. J. (2004) 'Integrins: dynamic scaffolds for adhesion and signaling in platelets', *Blood*, 104(6), pp. 1606–1615. doi: 10.1182/blood-2004-04-1257.

Shattil, S. J., Kim, C. and Ginsberg, M. H. (2010) 'The final steps of integrin activation: The end game', *Nature Reviews Molecular Cell Biology*. Nature Publishing Group, pp. 288–300. doi: 10.1038/nrm2871.

Shi, Q. (2003) 'A Novel Mode for Integrin-mediated Signaling: Tethering Is Required for Phosphorylation of FAK Y397', *Molecular Biology of the Cell*, 14(10), pp. 4306–4315. doi: 10.1091/mbc.E03-01-0046.

Simons, M. and Horowitz, A. (2001) 'Syndecan-4-mediated signalling', *Cellular Signalling*, 13(12), pp. 855–862. doi: 10.1016/S0898-6568(01)00190-5.

Singh, P., Carraher, C. and Schwarzbauer, J. E. (2010) 'Assembly of fibronectin extracellular marix', *Annu Rev Cell Dev Biol*, 26, pp. 397–419. doi: 10.1146/annurev-cellbio-100109-104020.

Sivakumar, P. *et al.* (2006) 'New insights into extracellular matrix assembly and reorganization from dynamic imaging of extracellular matrix proteins in living osteoblasts.', *Journal of cell science*. The Company of Biologists Ltd, 119(Pt 7), pp. 1350–60. doi: 10.1242/jcs.02830.

Smith, M. L. *et al.* (2007) 'Force-induced unfolding of fibronectin in the extracellular matrix of living cells', *PLoS Biology*. Edited by M. Schliwa. Public Library of Science, 5(10), pp. 2243–2254. doi: 10.1371/journal.pbio.0050268.

Sottile, J. *et al.* (2007) 'Fibronectin-dependent collagen I deposition modulates the cell response to fibronectin', *American Journal of Physiology-Cell Physiology*, 293(6), pp. C1934–C1946. doi: 10.1152/ajpcell.00130.2007.

Sottile, J. and Hocking, D. C. (2002) 'Fibronectin polymerization regulates the composition and stability of extracellular matrix fibrils and cell-matrix adhesions.', *Molecular biology of the cell*. American Society for Cell Biology, 13(10), pp. 3546–59. doi: 10.1091/mbc.E02-01-0048.

Springer, B. T. A. and À, J. W. (2004) 'THE THREE-DIMENSIONAL STRUCTURE OF INTEGRINS AND THEIR LIGANDS , AND CONFORMATIONAL REGULATION OF CELL ADHESION A bstract Integrins are a structurally elaborate family of adhesion molecules Members of the integrin family of adhesion molecules are non-cova', 68, pp. 29–63.

Stamatoglou, S. C. and Keller, J. M. (1983) 'Correlation between cell substrate attachment in vitro and cell surface heparan sulfate affinity for fibronectin and collagen', *Journal of Cell Biology*. Rockefeller University Press, 96(6), pp. 1820–1823. doi: 10.1083/JCB.96.6.1820.

Stegner, D. and Nieswandt, B. (2011) 'Platelet receptor signaling in thrombus formation', *Journal of Molecular Medicine*. Springer-Verlag, pp. 109–121. doi: 10.1007/s00109-010-0691-5.

Stepp, M. A. *et al.* (2010) 'Syndecan-1 regulates cell migration and fibronectin fibril assembly', *Experimental Cell Research*. Elsevier Inc., 316(14), pp. 2322–2339. doi: 10.1016/j.yexcr.2010.05.020.

Sun, Z., Guo, S. S. and Fässler, R. (2016) 'Integrin-mediated mechanotransduction.', *The Journal of cell biology*. Rockefeller University Press, 215(4), pp. 445–456. doi: 10.1083/jcb.201609037.

Sun, Z., Lambacher, A. and Fässler, R. (2014) 'Nascent adhesions: From fluctuations to a hierarchical organization', *Current Biology*, 24(17), pp. R801–R803. doi: 10.1016/j.cub.2014.07.061.

Takagi, J. *et al.* (2002) 'Global conformational earrangements in integrin extracellular domains in outside-in and inside-out signaling', *Cell*. Cell Press, 110(5), pp. 599–611. doi: 10.1016/S0092-8674(02)00935-2.

Takagi, J. *et al.* (2003) 'Structure of integrin alpha5beta1 in complex with fibronectin.', *The EMBO*

journal, 22(18), pp. 4607–15. doi: 10.1093/emboj/cdg445.

Takagi, J. (2004) 'Structural basis for ligand recognition by RGD (Arg-Gly-Asp)-dependent integrins', *Biochemical Society Transactions*. Portland Press Limited, 32(3), pp. 403–406. doi: 10.1042/bst0320403.

Takahashi, S. *et al.* (2007) 'The RGD motif in fibronectin is essential for development but dispensable for fibril assembly', *The Journal of Cell Biology*, 178(1), pp. 167–178. doi: 10.1083/jcb.200703021.

Takahashi, S. *et al.* (2015) 'C-type lectin-like domain and fibronectin-like type II domain of phospholipase A $_2$ receptor 1 modulate binding and migratory responses to collagen', *FEBS Letters*, 589(7), pp. 829–835. doi: 10.1016/j.febslet.2015.02.016.

Taubenberger, A. V. *et al.* (2010) 'The effect of unlocking RGD-motifs in collagen I on pre-osteoblast adhesion and differentiation', *Biomaterials*. Elsevier Ltd, 31(10), pp. 2827–2835. doi: 10.1016/j.biomaterials.2009.12.051.

Theodosiou, M. *et al.* (2016) 'Kindlin-2 cooperates with talin to activate integrins and induces cell spreading by directly binding paxillin', *eLife*, 5 (JANUARY2016), pp. 1–24. doi: 10.7554/eLife.10130.

Thomas, W. (2008) 'Catch bonds in adhesion.', *Annual review of biomedical engineering*, 10, pp. 39–57. doi: 10.1146/annurev.bioeng.10.061807.160427.

Tkachenko, E., Rhodes, J. M. and Simons, M. (2005) 'Syndecans: New kids on the signaling block', *Circulation Research*, 96(5), pp. 488–500. doi: 10.1161/01.RES.0000159708.71142.c8.

Tronik-Le Roux, D. *et al.* (2000) 'Thrombasthenic mice generated by replacement of the integrin alpha(IIb) gene: demonstration that transcriptional activation of this megakaryocytic locus precedes lineage commitment.', *Blood*, 96(4), pp. 1399–408.

Turner, C. J. *et al.* (2014) 'Integrin-α5β1 is not required for mural cell functions during development of blood vessels but is required for lymphatic-blood vessel separation and lymphovenous valve formation', *Developmental Biology*, 392(2), pp. 381–392. doi: 10.1016/j.ydbio.2014.05.006.

Uhrin, P. *et al.* (2010) 'Novel function for blood platelets and podoplanin in developmental separation of blood and lymphatic circulation', *Blood*, 115(19), pp. 3997–4005. doi: 10.1182/blood-2009-04-216069.

Vadasz, B. *et al.* (2015) 'Platelets and platelet alloantigens: Lessons from human patients and animal models of fetal and neonatal alloimmune thrombocytopenia', *Genes & Diseases*. Elsevier, 2(2), pp. 173–185. doi: 10.1016/j.gendis.2015.02.003.

Varga-Szabo, D., Pleines, I. and Nieswandt, B. (2008) 'Cell Adhesion Mechanisms in Platelets', *Arteriosclerosis, Thrombosis, and Vascular Biology*, 28(3), pp. 403–412. doi: 10.1161/ATVBAHA.107.150474.

Wang, Y. *et al.* (2014) 'Plasma fibronectin supports hemostasis and regulates thrombosis', *Journal of Clinical Investigation*, 124(10), pp. 4281–4293. doi: 10.1172/JCI74630.

Wang, Y. and Ni, H. (2016) 'Fibronectin maintains the balance between hemostasis and thrombosis', *Cellular and Molecular Life Sciences*. Springer International Publishing, 73(17), pp. 3265–3277. doi: 10.1007/s00018-016-2225-y.

Welsh, J. D., Kahn, M. L. and Sweet, D. T. (2016) 'Lymphovenous hemostasis and the role of

platelets in regulating lymphatic flow and lymphatic vessel maturation.', *Blood*. American Society of Hematology, 128(9), pp. 1169–73. doi: 10.1182/blood-2016-04-636415.

White, E., Baralle, F. and Muro, A. (2008) 'New insights into form and function of fibronectin splice variants', *The Journal of Pathology*, 216(1), pp. 1–14. doi: 10.1002/path.2388.

White, E. S. and Muro, A. F. (2011) 'Fibronectin splice variants: Understanding their multiple roles in health and disease using engineered mouse models', *IUBMB Life*, 63(7), pp. 538–546. doi: 10.1002/iub.493.

Wickström, S. A., Radovanac, K. and Fässler, R. (2011) 'Genetic analyses of integrin signaling', *Cold Spring Harbor Perspectives in Biology*. Cold Spring Harbor Laboratory Press, pp. 1–22. doi: 10.1101/cshperspect.a005116.

Wierzbicka-Patynowski, I. (2003) 'The ins and outs of fibronectin matrix assembly', *Journal of Cell Science*, 116(16), pp. 3269–3276. doi: 10.1242/jcs.00670.

Xia, W. and Springer, T. A. (2014) 'Metal ion and ligand binding of integrin α5β1.', *Proceedings of the National Academy of Sciences of the United States of America*, 111(50), pp. 17863–8. doi: 10.1073/pnas.1420645111.

Xian, X., Gopal, S. and Couchman, J. R. (2010) 'Syndecans as receptors and organizers of the extracellular matrix', *Cell and Tissue Research*, 339(1), pp. 31–46. doi: 10.1007/s00441-009-0829-3.

Xiong, J.-P. *et al.* (2002) 'Crystal structure of the extracellular segment of integrin alpha Vbeta3 in complex with an Arg-Gly-Asp ligand.', *Science (New York, N.Y.)*, 296(5565), pp. 151–155. doi: 10.1126/science.1069040.

Xu, X. R., Carrim, N., *et al.* (2016) 'Platelets and platelet adhesion molecules: novel mechanisms of thrombosis and anti-thrombotic therapies', *Thrombosis Journal*. Thrombosis Journal, 14(S1), p. 29. doi: 10.1186/s12959-016-0100-6.

Xu, X. R., Zhang, D., *et al.* (2016) 'Platelets are versatile cells: New discoveries in hemostasis, thrombosis, immune responses, tumor metastasis and beyond', *Critical Reviews in Clinical Laboratory Sciences*, pp. 409–430. doi: 10.1080/10408363.2016.1200008.

Yamamoto, H. *et al.* (2015) 'Integrin β1 controls VE-cadherin localization and blood vessel stability.', *Nature communications*. Nature Publishing Group, 6, p. 6429. doi: 10.1038/ncomms7429.

Yang, J. *et al.* (2009) 'Structure of an integrin IIb 3 transmembrane-cytoplasmic heterocomplex provides insight into integrin activation', *Proceedings of the National Academy of Sciences*, 106(42), pp. 17729–17734. doi: 10.1073/pnas.0909589106.

Yang, J. T. *et al.* (1999) 'Overlapping and independent functions of fibronectin receptor integrins in early mesodermal development.', *Developmental biology*, 215(2), pp. 264–77. doi: 10.1006/dbio.1999.9451.

Yang, J. T. and Hynes, R. O. (1996) 'Fibronectin receptor functions in embryonic cells deficient in alpha 5 beta 1 integrin can be replaced by alpha V integrins.', *Molecular biology of the cell*, 7(11), pp. 1737–1748. doi: 10.1091/mbc.7.11.1737.

Yang, J. T., Rayburn, H. and Hynes, R. O. (1993) 'Embryonic mesodermal defects in alpha 5 integrin-deficient mice.', *Development (Cambridge, England)*, 119(4), pp. 1093–1105.

Yoneda, A. and Couchman, J. R. (2003) 'Regulation of cytoskeletal organization by syndecan transmembrane proteoglycans', *Matrix Biology*, 22(1), pp. 25–33. doi: 10.1016/S0945-

053X(03)00010-6.

Zaidel-Bar, R. (2013) 'Job-splitting among integrins', *Nature Cell Biology*. Nature Publishing Group, pp. 575–577. doi: 10.1038/ncb2770.

Zeiler, M., Moser, M. and Mann, M. (2014) 'Copy number analysis of the murine platelet proteome spanning the complete abundance range.', *Molecular & cellular proteomics : MCP*, 13(12), pp. 3435–3445. doi: 10.1074/mcp.M114.038513.

Zhai, Z. *et al.* (2007) 'Fibrinogen controls human platelet fibronectin internalization and cell-surface retention', *Journal of Thrombosis and Haemostasis*, 5(8), pp. 1740–1746. doi: 10.1111/j.1538-7836.2007.02625.x.

Zhang, K. and Chen, J. F. (2012) 'The regulation of integrin function by divalent cations', *Cell Adhesion and Migration*. Taylor & Francis, pp. 20–29. doi: 10.4161/cam.6.1.18702.

Zhu, J. *et al.* (2008) 'Structure of a Complete Integrin Ectodomain in a Physiologic Resting State and Activation and Deactivation by Applied Forces', *Molecular Cell*, 32(6), pp. 849–861. doi: 10.1016/j.molcel.2008.11.018.

Zhu, J. *et al.* (2009) 'The Structure of a Receptor with Two Associating Transmembrane Domains on the Cell Surface: Integrin αIIbβ3', *Molecular Cell*. NIH Public Access, 34(2), pp. 234–249. doi: 10.1016/j.molcel.2009.02.022.

Zhu, J., Zhu, J. and Springer, T. A. (2013) 'Complete integrin headpiece opening in eight steps', *Journal of Cell Biology*. Rockefeller University Press, 201(7), pp. 1053–1068. doi: 10.1083/jcb.201212037.

Zollinger, A. J. and Smith, M. L. (2017) 'Fibronectin, the extracellular glue', *Matrix Biology*. Elsevier, 60–61, pp. 27–37. doi: 10.1016/J.MATBIO.2016.07.011.

GLOSSARY OF ABBREVIATIONS

α-SMA	Alpha-smooth muscle
ADP	Adenosine diphosphate
AU	Arbitrary units
BSA	Bovine serum slbumin
Col I	Collagen I
Col IV	Collagen IV
CT	Cytoplasmic tail (referred to integrins)
DMEM	Dulbecco's Modified Eagle's médium
DMSO	Dimethyl sulfoxide
DNA	Deoxyribonucleic acid
dNTP	Deoxynucleotide triphosphate
DOC	Sodium Deoxycholate
DOC ins	Insoluble in DOC
DOC sol	Soluble in DOC
DTSSP	3'-dithiobis (sulfosuccinimidyl propionate)
E(number)	Embryonic(days)
EC	Endothelial cells
ECM	Extracellular matrix
EDTA	Ethylendiaminoetetraacetic acid
FA	Focal adhesion
fl-FN	Full-length Fibronectin
FN	Fibronectin
FNcom	Commercial Fibronectin
FAK	Focal adhesion kinase
Fg	Fibrinogen
Hep	Heparin
HRP	Horseradish peroxidase
H&E	Haematoxylin/Eosin staining
KD	Knock-down
kDa	Kilo Dalton
KO	Knock-out

kPa	Kilo Pascal
LB	Luria Bertani medium
LEC	Lymphatic endothelial cell
Lyve-1	Lymphatic vessel endothelial hyaluronan receptor
NA	Nascent adhesion
NG2	Neuron-glial antigen 2
n.s.	Non-significative
P21	Postnatal 21 days
Pax	Paxillin
PBS	Phosphate buffered saline
PBST	PBS-tween
PCR	Polymerase chain reaction
PFA	Parafolmaldehide
PECAM	Platelet endothelial cell adhesion molecule
pFN	Plasmatic FN
pKO	pan-Knock-out
PPR	Platelet Rich Plasma
RT	Room temperature
Sdc	Syndecan
SRM	Serum replacement medium
TM	Transmembrane
vWF	von Willebrand Factor
WM	whole-mount
WT	wild-type

RESUMEN

La fibronectina (FN) es una glicoproteína que forma parte de la matriz extracelular (MEC). La FN se encuentra en dos formas: soluble, en el plasma sanguíneo, o formando fibras insolubles en la matriz que rodea las células de los tejidos. La FN es un dímero con una estructura modular que contiene varias regiones que unen receptores celulares, factores de crecimiento, otras proteínas de la MEC y otras moléculas de FN. Las MECs forman redes altamente dinámicas organizadas en fibras que constituyen un soporte para las células y regulan su comportamiento, como la proliferación, la migración o la diferenciación. La FN tiene una gran importancia en las MECs, ya que se ha visto que es esencial en procesos como el desarrollo embrionario o la coagulación de la sangre. Su participación en estos procesos se debe a las interacciones que establece con receptores celulares de la familia de las integrinas. Para la formación de una matriz fibrilar, los dímeros de FN tienen que establecer enlaces intermoleculares. Cuando la FN se secreta, el dímero presenta una conformación globular y soluble, ya que los motivos de unión a otras FNs permanecen ocultos en el glóbulo. El ensamblado de fibras de FN es un proceso dirigido por la célula y se cree que depende de la interacción FN-integrinas. Las integrinas son receptores de la membrana plasmática heterodiméricos que proporcionan un enlace transmembrana entre la MEC y el citosol. La región citosólica de las integrinas une filamentos de actina y promueve la contracción del citoesqueleto activando la miosina. De esta manera, la integrina ejerce una fuerza de tracción sobre el dímero de FN unido y permite la exposición de los sitios de unión FN-FN. Así, progresivamente se van generando fibrillas alargadas de FN en el espacio extracelular. Cuando la fibrilogénesis de FN está alterada, debido a una producción insuficiente de FN o a un ensamblaje defectuoso, puede provocar una disfunción de órganos o tejidos. Por lo tanto, es de gran importancia entender las reglas que rigen el proceso de fibrilogénesis. El principal sitio de unión a integrinas dentro de la molécula de FN es una secuencia RGD, localizada en la 10ª repetición de tipo III ($FNIII_{10}$). Este motivo RGD puede unir α5β1, αIIbβ3 y todas las integrinas que contienen la subunidad αv (integrinas clase αv). Además, las integrinas α5β1 y αIIbβ3 pueden unirse al denominado motivo sinérgico (DRVPPSRN) localizado en la 9ª repetición tipo III de la FN ($FNIII_9$). La interacción de estas dos integrinas con la FN está involucrada en procesos biológicos vitales como desarrollo embrionario o coagulación sanguínea, respectivamente. Es por ello por lo que para entender en detalle como tienen lugar dichos procesos y el papel tanto de la FN como de las integrinas en ellos debemos estudiar la interacción de estos receptores con los diferentes sitios de unión de la FN. En este trabajo, nuestro objetivo fue comprender la función *in vivo* de estos dos sitios de unión a integrinas y ver como cooperan entre sí. Para ello por un lado estudiamos la función del sitio RGD en el proceso de fibrilogénesis de FN, empleando los fibroblastos $Fn1^{\Delta RGD/\ \Delta RGD}$ genéticamente modificados para expresar FN que carece del sitio RGD. Por otro lado, desarrollamos una serie de aproximaciones *in vivo* e *in vitro* usando los ratones mutantes con el sitio sinérgico inactivo ($Fn1^{syn/syn}$), diferentes líneas de fibroblastos de ratón y FN mutante sinérgica (FN^{syn}) purificada del plasma de los ratones.

OBJETIVOS:

El objetivo de esta tesis fue estudiar la función de la interacción de las integrinas con su principal sitio de unión en la FN, el motivo RGD, localizado en la 10ª repetición tipo III

($FNIII_{10}$), desde diferentes perspectivas. Por un lado, estudiar el papel de la interacción RGD-integrina en la fibrilogénesis. Por otro lado, definir la función del denominado sitio sinérgico *in vivo*, que coopera con el sitio RGD en la unión de integrinas. Los objetivos concretos que nos propusimos fueron los siguientes:

a) Análisis de los requisitos mínimos para una fibrilogénesis de FN
   - Ensamblaje de fibronectina en fibroblastos que carecen del sitio RGD (*Fn1*$^{\Delta RGD/\ \Delta RGD}$)
   - Influencia de la activación de integrinas mediante diferentes sustratos: laminina, vitronectina, colágeno o gelatina
   - Contribución de los receptores sindecanos en el ensamblaje de FN sin el sitio RGD
b) Estudio de la función del sitio sinérgico *in vivo* e *in vitro*
   - Análisis de los ratones *Fn1*$^{syn/syn}$ para discernir si el sitio sinérgico es importante durante el desarrollo embrionario y para la homeostasis de los tejidos.
   - Investigar las implicaciones del sitio sinérgico de la FN en la hemostasia y en la función plaquetaria
   - Estudio de la fuerza del enlace entre α5β1 y FN en ausencia de adhesión al sitio sinérgico, así como su capacidad de soportar fuerzas laminares o formar adhesiones focales maduras
   - Evaluar posibles efectos compensatorios por las integrinas αvβ3 *in vitro* usando una línea celular que carece o expresa únicamente las integrinas del tipo αv, e *in vivo* generando los ratones doble mutantes *Fn1*$^{syn/syn}$*; Itgb3*$^{-/-}$.

METODOLOGÍA

1. Animales de experimentación

Los animales utilizados durante esta tesis se mantuvieron en un fondo genético mixto C57BL/6 x 129/Sv. Todo el trabajo realizado con ratones se hizo de acuerdo con la normativa del Gobierno de la Generalitat Valenciana (referencia de permiso A1327395471346) y con la normativa del Gobierno de Bavaria (Alemania). Los ratones se genotiparon mediante extracción de DNA de biopsia de la oreja o cola y PCR.

-La cepa *Fn1*^{syn}: se mantuvo en heterocigosis (*Fn1*$^{+/syn}$) u homocigosis (*Fn1*$^{syn/syn}$). Se realizaron cruces entre heterocigotos para obtener animales para experimentación que se sacrificaron a los 3 meses, y cruces entre homocigotos para la extracción de sangre y plasma.

-Cepa *Fn1*$^{syn/+}$*; Itgb3*$^{+/-}$: se generó cruzando las cepas *Fn1*$^{+/syn}$ y *Itgb3*$^{+/-}$ entre sí. Para analizar la viabilidad se entrecruzaron *Fn1*$^{syn/+}$*; Itgb3*$^{+/-}$x *Fn1*$^{syn/+}$*; Itgb3*$^{+/-}$ o *Fn1*$^{syn/syn}$*; Itgb3*$^{+/-}$ x *Fn1*$^{syn/syn}$*; Itgb3*$^{+/-}$, y se planificaron cesáreas a diferentes días del desarrollo embrionario entre E11.5 y E18.5.

2. Líneas celulares

Se emplearon las siguientes líneas de fibroblastos aisladas de embriones de ratón: *Fn1*$^{\Delta RGD/\Delta RGD}$, *Fn1*$^{WT/WT}$, *Fn1*$^{RGE/RGE}$, que expresan diferentes formas de FN; *Fn1*-KO que no expresa FN; pKO-β1, pKO-αv y pKO-β1/αv que expresan diferentes integrinas. También se usó la línea celular HT1080 de procedencia humana.

Las células se mantuvieron en medio DMEM con 10% de FCS y 1% de penicilina-estreptomicina. En los experimentos las células se cultivaron en DMEM con 1% de FCS sin FN, 9% de SRM y 1% de penicilina-estreptomicina. En los experimentos se prescindió de suero. Para el ensamblaje de matriz, los fibroblastos *Fn1*$^{\Delta RGD/\Delta RGD}$, *Fn1*$^{WT/WT}$, *Fn1*$^{RGE/RGE}$ se sembraron en SRM, y en los análisis de adhesión con *Fn1*-KO, pKO o HT1080 se empleó DMEM, ambos medios sin suero.

Los niveles de integrinas en la superficie de las células de origen murino se analizaron mediante citometría de flujo.

3. Silenciamiento génico con RNA de interferencia

Para bloquear la traducción de sindecanos, se empleó siRNA prediseñado de Dharmacon (SMARTpool, Dharmacon) contra sindecano 1 y 4. El siRNA (150 µM) se transfectó a las células con ayuda de lipofectamina 3000 (Invitrogen) y Optimem, siguiendo las instrucciones del fabricante. La reducción de los niveles de sindecanos se consiguió tras 96 h.

4. Inmunocitoquímica

Con el fin de analizar la formación de la matriz de fibronectina y las adhesiones focales, las células se sembraron sobre cristales recubiertos con proteínas de la MEC. Para el estudio de fibrilogénesis se empleó laminina, vitronectina, colágeno o gelatina. Para analizar las adhesiones focales se recubrieron los cristales con FN purificada del plasma de ratón. Tras el periodo de incubación establecido, las células se fijaron con 4% PFA (10 min), se permeabilizaron con 0.1% Triton-x100 en PBS (10 min) y se bloquearon con 3% de BSA en PBS (1 h). Posteriormente se incubaron con las diluciones de anticuerpos correspondientes en solución de bloqueo (anti-FN, paxilina o integrina β1) durante toda la noche a 4°C. Tras tres lavados en PBS, las células se incubaron con los anticuerpos secundarios y faloidina (detecta actina) marcados con determinados fluoróforos durante 1 h a temperatura ambiente, se lavaron e incubaron 10 min con DAPI para marcar los núcleos. Finalmente, las muestras se montaron con un medio de montaje para fluorescencia (elvanol). El análisis se llevó a cabo usando un microscopio confocal Zeiss LSM 780, y las imágenes se procesaron con ImageJ.

5. Detección de proteínas por Western blot

Los niveles de FN fibrilar, sindecanos, RhoA activa o FAK fosforilada se detectaron mediante western blot. Para ello las células se cultivaron un periodo de tiempo en adhesión y se lisaron con tampón RIPA o similar, conteniendo detergentes e inhibidores de proteasas y fosfatasas.

La FN fibrilar se detectó lisando las células adheridas a laminina con un tampón de alta (2%) concentración en deoxicolato de sodio. El deoxicolato de sodio hace precipitar las proteínas fibrilares permitiendo separar así la FN soluble de la fibrilar.

Los niveles de RhoA activo (unido a GTP) se analizaron por inmunoprecipitación de RhoA unido a GTP. Empleando una fracción de proteína que reconoce RhoA-GTP unida a GST, se separó RhoA activo del resto de proteínas del lisado, pudiéndola diferenciar de la proteína en su estado inactivo.

La concentración de proteínas se midió con el método de Pierce BCA (Thermofisher) siguiendo las instrucciones del fabricante para usar la misma cantidad proteína en el

western blot. Los lisados se incubaron con tampón de Laemmli conteniendo SDS durante 5 min a 95°C previamente y separaron por electroforesis en un gel de SDS-Poliacrilamida. Los geles se transfirieron en fluoruro de polivinilideno (PVDF). Las membranas se bloquearon en 5% de BSA o leche descremada en TBST durante 1 h, y se incubaron en la dilución de anticuerpo primario correspondiente en tampón de bloqueo toda la noche a 4°C. Posteriormente se lavaron con TBST, incubaron 1 h a temperatura ambiente con el anticuerpo secundario marcado con HRP (peroxidasa) diluido en tampón de bloqueo. Después de lavar las membranas, se revelaron con el sustrato quimioluminiscente de la peroxidasa (Immobilon, milipore).

6. Purificación de proteína plasmática

El plasma se extrajo de la sangre de los ratones *Fn1*^{syn} (ref. permiso 2016/VSC/PEA/00215) tras anestesiarlos, empleando EDTA como anticoagulante. El plasma se incubó con gelatina-sefarosa durante toda la noche a 4°C, para aislar la FN por cromatografía de afinidad. La gelatina-sefarosa con la FN unida se empaqueto en una columna, y tras lavados con tampones de tris-base para eliminar proteínas unidas a la columna de forma inespecífica, se eluyó la FN con urea 2M. Las fracciones eluídas de FN se analizaron por electroforesis en gel de SDS-poliacrilamida mediante tinción con azul Coomasie y western blot.

7. Análisis de adhesión

La adhesión de fibroblastos *Fn1*-KO, HT1080 y pKO a la FN^{syn} y FN^{wt} purificada de plasma se realizó de diferentes maneras:

- Adhesión en estático en placa de 96 pocillos: Se recubrieron los pocillos con FN^{syn} o FN^{wt} purificada, y con BSA y polilisina como control, durante una hora y se sembró el mismo número de células de las líneas *Fn1*-KO y pKO. Se dejaron adherir las células durante 2, 3, 5, 15, 30 y 60 min, y se lavaron para soltar todas aquellas células no adheridas. Las células adheridas se fijaron y tiñeron con metanol/cristal violeta toda la noche a 4°C, se lavaron con PBST. La tinción que penetro en las células adheridas y se midió por espectrofotometría a 595 nm de absorbancia.
- Adhesión en condiciones de fuerza laminar: Se recubrieron cristales con FN^{syn} o FN^{wt} purificada, y se dejaron adherir el mismo número de células *Fn1*-KO o HT1080 durante 1 h. Las células adheridas a los cristales se sumergieron en PBS y se sometieron a una fuerza laminar generada por el movimiento rotatorio de un aparato de *spining disk*. Seguidamente se fijaron con PFA y tiñeron con DAPI. El número de células y su situación en el cristal se contó de manera automatizada, y la aplicación del algoritmo $f = 1/\{1 + exp[b(\tau - \tau_{50}]\}$ permitió el cálculo de la fuerza del enlace.
- Adhesión a sustratos de distintas rigideces: Se emplearon sustratos de poliacrilamida de 0.4, 4 y 50 kPa que se recubrieron con FN^{syn} o FN^{wt}. Se sembró sobre ellos el mismo número de células *Fn1*-KO durante 1 h y se capturaron imágenes cada 15 min de las cuales se midió el número de células adheridas, así como su área. Tras 1 h de adhesión las células se lisaron con RIPA y mediante western blot se detectaron los niveles de fosforilación de FAK en Y397.

8. Histologías

Se realizaron análisis histológicos de secciones de parafina y de *whole mounts,* en ratones adultos y embriones de ratón.

Los ratones adultos se perfundieron con 4% PFA, y los tejidos diseccionados *postmortem* se fijaron con 4% PFA toda la noche a 4°C. Los embriones se fijaron *postmortem* con 4% PFA toda la noche a 4°C. Los tejidos fijados se deshidrataron en una gradación creciente de alcoholes y se embebieron en parafina, que se cortaron en secciones de 8 µm de grosor. Se realizaron tinciones de hematoxilina-eosina tanto en tejido adulto como en embriones. En las secciones de tejido adulto se realizaron inmunohistoquimicas para detectar FN y en las de embrión se detectaron vasos linfáticos (Lyve-1) y eritrocitos (Ter119).

Para preparar *whole mounts* de piezas de tejido de ratón adulto (oreja) y de embrión (piel) o embrión completo, estas se fijaron con solución DENT (20% DMSO, 80% metanol) toda la noche a 4°C y se hidrataron en soluciones decrecientes de metanol diluido en PBST. Los *whole mount* de ratón adulto se tiñeron para observar los vasos sanguíneos con laminina, FN, colágeno IV, marcador de células endoteliales (PECAM) y α-SMA. Los *whole mount* de embrión se tiñeron para detectar vasos linfáticos (Lyve-1), α-SMA, células endoteliales (PECAM), colágeno IV, pericitos (NG2) y eritrocitos (Ter119).

9. Análisis de adhesión y actividad plaquetaria

Para realizar ensayos de adhesión plaquetaria se estudió empleando como sustratos: colágeno, fibrinógeno, FN^{syn} o FN^{wt}. Para ello, se aislaron plaquetas de la sangre de ratones $Fn1^{syn/syn}$ y $Fn1^{+/+}$, y bien se activaron con trombina para estudiar la adhesión en condiciones estáticas o se pasaron por una cámara de flujo para estudiar la adhesión en condiciones de corriente, en la que se trata de mimetizar las condiciones del flujo sanguíneo. En el caso de la adhesión en condiciones estáticas se adquirieron imágenes de las plaquetas a los 15, 30 y 60 min, y se midió el área de las plaquetas adheridas. En el caso de la adhesión en condiciones de corriente las plaquetas se marcaron con un fluorocromo, y tras someterlas a un flujo constante durante 10 min, se observo en un microscopio de fluorescencia el área recubierto por plaquetas.

La actividad plaquetaria se midió en ratones $Fn1^{syn/syn}$ *in vivo* mediante la observación de la formación del agregado plaquetario post-daño vascular con microscopía intravital, en el laboratorio de Prof. C. Reichel.

RESULTADOS:

Capitulo I. Análisis del papel de la adhesión de la integrina al motivo RGD en la fibrilogénesis de FN

Clásicamente se consideraba que la unión de la integrina α5β1 al sitio RGD era el sitio necesario para que se produjera una fibrilogénesis de FN. Sin embargo, pudo comprobarse en ratones que no expresaban α5 que había formación de fibras de FN y otras integrinas αvβ3 y pueden sustituir a α5β1 en el ensamblaje de matrices de FN. Lo mismo se observó en ratones que expresaban FN con la mutación RGD>RGE, lo cual condujo a la hipótesis de que existían otras regiones en la FN que también podían unir integrinas de la clase αv y promover la fibrilogénesis de manera independiente del motivo RGD. De hecho, se llegó a describir una región localizada en el extremo N-terminal de la molécula. Sin embargo, pronto aparecieron

evidencias que demostraban que esa región N-terminal no era accesible en la molécula nativa. Para resolver esta polémica, en mi laboratorio se generaron los ratones que expresan FN que carece de la secuencia RGD ($FN^{\Delta RGD}$). Estos ratones mueren durante el desarrollo temprano, presentando un fenotipo similar a los ratones que no expresan FN ($FN^{-/-}$), lo que indicaba que las integrinas α5β1 y la clase αv no pueden interaccionar con la $FN^{\Delta RGD}$. Sin embargo, al contrario que los ratones $FN^{-/-}$, los ratones *Fn1*$^{\Delta RGD/\Delta RGD}$ ensamblan matrices de FN. Con el fin de esclarecer como tiene lugar el ensamblaje de $FN^{\Delta RGD}$ analizamos la fibrilogénesis de FN realizada por fibroblastos *Fn1*$^{\Delta RGD/\Delta RGD}$ aislados de embriones y la comparamos con el ensamblaje de FN realizado por fibroblastos *Fn1*$^{+/+}$ y *Fn1*$^{RGE/RGE}$. En primer lugar, comprobamos que las células *Fn1*$^{\Delta RGD/\Delta RGD}$ expresaban las integrinas α5β1 y αvβ3 implicadas en la fibrilogénesis y analizamos la actividad del citoesqueleto, medida por la activación de la GTPasa RhoA, que no estaba alterada en dichas células. Además, también analizamos la expresión de otros receptores de FN, los sindecanos, comprobando que las células *Fn1*$^{\Delta RGD/\Delta RGD}$ expresaban sindecanos en niveles superiores a los observados en las otras dos líneas. Para analizar el proceso de fibrilogénesis, las 3 líneas celulares se cultivaron sobre diferentes sustratos (laminina, colágeno, vitronectina o gelatina) durante 24-120 h y observamos la matriz mediante inmunofluorescencia y western blot. En estos ensayos observamos que la matriz ensamblada por los fibroblastos *Fn1*$^{\Delta RGD/\Delta RGD}$ está desorganizada y es menos densa en comparación con la ensamblada por fibroblastos *Fn1*$^{+/+}$ y *Fn1*$^{RGE/RGE}$ sobre todos los sustratos analizados. Mediante western blot confirmamos que la deleción del sitio RGD no impide la fibrilogénesis de FN, pero que las células *Fn1*$^{\Delta RGD/\Delta RGD}$ generaban menos FN fibrilar. También analizamos la cantidad de FN en el medio de cultivo de las células para detectar si la reducción de FN fibrilar en las células *Fn1*$^{\Delta RGD/\Delta RGD}$ era debido a una menor secreción o a la formación de una matriz más soluble, y comprobamos que de hecho había más FN en el medio acondicionado por las células *Fn1*$^{\Delta RGD/\Delta RGD}$. Esto nos indicó que de hecho la reducción de fibras en la matriz $FN^{\Delta RGD}$ se debía a que no toda la FN secretada por las células *Fn1*$^{\Delta RGD/\Delta RGD}$ puede ser incorporada en la matriz insoluble. Dado que las integrinas α5β1 y αvβ3 no podían interaccionar con el sitio RGD en la $FN^{\Delta RGD}$, y que los fibroblastos *Fn1*$^{\Delta RGD/\Delta RGD}$ presentaban niveles superiores de receptores sindecanos, hipotetizamos que la fibrilogénesis de $FN^{\Delta RGD}$ podría tener lugar a través de la región de FN denominada heparina II (repeticiones 12-14ª tipo III), que interacciona con sindecanos. Para comprobar esto, realizamos ensayos de ensamblaje de FN en presencia de heparina. La heparina se une a los sitios de unión a heparina en la FN, bloqueándolos e impidiendo su interacción con otras proteínas. Así, la presencia de heparina durante los ensayos de ensamblaje de matriz bloqueó la fibrilogénesis en las células *Fn1*$^{\Delta RGD/\Delta RGD}$, mientras que no altero la fibrilogénesis realizada por las células *Fn1*$^{+/+}$ y *Fn1*$^{RGE/RGE}$. Este resultado nos sugirió que la fibrilogénesis en $FN^{\Delta RGD}$ tiene lugar mediante los sitios heparina, probablemente por su unión a sindecanos. Igualmente, para descartar un papel de las integrinas en la fibrilogénesis de la $FN^{\Delta RGD}$, realizamos experimentos de ensamblaje usando $MnCl_2$ como activador de integrinas. No observamos un aumento en la cantidad de fibras ni en su organización en la matriz de $FN^{\Delta RGD}$ tras el tratamiento con $MnCl_2$, pero Mn^{+2} sí que incrementó la densidad de matriz generada por las células *Fn1*$^{+/+}$ y *Fn1*$^{RGE/RGE}$. Estos experimentos nos permitieron constatar que las integrinas no están implicadas en la formación de una matriz $FN^{\Delta RGD}$ ya que su activación en las células *Fn1*$^{\Delta RGD/\Delta RGD}$ no mejora o incrementa la

formación de matriz de $FN^{\Delta RGD}$. Para esclarecer el mecanismo detrás del proceso de fibrilogénesis de $FN^{\Delta RGD}$, inhibimos la expresión de sindecanos en las células *Fn1*$^{\Delta RGD/\Delta RGD}$ mediante ARN de interferencia (siRNA). El siRNA redujo específicamente los niveles de sindecanos entre el 30-70% en los fibroblastos *Fn1*$^{\Delta RGD/\Delta RGD}$, e impidió la fibrilogénesis. Esto confirmó que la fibrilogénesis de $FN^{\Delta RGD}$ tiene lugar por la unión de receptores celulares distintos de las integrinas: la familia de proteoglicanos de heparansulfato denominada sindecan. Estos sindecanos se unen a la región de FN denominada heparina II (repeticiones 12-14ª tipo III). Sin embargo, el hecho de que la matriz fibrilar de $FN^{\Delta RGD}$ no esté bien estructurada indica que el motivo RGD es crítico para este proceso.

Capítulo II. Estudio de la función del sitio sinérgico

Aunque la secuencia RGD en el dominio $FNIII_{10}$ es esencial para la unión de integrinas, experimentos de adhesión *in vitro* habían demostrado que la secuencia del sitio sinérgico (DRVPPSRN en ratones) localizado en el módulo adyacente al RGD cooperaba en la adhesión de α5β1 y αIIbβ3. La secuencia sinérgica no tiene actividad adhesiva por sí misma, pero aumenta unas 100 veces la adhesión celular a FN mediante α5β1, a diferencia de las integrinas que contienen αv que se unen de manera independiente del sitio sinérgico. Con el objetivo de analizar el papel del sitio de sinérgico *in vivo*, en este proyecto analizamos una cepa de ratón en la que las dos argininas de la secuencia DRVPPSRN se sustituyeron por alaninas. Esperábamos que las mutaciones afectasen a las funciones α5β1 y αIIbβ3, sin modificar las funciones αv. Concretamente, se ha demostrado que la integrina α5β1 se expresa principalmente en células mesenquimales y su interacción con FN es esencial durante el desarrollo. A su vez, la integrina αIIbβ3 solo se expresa en plaquetas, junto con α5β1, e interactúa con la FN plasmática durante la formación del coágulo sanguíneo. Pese a que estaba demostrado que el sitio de sinérgico era esencial para el desarrollo de *Xenopus*, nosotros pudimos constatar que la inactivación del sitio sinérgico no afectaba al desarrollo del ratón, ni a la homeostasis de sus tejidos. Para confirmarlo realizamos un análisis histológico del corazón, hígado, pulmón y riñón en los ratones adultos (3 meses), tiñéndolos con hematoxilina-eosina e inmunohistoquímicas de FN. Ambas aproximaciones mostraron que no hay diferencias morfológicas ni en la deposición de la matriz de FN en los tejidos de los ratones *Fn1*$^{syn/syn}$ en comparación con los ratones *Fn1*$^{+/+}$. Además, para descartar cualquier problema en vasos sanguíneos analizamos por inmunocitoquímicas de células endoteliales (PECAM), eritrocitos (Ter119) y proteínas de membrana basal (laminina, FN y colágeno) con *whole mounts* de oreja de ratones *Fn1*$^{syn/syn}$ y *Fn1*$^{+/+}$, que mostraron que presentan una morfología similar y no hay pérdidas de sangre ya que no había filtración de eritrocitos fuera de los vasos. Sin embargo, mediante microscopía intravital observamos que los ratones con la mutación en el sitio sinérgico (*Fn1*$^{syn/syn}$) tienen hemorragias prolongadas tras lesiones vasculares, lo que indica que la interacción plaquetas-FN está alterada. Mediante diferentes ensayos de adhesión y ensamblaje de matriz pudimos demostrar que el sitio sinérgico no es esencial para la adhesión celular o la fibrilogénesis de FN, pero es importante para fortalecer la unión a FN cuando la asociación FN-integrina está muy tensionada, por ejemplo, debido a fuerzas de laminación. Así, el refuerzo de enlace vía el sitio sinérgico permite la transmisión de señales más intensas corriente abajo, como es el grado de fosforilación de la tirosina 397 en FAK, y el ensamblaje de

mayore adhesiones focales. El refuerzo del enlace integrina-FN a través del sitio de sinérgico también modula la adaptación celular a diferentes rigideces. En nuestro estudio corroboramos que todos estos procesos se ven mermados por la falta el sitio sinérgico. Además, nos planteamos que la falta de defectos durante el desarrollo en los ratones *Fn1*$^{syn/syn}$ posiblemente se debía a un efecto compensador producido por integrinas αv. Por otra parte, el fibrinógeno, una proteína plasmática que se une a la integrina αIIbβ3, además de la FN, también podía compensar la ausencia del sitio sinérgico en la adhesión plaquetaria. La compensación de la inactivación del sitio sinérgico la demostramos, tanto en cultivos celulares como *in vivo*. En cultivos celulares utilizamos fibroblastos genéticamente modificados que solo expresan un tipo de integrinas: α5β1 o integrinas de la clase αv. Para demostrarlo *in vivo* cruzamos los ratones *Fn1*$^{syn/syn}$ con ratones deficientes para la integrina β3 (*Itgb3*$^{-/-}$) que, por lo tanto, no expresan integrinas αvβ3 y αIIbβ3, generando la cepa *Fn1*$^{syn/syn}$; *Itgb3*$^{-/-}$. *In vitro* observamos que las células que carecen de las integrinas αv no forman adhesiones focales sobre la FN con el sitio sinérgico inactivo. En el caso de los ratones *Fn1*$^{syn/syn}$;*Itgb3*$^{-/-}$ demostramos que mueren durante el desarrollo, a E15.5 y mostraban múltiples hemorragias cutáneas y edema. Mediante un análisis histológico exhaustivo de los embriones *Fn1*$^{syn/syn}$; *Itgb3*$^{-/-}$, empleando tinciones de *whole mount* y secciones en parafina, demostramos que sus vasos sanguíneos son inestables y se retraen, y que el desarrollo de los vasos linfáticos es defectuoso. Dado que la separación de los vasos linfáticos comienza tras la formación de un agregado plaquetario en la vena cardinal, hipotetizamos que la falta de agregación plaquetaria en los embriones *Fn1*$^{syn/syn}$;*Itgb3*$^{-/-}$ era la causa de un mal desarrollo de los vasos linfáticos. Para comprobar nuestra hipótesis aislamos plaquetas *Itgb3*$^{-/-}$ e *Itgb3*$^{+/+}$ para estudiar su adhesión a FN^{syn} y FN^{wt}. Los ensayos de adhesión plaquetaria demostraron que en efecto, las plaquetas *Itgb3*$^{-/-}$ no se unen a la FN^{syn} en condiciones estáticas, y ni las plaquetas *Itgb3*$^{-/-}$ ni las *Itgb3*$^{+/+}$ se adhieren a la FN^{syn} en condiciones de flujo, indicando que el sitio sinérgico de la FN es necesario para mantener las plaquetas unidas durante la agregación plaquetaria, aunque la interacción αIIbβ3-Fibrina puede compensar la falta de función del sitio sinérgico.

En conjunto, los datos presentados en este estudio demuestran que el motivo RGD es necesario y el único sitio de adhesión de integrinas α5β1 y αv a la FN, y que sitio sinérgico de la FN refuerza la adhesión de integrinas α5β1 y αIIbβ3 a FN cuando la unión está sometida a fuerzas o tensión, como las fuerzas del citoesqueleto o el constante flujo sanguíneo. Finalmente, demostramos que las integrinas de clase αv y el fibrinógeno pueden compensar la ausencia de sitio sinérgico en células de origen mesenquimal y en el plasma respectivamente.

CONCLUSIONES:

En este trabajo se han analizado los dos principales sitios de unión a la integrina α5β1 en la FN, los motivos RGD y sinérgico, con diferentes objetivos y aproximaciones. En el estudio del sitio RGD nos hemos centrado en el proceso de fibrilogénesis. Para el sitio sinérgico hemos resulto su función *in vivo.* Demostramos con fibroblastos en cultivo que la eliminación de la secuencia RGD no elimina la fibrilogénesis de FN, aunque las fibras de FN$^{\Delta RGD}$ presentan una

morfología diferente que FN^{wt}, lo que sugiere que el motivo RGD es esencial para una matriz de FN bien estructurada.

1. El proceso de fibrilogénesis $FN^{\Delta RGD}$ se produce después de la participación de los sitios de heparina FN por los receptores sindecanos.
2. La mutación R> A de la secuencia del sitio sinérgico de la FN no afecta el desarrollo del ratón ni la homeostasis de los tejidos en adultos.
3. Los ratones que expresan la FN con sitio sinérgico mutante tienen tiempos de sangrado prolongados y la formación de trombos es retardada cuando se induce una lesión vascular, en comparación con ratones de tipo salvaje, lo que indica un defecto en la función plaquetaria. Los experimentos de cámara de flujo confirman que, aunque en condiciones estáticas, las plaquetas se pueden unir a FN^{syn}, bajo condiciones de corriente de flujo se suprime su adhesión a FN^{syn}.
4. Las células se adhieren a la proteína FN^{syn} y pueden ensamblar fibras de FN normales, sin embargo, la maduración de adhesiones nacientes a adhesiones focales se retrasa sobre FN^{syn}.
5. El reforzamiento del enlace α5β1-FN es menor tras la aplicación de fuerzas y las células forman enlaces tipo *catch bond* significativamente menores entre la integrina α5β1 y la FN^{syn} mutada. Este efecto se observa en diferentes líneas celulares de ratón (*Fn1*-KO) y humano (HT1080).
6. La fosforilación de FAK en la tirosina 397, un marcador de la tensión de la integrina α5β1, se reduce en las células adheridas a las superficies recubiertas con FN^{syn} y no se ve alterada por la rigidez del sustrato.
7. El fenotipo de los ratones $Fn1^{syn/syn}$ se vuelve letal embrionario cuando se anula la expresión de las integrinas β3, señalando los efectos compensatorios por la integrina αvβ3 y por la proteína plasmática fibrinógeno.
8. En células en cultivo, la expresión de la integrina αvβ3 permite la buena adhesión y extención celular, la formación de fibras de estrés y el ensamblaje FA en superficies revestidas con FN^{syn}.
9. En el embrión, la falta de expresión de αvβ3 junto con la inactivación del sitio sinérgico deteriora la estabilidad de los vasos sanguíneos, causada por una adhesión alterada de las células mural y endoteliales a su MEC.
10. En las plaquetas, la falta de función del sitio sinérgico está parcialmente compensada por el fibrinógeno que se une a las integrinas αIIbβ3. Esto se evidencia en los ratones dobles mutantes $Fn1^{syn/syn}$;$Itgb3^{-/-}$ que muestran la falta de separación entre los vasos linfáticos y sanguíneos, un defecto del desarrollo causado por deficiencias graves en la adhesión de las plaquetas.
11. En conjunto, nuestros resultados indican que el sitio sinérgico es importante para reforzar el enlace integrina-FN en situaciones de estrés y que las integrinas que contienen la subunidad αv pueden compensar parcialmente su ausencia.

eLIFE elifesciences.org

RESEARCH ARTICLE

The fibronectin synergy site re-enforces cell adhesion and mediates a crosstalk between integrin classes

Maria Benito-Jardón[1,2], Sarah Klapproth[3], Irene Gimeno-LLuch[1,2], Tobias Petzold[4], Mitasha Bharadwaj[5], Daniel J Müller[5], Gabriele Zuchtriegel[3], Christoph A Reichel[3,6], Mercedes Costell[1,2]*

[1]Department of Biochemistry and Molecular Biology, Universitat de València, Burjassot, Spain; [2]Estructura de Recerca Interdisciplinar en Biotecnologia i Biomedicina, Universitat de València, Burjassot, Spain; [3]Walter Brendel Centre of Experimental Medicine, Ludwig-Maximilians-Universität München, Munich, Germany; [4]Medizinische Klinik und Poliklinik I, Klinikum der Universität München, Munich, Germany; [5]Eidgenössische Technische Hochschule Zürich, Basel, Switzerland; [6]Departement of Otorhinolaryngology, Ludwig-Maximilians-Universität München, Munich, Germany

Abstract Fibronectin (FN), a major extracellular matrix component, enables integrin-mediated cell adhesion *via* binding of $\alpha5\beta1$, $\alpha IIb\beta3$ and αv-class integrins to an RGD-motif. An additional linkage for $\alpha5$ and αIIb is the synergy site located in close proximity to the RGD motif. We report that mice with a dysfunctional FN-synergy motif ($Fn1^{syn/syn}$) suffer from surprisingly mild platelet adhesion and bleeding defects due to delayed thrombus formation after vessel injury. Additional loss of $\beta3$ integrins dramatically aggravates the bleedings and severely compromises smooth muscle cell coverage of the vasculature leading to embryonic lethality. Cell-based studies revealed that the synergy site is dispensable for the initial contact of $\alpha5\beta1$ with the RGD, but essential to re-enforce the binding of $\alpha5\beta1/\alpha IIb\beta3$ to FN. Our findings demonstrate a critical role for the FN synergy site when external forces exceed a certain threshold or when $\alpha v\beta3$ integrin levels decrease below a critical level.

DOI: 10.7554/eLife.22264.001

***For correspondence:** mercedes.costell@uv.es

Competing interests: The authors declare that no competing interests exist.

Funding: See page 21

Received: 11 October 2016
Accepted: 15 January 2017
Published: 16 January 2017

Reviewing editor: Reinhard Fässler, Max Planck Institute of Biochemistry, Germany

Introduction

Fibronectin (FN) is a large extracellular matrix (ECM) glycoprotein that triggers biochemical and mechanical signaling via integrin binding. FN is essential for mammalian development and tissue regeneration, and can influence disease such as cancer progression. FN is abundant in blood and in most tissues and is present in provisional matrices of healing wounds and in the stroma of tumors. FN is secreted as a disulfide-bonded dimer, assembled into fibrils of variable diameters and then crosslinked into a fibrillar network of variable rigidity (***Leiss et al., 2008***) that binds to and serves as a scaffold for numerous other ECM molecules. FN consists of three different repeating Ig-like folded units, called type I-III modules. Whereas type I and II modules are stabilized by internal disulfide bonds, the 15 type III repeats of FN lack disulfide bonds, which confers elasticity to FN fibrils and the ability to modulate fibril rigidity (***Erickson, 1994***; ***Oberhauser et al., 2002***). The major cell-binding site in FN is an arginine-glycine-aspartate (RGD) motif located in the 10^{th} type III module (FNIII10) that is recognized by $\alpha5\beta1$, $\alpha IIb\beta3$, and αv-class integrins. In addition to the RGD motif, FN harbors the so-called FN synergy site in the FNIII9 module (***Obara et al., 1988***), which binds $\alpha5\beta1$

and αIIbβ3 integrins but not αv-class integrins (**Bowditch et al., 1994**). The synergy site encompasses the DRVPHSRN sequence in mouse FN and site directed mutagenesis identified the two arginine residues to be essential for all synergy site-induced functions (**Aota et al., 1994**; **Friedland et al., 2009**; **Chada et al., 2006**; **Nagae et al., 2012**).

In vitro studies have shown that the synergy site increases cell spreading (**Aota et al., 1991**), FN fibril assembly (**Sechler et al., 1997**) and platelet adhesion to FN (**Chada et al., 2006**). Based on the crystal structures, the RGD motif forms a flexible loop that physically interacts with both the α5 and β1 integrin subunits, while the synergy site contacts only the head domain of the α subunit (**Redick et al., 2000**; **Nagae et al., 2012**). The synergy site has been studied using protein- and cell-based assays, which produced different results giving rise to diverse hypotheses regarding the mechanistic properties. One hypothesis based on ultra-structural analyses of the recombinant α5β1 ectodomain and the FNIII7-10 polypeptide proposes that the synergy site aligns the binding interface of the integrin heterodimer with the RGD motif to increase the on-rate constant (K_{on}) of α5β1 binding to FN (**Leahy et al., 1996**; **García et al., 2002**; **Takagi et al., 2003**). A combination of theoretical and cell-based studies with FRET sensors inserted into the linker region between FNIII9 and FNIII10 concluded that cell-induced forces reversibly stretch the linker, separate the FN-RGD motif from the synergy site and switch the binding of α5β1 integrins to αv-class integrins (**Grant et al., 1997**; **Krammer et al., 2002**). Finally, using a spinning disk device, it was shown that the engagement of the synergy site allows FN-α5β1 bonds (or FN-αIIbβ3 bonds on platelets) to resist shear forces, suggesting that force exposure allows to switch the bonds from a relaxed to a tensioned state, leading to an extension of the FN-integrin bond lifetime and to adhesion strengthening (**Friedland et al., 2009**). Although these in vitro studies highlight the importance of α5β1 and αIIbβ3 integrin-binding to the synergy site, the mode of action is still unclear and the apparently important roles of these interactions have never been scrutinized in vivo using genetic loss-of-function approaches.

We decided to directly test the role of the synergy site in vivo by substituting critical residues of the FN-synergy site in mice. We report that mice carrying a homozygous inactivating mutation in the fibronectin gene (*Fn1*)-synergy site ($Fn1^{syn/syn}$) are viable, fertile, show no overt organ defects, however, display a mild bleeding tendency and delayed thrombus formation after vessel injury. The lethal intercrosses of $Fn1^{syn/syn}$ mice with β3 integrin (*Itgb3*)-deficient mice and in vitro assays with purified FN^{syn} isolated from the blood of $Fn1^{syn/syn}$ mice revealed three important findings: (i) the synergy site does not influence the K_{on} of α5β1 integrin binding to FN-RGD, (ii) the synergy site strengthens α5β1/αIIbβ3 integrin binding to FN upon application of external force such as blood flow or internal force such as actomyosin pulling forces, and (iii) during force-induced adhesion strengthening the synergy site binding to α5β1 and αv-class integrin binding to FN compensate each other, at least in part, up to a certain force threshold.

Results

Normal development and prolonged trauma-induced bleeding in $Fn1^{syn/syn}$ mice

To directly test the in vivo role(s) of the FN synergy site, we generated the $Fn1^{syn}$ allele by substituting the two arginines (R_{1374} and R_{1379}) of the synergy motif (DRVPPSRN) in the FN-III9 module with alanines (A) (**Figure 1A** and **Figure 1—figure supplement 1A–C**). Intercrossing of heterozygous mice ($Fn1^{+/syn}$), which showed no apparent phenotype, gave rise to homozygous offspring ($Fn1^{syn/syn}$) with a normal Mendelian ratio before and after weaning. $Fn1^{syn/syn}$ mice were fertile, had normal size and weight, and aged normally. The morphology, ultrastructure, and FN distribution in heart (**Figure 1B**), liver, kidney, and lung (**Figure 1—figure supplement 1D**) were indistinguishable between $Fn1^{syn/syn}$ and control littermates. Blood vessel organization in whole mount ear samples analyzed by anti-PECAM-1 and anti-αSMA immunostainings revealed no abnormalities (**Figure 1C**), and the subendothelial matrix visualized with antibodies to laminin-1, collagen IV and FN, was also normally organized in $Fn1^{syn/syn}$ mice (**Figure 1—figure supplement 1E**). Altogether, these data indicate that the FN synergy site is dispensable for development and postnatal homeostasis.

Soluble plasma (p) FN is required for the stability of blood clots (**Ni et al., 2003b**). Therefore, we performed several experiments to test whether platelets require the synergy site to firmly bind FN

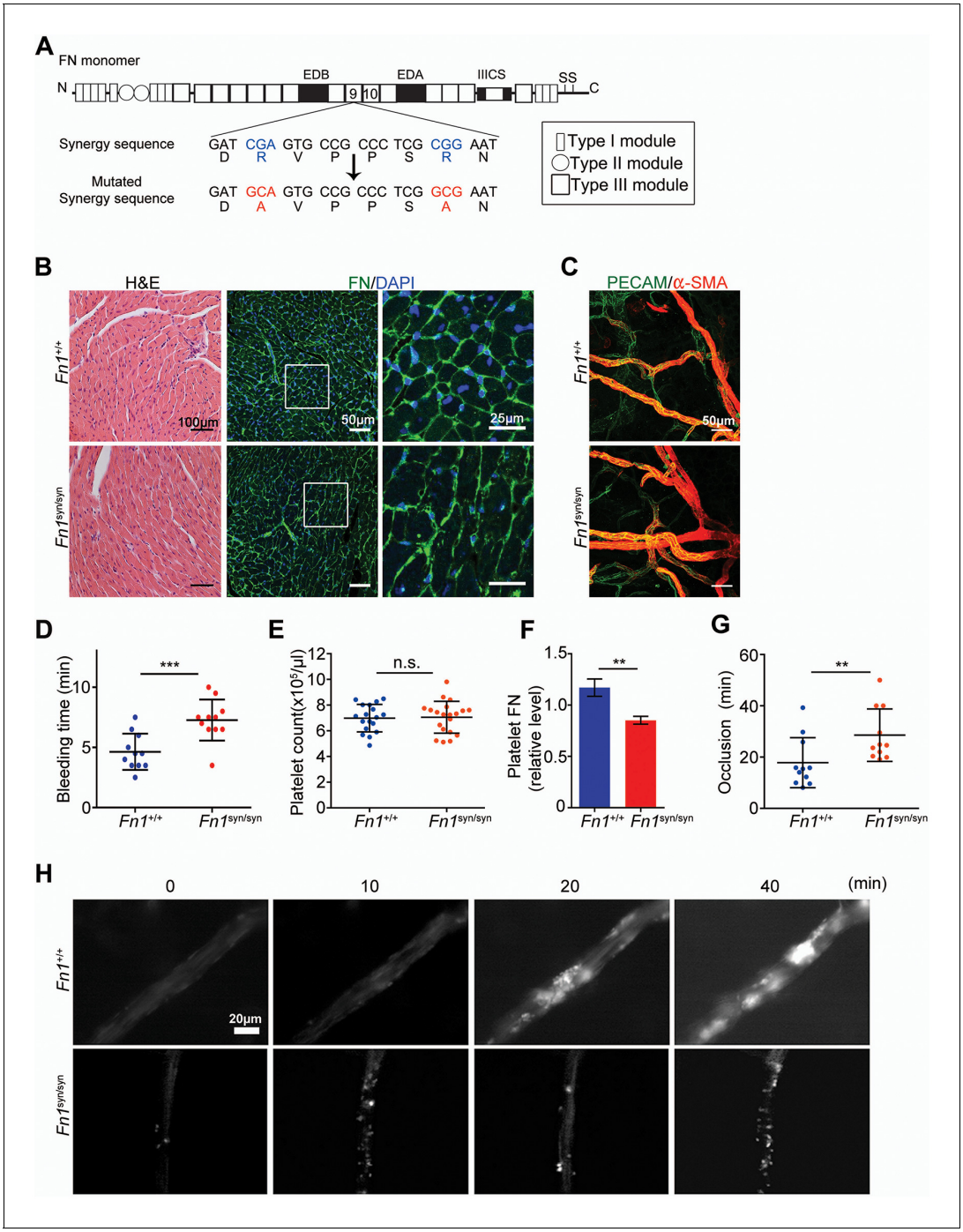

Figure 1. Normal tissue development and prolonged bleeding in *Fn1*$^{syn/syn}$ mice. (**A**) Cartoon of FN and the nucleotide point mutations disrupting the function of the synergy site. (**B**) Representative images of 3-months-old *Fn1* $^{+/+}$ and *Fn1*$^{syn/syn}$ heart sections stained with **H** and **E** and immunostained for FN. (**C**) Confocal images of ear whole-mounts from 3 months-old mice immunostained with anti-PECAM-1 and anti-αSMA to visualize the dermal endothelial cell tubes and smooth muscle cells. (**D**) Bleeding time of 3-months-old *Fn1*$^{+/+}$ (n = 11) and *Fn1*$^{syn/syn}$ (n = 11) mice. (**E**) Platelet counts in blood samples of *Fn1*$^{+/+}$ (n = 18) and *Fn1*$^{syn/syn}$ (n = 19) mice. (**F**) FN content in platelets derived from *Fn1*$^{+/+}$ (n = 6) and *Fn1*$^{syn/syn}$ (n = 6) mice relative to their vinculin levels. (**G**) Occlusion time of injured arterioles in the cremaster muscle of 3-months-old *Fn1*$^{+/+}$ (n = 11) and *Fn1*$^{syn/syn}$ (n = 11) mice. (**H**) Representative still images of the arteriolar occlusion (white:platelets). Values are shown as mean ± SD; statistical significances were calculated using the Student *t*-test; **p<0.01 and ***p<0.001.

DOI: 10.7554/eLife.22264.002

The following figure supplements are available for figure 1:

Figure supplement 1. Strategy used to generate the *Fn1*$^{syn/syn}$ mice and tissue and platelet analysis.

Figure 1 continued on next page

Figure 1 continued

DOI: 10.7554/eLife.22264.003

Figure supplement 2. FN levels in platelets and blood from *Fn1*$^{syn/syn}$ mice and platelet aggregation assays.

DOI: 10.7554/eLife.22264.004

via their αIIbβ3 and α5β1 integrins. We measured tail bleeding time after tail biopsy (***Figure 1D***) and found a significant increase from 4.64 ± 1.50 min (mean ± SD) in *Fn1*$^{+/+}$ mice to 7.27 ± 1.71 min in *Fn1*$^{syn/syn}$ mice ($p<0.001$). Importantly, blood platelet counts were normal in *Fn1*$^{syn/syn}$ mice (***Figure 1E***). Since αIIbβ3 integrins mediate the uptake of pFN into platelet α-granules (***Ni et al., 2003a***), we performed Western-blotting with lysates from washed platelets and found that the FN content was significantly reduced to 70% in platelets from *Fn1*$^{syn/syn}$ mice (***Figure 1F*** and ***Figure 1—figure supplement 2A***), while the levels of pFN were similar in *Fn1*$^{+/+}$ (318.7 ± 24.1 µg/ml) and *Fn1*$^{syn/syn}$ (316.1 ± 31.0 µg/ml) mice (***Figure 1—figure supplement 2B***).

Importantly, plasma levels of fibrinogen were also similar in *Fn1*$^{+/+}$ (2.10 ± 0.17 mg/ml) and *Fn1*$^{syn/syn}$ (2.08 ± 0.07 mg/ml) mice. In vitro aggregation of washed platelets, induced with either collagen I, thrombin or ADP, triggered normal shape changes and aggregations (***Figure 1—figure supplement 2C–E***). To quantitatively study the velocity of thrombus formation in vivo, thrombi induction was measured in the arterioles of the cremaster muscle upon vessel injury. The experiments revealed a small delay in the onset of thrombus formation in the *Fn1*$^{syn/syn}$ mice (10.29 ± 9.04 min) that, however, was not significantly different compared to the *Fn1*$^{+/+}$ littermates (5.13 ± 3.89 min). In contrast, the time required for arteriole occlusion was significantly increased in *Fn1*$^{syn/syn}$ mice (28.56 ± 10.24 min) compared to *Fn1*$^{+/+}$ mice (17.82 ± 9.74 min) (***Figure 1G***). Notably, in 3 out of 11 *Fn1*$^{syn/syn}$ mice no total occlusion was observed after 40 min (***Figure 1H***), a defect that was never observed in control mice.

These results demonstrate that the synergy site is dispensable for development and postnatal homeostasis but is required to stabilize platelet clots in vivo and to prevent prolonged bleeding times.

Fibroblasts delay their focal adhesion maturation on FN^{syn}

The assembly of FN into a fibrillar network depends on α5β1 binding to FN (***Fogerty et al., 1990***). To test whether FN assembly proceeds normally in the absence of the synergy site, we incubated FN-deficient (*Fn1*-KO) fibroblasts that express high levels of α5, αv, β1 and β3 integrins on their cell surface (***Figure 2—figure supplement 1A***) with blood plasma derived from either *Fn1*$^{+/+}$ or *Fn1*$^{syn/syn}$ mice. In line with our immunostaining of FN in tissues from *Fn1*$^{syn/syn}$ mice, *Fn1*-KO cells assembled fibrillar FN networks of indistinguishable complexity, fibril diameter and length with plasma from *Fn1*$^{syn/syn}$ and *Fn1*$^{+/+}$ mice, respectively (***Figure 2A***).

Next, we coated glass coverslips with plasma FN (pFN) purified from *Fn1*$^{+/+}$ or *Fn1*$^{syn/syn}$ mice (***Figure 2—figure supplement 1B–E***), seeded *Fn1*-KO fibroblasts and measured adhesion and spreading (***Figure 2B–E***). Adhesion of *Fn1*-KO cells to pFN^{wt} and pFN^{syn} began around 3 min after cell seeding and increased with time without noticeable differences (***Figure 2—figure supplement 1F***). While the formation of nascent adhesions (NAs) was similar on pFN^{wt} and pFN^{syn} (***Figure 2B***), the numbers as well as percentage of paxillin-positive focal adhesions (FAs) linked to stress fibers were significantly reduced in *Fn1*-KO fibroblasts seeded for 30 min on pFN^{syn} (***Figure 2D,E***) indicating that the transition from NAs to mature, stress fiber-anchored FAs is delayed on pFN^{syn}. Furthermore, cell spreading determined as cell area at different time points after cell seeding onto pFN^{syn}-coated substrates was also delayed in the first 30 min (***Figure 2C***). Time-lapse video microscopy confirmed the delayed cell spreading on pFN^{syn} and revealed unstable adhesions consisting of several cycles of binding and release from the substrate (see ***Video 1***, ***Video 2*** and still images in ***Figure 2—figure supplement 2***).

These findings indicate that the synergy site is dispensable for FN fibril formation but promotes the transition from NAs to FAs.

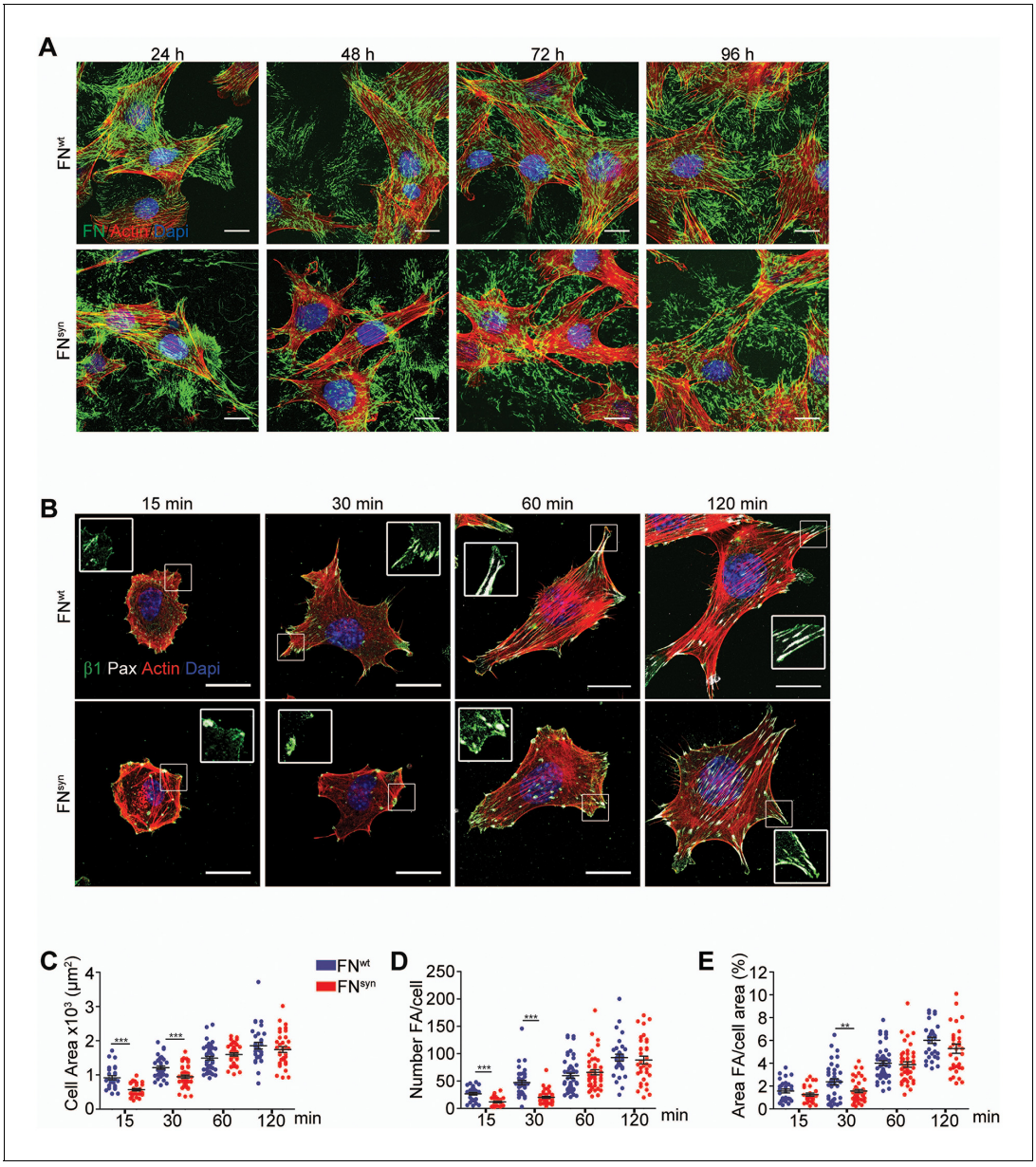

Figure 2. The FN synergy site is dispensable for FN fibrillogenesis, cell adhesion and spreading. (**A**) *Fn1*-Knock-Out (*Fn1*-KO) fibroblasts grown in 1% plasma derived from either $Fn1^{+/+}$ or $Fn1^{syn/syn}$ mice, fixed at the indicated times and stained for FN (green), F-actin stain (with Phalloidin; red) and nuclei (with DAPI; blue). Scale bar, 10 µm. (**B**) *Fn1*-KO cells seeded on pFN^{wt} or pFN^{syn}, fixed at the indicated times and stained for F-actin (red), paxillin (white) and total β1 integrin (green). Scale bar, 20 µm. (**C–E**) Cell size (**C**), number of FAs per cell (**D**) and percentage coverage by FAs (paxillin-positive) (**E**) were quantified (n = 25 cells assessed from three independent experiments; mean ± sem). Statistical significances were calculated using the Student *t*-test; **p<0.01 and ***p<0.001.

DOI: 10.7554/eLife.22264.005

The following figure supplements are available for figure 2:

Figure supplement 1. Integrin surface levels and plasma FN purification and glass coating.

DOI: 10.7554/eLife.22264.006

Figure supplement 2. Captures of life-time microscopy videos of *Fn1*-KO fibroblasts spreading on pFN^{wt} or pFN^{syn}.

DOI: 10.7554/eLife.22264.007

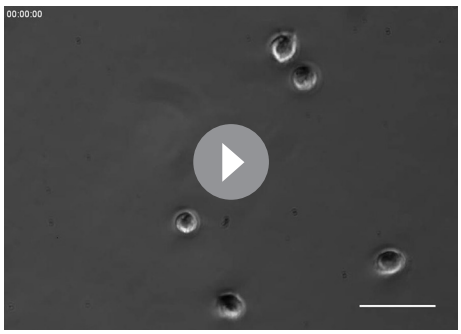

Video 1. Life-time microscopy video of *Fn1*KO fibroblasts on pFN^{wt}.
DOI: 10.7554/eLife.22264.008

The FN synergy site is required to tension FN-α5β1 bonds and to resist shear forces

It has been reported that HT1080 cells seeded on the FNIII7-10 polypeptide, increase adhesion strength to FN upon force application (***Friedland et al., 2009***). Therefore, we next tested whether the force-induced adhesion strengthening is FN-synergy site-dependent when *Fn1*-KO cells adhere to plasma-derived, purified full-length pFN^{syn}. We seeded overnight-starved *Fn1*-KO fibroblasts for 1 hr onto substrates coated with pFN^{wt} or pFN^{syn} and recombinant FNIII7-10^{wt} or FNIII7-10^{syn} polypeptides, respectively, and applied a hydrodynamic shear force with a spinning disk device (***García et al., 1998***). Typically, the number of *Fn1*-KO fibroblasts adhering to pFN^{wt}-coated coverslips and spun for 5 min decreased non-linearly with the applied force and followed a sigmoidal curve (***Figure 3—figure supplement 1***), whose inflection point (τ50) corresponds to the mean shear stress for 50% detachment, and hence to a quantitative measure of adhesion strength. Interestingly, the τ50 values of *Fn1*-KO cells decreased on purified full-length pFN^{syn} by 16% compared to pFN^{wt} (***Figure 3A***), and by 43% on FNIII7-10^{syn} fragment compared to FNIII7-10^{wt}, indicating that cells develop less adhesion strength on the synergy site-deficient pFN and that higher adhesion strengths arise on full-length FN compared to FNIII7-10 fragments.

Simultaneous engagement of the RGD motif and the synergy site was suggested to enable α5β1 and αIIbβ3 integrins to induce tensioned bonds, which form when receptor and ligand are in close proximity and hence, can be chemically cross-linked (***Shi and Boettiger, 2003***). To test the extent of bond tensioning on pFN^{syn}, we seeded (15, 30 and 60 min) serum-starved *Fn1*-KO fibroblasts onto pFN^{wt}- and pFN^{syn}-coated substrates, respectively, spun them and treated them with 3,3'-dithiobis (sulfosuccinimidyl propionate; DTSSP) to crosslink extracellular secondary amines that are within 1.2 nm proximity to each other. We found that the amount of α5 integrins crosslinked to FN in *Fn1*-KO fibroblasts was reduced to 60% on pFN^{syn} (***Figure 3B***). Upon spinning, *Fn1*-KO cells increased the proportion of α5 integrins crosslinked to pFN^{wt}. Importantly, in cells on pFN^{syn}, the tension was unable to increase the number of crosslinked bonds upon spinning and their numbers remained at the same levels as before spinning (***Figure 3B***), which altogether indicates that the spinning force strengthens α5β1-mediated adhesion to FN in a synergy site-dependent manner. Furthermore and in line with a report showing that the conversion of FN-α5β1 bonds from a relaxed to a tensioned state induces phosphorylation of focal adhesion kinase (FAK) on Y397 (***Guan et al., 1991***; ***Kornberg et al., 1992***), pY397-FAK levels were reduced by 54% when cells were plated on pFN^{syn} compared to pFN^{wt} (***Figure 3C***). Importantly, phosphorylation of Y861-FAK, which occurs independent of substrate binding (***Shi and Boettiger, 2003***), was indistinguishable in cells seeded on pFN^{wt} or pFN^{syn} (***Figure 3C***). Since the intensity of FAK Y397 phosphorylation was shown to operate as a sensor for ECM rigidity (***Seong et al., 2013***), we conclude that fibroblasts attached to pFN^{syn} perceive insufficient information regarding substrate stiffness.

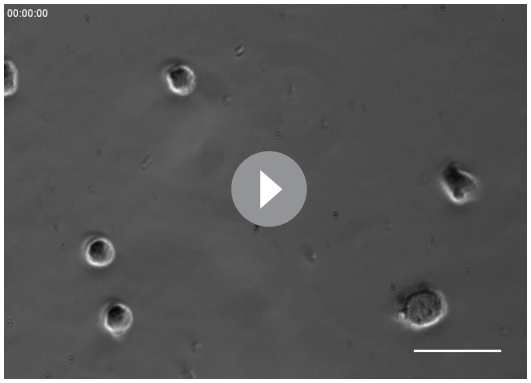

Video 2. Life-time microscopy video of *Fn1*KO fibroblasts on pFN^{syn}.
DOI: 10.7554/eLife.22264.009

αv-class integrins compensate for the absent FN synergy site

Fn1-KO cells express high levels of αv-class integrins (***Figure 2—figure supplement 1G***),

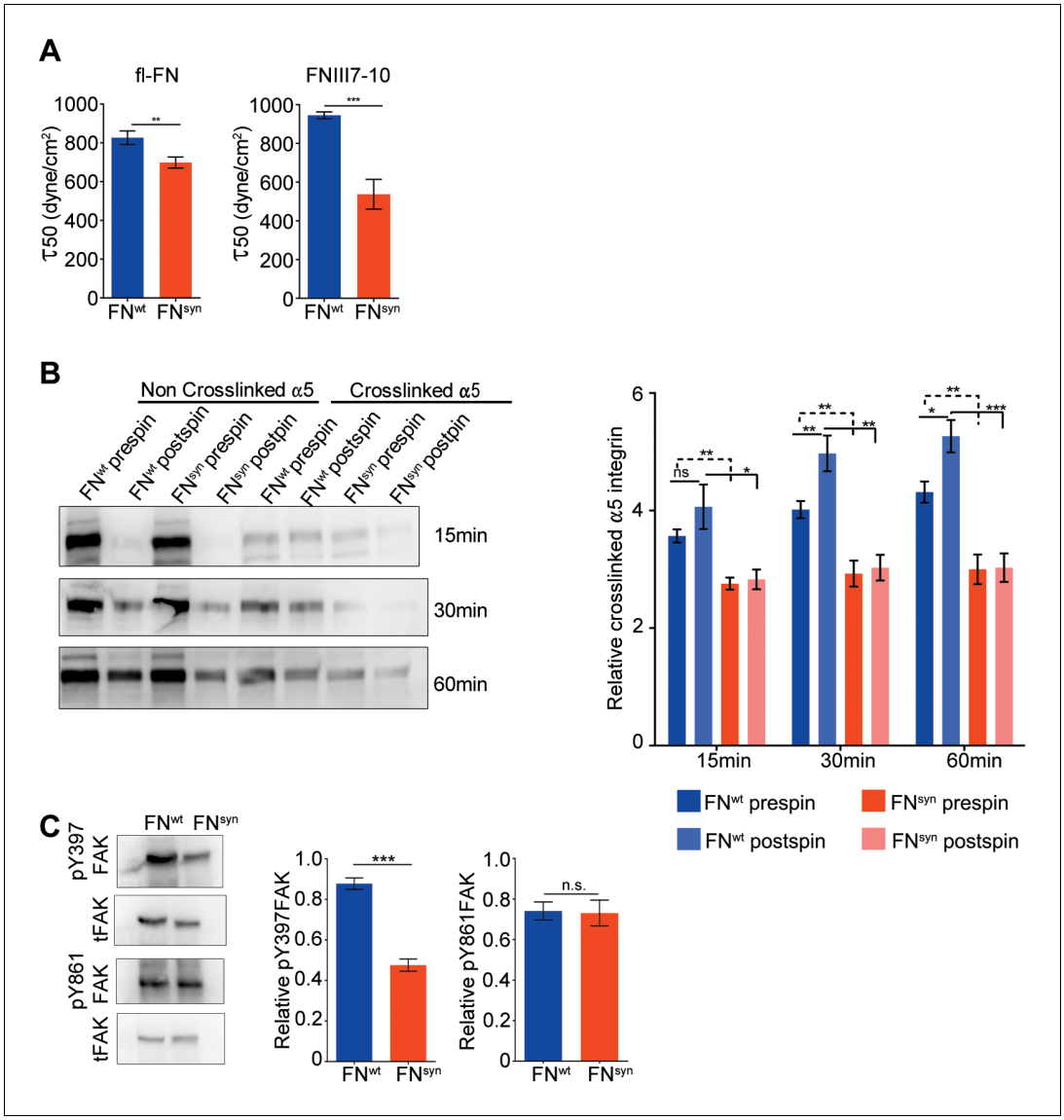

Figure 3. The FN synergy site is required to establish tensioned FN-α5β1 bonds. (**A**) Quantification of adhesion strength. 7×10^5 *Fn1*-KO cells attached onto purified, full-length (fl) pFN^{wt} or pFN^{syn} or FNIII7-10^{wt} or FNIII7-10^{syn} and spun with a spinning disk device (n = 7 independent experiments with fl-FN; n = 3 independent experiments with FNIII7-10; mean ± sem). (**B**) Western-blot analysis (left) and quantification (right) of cross-linked α5 integrins to pFN^{wt} or pFN^{syn} before and after applying shear forces (n = 6 independent experiments; mean ± sem). (**C**) Western-blot analysis (left) and quantification (right) of pY397- and pY861-FAK levels in *Fn1*-KO cells plated on pFN^{wt} or pFN^{syn} (n = 6 independent experiments; mean ± sem). Statistical significances were calculated using the Student *t*-test; *p<0.05, **p<0.01 and ***p<0.001.

DOI: 10.7554/eLife.22264.010

The following figure supplement is available for figure 3:

Figure supplement 1. Representative spinning disk experiment showing the cell distribution profile against the shear force.

DOI: 10.7554/eLife.22264.011

which could, at least in part, compensate for the absence of the synergy site during adhesion strengthening (***Figure 3***). To test this hypothesis, we seeded pan-integrin-null fibroblasts (pKO) reconstituted with β1-class integrins to express α5β1 (pKO-β1), or with αv integrins (pKO-αv) to express αvβ3 and αvβ5 integrins, or with both β1 and αv integrins (pKO-αv/β1) (***Schiller et al., 2013***) on pFN^{wt}- and pFN^{syn}-coated substrates and evaluated cell adhesion, spreading, and

adhesion site formation. From the three cell lines, only pKO-β1 cells exhibited reduced adhesion on pFN^{syn} compared to pFN^{wt} at all-time points analyzed (***Figure 4A***). Moreover, pKO-β1 cells had significantly fewer FAs, contained fewer stress fibers, and spread less on pFN^{syn} compared to pFN^{wt} (***Figure 4B–F***, see ***Videos 3*** and ***4*** and still images in ***Figure 4—figure supplement 1***). Moreover, the areas of FAs determined with paxillin and β1 integrin stainings were significantly reduced on pFN^{syn} compared to pFN^{wt} (***Figure 4G,H***), which altogether suggests that pFN^{syn}-bound $\alpha5\beta1$ integrins fail to organize functional adhesion sites and to induce contractile stress fibers required for cell spreading. pKO-αv cells adhered and spread similarly on pFN^{wt} and pFN^{syn}, and developed comparably large, paxillin-positive FAs that were anchored to thick stress fibers (***Figure 4B,D***). Importantly, pKO-αv/β1 cells also showed the same adhesion and spreading behavior, and developed similar adhesion sites on pFN^{syn} indicating that αv-containing integrins compensate for the absence of a functional synergy site (***Figure 4B,E***). Interestingly, the pKO-αv/β1 cells do not show a delay in the transition from NAs to mature FAs on pFN^{syn}, as we observed with *Fn1*-KO cells, which could be due to the significantly higher β3 and lower α5 integrin cell surface levels on pKO-αv/β1 as compared to *Fn1*-KO cells (***Figure 2—figure supplement 1F***).

The FN synergy site is dispensable for the on-rate of FN binding to $\alpha5\beta1$ integrins

Electron microscopy studies of the ligand-binding headpiece of integrin $\alpha5\beta1$ complexed with fragments of FN indicated no contact with the synergy site region while kinetic data suggested a role of the synergy site for enhancing the K_{on} of the complex (***Takagi et al., 2003***). These findings gave rise to the hypothesis that the synergy site contributes to accelerate the initial encounter of $\alpha5\beta1$ with FN-RGD, which was in conflict with our observations that adhesion initiation was unaffected in *Fn1*-KO cells seeded on pFN^{syn} (***Figure 2—figure supplement 1F***). To further test whether the synergy site is required for the FN binding on-rate, we quantified the probability of pKO-β1, pKO-αv, pKO-αv/β1 and pKO cells binding to FNIII7-10^{wt} or FNIII7-10^{syn} fragments and to purified full-length pFN^{wt} or pFN^{syn} using single-cell force spectroscopy (***Figure 4I,J***). To this end, a single cell was attached to the ConA-coated cantilever, lowered onto the FN with a speed of 1 µm/s until a contact force of 200 pN was recorded. After a very short contact time of $\approx$ 50 ms, cell and substrate were separated to detect the rupture of the few specific bonds formed between integrins and FN. On FNIII7-10^{wt}, the experiments revealed a 3-fold higher binding probability of pKO-αv and pKO-αv/β1 cells compared to pKO-β1 cells, indicating that $\alpha v\beta3$ integrins have a higher affinity for FN-RGD than $\alpha5\beta1$ integrins. Similar results were observed with full-length pFN^{wt} or pFN^{syn} (***Figure 4J***). Interestingly, however, full-length pFN showed higher binding probability than fragments for all cell lines tested including the pKO cells that lack integrin expression, which altogether suggests that in addition to integrins also other FN-binding cell surface receptor(s) contribute to the initial binding.

These findings indicate that the FN synergy site promotes the maturation of FAs but accelerates neither the rates of FN binding to $\alpha5\beta1$ integrins nor the formation of NAs.

The FN synergy site compensates for $\alpha IIb\beta3$ integrin loss on platelets

To test whether the FN synergy site can also compensate for the loss of β3-class integrin expression in vivo, we generated homozygous compound mice carrying the *Fn1*^{syn} mutation and the *Itgb3* null mutation (*Itgb3*$^{-/-}$) (***Hodivala-Dilke et al., 1999***). *Itgb3*-null mice fail to express the widely expressed $\alpha v\beta3$ integrins and the platelet-specific $\alpha IIb\beta3$ integrin, and suffer from a bleeding disorder resembling human Glanzmann thrombasthenia. Around 87% of *Itgb3*-null mice are born and around 40% of them survive the first year of life (***Hodivala-Dilke et al., 1999***). To test how the *Fn1*^{syn} alleles affect development and survival of *Itgb3*$^{-/-}$ mice, we intercrossed *Fn1*$^{syn/+}$;*Itgb3*$^{+/-}$ as well as *Fn1*$^{syn/syn}$;*Itgb3*$^{+/-}$ mice and obtained a total of 245 and 90 live offspring at P21, respectively (***Table 1*** and ***Table 1—source data 1***). Out of the 335 offspring altogether, one instead of the expected 38 compound homozygous *Fn1*$^{syn/syn}$;*Itgb3*$^{-/-}$ mice survived to P21. The survivor died at the age of 5 months from excessive bleeding. To determine the time-point of lethality, embryos were collected at different gestation times and genotyped. While compound homozygous *Fn1*$^{syn/syn}$;*Itgb3*$^{-/-}$ embryos were present at the expected Mendelian distribution until E15.5, no live embryos were present at E16.5 or later. Interestingly, mice with one wild-type *Itgb3* allele (*Fn1*$^{syn/syn}$;*Itgb3*$^{-/+}$) were normally

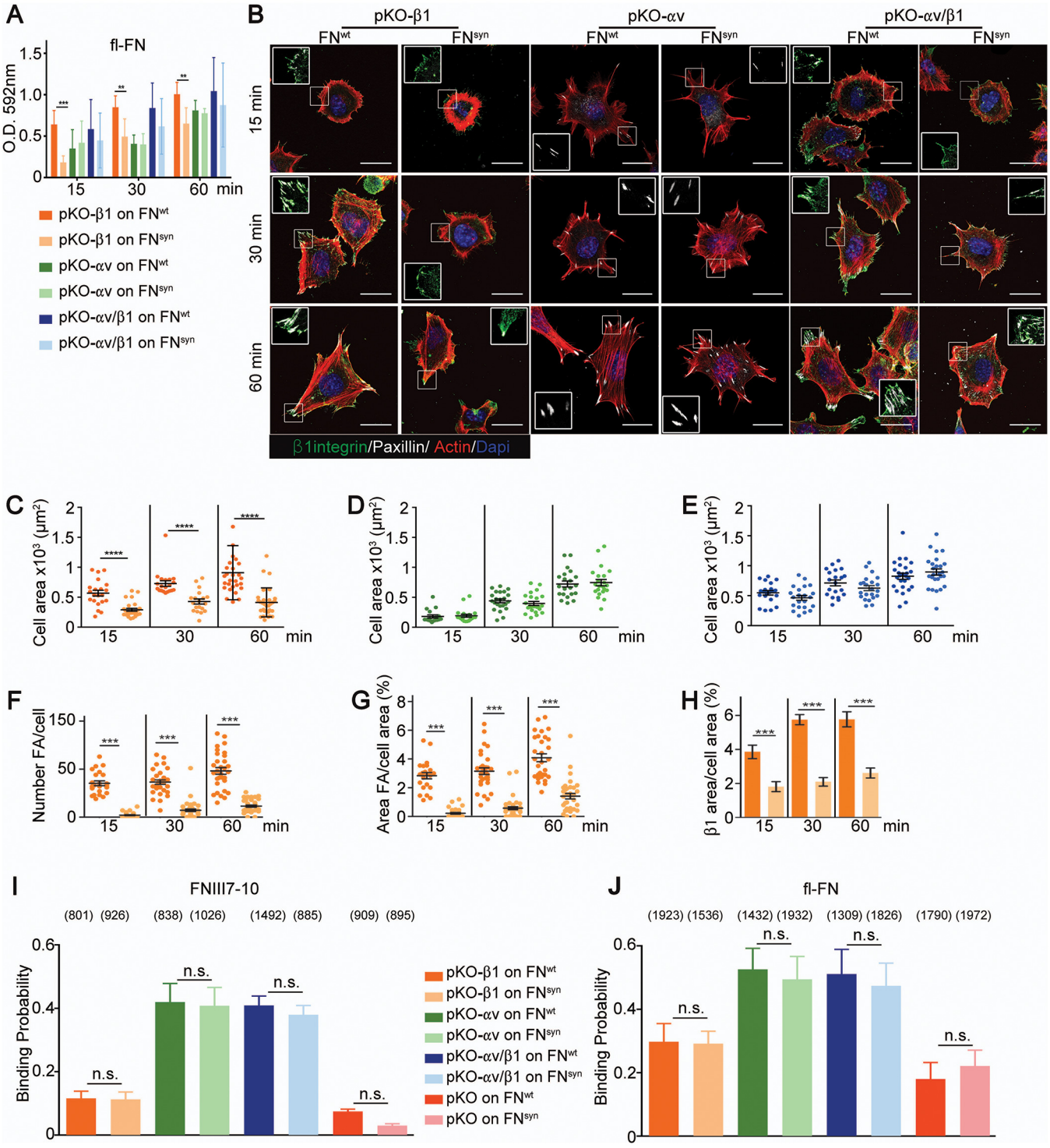

Figure 4. α5β1 integrins require the synergy site in FN to induce cell spreading. (**A**) Adhesion of pKO-β1, pKO-αv and pKO-αv/β1 fibroblasts seeded on pFN^{wt} or pFN^{syn} for indicated times (n = 3 independent experiments; mean ± sem). (**B**) pKO-β1, pKO-αv and pKO-αv/β1 fibroblasts were seeded on pFN^{wt} or pFN^{syn}, fixed at the indicated times and stained for total β1 integrin (green), paxillin (white) and F-actin (red). Scale bar, 50 μm. (**C–E**) Quantification of cell area of pKO-β1 (**C**), pKO-αv (**D**) and pKO-αv/β1 (**E**) cells seeded on pFN^{wt} or pFN^{syn} for indicated times. (**F–H**) Quantification of the number of FAs (**F**), the percentage of FA coverage measured as paxillin-positive area (**G**) and the percentage of β1 integrin-positive areas referred to the total cell area (**H**) in pKO-β1 cells (n = 25 cells for each measurement and three independent experiments; mean ± sem). The binding probability

Figure 4 continued on next page

Figure 4 continued

of integrins to FNIII7-10^{wt} or FNIII7-10^{syn} fragments (I) and to full length (fl-FN) pFN^{wt} or pFN^{syn} (J) determined by single-cell force spectroscopy. Numbers in parentheses indicate events studied for each condition. Statistical significances were calculated using the Student *t*-test; *p<0.05, **p<0.01, ***p<0.001 and ****p<0.0001.

DOI: 10.7554/eLife.22264.012

The following figure supplement is available for figure 4:

Figure supplement 1. Captures of life-time microscopy videos of pKO-β1 fibroblasts spreading on pFN^{wt} or pFN^{syn}.

DOI: 10.7554/eLife.22264.013

distributed, which altogether indicates that one β3 integrin allele is sufficient to compensate for normal development.

Compound homozygous *Fn1$^{syn/syn}$;Itgb3$^{-/-}$* embryos displayed multiple cutaneous hemorrhages and edema, which were first visible at E11.5/12.5 (***Figure 5A*** and ***Figure 5—figure supplement 1A***) and then spread over the whole body at E15.5 (***Figure 5B***). Interestingly, at E12.5 the bleeds were visible at sites where the lymphatic vessels form (arrowheads in ***Figure 5A***) and therefore, we hypothesized that the newly formed lymphatic vessels fail to separate from the cardinal vein, which occurs between E11-13 (***Carramolino et al., 2010***). In line with our hypothesis, Lyve1-positive lymphatic vessels in the skin of *Fn1$^{syn/syn}$;Itgb3$^{-/-}$* embryos were dilated and covered with ectopic α-smooth muscle actin (α-SMA)-positive cells and filled with Ter119-positive erythroblasts (***Figure 5C–E***). In contrast, lymphatic vessels in the skin of *Itgb3*-null or wild-type littermates neither contained Ter119-positive cells nor were surrounded with α-smooth muscle actin-positive cells.

The separation of the primary lymphatic sac from the cardinal vein is driven by platelet adhesion to and aggregation at the lymphatic endothelium (***Carramolino et al., 2010***; ***Uhrin et al., 2010***). We therefore hypothesized that the platelet functions are severely compromised in *Fn1$^{syn/syn}$;Itgb3$^{-/-}$* embryos as they lack αIIbβ3-mediated binding to fibrinogen and FN (***Figure 6A***), as well as the ability to strengthen adhesion and signaling via $\alpha5\beta1$ integrin-mediated binding to FN. To test the hypothesis, we performed spreading assays as well as adhesion assays under flow with wild-type or *Itgb3$^{-/-}$* platelets. The mean spreading area of wild-type platelets seeded for 60 min on fibrinogen, pFN^{wt}, and pFN^{syn} was 15–16 μm^2. As expected, *Itgb3$^{-/-}$* platelets failed to spread on fibrinogen (mean spreading area of 4.6 μm^2). Furthermore, they showed a reduced mean spreading area of 8.9 μm^2 on pFN^{wt} and failed to spread on pFN^{syn} (mean spreading area of 3.8 μm^2) (***Figure 6B,C***). Application of shear flow reduced adhesion of wild-type platelets to pFN^{syn} by 10-fold compared to pFN^{wt}, while adhesion of *Itgb3*-null platelets was lost on fibrinogen as well as pFN^{syn}, and only slightly diminished on pFN^{wt} (***Figure 6D,E***). Importantly, adhesion and spreading of platelets isolated from *Itgb3$^{-/-}$* mice to collagen were unaffected, irrespective of whether shear flow was applied or not (***Figure 6C,E***).

These in vitro experiments demonstrate that adhesion of αIIbβ3-deficient platelets to wild-type FN is partially compensated by $\alpha5\beta1$ integrins in a FN synergy site-dependent manner, and that $\alpha5\beta1$ as well as αIIbβ3 integrins require the FN synergy site for stabilizing platelet adhesion to FN, under shear flow.

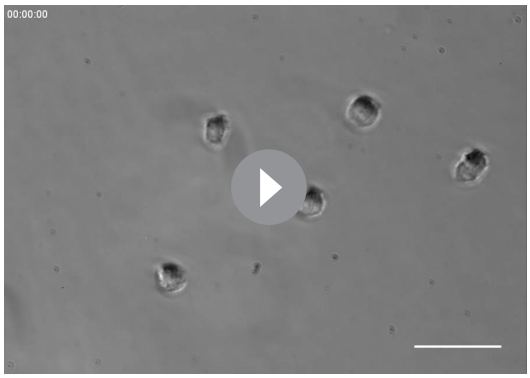

Video 3. Life-time microscopy video of pKO-β1 fibroblasts on pFN^{wt}.

DOI: 10.7554/eLife.22264.014

The FN synergy site compensates for $\alpha v\beta3$ during vessel maturation

The absence of $\alpha5\beta1$ integrins leads to vascular defects (***Abraham et al., 2008***). To test whether vascular abnormalities due to an impaired $\alpha5\beta1$ function contribute to the severe bleeds and the lethality of *Fn1$^{syn/syn}$;Itgb3$^{-/-}$* embryos, we analyzed the mural coverage and anchorage to the ECM. While immunostaining of E11.5 whole mount embryos with an anti-PECAM-1 antibody revealed that the vessels in the trunk of *Fn1$^{syn/syn}$;Itgb3$^{-/-}$* embryos showed normal sprouting

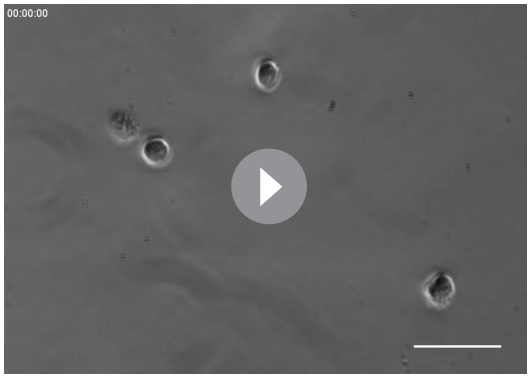

Video 4. Life-time microscopy video of pKO-β1 fibroblasts on pFN^{syn}.
DOI: 10.7554/eLife.22264.015

(***Figure 5—figure supplement 1B***), the arteries and veins of the dermal vasculature of E15.5 embryos were tortuous and irregularly covered with α-SMA-positive cells (***Figure 7A***). Furthermore, the vascular network was less intricate and had significantly fewer branching points in *Fn1$^{syn/syn}$;Itgb3$^{-/-}$* embryos compared to wild-type littermates (***Figure 7B***). Interestingly, collagen IV immunostaining indicated that many small vessels in E15.5 *Fn1$^{syn/syn}$;Itgb3$^{-/-}$* embryos lacked a clear lumen and PECAM-1 immunosignals (see arrowheads in ***Figure 7C***). They probably represent retracted vessels and were significantly more frequent in *Fn1$^{syn/syn}$;Itgb3$^{-/-}$* embryos compared to wild-type, *Fn1$^{syn/syn}$;Itgb3$^{+/+}$* and *Fn1$^{+/+}$;Itgb3$^{-/-}$* littermates (***Figure 7D***). Moreover, small vessels in *Fn1$^{syn/syn}$;Itgb3$^{-/-}$* embryos were often less covered by pericytes. Instead, NG2-positive pericytes were either detached or formed patchy aggregates on the vessel surface (see arrowheads in ***Figure 7E***). Altogether, these observations indicate that the vessel wall coverage and stability are decreased in the *Fn1$^{syn/syn}$;Itgb3$^{-/-}$* embryos and probably contribute to their severe hemorrhages.

Discussion

Although cell-based studies suggested that the FN synergy site is required for αIIbβ3 and α5β1 integrin function, the in vivo evidence was missing and the mechanistic property controversial. We report here the characterization of a mouse strain, in which the synergy site of FN (*Fn1^{syn}*) was disrupted. Contrary to expectations, the *Fn1$^{syn/syn}$* mice were born without developmental defects indicating that the synergy site is dispensable for organogenesis and tissue homeostasis. However, when *Fn1$^{syn/syn}$* mice are exposed to stress such as tail bleeding and arteriole injury, or the genetic ablation of the FN-binding β3-class integrins (αvβ3, αIIbβ3), the synergy site becomes essential for cells that have to resist or produce high forces such as platelets and vascular smooth muscle cells (***Figure 8***).

Table 1. Progeny of *Fn1$^{syn/+}$;Itgb3$^{+/-}$* x *Fn1$^{syn/+}$;Itgb3$^{+/-}$* intercrosses.

Age	Num.	*Fn1$^{syn/syn}$ Itgb3$^{+/-}$*	*Fn1$^{syn/syn}$ Itgb3$^{+/+}$*	*Fn1$^{syn/syn}$ Itgb3$^{-/-}$*	*Fn1$^{+/syn}$ Itgb3$^{+/-}$*	*Fn1$^{+/syn}$ Itgb3$^{+/+}$*	*Fn1$^{+/syn}$ Itgb3$^{-/-}$*	*Fn1$^{+/+}$ Itgb3$^{+/-}$*	*Fn1$^{+/+}$ Itgb3$^{+/+}$*	*Fn1$^{+/+}$ Itgb3$^{-/-}$*
E11.5	36	6 (16.7%)	1 (2.8%)	1 (2.8%)	10 (27.8%)	6 (16.7%)	4 (11.1%)	5 (13.9%)	2 (5.6%)	1 (2.8%)
E14.5	23	2 (8.7%)	2 (8.7%)	2 (8.7%)	5 (21.7%)	5 (21.7%)	1 (4.3%)	1 (4.3%)	4 (17.3%)	1 (4.3%)
E15.5	121	12 (9.9%)	5 (4.1%)	3 (2.5%)	39 (32.2%)	5 (15.4%)	12 (9.9%)	14 (11.6%)	17 (14%)	4 (3.3%)
E16.5	16	2 (12.5%)	1 (6.25%)	0	5 (31.5%)	1 (6.25%)	1 (6.25%)	3 (37.5%)	1 (6.25%)	2 (12.5%)
E17.5	16	2 (12.5%)	0	0	6 (23%)	3 (19%)	2 (12.5%)	2 (12.5%)	1 (8%)	0
P 21	245	33 (13.5%)	32 (13%)	0	57 (23%)	46 (18.7%)	13 (5.3%)	35 (14.4%)	17 (3.9%)	12 (4.9%)
Mendelian Distribution	100	12.5%	6.25%	6.25%	25%	12.5%	12.5%	12.5%	6.25%	6.25%

DOI: 10.7554/eLife.22264.016
Source data 1. Progeny of *Fn1$^{syn/syn}$;Itgb3$^{+/-}$* x *Fn1$^{syn/syn}$;Itgb3$^{+/-}$* crosses
DOI: 10.7554/eLife.22264.017

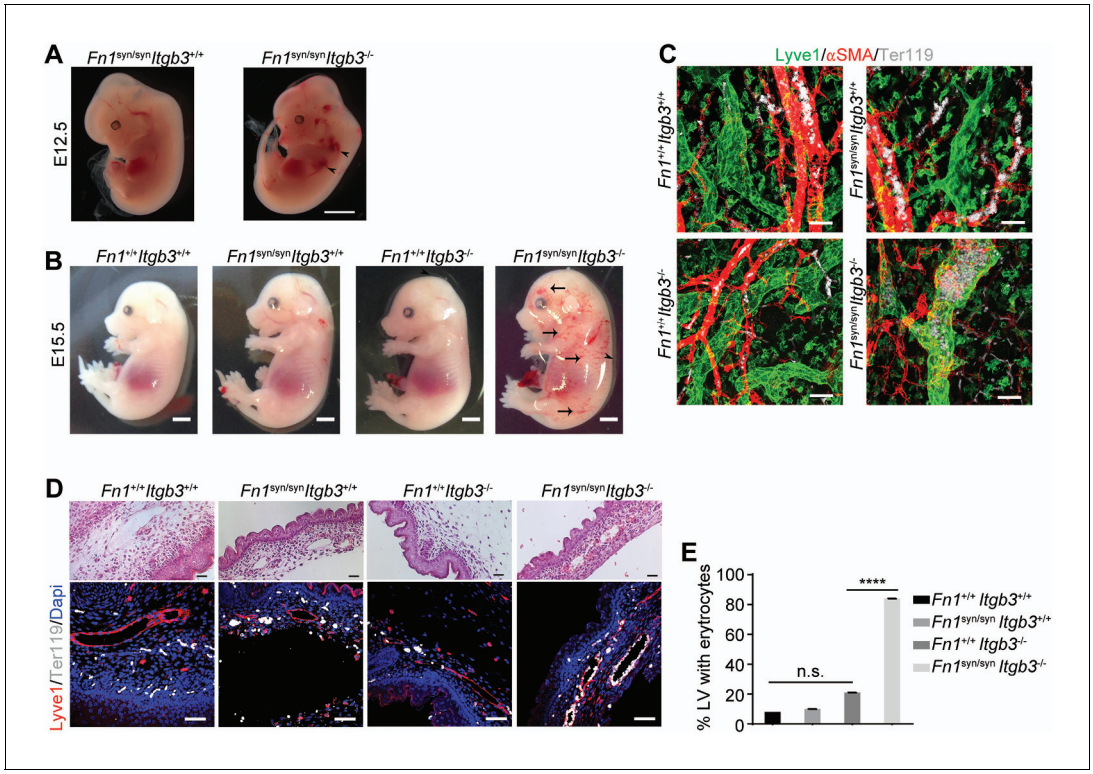

Figure 5. *Fn1*$^{syn/syn}$;*Itgb3*$^{-/-}$ mice suffer from severe hemorrhages and fail to separate the blood and lymphatic vasculatures. (**A**) E12.5 *Fn1*$^{syn/syn}$;*Itgb3*$^{-/-}$ embryos display hemorrhages in the jugular and axilar areas in the left side (arrowheads). Scale bar, 50 mm. (**B**) Representative images from E15.5 littermates embryos resulting from *Fn1*$^{syn/+}$;*Itgb3*$^{-/+}$ intercrosses. Compound *Fn1*$^{syn/syn}$;*Itgb3*$^{-/-}$ embryos display cutaneous edema (arrowhead) and abundant skin hemorrhages (arrows); scale bars, 50 mm. (**C**) Skin whole-mount from E15.5 embryos showing Lyve1-positive lymphatic vessels (green), αSMA-positive blood vessels (red) and Terr119-positive erythrocytes (white). The lymphatic vessels of compound *Fn1*$^{syn/syn}$;*Itgb3*$^{-/-}$ embryos are dilated, covered by ectopic αSMA-positive cells and filled with erythrocytes. Scale bar, 50 μm. (**D**) Representative images of skin sections stained with H and E (upper panel) and Lyve1 and Terr119 (lower panel) showing erythrocytes in lymphatic vessels. Scale bar, 50 μm. (**E**) Quantification of the percentage of lymphatic vessels filled with Ter119-positive erythrocytes (n = 40 vessels counted per embryo, in two embryos per each genotype; mean ± sem). Statistical significances were calculated using the Student *t*-test: ****p<0.0001.

DOI: 10.7554/eLife.22264.018

The following figure supplement is available for figure 5:

Figure supplement 1. Blood vessel formation in *Fn1*$^{syn/syn}$; *Itgb3*$^{-/-}$embryos.

DOI: 10.7554/eLife.22264.019

Ablation of the *Fn1* gene in mice, as well as the simultaneous ablations of the *Itga5*/*Itgav* integrin genes in mice arrests development at embryonic day 8.5 (E8.5) due to defects in the formation of mesoderm and mesoderm-derived structures (***George et al., 1993***; ***Georges-Labouesse et al., 1996***; ***Yang et al., 1999***). The replacement of the FNIII10 RGD motif with the RGE in mice also affects mesoderm development, although less severe and restricted to the vascular system and to the posterior region of the developing embryo (***Takahashi et al., 2007***; ***Girós et al., 2011***). Interestingly, these defects resemble those observed in *Itga5*-deficient mice indicating that the RGE mutation is sufficient to abrogate α5β1 integrin function and that the synergy site cannot compensate for a dysfunctional RGD motif. Furthermore, the normal development of *Fn1*$^{syn/syn}$ mice also excludes an essential role of the synergy site for α5 integrin function in vivo (***Grant et al., 1997***; ***Krammer et al., 2002***). A reduced α5β1 integrin function would probably have occurred if the synergy site would indeed guide the binding pocket of α5β1 towards the RGD motif and increase the FN-binding on-rate (***Takagi et al., 2003***). However, the absence of obvious 'α5β1-loss-of-function defects' (***Yang et al., 1993***) in *Fn1*$^{syn/syn}$ mice and the normal FN-binding on-rates of pKO-β1 cells in single-cell force spectroscopy experiments indicate that the synergy site is probably dispensable to accelerate α5β1 integrin-FN binding.

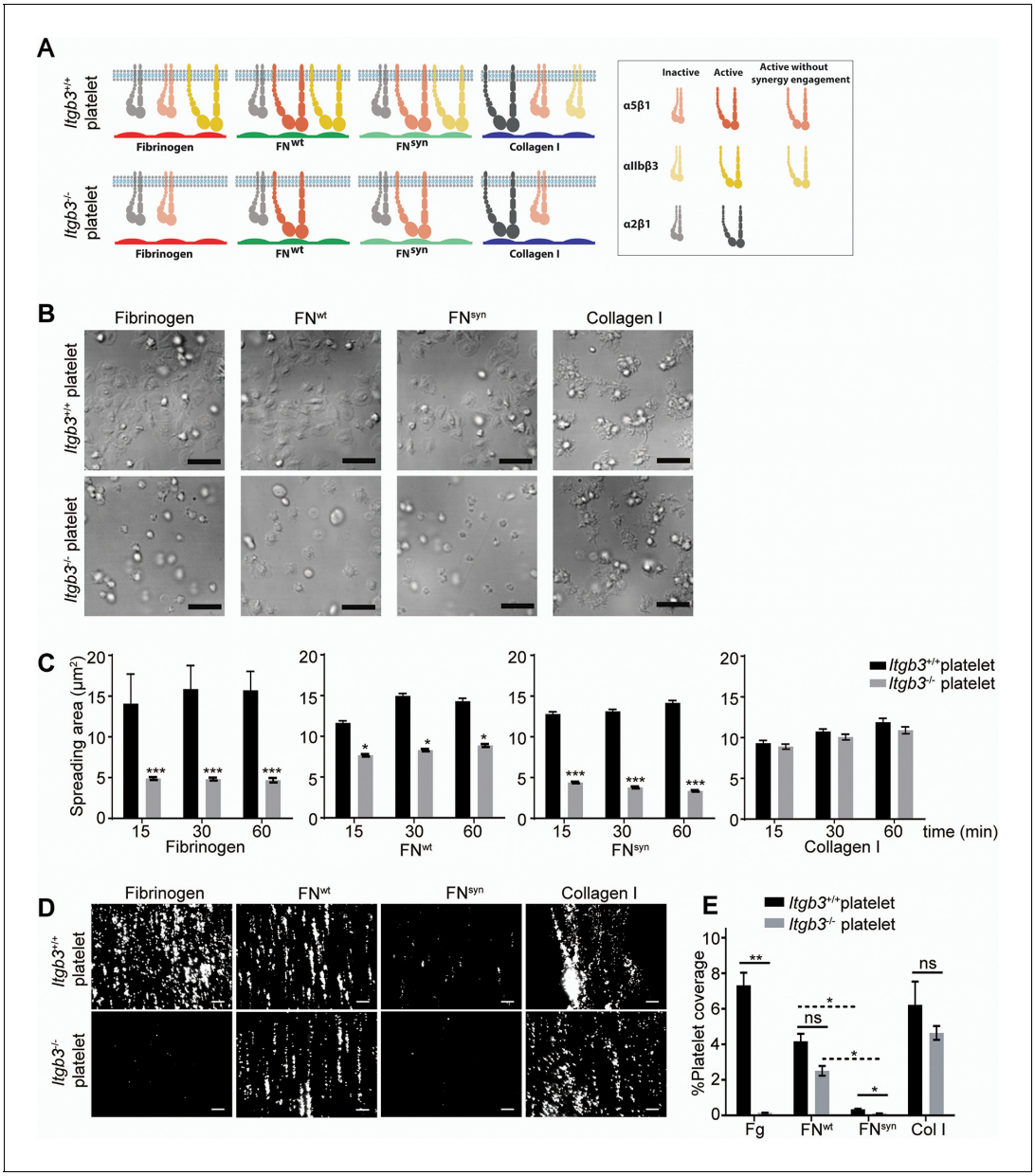

Figure 6. Shear flow exposed platelets fail to adhere to pFN^{syn}. (**A**) Cartoon showing the platelet integrins that can be ligated to the different substrates used in the experiments. The color intensity of the integrin denotes whether the integrin is active or inactive. (**B**) Spreading of *Itgb3*$^{+/+}$ and *Itgb3*$^{-/-}$ platelets after 1 hr on fibrinogen, pFN^{wt}, pFN^{syn} and type I collagen. Scale bars, 10 μm. (**C**) Quantification of the platelet area at indicated times (n = 100 platelets per each condition in three independent experiments; mean ± sem). (**D**) Representative figures of fluorescently labeled *Itgb3*$^{+/+}$ or *Itgb3*$^{-/-}$ platelets seeded on indicated substrates and exposed to shear flow. Scale bar, 40 μm. (**E**) Platelet coverage after 10 min shear flow of 1000 s^{-1}. (n = 10 pictures per experiment, four independent experiments for each condition; mean ± sem). Statistical significances were calculated using the Student *t*-test; *p<0.05, **p<0.01 and ***p<0.001.

DOI: 10.7554/eLife.22264.020

We also demonstrate an unexpected, compensatory role between the FN synergy site and αvβ3 integrins for the vascular coverage by smooth muscle cells. Apparently, the high myosin II-induced forces generated by these cells are only efficiently absorbed with either high αv-class integrin surface levels or a fully functional FN. Whether a similar functional relationship operates also during paraxial mesoderm, whose formation critically depends on the expression of α5β1 and αv-class integrins (***Yang et al., 1999***), cannot be deduced from our experiments. However, the normal mesoderm formation in *Fn1*$^{syn/syn}$ mice indicates that mesodermal cells require α5β1 to bind the RGD motif but

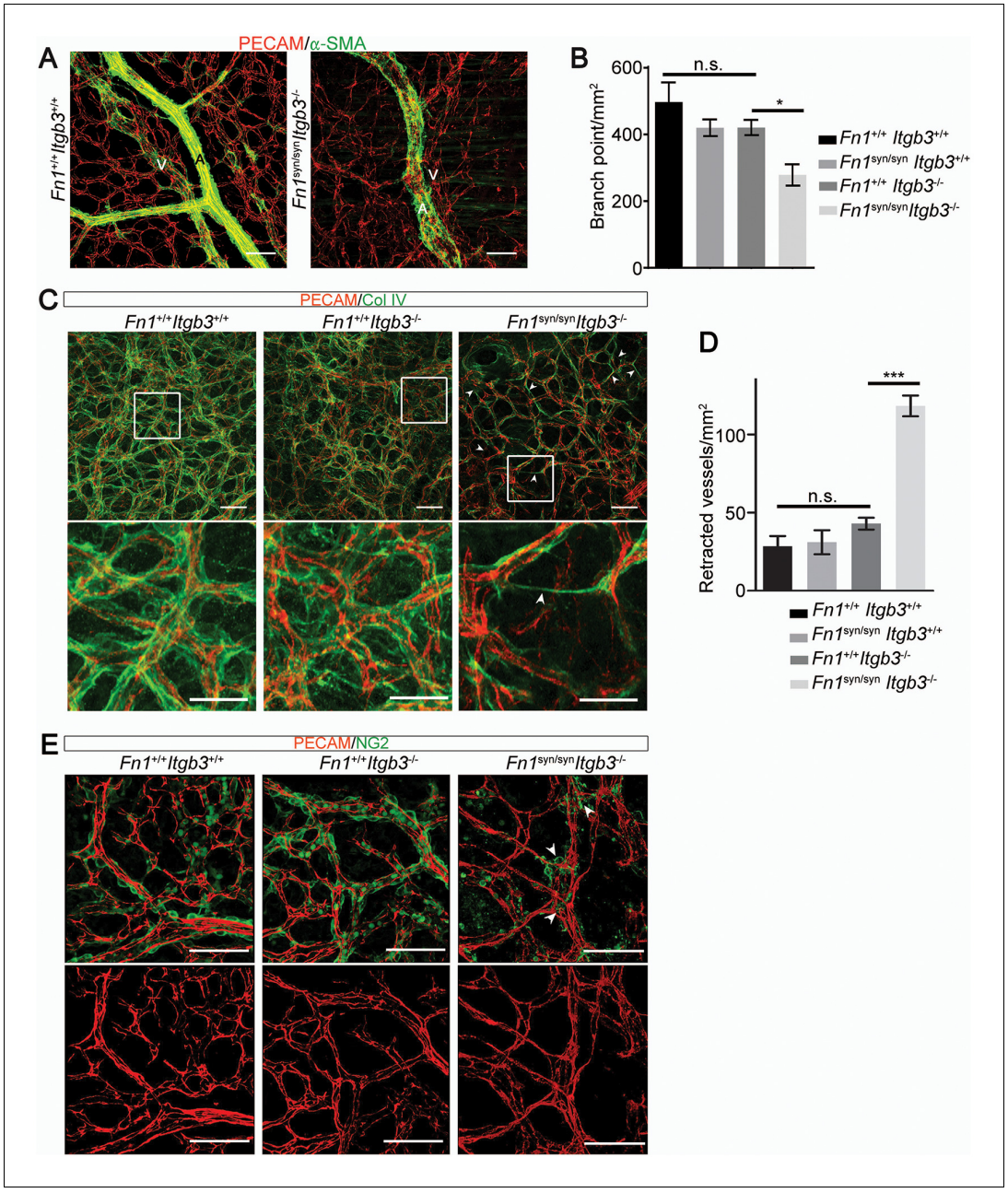

Figure 7. Malformed blood vessels in *Fn1*$^{syn/syn}$;*Itgb3*$^{-/-}$ embryos. (**A**) PECAM-positive endothelial cells (red) and α-SMA-positive smooth muscle cells (green) in dermal whole mounts from E15.5 *Fn1*$^{+/+}$;*Itgb3*$^{+/+}$ and *Fn1*$^{syn/syn}$; *Itgb3*$^{-/-}$ littermate embryos indicate veins (V) and arteries (**A**). (**B**) Quantification of the number of branching points (n = 10–15 images of 2–3 embryos; mean ± sem). (**C**) Vascular basement membranes in dermal whole mounts from E15.5 *Fn1*$^{+/+}$;*Itgb3*$^{+/+}$, *Fn1*$^{+/+}$;*Itgb3*$^{-/-}$ and *Fn1*$^{syn/syn}$;*Itgb3*$^{-/-}$ littermate embryos stained for type IV collagen (green) and PECAM-positive endothelial cells (red). Arrowheads show small vessels lacking lumen. (**D**) Quantification of retracted vessels (n = 14–23 from 4–7 embryos; mean ± sem). (**E**) PECAM-positive endothelial cells (red) and NG2-positive pericytes (green) in dermal whole-mounts from E15.5 *Fn1*$^{+/+}$;*Itgb3*$^{+/+}$, *Fn1*$^{+/+}$;*Itgb3*$^{-/-}$ and *Fn1*$^{syn/syn}$;*Itgb3*$^{-/-}$ littermate embryos. Note pericytes are sparse, absent or aggregate on mutant vessels (arrowheads). Statistical significances were calculated using the Student *t*-test; *p<0.05, and ***p<0.001. Scale bars, 50 μm.

DOI: 10.7554/eLife.22264.021

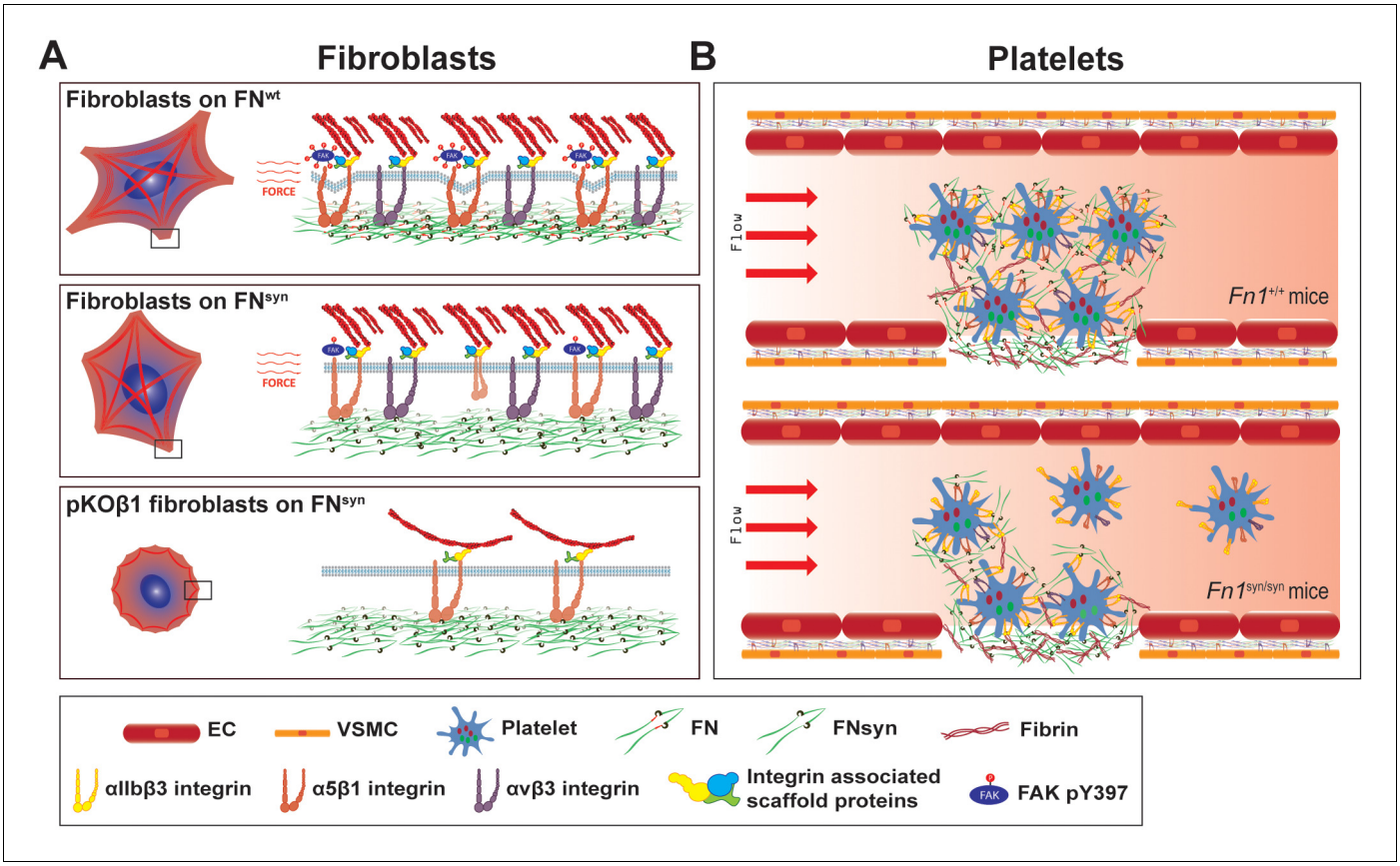

Figure 8. The major role of the FN synergy site is to re-enforce cell adhesion. (**A**) Hydrodynamic shear force-exposed fibroblasts seeded on a FN^{wt}-coated surface form catch-bonds that strengthen α5β1 integrin-mediated adhesions to FN and trigger phosphorylation of Y397-FAK (upper image). On FN^{syn}-coated surfaces, the αvβ3 integrins compensate for the absent synergy site allowing fibroblast adhesion and the reduced α5β1 binding strength leads to diminished phosphorylation of pY397-FAK (middle image). The elimination of αv-class integrins decreases cell adhesion on FN^{syn}-coated surfaces, reduces cell spreading and delays the maturation of FA and fibrillar adhesions (lower image). (**B**) Platelets in $Fn1^{+/+}$ mice form tight aggregates on injured vessel walls that withstand the shear forces of the blood flow (upper image), while platelets in an injured vessel in $Fn1^{syn/syn}$ mice fail to withstand the blood flow leading to a delayed thrombus formation (lower image). Endothelial cells (EC); vascular smooth muscle cells (VSMC).
DOI: 10.7554/eLife.22264.022

not the synergy site. Interestingly, we also find clear evidence for a compensatory role of the FN synergy site and αv-class integrins for cell spreading and FA maturation in vitro (***Figure 8***), which differs from previous reports showing that α5β1 and αv-class integrins have non-overlapping functions for inducing myosin contractility (***Schiller et al., 2013***) or controlling directional migration (***Missirlis et al., 2016***).

It is well known that platelet adhesion to pFN, mediated by αIIbβ3 with contributions from α5β1 and other integrins, plays a critical role for hemostasis (***Wang et al., 2014***; ***Ni et al., 2003b***). Our findings revealed that the FN synergy site is critically important for the adhesion of wild type platelets in in vitro flow chamber settings, while impaired spreading or defects under static adhesion only arise when αIIbβ3 expression is lost. These findings indicate that the synergy site plays a central role as soon as force is applied to the bonds between FN and platelet integrins. A similar force-dependent requirement of the synergy site was also apparent after arteriolar injuries in vivo, which showed that $Fn1^{syn/syn}$ mice display diminished platelet adhesion and delayed thrombus formation. This requirement of the synergy site for platelets to resist the shear forces of the blood flow also provides a rational explanation for the prolonged bleeding times observed in $Fn1^{syn/syn}$ mice after tail tip excisions. Interestingly, the in vivo platelet dysfunctions in $Fn1^{syn/syn}$ mice as well as $Itgb3^{-/-}$ mice profoundly aggravate in compound $Fn1^{syn/syn}$;$Itgb3^{-/-}$ embryos where they cause fatal bleedings and an insufficient platelet-mediated separation of the lymphatic vessels from the cardinal vein. Since murine platelets contain around 100 times more αIIbβ3 than α5β1 integrins (***Zeiler et al., 2014***) the

compensation of the entire αIIbβ3 pool by the minor α5β1-FN^{wt} complexes underscores the fundamental role of the adhesion strengthening property of the synergy site in FN.

Our mouse strain will allow now to test how the synergy site-mediated adhesion re-enforcement affects the course of tissue fibrosis or cancer development and progression, which are heavily influenced by integrin surface levels as well as tissue rigidity that in turn is modulated by the strength of integrin-ligand bonds (**Zilberberg et al., 2012**; **Laklai et al., 2016**).

Materials and methods

Animals

Mice were housed in special pathogen free animal facilities. All mouse work was performed in accordance with the Government of the Valencian Community (Spain) guidelines (permission reference A1327395471346) and with the Government of Upper Bavaria. Mice containing the integrin β3 deletion were bred under the permission reference 55.2-1-54-2532-96-2015. The tail-bleeding and cremaster muscle venules injury assays performed under the permission reference 55.2-1-54-2532-115-12.

Generation of *Fn1$^{syn/syn}$* knockin mice

A 129/Sv mouse PAC clone was used to construct the targeting vector (**Figure 1—figure supplement 1A**), which consisted of a 2.1 kb fragment containing exons 26 and 27, a neomycin cassette flanked by *loxP* sites, a 2.4 kb fragment containing the exon 28 carrying the mutated nucleotides, and a 3.5 kb fragment with the exons 29 to 32. The targeting construct was linearized with NotI and electroporated into R1 embryonic stem (ES) cells. Approximately 300 G418-resistant clones were isolated and screened by Southern blot for homologous recombination. The genomic DNAs were digested with SacI, XbaI or BstEII and probed with external probes 1 and 2 (**Figure 1—figure supplement 1A**). Two correctly targeted clones were injected into C57BL/6 host blastocysts to generate germline chimeras. The *Fn1$^{syn\text{-}neo/+}$* mice were crossed with a deleter-Cre strain to eliminate the *loxP* flanked neomycin cassette. The elimination of neomycin was analyzed by Southern blot, genomic DNA was digested with Eco RI and probed with probe 3 (**Figure 1—figure supplement 1B**). The *Fn1$^{syn/+}$* mice were intercrossed to generate homozygous *Fn1$^{syn/syn}$* mice. The following primers were used to genotype the mouse strain by PCR: 5′-TCACAAGGAAACCAGGGAAC-3′ (forward); 5′-CCGTTTTCACTCTCGTCAT-3′ (reverse).

Cell lines

The mouse *Fn1*-KO cell line and the integrin pan-KnockOut fibroblast lines were isolated from a mouse kidney and immortalized by retroviral delivery of the SV40 large T. To generate *Fn1*-KO cells, the *Fn1* gene was deleted from *Fn1$^{flox/flox}$* with the adenoviral transduction of the *Cre* recombinase. Integrin pKO fibroblasts were generated as described by **Schiller et al. (2013)**. *Itgav$^{flox/flox}$*; *Itgb1$^{flox/flox}$*; *Itgb2$^{-/-}$*;*Itgb7$^{-/-}$* immortalized fibroblasts were treated with adenoviral *Cre* recombinase and reconstituted with mouse *Itgb1* and/or *Itgav* integrin cDNAs to generate pKO-β1, pKO-αv and pKO-αv/β1 cells. The cells were provided by H. Schiller (Max-Planck Institute for Biochemistry, Martinsried, Germany). Cell lines were not tested for mycoplasma.

Antibodies

For flow cytometry, we used the following antibodies conjugated to PE: 1:200; hamster anti-β1 integrin (102207, from from BioLegend, San Diego, CA, USA), rat anti-α5 integrin (557447, from from PharMingen, Madrid, Spain), hamster anti-β3 integrin (12–0611, from BD Bioscience, Madrid, Spain) and rat anti-αv integrin (551187, from from PharMingen). For immunostainings or western blots, we used the following antibodies: rabbit anti-β1 integrin (obtained from Reinhard Fässler) IF 1:500; rabbit anti-α5 integrin (4705, from Cell Signaling, Barcelona, Spain) WB 1:2000; rabbit anti-pTyr397FAK (44–624G, from Biosource, Madrid, Spain) WB 1:1000; rabbit anti-pTyr861FAK (44–626G, from Biosource) WB 1:1000; rabbit anti-FAK (06–543, from Millipore, Ille de France, France) WB 1:1000; rabbit anti-Fibronectin (AB2033, from Millipore) WB 1:2000, IF 1:300–500; mouse anti-Paxillin (610051, from PharMingen) IF 1:300; rabbit anti-Lyve1 (ab14914, from Abcam, Cambridge, UK) IF 1:300, WM 1:100; rat anti-Ter119 (09082D, from PharMingen) IF 1:400,

WM 1:100; rat anti-PECAM (553370, from PharMingen) IF 1:300, WM 1:100; rabbit anti-Collagen IV (2150–1470, from Bio-Rad, Madrid, Spain) WM 1:100; mouse anti-smooth muscle actin conjugated with Cy3 (A2547, from Sigma-Aldrich, Madrid, Spain) IF 1:500, WM 1:200; anti-NG2 chondroitin sulfate proteoglycan (AB5320, from Merck Millipore) WM 1:100; mouse anti-gamma chain fibrinogen (ab119948, from Abcam), WB 1:200; rabbit anti-laminin-1 (L9393, from Sigma-Aldrich) WM 1:100. F-actin was stained with Phalloidin coupled with TRITC (P1951, from Sigma-Aldrich) IF 1:500. For immunofluorescence the following secondary antibodies were used diluted 1:400: goat anti-rabbit conjugated with Alexa488 (A11008); goat anti-rabbit conjugated with A546 (A11010); donkey anti-mouse conjugated with A647 (A31571); goat anti-rat conjugated with A488 (A21208); goat anti-rat conjugated with A546 (A11081); goat anti-rat conjugated with A647 (A21247) (all from Invitrogen, Madrid, Spain). For western-blot, goat anti–rabbit conjugated with horseradish peroxidase (172–1019, from Bio-Rad) was used as secondary antibody.

Purification of plasma fibronectin (pFN)

Blood was collected from $Fn1^{+/+}$ and $Fn1^{syn/syn}$ mice using 0.5 M EDTA as anticoagulant in non-heparinized capillaries, centrifuged at 3000 rpm for 20 min and the pFN was purified from the supernatant (plasma) using Gelatin-Sepharose (GE Healthcare Life Sciences, Valencia, Spain) affinity chromatography (***Retta et al., 1999***) adapted to minicolumns (Poly-Prep, Bio-Rad). Briefly, the columns were washed with 0.5 NaCl in 10 mM Tris-HCl pH7.4 and pFN was eluted with 2 M urea in TBS (0.15 M NaCl in 10 mM Tris-HCl, pH 7.4) and dialyzed against TBS. Purified FN was analyzed by 8% SDS-PAGE and stained with Coomassie brilliant blue, and by Western blot.

Production of the FNIII7-10 fragment

We used the human cDNA encoding the FNIII7-10 fragment and subcloned in the expression vector pET-15b (***Takahashi et al., 2007***). To generate the FNIII7-10^{syn} we mutated by site-directed mutagenesis the two arginines in the synergy sequence: DRVPHSRN>DAVPHSAN. We performed two rounds of PCR using the following primers: 5´-GATGCGGTGCCCCACTCTCGGAAT-3´ (forward) and 5´-GATGCGGTGCCCCACTCTGCGAAT-3´ (forward) and the complementary reverse primers. The expression of recombinant FN fragments was done in the *E. coli* strain Rosetta T1R. Purification was performed using TALON Metal Affinity chromatography (Clontech, Saint Germain en Laye, France). Finally the protein was obtained by gel filtration chromatography using Superdex 200 10/300 GL columns (GE Healthcare) and Superdex Size Exclusion Media (GE Healthcare, Valencia, Spain) and eluted in PBS.

Adsorption of purified pFN onto glass

Glass coverslips of 18 mm diameter were poly-maleic anhydride-1-octadecene (POMA; Polysciences Inc)-treated (***Prewitz et al., 2013***) and coated with 0.1–10 µg/ml of purified mouse pFN during 1 hr at RT, followed by a blocking step of 1 hr using 1% BSA in PBS. To quantify the adsorbed FN, the coverslips were then incubated for 2 hr at RT with anti-FN antibodies (Ab; diluted 1/300 in blocking solution), washed, incubated with anti-rabbit Ab conjugated-HRP (diluted 1/500 in blocking solution) 1 hr at RT and finally treated with 50 µl of 2,2'-azino-bis(3-ethylbenzthiazoline-6-sulfonic acid (ABTS; Peroxidase substrate kit, Vector SK-4500) for 30 min in the dark. The ABTS-containing solution was collected and the absorbance was measured at 405 nm.

Cell adhesion assay

96 well plates were coated with 10 µg/ml of pFN or poly-lysine (Sigma-Aldrich, Madrid, Spain) or 3% BSA in PBS during 1 hr at RT, followed by a blocking step of 30 min using 3% BSA in PBS. The cells were starved overnight in 9% serum replacement medium (SRM) composed of 46.5% AIM-V (Life Technologies, Madrid, Spain), 5% RPMI (Life Technologies) and 1% NEAA (Non-Essential Amino Acid Solution, Sigma-Aldrich) supplemented with 1% FN-depleted calf serum. 5×10^4 cells were plated, allowed to adhere for the indicated times and medium was removed and wells washed three times with PBS. The cells were stained with crystal violet (20% Methanol, 0.1% Crystal Violet) overnight at 4°C, washed, 0.1% triton X-100 was added and incubated for 2 hr at RT. Absorbance was measured at 595 nm.

Spinning disk assay

The spinning disk assay was done as previously described (**Boettiger, 2007**) on POMA-treated glass coverslips of 25 mm diameter, coated with a solution of 10 µg/ml of purified pFN during 1 hr at RT and afterwards blocked 1 hr with 1% BSA in PBS. The *Fn1*-KO or HT1080 cells were starved overnight in 9% SRM supplemented with 1% FN-depleted serum. 7×10^5 cells were seeded, allowed to adhere for 1 hr and spun for 5 min at 6000 rpm in Dulbecco´s PBS supplemented with 80 mM $CaCl_2$ and 80 mM $MgCl_2$. After spinning the cells were fixed with 4% PFA and nuclei stained with DAPI. The nuclei were counted with a Zeiss Axiovert (objective 10x) controlled by Metamorph software, which allows taking images at determined positions. Data were analyzed as described (**Boettiger, 2007**). We calculated for each condition the τ50, which is the mean force for cell detachment.

pFN-integrin crosslinking assay

Cells were seeded onto pFN-coated glass coverslips and spun and non-spun cells were incubated with 1 mM 3,3'-dithiobis (sulfosuccinimidyl propionate) (DTSSP; Thermo Scientific, Madrid, Spain) during 15 min at 4°C. Quenching was carried out with 50 mM Tris, pH 7.4 for 15 min at RT and cells were extracted with 20 mM Tris, pH 7.4, 0.1% SDS and proteinase inhibitors (Inhibitors cocktail, Roche , Barcelona, Spain). Cell lysates were collected and coverslips were thoroughly washed with 20 mM Tris, pH 8.5 followed by incubation with 20 mM Tris, pH 8.5, 0.1% SDS and 25 mM DTT for 1 hr at 37°C to break the crosslinks. The whole crosslinked fractions and the cell lysates were separated by SDS-PAGE and transferred to a nitrocellulose membrane. Western-blots were analyzed with ImageJ and the levels of crosslinked integrins were calculated as the relation between the crosslinked and the total integrin fractions (cell lysates + crosslinked fraction).

Single-cell force spectroscopy (SCFS)

For cell attachment, cantilevers were plasma cleaned (PDC-32G, Harrick Plasma, Ithaca, NY, USA) and then incubated overnight at 4˚C in PBS containing ConA (2 mg/ml, Sigma-Aldrich) (**Friedrichs et al., 2013**). For substrate coatings, 200 µm thick four-segmented polydimethylsilane (PDMS) mask fused to the surface of glass bottom Petri dishes (WPI, Sarasota, FL, USA) was used (**Yu et al., 2015**). Each of the four PDMS framed glass surfaces were incubated overnight at 4°C either with the FNIII7-10^{wt} or FNIII7-10^{syn} fragments or full-length FN (50 µg/ml) in PBS. For SCFS, we mounted an AFM (Nanowizard II, JPK Instruments, Berlin, Germany) on an inverted fluorescence microscope (**Puech et al., 2006**) (Observer Z1/A1, Zeiss, Germany). The temperature was kept at 37°C throughout the experiment by a Petri dish heater (JPK Instruments,Berlin, Germany). 200 µm long tip-less V-shaped silicon nitride cantilevers having nominal spring constants of 0.06 N/m (NP-0, Bruker, USA) were used. Each cantilever was calibrated prior the measurement by determining its sensitivity and spring constant using the thermal noise analysis of the AFM (**Hutter and Bechhoefer, 1993**). To adhere a single fibroblast to the AFM cantilever, overnight serum-starved fibroblasts with confluency up to ≈80% were washed with PBS, trypsin-detached for up to 2 min, suspended in SCFS media (DMEM supplemented with 20 mM HEPES) containing 1% (v/v) FCS, pelleted and resuspended in serum free SCFS media. Fibroblasts were allowed to recover for at least 30 min from trypsin treatment. Adhesion of a single fibroblast to the free cantilever end was achieved by pipetting the fibroblast suspension onto the functionalized Petri dishes. The functionalized cantilever was lowered onto a fibroblast with a speed of 1 µm/s until a force of 1 nN was recorded. After ≈5 s contact, the cantilever was retracted with 1 µm/s for 10 µm and the cantilever bound fibroblast was incubated for 7–10 min to assure firm binding to the cantilever. Using differential interference contract (DIC) microscopy, the morphological state of the fibroblast was monitored. For single molecule sensitivity, the fibroblast bound to the cantilever was lowered onto the coated substrate with a speed of 1 µm/s until a contact force of 200 pN was recorded for ≈50 ms contact time. Subsequently, the cantilever was retracted at 1 µm/s and for ≥13 µm until the fibroblast and substrate were fully separated. After the experimental cycle, the fibroblast was allowed to recover for 0.5 s. For each measurement, the area of the substrate was varied. Force-distance curves were analyzed to determine binding probability using JPK software. Mann-Whitney tests were applied to determine significant differences between the binding probability of fibroblast lines at different conditions. Tests were done using Prism (GraphPad, La Jolla, USA).

pFAK analysis

Cells were plated on pFN-coated glass coverslips and spun in the spinning disk device, then lysed in RIPA buffer (50 mM Tris, pH 7.4; 1% NP-40; 0.5% Na-Deoxycolate; 0.1% SDS; 2 mM EDTA) supplemented with proteinase inhibitors (Complete Proteinase Inhibitor Cocktail tablet, Roche), phosphatase inhibitors (Protease Inhibitors Cocktail 2 Aqueous Solution and Cocktail 3, Sigma-Aldrich), 1 mM Na_3VO_4 and 5 mM NaF for 10 min on ice, and sonicated for 1 min. The protein concentrations were quantified using the Pierce BCA Protein Assay Kit (Thermo Scientific) assay and 30–50 µg of protein were separated by SDS-PAGE gel, transferred to nitrocellulose membranes and hybridized with specific antibodies. Western-blots were analyzed with ImageJ and the levels of phospho-Tyr_{397}-FAK or phospho-Tyr_{861}FAK were referred to the total FAK content.

FN matrix assembly assay

Fn1-KO fibroblasts were starved overnight in 9% SRM supplemented with 1% FN-depleted serum, trypsinized and transferred into 8-well Lab-Tek chambers (Thermo Scientific) coated for 1 hr with a solution of 20 µg/ml of Laminin (Roche) at RT. After 3 hr, the 9% SRM was supplemented with 1% mouse plasma and cells were incubated for 24, 48, 72 and 96 hr, fixed with 4% PFA and prepared for immunofluorescence staining.

Cell spreading assay

Glass coverslips (18 × 18 mm) were POMA treated, coated with pFN and then incubated with 2×10^4 *Fn1*-KO or pKO-β1, pKO-αv and pKO-αv/β1 cells starved overnight in 9% SRM supplemented with 1% FN-depleted serum. After 15, 30, 60 and 120 min of adhesion, cells were fixed with 2% PFA and immunostained. Focal adhesions were quantified with imageJ.

Integrin expression analysis by FACS

Flow cytometry to analyse integrin levels on the *Fn1*-KO fibroblasts was carried out as previously described (***Theodosiou et al., 2016***).

Live imaging of cell spreading

10^4 cells (*Fn1*-KO, pKO-β1, pKO-αv or pKO-αv/β1) were starved overnight, cultured on µ-Slide eight well chambers (Ibidi, Martinsried, Munich) coated with 10 µg/ml of pFN during 1 hr and imaged with frame rates of 90 s in a Zeiss Axiovert microscope using the VisiView (Visitron Systems, Puchheim, Germany) software.

Histological analysis

Adult mice were perfused with 4% parafolmaldehyde (PFA) in PBS or tissue pieces and embryos were fixed overnight with 4% PFA at 4˚C. Fixed tissues were dehydrated in graded alcohol series, embedded in paraffin (Paraplast X-tra, Sigma-Aldrich), sectioned into 8 µm thick sections and stained with Haematoxylin-Eosin (H and E) using standard protocols. For immunostainings, sections were hydrated with inverse graded alcohol series, unmasked by heating in 10 mM citrate buffer (pH 6) for 10 min, blocked for 1 hr with 3% BSA at RT and incubated overnight with the primary antibody, washed, incubated with secondary antibodies for 1 hr at room temperature, washed, DAPI stained and mounted on glass slides with elvanol.

Embryo and skin whole mount immunostaining

Embryos were isolated from pregnant mothers at the stages of E11.5, E15.5 and E16.5 and fixed overnight at 4˚C with DENT´s fixative consisting of 80% Methanol, 20% DMSO. The skin was dissected after fixation from the E15.5 and E16.5 embryos, washed 3 times with 100% methanol (5 min) and kept at −20˚C in 100% methanol. For staining, fixed pieces of skin or whole E11.5 embryos were hydrated in decreasing (75, 50 and 25%) methanol series, diluted in PBS supplemented with 0.1% Tween20 (PBST) and blocked for 2 hr at RT with 3% BSA in PBST. Incubations with primary and secondary antibodies were done overnight at 4˚C with gentle rocking and after washing with PBST, tissues were mounted with elvanol.

Platelet isolation and quantification

Blood from *Fn1*$^{syn/syn}$ or *Fn1*$^{+/+}$ mice was collected in heparinized Microvette CB 300 LH tubes (Sarstedt) and platelets were counted using a ProCyte Hematology Analyzer (IDEXX Laboratories, Ludwigsburg, Germany). To isolate platelets, heparinized blood from $\beta3^{+/+}$ or $\beta3^{-/-}$ mice was centrifuged at 70xg for 10 min at RT, the platelet enriched upper phase was then centrifuged at 800xg for 10 min and the platelet pellet was finally washed twice with Tyrodes buffer pH 6.5 (134 mM NaCl, 2.9 mM KCl, 12 mM $NaHCO_3$, 10 mM *N*-2-hydroxyethylpiperazine-*N*-2-ethanesulfonic acid, 5 mM glucose, 0.35% bovine serum albumin (BSA)). Washed platelets were resuspended in Tyrodes buffer pH 7.4 and counted using a ProCyte Hematology Analyzer (IDEXX Laboratories). For experiments, platelet numbers were adjusted to equivalent concentrations with Tyrodes buffer pH 7.4 complemented with 1 mM $CaCl_2$, 1 mM $MgCl_2$.

Platelet aggregation in vitro assays

Platelet aggregation was measured with 1×10^8 washed platelets stimulated with 0.5 U/ml thrombin (Sigma-Aldrich) or 5 µg/ml fibrillar type I collagen (Nycomed, Munich, Germany) in the presence of 10 µg/ml pFN isolated either from *Fn1*$^{+/+}$ or *Fn1*$^{syn/syn}$ mice. For platelet aggregation with 20 µM ADP, platelet rich plasma (PRP) was isolated. The mouse blood was collected with citrate buffer (1:9, buffer:blood), centrifuged at 110xg and the supernatant (PRP) was collected. A volume of 225 µl of PRP containing 6.75×10^7 platelets was used for each experiment adding 20 µM ADP. Light transmission was recorded with a ChronoLog aggregometer over 15 min as arbitrary units with the transmission through buffer defined as 100% transmission.

FN and fibrinogen quantification in isolated platelets and blood plasma

Platelets were isolated from *Fn1*$^{+/+}$and *Fn1*$^{syn/syn}$ heparinized blood as described above. About 5×10^6 platelets were lysed with 0,1% Triton in TBS with proteinase inhibitors (Complete Proteinase Inhibitor Cocktail tablet, Roche) during 10 min on ice. After centrifugation at 13,000 rpm, the supernatant was run in an 8% SDS-PAGE under reducing conditions, transferred to nitrocellulose membranes and incubated with anti-FN antibodies. To quantify the plasma content of FN and fibrinogen, 2 µl of plasma were loaded onto the 8% SDS-PAGE. As a reference, we used pure human pFN (Millipore) and human fibrinogen (Sigma-Aldrich). Western-blots were analyzed with ImageJ. To know the FN levels in platelets derived from the different mouse strains the FN levels were related to their vinculin contents.

Platelet spreading assay

To study platelet spreading, glass bottom dishes were coated with 10 µg/ml of pFN^{wt}, pFN^{syn}, fibrinogen (Sigma-Aldrich) or soluble collagen type I (PureCol, Advanced Biomatrix, San Diego, CA, USA) at RT for 1 hr and blocked with 1% BSA in PBS. Washed platelets ($0.5–1 \times 10^6$) were added to the dishes in a final volume of 1 ml and activated with 0.01% thrombin (Sigma-Aldrich). Images were taken after 15, 30 and 60 min under a differential interference contrast microscopy (Zeiss Axiovert 200M microscope with a Plan-NEOFLUAR,×100, 1.45 oil objective; Zeiss, Jena, Germany) using the Metamorph software (Molecular Devices, Sunnyvale, CA, USA). The platelet spreading area was analysed using the ImageJ software.

Platelets adhesion assay under flow

Flow chamber experiments were carried out as described previously (***Schulz et al., 2009***) using the air-driven continuous flow pump system from Ibidi. Briefly, platelets were isolated, fluorescently labelled with 5 µM carboxyfluorescein succinimidyl ester (CFSE; Invitrogen) in Tyrodes buffer pH 6.5 for 15 min and then washed. To achieve near-physiological conditions during perfusion of the pFN-coated flow chamber slides, 2 ml of washed platelets with a platelet count of 1×10^7 were combined with 1 ml of human erythrocytes isolated from the blood of a healthy volunteer.

For each experiment, 4 channels of a flow chamber slide (µ-Slide VI 0.1 ibiTreat, Ibidi) were coated with 10 µg/ml fibrillar collagen, fibrinogen, pFN^{wt} or pFN^{syn} over night at 4°C and blocked with 1% BSA the following day. The coated channels of one µ-slide were connected in series with connector tubings for simultaneous perfusion. The platelet suspension was filled in one reservoir of a Perfusion Set Black (Ibidi) and the pump was started with unidirectional flow at the highest possible

pressure 100 mbar) until all channels were filled with the blood-like fluid. Then, the experiment was started by adjusting the shear rate to approximately 1000/s. The channels were perfused for 10 min and subsequently washed by perfusing Tyrodes buffer for another 10 min. Platelets were imaged after performing the perfusion with a Zeiss Apotome microscope and platelet surface coverage was analysed using ImageJ.

Microvascular thrombus formation

The surgical preparation of the mouse cremaster muscle was performed as described (***Baez, 1973***). Mice were anesthetized using a mixture of 100 mg/kg ketamine and 10 mg/kg xylazin. The left femoral artery was cannulated in a retrograde manner to administer FITC-labeled dextran (MW 150 kDa; Sigma Aldrich). The right cremaster muscle was exposed through a ventral incision of the scrotum. The muscle was opened ventrally in a relatively avascular zone and spread over the pedestal of a custom-made microscopy stage. Epididymis and testicle were detached from the cremaster muscle and placed into the abdominal cavity. Throughout the surgical procedure and in vivo microscopy, the muscle was superfused with warm saline solution. At the end of each experiment, blood samples were collected by cardiac puncture to determine systemic cell counts using a hematology analysis system (ProCyte DX, IDEXX Laboratories).

Microvascular thrombus formation was induced by phototoxic injury as described (***Rumbaut et al., 2005***) with slight modifications. Briefly, after surgical preparation of the cremaster muscle, 4 ml/kg body weight of a 2.5% solution of FITC-dextran was infused intraarterially and the exposed the vessel segment under investigation was continuously epi-illuminated with a wavelength of 488 nm (Polychrome II, TILL Photonics, Gräfelfing, Germany). An Olympus water immersion lens (60 × /NA 0.9) in an upright microscope (BX50; Olympus Microscopy, Hamburg, Germany) was used to focus the light onto the cremaster muscle and to visualize the microvascular thrombus formation in real-time. Thrombus formation was induced in one arteriole (25–35 µm) per experiment by analyzing the time until the first platelet adhesion to the vessel wall (defined as the onset of thrombus formation) occurred and the time until blood flow ceased (defined as the complete occlusion of the vessel).

Tail bleeding assay

The tail bleeding assay was performed in anesthetized mice directly after the analysis of microvascular thrombus formation. For this purpose, the distal 2 mm segment of the tail was removed with a scalpel. Bleeding was monitored by absorbing the bead of blood with a filter paper in 30 s intervals without touching the wound. Tail bleeding time was defined as the time until hemorrhage ceased.

Acknowledgements

We acknowledge support from the Spanish Ministry for Economy and Competitiveness (MINECO) and Fondo Europeo de Desarrollo Regional (FEDER): Mat2012-38359 (MINECO) and Mat2015-69315 (MINECO/FEDER) as well as from the Sonderforschungsbereich 914 (SFB 914; project B3) granted by the Deutsche Forschungsgemeinschaft (DFG). MB-J was supported by a contract from the Conselleria Valenciana d'Educació i Ciència. We thank Kairbaan Hodivala-Dilke for providing the *Itgb3*$^{-/-}$ mouse strain and Herbert Schiller for cell lines.

Additional information

Funding

Funder	Grant reference number	Author
Ministerio de Economía y Competitividad	National grant	Maria Benito-Jardón Irene Gimeno-LLuch Mercedes Costell
Conselleria Valenciana d'Educació i Ciència	Graduate student fellowship	Maria Benito-Jardón

The funders had no role in study design, data collection and interpretation, or the decision to submit the work for publication.

Author contributions

MB-J, Formal analysis, Investigation, Writing—review and editing; SK, MB, Investigation, Writing—review and editing; IG-L, Resources, Investigation, Writing—review and editing; TP, Conceptualization, Formal analysis, Writing—review and editing; DJM, Conceptualization, Supervision, Investigation, Writing—original draft; GZ, Investigation, Writing—original draft; CAR, Conceptualization, Supervision, Writing—original draft; MC, Conceptualization, Resources, Supervision, Funding acquisition, Validation, Investigation, Visualization, Methodology, Writing—original draft, Project administration, Writing—review and editing

Author ORCIDs

Maria Benito-Jardón, http://orcid.org/0000-0001-9562-5430
Mercedes Costell, http://orcid.org/0000-0001-6146-996X

Ethics

Animal experimentation: Mice were housed in special pathogen free animal facilities. All mouse work was performed in accordance with the Government of the Valencian Community (Spain) guidelines (permission reference A1327395471346). Mice containing the integrin Î²3 deletion were bred under the permission reference 55.2-1-54-2532-96-2015 (Government of Upper Bavaria). The tail-bleeding and cremaster muscle venules injury assays performed under the permission reference 55.2-1-54-2532-115-12 (Government of Upper Bavaria).

References

Abraham S, Kogata N, Fässler R, Adams RH. 2008. Integrin beta1 subunit controls mural cell adhesion, spreading, and blood vessel wall stability. *Circulation Research* **102**:562–570. doi: 10.1161/CIRCRESAHA.107.167908, PMID: 18202311

Aota S, Nagai T, Yamada KM. 1991. Characterization of regions of fibronectin besides the arginine-glycine-aspartic acid sequence required for adhesive function of the cell-binding domain using site-directed mutagenesis. *The Journal of Biological Chemistry* **266**:15938–15943. PMID: 1874740

Aota S, Nomizu M, Yamada KM. 1994. The short amino acid sequence Pro-His-Ser-Arg-Asn in human fibronectin enhances cell-adhesive function. *The Journal of Biological Chemistry* **269**:24756–24761. PMID: 7929152

Baez S. 1973. An open cremaster muscle preparation for the study of blood vessels by in vivo microscopy. *Microvascular Research* **5**:384–394. doi: 10.1016/0026-2862(73)90054-X, PMID: 4709735

Boettiger D. 2007. Quantitative measurements of integrin-mediated adhesion to extracellular matrix. In: *Methods in Enzymology*. Elsevier. p 1–25. doi: 10.1016/S0076-6879(07)26001-X

Bowditch RD, Hariharan M, Tominna EF, Smith JW, Yamada KM, Getzoff ED, Ginsberg MH. 1994. Identification of a novel integrin binding site in fibronectin. differential utilization by beta 3 integrins. *The Journal of Biological Chemistry* **269**:10856–10863. PMID: 7511609

Carramolino L, Fuentes J, García-Andrés C, Azcoitia V, Riethmacher D, Torres M. 2010. Platelets play an essential role in separating the blood and lymphatic vasculatures during embryonic angiogenesis. *Circulation Research* **106**:1197–1201. doi: 10.1161/CIRCRESAHA.110.218073, PMID: 20203303

Chada D, Mather T, Nollert MU. 2006. The synergy site of fibronectin is required for strong interaction with the platelet integrin alphaIIbbeta3. *Annals of Biomedical Engineering* **34**:1542–1552. doi: 10.1007/s10439-006-9161-1, PMID: 16933105

Erickson HP. 1994. Reversible unfolding of fibronectin type III and immunoglobulin domains provides the structural basis for stretch and elasticity of titin and fibronectin. *PNAS* **91**:10114–10118. doi: 10.1073/pnas.91.21.10114, PMID: 7937847

Fogerty FJ, Akiyama SK, Yamada KM, Mosher DF. 1990. Inhibition of binding of fibronectin to matrix assembly sites by anti-integrin (alpha 5 beta 1) antibodies. *The Journal of Cell Biology* **111**:699–708. doi: 10.1083/jcb.111.2.699, PMID: 2380248

Friedland JC, Lee MH, Boettiger D. 2009. Mechanically activated integrin switch controls alpha5beta1 function. *Science* **323**:642–644. doi: 10.1126/science.1168441, PMID: 19179533

Friedrichs J, Legate KR, Schubert R, Bharadwaj M, Werner C, Müller DJ, Benoit M. 2013. A practical guide to quantify cell adhesion using single-cell force spectroscopy. *Methods* **60**:169–178. doi: 10.1016/j.ymeth.2013.01.006, PMID: 23396062

García AJ, Huber F, Boettiger D. 1998. Force required to break alpha5beta1 integrin-fibronectin bonds in intact adherent cells is sensitive to integrin activation state. *Journal of Biological Chemistry* **273**:10988–10993. doi: 10.1074/jbc.273.18.10988, PMID: 9556578

García AJ, Schwarzbauer JE, Boettiger D. 2002. Distinct activation states of alpha5beta1 integrin show differential binding to RGD and synergy domains of fibronectin. *Biochemistry* **41**:9063–9069. doi: 10.1021/bi025752f, PMID: 12119020

George EL, Georges-Labouesse EN, Patel-King RS, Rayburn H, Hynes RO. 1993. Defects in Mesoderm, neural tube and vascular development in mouse embryos lacking fibronectin. *Development* **119**:1079–1091. PMID: 8306876

Georges-Labouesse EN, George EL, Rayburn H, Hynes RO. 1996. Mesodermal development in mouse embryos mutant for fibronectin. *Developmental Dynamics* **207**:145–156. doi: 10.1002/(SICI)1097-0177(199610)207:2<145::AID-AJA3>3.0.CO;2-H, PMID: 8906418

Girós A, Grgur K, Gossler A, Costell M. 2011. α5β1 integrin-mediated adhesion to fibronectin is required for axis elongation and somitogenesis in mice. *PLoS One* **6**:e22002. doi: 10.1371/journal.pone.0022002, PMID: 21799763

Grant RP, Spitzfaden C, Altroff H, Campbell ID, Mardon HJ. 1997. Structural requirements for biological activity of the ninth and tenth FIII domains of human fibronectin. *Journal of Biological Chemistry* **272**:6159–6166. doi: 10.1074/jbc.272.10.6159, PMID: 9045628

Guan JL, Trevithick JE, Hynes RO. 1991. Fibronectin/integrin interaction induces tyrosine phosphorylation of a 120-kDa protein. *Molecular Biology of the Cell* **2**:951–964. doi: 10.1091/mbc.2.11.951, PMID: 1725602

Hodivala-Dilke KM, McHugh KP, Tsakiris DA, Rayburn H, Crowley D, Ullman-Culleré M, Ross FP, Coller BS, Teitelbaum S, Hynes RO. 1999. Beta3-integrin-deficient mice are a model for glanzmann thrombasthenia showing placental defects and reduced survival. *Journal of Clinical Investigation* **103**:229–238. doi: 10.1172/JCI5487, PMID: 9916135

Hutter JL, Bechhoefer J. 1993. Calibration of atomic-force microscope tips. *Review of Scientific Instruments* **64**:1868–1873. doi: 10.1063/1.1143970

Kornberg L, Earp HS, Parsons JT, Schaller M, Juliano RL. 1992. Cell adhesion or integrin clustering increases phosphorylation of a focal adhesion-associated tyrosine kinase. *The Journal of Biological Chemistry* **267**:23439–23442. PMID: 1429685

Krammer A, Craig D, Thomas WE, Schulten K, Vogel V. 2002. A structural model for force regulated integrin binding to fibronectin's RGD-synergy site. *Matrix Biology* **21**:139–147. doi: 10.1016/S0945-053X(01)00197-4, PMID: 11852230

Laklai H, Miroshnikova YA, Pickup MW, Collisson EA, Kim GE, Barrett AS, Hill RC, Lakins JN, Schlaepfer DD, Mouw JK, LeBleu VS, Roy N, Novitskiy SV, Johansen JS, Poli V, Kalluri R, Iacobuzio-Donahue CA, Wood LD, Hebrok M, Hansen K, et al. 2016. Genotype tunes pancreatic ductal adenocarcinoma tissue tension to induce matricellular fibrosis and tumor progression. *Nature Medicine* **22**:497–505. doi: 10.1038/nm.4082, PMID: 27089513

Leahy DJ, Aukhil I, Erickson HP. 1996. 2.0 A crystal structure of a four-domain segment of human fibronectin encompassing the RGD loop and synergy region. *Cell* **84**:155–164. doi: 10.1016/S0092-8674(00)81002-8, PMID: 8548820

Leiss M, Beckmann K, Girós A, Costell M, Fässler R. 2008. The role of integrin binding sites in fibronectin matrix assembly in vivo. *Current Opinion in Cell Biology* **20**:502–507. doi: 10.1016/j.ceb.2008.06.001, PMID: 18586094

Missirlis D, Haraszti T, Scheele C, Wiegand T, Diaz C, Neubauer S, Rechenmacher F, Kessler H, Spatz JP, Scheele CVC, Spatz JP. 2016. Substrate engagement of integrins α5β1 and αvβ3 is necessary, but not sufficient, for high directional persistence in migration on fibronectin. *Scientific Reports* **6**:23258–18. doi: 10.1038/srep23258, PMID: 26987342

Nagae M, Re S, Mihara E, Nogi T, Sugita Y, Takagi J. 2012. Crystal structure of α5β1 integrin ectodomain: atomic details of the fibronectin receptor. *The Journal of Cell Biology* **197**:131–140. doi: 10.1083/jcb.201111077, PMID: 22451694

Ni H, Papalia JM, Degen JL, Wagner DD. 2003a. Control of thrombus embolization and fibronectin internalization by integrin alpha IIb Beta 3 engagement of the fibrinogen gamma chain. *Blood* **102**:3609–3614. doi: 10.1182/blood-2003-03-0850, PMID: 12855554

Ni H, Yuen PS, Papalia JM, Trevithick JE, Sakai T, Fässler R, Hynes RO, Wagner DD. 2003b. Plasma fibronectin promotes thrombus growth and stability in injured arterioles. *PNAS* **100**:2415–2419. doi: 10.1073/pnas.2628067100, PMID: 12606706

Obara M, Kang MS, Yamada KM. 1988. Site-directed mutagenesis of the cell-binding domain of human fibronectin: separable, synergistic sites mediate adhesive function. *Cell* **53**:649–657. doi: 10.1016/0092-8674(88)90580-6, PMID: 3286012

Oberhauser AF, Badilla-Fernandez C, Carrion-Vazquez M, Fernandez JM. 2002. The mechanical hierarchies of fibronectin observed with single-molecule AFM. *Journal of Molecular Biology* **319**:433–447. doi: 10.1016/S0022-2836(02)00306-6, PMID: 12051919

Prewitz MC, Seib FP, von Bonin M, Friedrichs J, Stißel A, Niehage C, Müller K, Anastassiadis K, Waskow C, Hoflack B, Bornhäuser M, Werner C. 2013. Tightly anchored tissue-mimetic matrices as instructive stem cell microenvironments. *Nature Methods* **10**:788–794. doi: 10.1038/nmeth.2523

Puech PH, Poole K, Knebel D, Muller DJ. 2006. A new technical approach to quantify cell-cell adhesion forces by AFM. *Ultramicroscopy* **106**:637–644. doi: 10.1016/j.ultramic.2005.08.003, PMID: 16675123

Redick SD, Settles DL, Briscoe G, Erickson HP. 2000. Defining fibronectin's cell adhesion synergy site by site-directed mutagenesis. *The Journal of Cell Biology* **149**:521–527. doi: 10.1083/jcb.149.2.521, PMID: 10769040

Retta SF, Ferraris P, Tarone G. 1999. Purification of fibronectin from human plasma. In: *Adhesion Protein Protocols*. New Jersey: Humana Press. p 119–124. doi: 10.1385/1-59259-258-9:119

Rumbaut RE, Slaff DW, Burns AR. 2005. Microvascular Thrombosis models in Venules and Arterioles *in vivo*. *Microcirculation* **12**:259–274. doi: 10.1080/10739680590925664, PMID: 15814435

Schiller HB, Hermann MR, Polleux J, Vignaud T, Zanivan S, Friedel CC, Sun Z, Raducanu A, Gottschalk KE, Théry M, Mann M, Fässler R. 2013. β1- and αv-class integrins cooperate to regulate myosin II during rigidity sensing of fibronectin-based microenvironments. *Nature Cell Biology* **15**:625–636. doi: 10.1038/ncb2747, PMID: 23708002

Schulz S, Schuster T, Mehilli J, Byrne RA, Ellert J, Massberg S, Goedel J, Bruskina O, Ulm K, Schömig A, Kastrati A. 2009. Stent thrombosis after drug-eluting stent implantation: incidence, timing, and relation to discontinuation of clopidogrel therapy over a 4-year period. *European Heart Journal* **30**:2714–2721. doi: 10.1093/eurheartj/ehp275, PMID: 19596658

Sechler JL, Corbett SA, Schwarzbauer JE. 1997. Modulatory roles for integrin activation and the synergy site of fibronectin during matrix assembly. *Molecular Biology of the Cell* **8**:2563–2573. doi: 10.1091/mbc.8.12.2563, PMID: 9398676

Seong J, Tajik A, Sun J, Guan JL, Humphries MJ, Craig SE, Shekaran A, García AJ, Lu S, Lin MZ, Wang N, Wang Y. 2013. Distinct biophysical mechanisms of focal adhesion kinase mechanoactivation by different extracellular matrix proteins. *PNAS* **110**:19372–19377. doi: 10.1073/pnas.1307405110, PMID: 24222685

Shi Q, Boettiger D. 2003. A novel mode for integrin-mediated signaling: tethering is required for phosphorylation of FAK Y397. *Molecular Biology of the Cell* **14**:4306–4315. doi: 10.1091/mbc.E03-01-0046, PMID: 12960434

Takagi J, Strokovich K, Springer TA, Walz T. 2003. Structure of integrin alpha5beta1 in complex with fibronectin. *The EMBO Journal* **22**:4607–4615. doi: 10.1093/emboj/cdg445, PMID: 12970173

Takahashi S, Leiss M, Moser M, Ohashi T, Kitao T, Heckmann D, Pfeifer A, Kessler H, Takagi J, Erickson HP, Fässler R. 2007. The RGD motif in fibronectin is essential for development but dispensable for fibril assembly. *The Journal of Cell Biology* **178**:167–178. doi: 10.1083/jcb.200703021, PMID: 17591922

Theodosiou M, Widmaier M, Böttcher RT, Rognoni E, Veelders M, Bharadwaj M, Lambacher A, Austen K, Müller DJ, Zent R, Fässler R. 2016. Kindlin-2 cooperates with talin to activate integrins and induces cell spreading by directly binding paxillin. *eLife* **5**:e10130. doi: 10.7554/eLife.10130, PMID: 26821125

Uhrin P, Zaujec J, Breuss JM, Olcaydu D, Chrenek P, Stockinger H, Fuertbauer E, Moser M, Haiko P, Fässler R, Alitalo K, Binder BR, Kerjaschki D. 2010. Novel function for blood platelets and podoplanin in developmental separation of blood and lymphatic circulation. *Blood* **115**:3997–4005. doi: 10.1182/blood-2009-04-216069, PMID: 20110424

Wang Y, Reheman A, Spring CM, Kalantari J, Marshall AH, Wolberg AS, Gross PL, Weitz JI, Rand ML, Mosher DF, Freedman J, Ni H. 2014. Plasma fibronectin supports hemostasis and regulates thrombosis. *Journal of Clinical Investigation* **124**:4281–4293. doi: 10.1172/JCI74630, PMID: 25180602

Yang JT, Rayburn H, Hynes RO. 1993. Embryonic mesodermal defects in Alpha 5 integrin-deficient mice. *Development* **119**:1093–1105. PMID: 7508365

Yang JT, Bader BL, Kreidberg JA, Ullman-Culleré M, Trevithick JE, Hynes RO. 1999. Overlapping and independent functions of fibronectin receptor integrins in early mesodermal development. *Developmental Biology* **215**:264–277. doi: 10.1006/dbio.1999.9451, PMID: 10545236

Yu M, Strohmeyer N, Wang J, Müller DJ, Helenius J. 2015. Increasing throughput of AFM-based single cell adhesion measurements through multisubstrate surfaces. *Beilstein Journal of Nanotechnology* **6**:157–166. doi: 10.3762/bjnano.6.15, PMID: 25671160

Zeiler M, Moser M, Mann M. 2014. Copy number analysis of the murine platelet proteome spanning the complete abundance range. *Molecular & Cellular Proteomics* **13**:3435–3445. doi: 10.1074/mcp.M114.038513, PMID: 25205226

Zilberberg L, Todorovic V, Dabovic B, Horiguchi M, Couroussé T, Sakai LY, Rifkin DB. 2012. Specificity of latent TGF-β binding protein (LTBP) incorporation into matrix: role of fibrillins and fibronectin. *Journal of Cellular Physiology* **227**:3828–3836. doi: 10.1002/jcp.24094, PMID: 22495824

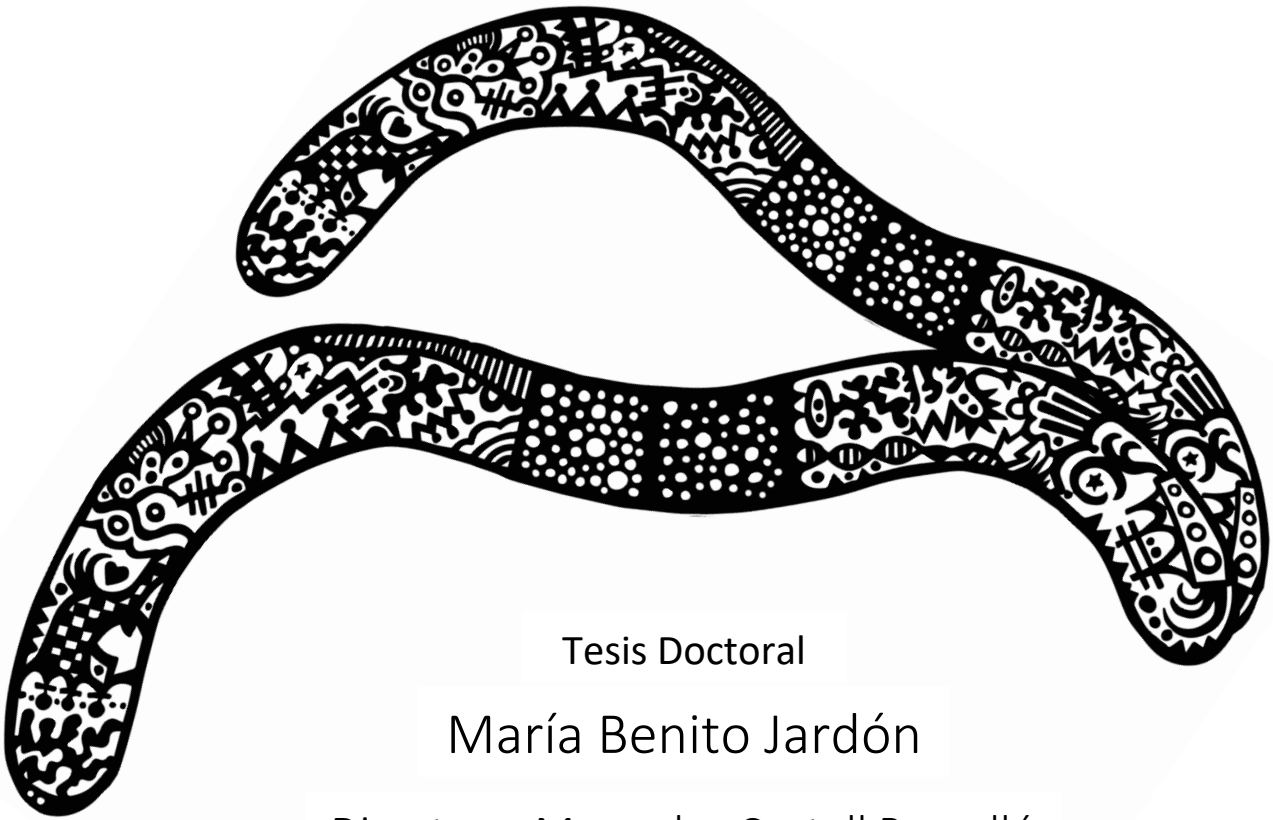

Tesis Doctoral

María Benito Jardón

Directora: Mercedes Costell Rosselló

Valencia, Junio 2018